

Study on Physicochemical Properties of Some Soft Matter Systems Using Fluorescence and Conductometric Methods

THESIS

Submitted in partial fulfillment
of the requirements for the degree of

DOCTOR OF PHILOSOPHY

by

Sonu

Under the supervision of
Prof. Subit Kumar Saha



BITS Pilani
Pilani | Dubai | Goa | Hyderabad

**BIRLA INSTITUTE OF TECHNOLOGY & SCIENCE
PILANI – 333 031 (RAJASTHAN) INDIA**

2016

Study on Physicochemical Properties of Some Soft Matter Systems Using Fluorescence and Conductometric Methods

THESIS

Submitted in partial fulfillment
of the requirements for the degree of

DOCTOR OF PHILOSOPHY

by

Sonu
2009PHXF409P

Under the supervision of
Prof. Subit Kumar Saha



BITS Pilani
Pilani | Dubai | Goa | Hyderabad

BIRLA INSTITUTE OF TECHNOLOGY & SCIENCE
PILANI – 333 031 (RAJASTHAN) INDIA

2016



**BIRLA INSTITUTE OF TECHNOLOGY & SCIENCE
PILANI – 333 031 (RAJASTHAN) INDIA**

CERTIFICATE

This is to certify that the thesis entitled “**Study on Physicochemical Properties of Some Soft Matter Systems Using Fluorescence and Conductometric Methods**” submitted by **Sonu, ID.No. 2009PHXF409P** for award of Ph.D. Degree of the Institute embodies original work done by him under my supervision.

Signature of the supervisor : _____

Name of the supervisor : Dr. Subit Kumar Saha

Designation : Professor

Date : _____

*Dedicated to my Parents
and Teachers*

Acknowledgement

This thesis, as I see it, is not the end but just the beginning of my research journey. However before continuing the journey further, I would like to thank all those who have supported, guided and taught me how to make this travel in a safe way and explore things in order to get as much as possible out of the journey.

First of all, I would like to thank the Supreme Power of Universe, almighty God for his/her unparalleled grace that leads me toward the ultimate goal through the lows and highs of my PhD journey. I am thankful, for your love and care.

I would like to express my sincere gratitude to Prof. Subit Kumar Saha, my supervisor, without whom this research could not have been completed. The time he spent for me to complete this research is extremely appreciable and I will always be indebted for his guidance, understanding, patience, and most importantly, his tremendous mentorship.

I am thankful to the Doctoral Advisory Committee (DAC) members Prof. Inamur R. Laskar and Dr. Madhushree Sarkar who spared their valuable time to review my draft thesis. They critically evaluated my work and provided me with constructive criticisms and valuable suggestions, which have immensely helped in improving the quality of this thesis. Indeed, it is a pleasure to extend my sincere gratitude to all the faculty members of Department of Chemistry BITS Pilani, for their excellent teaching and enthusiastic corporation throughout my doctoral study.

I am immensely thankful to the Vice-Chancellor, Directors, Deputy Directors and Deans of Birla Institute of Technology & Science (BITS), Pilani for providing me the opportunity to pursue my doctoral studies by providing necessary facilities and financial support.

I express my gratitude to Prof. Sanjay Kumar Verma, Dean, Academic Research Division (ARD), BITS Pilani, Pilani Campus and Prof. Ajay Kumar Sah, Convenor, Departmental Research Committee (DRC), Department of Chemistry, BITS Pilani, Pilani Campus for his official support and encouragement. I thank Prof. Hemanth Jadhav, Dr. Navin Singh, nucleus members of ARD and Prof. S.C. Sivasubramanian,

Prof. Ram Kinkor Roy, Prof. Dalip Kumar and Prof. Anil Kumar, member of DRC, Department of Chemistry, BITS Pilani, Pilani Campus for their cooperation and constant guidance during each of the past few years. I also express my gratitude to the office staff of ARD, whose secretarial assistance helped me in submitting the various evaluation documents in time.

I thank SAIF, Panjab University, Chandigarh and AIRF, Jawaharlal Nehru University, New Delhi for their technical support to access NMR.

I am thankful to past and current lab members who always supported me, whenever I am in need of any help Dr. M. Sowmiya, Dr. Amit Kumar Tiwari and Ms. Sunita along with all research scholars of the Department of Chemistry.

Most importantly, my family deserves credit. I would like to express my sincere gratitude to my parents for their unquestioning support. They are the source of inspiration and courage in every ups-and-down of my life. I thank to my teachers Sh. Kartar Singh (Primary school teacher) and Sh. Surender Kumar (Principal) for their highly motivational support. Special thanks to my brother Mr. Satish Kumar for his priceless support in my life especially in school and college life. I thank to my uncles Mr. Hariom Singh and Mr. Krishan Kumar for their support and encouragement. I thank my mother-in-law for her constant help and care. These phrases will remain incomplete without mentioning the contribution of my wife, Babli for her continual support, understanding, motivation and care. Every achievement of this thesis is the result of her prayers, encouragement, and love.

There are several people whom I would like to acknowledge. Unfortunately, due to space limitations, I could not mention about everybody. However, I would like to thank each and everyone, who had supported me directly or indirectly in completing this research work.

Sonu

Abstract

In the present thesis work, the physicochemical properties of some soft matter systems like micelles, reverse micelles, mixed micelles, and protein have been studied by using conductometry, UV-Visible absorption spectroscopy, steady-state fluorescence and fluorescence anisotropy, time-resolved fluorescence and fluorescence anisotropy techniques. The micellization behavior of conventional surfactants with different counterions and hydrophobic chain length and synthesized gemini surfactants have been studied. The probe molecules showing the twisted intramolecular charge transfer (TICT) fluorescence have been used to explore the microenvironmental properties of micelles as well as mixed micelles. The concept of TICT fluorescence and its properties have been explained. The solvation dynamics and rotational relaxation of fluorescence dyes, Coumarin-153 (C-153), Coumarin-480 (C-480), and Coumarin-490 (C-490) have been studied in various micellar systems. The solvation dynamics and rotational relaxation of fluorescence dye, C-490 have been studied in a reverse micellar system. The effect of added urea on solvation dynamics and rotational relaxation of C-480 has been studied in aqueous micelles of cationic gemini surfactant, 12-4-12, 2Br^- . Interactions of gemini surfactants with a protein, bovine serum albumin (BSA) also have been investigated.

A concise review of literature, objectives and motivation behind the present work are discussed in the chapter 1 of the thesis. The scope of the present study is briefed by stating the research gap and the work done in this thesis. The materials, methods and instruments used in the present study are explained in the chapter 2.

In chapter 3 photophysical properties of trans-2-[4-(N,N-dimethylaminostyryl)]pyridine (2-DMASP), a “push-pull” molecule, have been studied experimentally and theoretically. The possible pathway for the TICT fluorescence, such as donor and acceptor twisting has been explored by performing theoretical calculations and the results are corroborated with the experimental observations. Theoretical calculations suggest donor twisting as a possible path for the creation of a charge transfer state rather than acceptor twisting. Excited state dipole moment value obtained from theoretical calculation corroborates well with the value determined experimentally. The

TICT fluorescence properties of 2-DMASP are explored to study the microenvironmental properties of cetyltrimethylammonium surfactants with different counterions.

Chapter 4 explores the micellar properties of binary mixtures of the monomeric cationic surfactants, hexadecyltrimethylammonium bromide (CTAB), tetradecyltrimethylammonium bromide (TTAB), and dodecyltrimethylammonium bromide (DTAB) with the cationic gemini surfactants, 12-3(OH)-12, 2Br⁻ and 12-4(OH)-12, 2Br⁻ in aqueous solutions. The presence of a small amount of gemini surfactant is found to improve the physicochemical properties of the conventional surfactants. The participation of gemini surfactant molecules in mixed micelle formation is found to increase with decreasing spacer chain length and number of substituted hydroxyl groups in it. The *cmc* value of each mixed micellar system is decreased with increasing bulk mole fraction of a gemini surfactant. The formation of mixed micelles is found to be thermodynamically spontaneous for all the mixed systems. The microviscosity and micropolarity of all the mixed micellar systems are determined using the viscosity and polarity-sensitive TICT fluorescence probe, N,N-dimethylaminocinnamaldehyde (DMACA).

Chapter 5 deals with the study on solvation dynamics and rotational relaxation of C-153 in the micelles of a series of cationic gemini surfactants, 12-s-12, 2Br⁻ containing a hydrophobic polymethylene spacer with $s = 3, 4, 6, 8, 12$. Solvation dynamics at the Stern layer of gemini micelles is bimodal in nature. Counter ions and water molecules bonded with the polar headgroups of surfactant molecules are responsible for the slow component. Average solvation time increases with spacer chain length because of the increased degree of counterion dissociation. The hydrophobic spacer chain also has an effect on increasing the solvation time with increasing chain length. The average rotational relaxation time for C-153 decreases with spacer chain length with a rapid decrease at $s > 4$. The anisotropy decay of C-153 in micelles is biexponential in nature. The slow rotational relaxation is due to the lateral diffusion of C-153 in micelles. Lateral diffusion is much faster than the rotational motion of a micelle as a whole. The rotational motion of the micelle as a whole becomes faster with the decreasing size of micelles. The average rotational relaxation time for C-153 decreases with increasing spacer chain length as the

micelles become progressively less compact and less viscous. The slow relaxation in micellar media is due to the lateral diffusion of the fluorophore.

Chapter 6 deals with the study on solvation dynamics and rotational relaxation of C-153 in mixed micelles of non-ionic surfactant, Triton X-100 and a series of cationic gemini surfactants, 12-s-12, 2Br with varying polymethylene spacer chain length ($s = 3, 6, 8, 12$) at different bulk mole fractions of a surfactant. While micropolarity of the environment around C-153 in the mixed micelles is increased, the microviscosity is decreased with increasing amount of a gemini surfactant. This is because the thickness of the Stern layer of micelles increases as a result of greater extent of penetration of water molecules. Solvation dynamics and rotational relaxation of C-153 become faster with increasing mole fraction of a gemini surfactant in the mixed micelles. Increasing the thickness of the Stern layer leads to an increase in the number of water molecules hydrogen bonded among themselves, resulting in an increase in polarity and microfluidity of the environment. At a given bulk mole fraction of a surfactant, the microviscosity of micelles decreases with increasing the spacer chain length of the gemini surfactant resulting in an increase in the rate of the rotational relaxation process. At a given bulk mole fraction of a surfactant, solvation dynamics becomes slower with increasing spacer chain length from $s = 3$ to 8 because of the increasing degree of counterion dissociation. The slow rotational relaxation process is mainly due to the lateral diffusion of C-153 along the surface of the mixed micelles. Rotational motion of the mixed micelle as a whole is much slower than the lateral diffusion of C-153.

Chapter 7 discloses the effect of added urea on solvation dynamics and rotational relaxation of C-480 in aqueous micelles of cationic gemini surfactant, 12-4-12, 2Br⁺. The *cmc* value of 12-4-12, 2Br⁺ increases with increasing the concentration of urea. Microviscosity, mole fraction partition coefficient and Gibbs free energy of micellization are decreased with the addition of urea. Time resolved anisotropy measurements are bimodal in nature. The average rotational relaxation time decreases with increasing the concentration of urea in the micelles. Solvation dynamics in aqueous micelles depends upon the concentration of urea. While at low concentration of urea the process of solvation dynamics is fast due to the disruption of tetrahedral structure of water, at high

concentration of urea solvation dynamics becomes slower which is due to hydrogen bonding interaction between water and urea.

Chapter 8 demonstrates the solvation dynamics and rotational relaxation of C-490 in presence of 12-4-12, 2Br⁻/cyclohexane/*n*-pentanol/water reverse micelles (RMs). A lesser extent of hydrogen bonding interactions occurs between the –OH group of the alcohol and the C-490 molecule at the interface of the present RMs as compared to the RMs of reported conventional cationic surfactants. Probe molecules move towards the water pool on increasing the content of water molecules, and thus the rotational relaxation and solvation dynamics depend on w_o . The time constants for solvation dynamics and rotational relaxation of C-490 decreases with increasing the value of w_o . The microenvironment around the C-490 has been determined in presence of RMs.

Chapter 9 deals with the interactions of gemini surfactants, 12-4-12, 2Br⁻ and 12-4(OH)-12, 2Br⁻ with BSA. The effect of spacer group of the gemini surfactants has been investigated. Gemini surfactant with hydroxyl group in the spacer part (12-4(OH)-12, 2Br⁻) interacts with native BSA more strongly than the gemini surfactant without hydroxyl group (12-4-12, 2Br⁻) in the spacer. Both the gemini surfactants interact with BSA in a sequential manner. Hydrophobic and electrostatic interactions of gemini surfactant show specific, noncooperative and cooperative bindings with BSA. With increasing concentration of gemini surfactant, BSA unfolds and wraps around the micelles of gemini surfactants. Microenvironment around Trp residues is altered during the interaction of gemini surfactant. Excited singlet state lifetime data also support the fact of sequential manner of interaction of gemini surfactants with BSA. Interactions of gemini surfactants with unfolded BSA also has been studied. 12-4-12, 2Br⁻ interacts with the unfolded BSA to a greater extent than that by 12-4(OH)-12, 2Br⁻.

Table of contents

Contents	Page No.
<i>Certificate</i>	i
<i>Dedication</i>	ii
<i>Acknowledgements</i>	iii
<i>Abstract</i>	v
<i>Table of contents</i>	ix
<i>List of figures</i>	xvii
<i>List of schemes</i>	xxiv
<i>List of tables</i>	xxv
<i>List of abbreviations and symbols</i>	xxviii
Chapter 1 Introduction	1-73
1.1 Surfactant	1
1.1.1 Classification of surfactant	2
1.1.2 Gemini surfactant	4
1.1.3 Micelles formation by surfactant	5
1.1.4 Factors affecting micellization	7
1.1.4.1 The structure of surfactant	7
1.1.4.1.1 Effect of hydrophobic chain length	7
1.1.4.1.2 Effect of headgroups	8
1.1.4.1.3 Effect of spacer (in case of gemini surfactants)	8
1.1.4.1.4 Effect of counterion binding	9
1.1.4.2 Presence of electrolytes	9
1.1.4.3 Effect of organic additives	10
1.1.4.4 Effect of temperature	11
1.1.5 Aggregation number	12
1.1.6 Structure and shape of micelles	12
1.1.7 Thermodynamics of micellization	15
1.1.7.1 Phase separation model	15
1.1.7.2 Mass action model	16
1.1.8 Mixed micelles	18

Contents		Page No.
1.2	Reverse micelles	19
1.3	Protein	21
1.3.1	Significance of serum albumins	21
1.3.2	Structure of BSA	22
1.3.3	Intrinsic fluorescence of BSA	22
1.3.4	Interaction of BSA with surfactant	23
1.4	Fluorescence spectroscopy	24
1.4.1	Effect of substituent	26
1.4.2	Solvent effect	27
1.4.2.1	Dispersive or general solvent interaction	27
1.4.2.2	Specific interaction	28
1.4.3	Excited state dipole moment	32
1.4.4	Dual fluorescence by charge transfer	33
1.4.5	Twisted intramolecular charge transfer (TICT)	34
1.4.6	Twisted geometry	36
1.4.7	Kinetics of TICT	37
1.4.8	Intermolecular proton transfer reaction	39
1.4.9	Fluorescence intensity decay and lifetime	39
1.4.10	Fluorescence quenching	40
1.4.10.1	Dynamic quenching	40
1.4.10.2	Static quenching	41
1.4.11	Fluorescence anisotropy	42
1.4.11.1	Steady-state fluorescence anisotropy	43
1.4.11.2	Time-resolve fluorescence anisotropy	43
1.4.12	Solvation dynamics	44
1.4.12.1	Application of solvation dynamics	45
1.4.12.1.1	Solvation dynamics in presence of pure solvent	46
1.4.12.1.2	Solvation dynamics in microheterogeneous systems	47
1.5	Scope of the present research work	49
	<i>References</i>	57

Contents		Page No.
Chapter 2	Materials, methods, and instrumentation	74-104
2.1	Material	74
2.1.1	Fluorescence probe	74
2.1.2	Surfactants (Conventional and gemini surfactants)	75
2.1.2.1	Conventional surfactants	75
2.1.2.2	Gemini surfactant	75
2.1.2.2.1	Synthesis of gemini surfactants	75
2.1.3	Solvents and other materials	78
2.2	Methods	79
2.2.1	Preparation of different solutions	79
2.2.2	Determination of dissociation constant	81
2.2.2.1	Ground state dissociation constant (pK_a)	81
2.2.2.2	Excited state dissociation constant	82
2.2.3	Solvatochromic comparison method (SCM)	82
2.2.4	Quantum chemical calculation	83
2.2.5	Determination of micropolarity of environment around 2-DMASP, DMACA, C-490, C-153, and pyrene	83
2.2.6	Determination of microviscosity of environment around, 2-DMASP, DMACA, and DPH	84
2.2.7	Steady-state fluorescence anisotropy measurements	85
2.2.8	Fluorescence quantum yield, radiative and non-radiative rate constants calculations	85
2.2.9	Binding constant of probe to micelles	86
2.2.10	Determination of aggregation number	87
2.2.11	Solvation dynamics	87
2.2.12	Time-resolved fluorescence anisotropy	89
2.2.12.1	Two-step model	90
2.2.12.2	Wobbling in a cone model	90
2.2.13	Conductivity measurement	92
2.2.14	Methods to study thermodynamics of mixed micelles	93
2.2.14.1	Clint's method	94
2.2.14.2	Rubingh's method	94
2.2.14.3	Rodenas method	95

Contents		Page No.
2.2.14.4	Motomura method	95
2.3	Instrumentation	96
2.3.1	UV-Visible spectrophotometer	96
2.3.2	Steady-state spectrofluorimeter	97
2.3.3	Time-resolved spectrofluorimeter	99
2.3.3.1	Time-Correlated single photon counting (TCSPC) technique	99
2.3.3.2	Deconvolution procedure	100
2.3.3.3	Analysis of fluorescence decays	101
2.3.4	Other instruments	101
	<i>References</i>	103
Chapter 3 Study on intramolecular charge transfer fluorescence properties of trans-2-[4-(N,N-dimethylaminostyryl)] pyridine in homogeneous and micellar media		105-134
3.1	Study on photophysical properties and prototropic equilibria of trans-2-[4-(N,N-dimethylaminostyryl)]pyridine	105
3.1.1	Results and discussions	106
3.1.1.1	UV-Visible absorption spectra of 2-DMASP\	106
3.1.1.2	Fluorescence study of 2-DMASP	109
3.1.1.3	Effect of nature of solvents on excited singlet state lifetime	115
3.1.1.4	Effect of pH on absorption and fluorescence spectra of 2-DMASP	117
3.1.1.5	Theoretical calculations	121
3.1.1.6	Conclusions	125
3.2	Study on microenvironmental properties of cetyltrimethylammonium surfactants with various counterions by using fluorescence properties of 2-DMASP	126
3.2.1	Results and discussions	127
3.2.1.1	UV-Visible absorption and fluorescence spectra of 2-DMASP	127
3.2.1.2	Micropolarity and microviscosity	130
3.2.1.3	Conclusions	132
	<i>References</i>	133

Contents		Page No.
Chapter 4 Study on mixed micelles of cationic gemini surfactants having hydroxyl group in the spacers with conventional cationic surfactants: effects of spacer group and hydrocarbon tail length		135-166
4.1	Results and discussion	136
4.1.1	Determination of cmc	136
4.2	Pure gemini surfactants: Aggregation behavior	144
4.3	Mixed surfactant systems	145
4.3.1	Aggregation behavior	145
4.3.2	Interactions and thermodynamic properties	146
4.4	Microenvironmental properties	159
4.5	Binding of DMACA with mixed surfactant systems	162
4.6	Conclusions	163
	<i>References</i>	165
Chapter 5 Effect of polymethylene spacer of cationic gemini surfactants on solvation dynamics and rotational relaxation of Coumarin 153 in aqueous micelles		167-186
5.1	Results and discussion	168
5.1.1	UV-Visible absorption and steady-state fluorescence spectra	168
5.1.2	Micropolarity	170
5.1.3	Microviscosity	172
5.1.4	Binding of C-153 with micelles	173
5.2	Solvation dynamics	174
5.3	Rotational relaxation or time-resolved fluorescence anisotropy	180
5.4	Conclusions	184
	<i>References</i>	185

Contents		Page No.
Chapter 6	Solvation dynamics and rotational relaxation of Coumarin 153 in mixed micelles of Triton X-100 and cationic gemini surfactants: Effect of composition and spacer chain length of gemini surfactant	187-210
6.1	Results and discussion	188
6.1.1	UV-visible absorption and steady-state fluorescence spectra	188
6.1.2	Micropolarity	191
6.1.3	Microviscosity	192
6.2	Solvation dynamics	195
6.3	Rotational relaxation or time-resolved fluorescence anisotropy	202
6.4	Conclusions	207
	<i>References</i>	208
Chapter 7	Effect of added urea on solvation dynamics and rotational relaxation of Coumarin 480 in aqueous micelles of cationic gemini surfactant	211-228
7.1	Results and discussions	211
7.1.1	Effect of urea on cmc value of 12-4-12: Study with DMACA	211
7.1.2	UV-Visible absorption and steady-state fluorescence study of C-480	214
7.1.3	Micropolarity	215
7.1.4	Microviscosity	216
7.2	Rotational Relaxation study	219
7.3	Solvation dynamics	222
7.4	Conclusions	226
	<i>References</i>	227

Contents		Page No.
Chapter 8 Study on intramolecular charge transfer processes, solvation dynamics and rotational relaxation of Coumarin 490 in reverse micelles of cationic gemini surfactant		229-246
8.1	Results and discussions	229
8.1.1	UV-Visible absorption spectra	229
8.1.2	Steady-state fluorescence spectra	231
8.1.3	Micropolarity and microviscosity	234
8.2	Excited singlet state lifetime	236
8.2.1	Radiative and non-radiative rate constants in RMs	236
8.3	Time-resolved fluorescence anisotropy	237
8.4	Solvation dynamics	238
8.5	Conclusions	244
	<i>References</i>	245
Chapter 9 Study on interaction of bovine serum albumin with cationic gemini surfactants: The spacer group effect		247-264
9.1	Results and discussions	247
9.1.1	UV-Visible absorption study	247
9.1.2	Steady-state fluorescence study	249
9.1.3	Synchronous fluorescence spectroscopy study	251
9.1.4	Binding of gemini surfactant with BSA: Study of binding isotherm	253
9.2	Time-resolved fluorescence spectroscopy study	255
9.3	Fluorescence quenching of BSA by acrylamide	258
9.4	Interaction of gemini surfactant with unfolded BSA	260
9.5	Conclusions	263
	<i>References</i>	264

Contents	Page No.
Overall conclusions	265
Future scope of the research work	267
Appendix A	A1-A4
List of publications	B1
Brief biography of the candidate	B4
Brief biography of the supervisor	B5

List of figures

Figure No.	Caption	Page No.
1.1	Structures of various types of surfactants	1
1.2	Schematic representation of formation of micelle	6
1.3	Spherical cross section of idealized micelles of (a) cationic conventional surfactant and (b) cationic gemini surfactant	13
1.4	Different shapes of micelle based on critical packing parameter.	14
1.5	Formation of mixed micelles of a conventional surfactant with a gemini surfactant	19
1.6	Diagrammatic representation of reverse micelles formed by gemini surfactants and co-surfactants	20
1.7	Jablonski diagram showing fates of polyatomic molecules upon photoexcitation	25
1.8	Schematic representations of equilibrium and Frank-Condon (F-C) electronic states	28
1.9	Excited state reversal of DMABN	33
1.10	TICT model of DMABN	35
1.11	Model of a TICT excited state for a D-A molecule	35
1.12	Comparison of dynamic and static quenching	42
1.13	Schematic diagram showing mechanism of solvation dynamics	44
2.1	$^1\text{H-NMR}$ spectrum of gemini 12-4-12	78
2.2	Schematic representation of wobbling-in-a-cone model of rotational dynamics	91
2.3	Photograph of the (a) Hitachi U-2900 and (b) Jasco V-630 UV-Visible spectrophotometers	96
2.4	Photograph of the steady-state spectrofluorimeter	97
2.5	Photograph of the time-resolved spectrofluorimeter	99
2.6	Photograph of the Zeta Sizer instrument	102
2.7	Photograph of the conductometer	102
3.1	Absorption spectra of 2-DMASP in different pure solvents. $[2\text{-DMASP}] = 5\mu\text{M}$. Inset shows the absorption spectra in H_2O and MeOH	107
3.2	Emission spectra of 2-DMASP in different pure solvents at $[2\text{-DMASP}] = 5\mu\text{M}$. Spectra 1 to 6 correspond to cyclohexane, diethylether, ethylacetate, MeCN, MeOH, and H_2O , respectively. $\lambda_{\text{ex}} = 356\text{ nm}$	110
3.3	Excitation spectra of 2-DMASP in MeOH at different emission wavelengths. 445(1), 455(2), 465(3), 490(4), and 480(5). Inset represents clear change in excitation spectra with respect to emission wavelength 410(1), 415(2), 420(3), and 425(4)	110

Figure No.	Caption	Page No.
3.4	Fluorescence spectra of 2-DMASP in different percentages of dioxane-water mixtures, From 1 to 11, % of dioxane is 100, 94, 90, 80, 70, 60, 50, 40, 30, 20 and 10 respectively. Inset shows the fluorescence intensity ratio of 2-DMASP in different percentages of dioxane-water mixtures. $\lambda_{ex} = 374$ nm	112
3.5	Absorption (1) and excitation (2) spectrum ($\lambda_{em} = 470$ nm) of 2-DMASP in cyclohexane and excitation (3) spectrum of 2-DMASP in MeOH ($\lambda_{em} = 410$ nm)	113
3.6	Plot of Stokes shift, $\Delta\nu$ (cm^{-1}) of 2-DMASP vs. solvent parameter, Δf in (1) cyclohexane, (2) diethylether, (3) ethylacetate, (4) THF, (5) DMF and (6) MeCN	114
3.7	Plot of Stokes shift, $\Delta\nu$ (cm^{-1}) versus solvent polarity parameter, $E_T(30)$ (kcal mol^{-1}) for 2-DMASP in different polar aprotic and polar protic solvents. Inset shows the plot of emission maxima in terms of wavenumber, $\bar{\nu}_f$ (cm^{-1}) versus hydrogen bonding parameter, α . H_2O (1), MeOH(2), EtOH(3), <i>i</i> PrOH(4)	114
3.8	TCSPC fluorescence intensity decay profiles of 2-DMASP in some selected solvents, $\lambda_{ex} = 375$ nm. λ_{em} are peak maxima in respective solvents	116
3.9	Absorption spectra of neutral-III and monocation-II species of 2-DMASP (Scheme 3.2) in equilibrium in aqueous solutions at different pH. Spectra from 1 to 8 correspond to the pH 4.65, 5.21, 5.46, 5.58, 5.70, 6.23, 7.25, and 7.89, respectively	118
3.10	Absorption spectra of monocation-II and dication-I (Scheme 3.2) in equilibrium in aqueous solutions at different pH. Spectra from 1 to 8 correspond to the pH 1.92, 2.11, 2.43, 2.74, 2.97, 3.28, 3.61, and 3.88, respectively	119
3.11	Fluorescence spectra of 2-DMASP in aqueous solution at different pH. Spectra from 1 to 5 correspond to the pH 4.59, 4.91, 5.31, 5.66, and 7.65, respectively. Inset shows the emission spectra of 2-DMASP in aqueous solution at pH 3.91, 4.27, and 4.37 (bottom to top)	120
3.12	Fluorescence spectra of 2-DMASP in aqueous solution at different pH. Spectra from 1 to 6 correspond to the pH 2.11, 2.58, 2.74, 2.97, 3.28, and 3.61, respectively	120
3.13	Potential energy surfaces for the ground and first two excited singlet states along the twisting coordinate of donor (θ_1) in (a) vacuuo and in (b) MeCN solvent. Insets show the plots of variation of oscillator strength along twist angle	124
3.14	Potential energy surfaces for the ground and first two excited singlet states along the twisting coordinate of acceptor (θ_2) in (a) vacuuo and in (b) MeCN. Insets show the plots of variation of oscillator strength along twist angle	124
3.15	Frontier molecular orbitals (FMO) of 2-DMASP with (a) optimized planar structure in vacuuo, (b) donor twisted structure in acetonitrile, and (c) acceptor twisted structure in acetonitrile	125

Figure No.	Caption	Page No.
3.16	UV-Visible absorption spectra of 2-DMASP in presence of various concentration of CTAB	127
3.17	Fluorescence spectra of 2-DMASP with increasing concentration (from bottom to top) of CTAB	129
3.18	Variation of steady-state fluorescence intensity of 2-DMASP in presence of varying concentration of CTAB	129
3.19	Plot of fluorescence energy at peak maxima ($\epsilon_{\max}^{\text{fl}}$) of 2-DMASP versus $E_T(30)$ of different percentage of dioxane-water mixture	131
3.20	Variation of fluorescence anisotropy value of 2-DMASP in presence of different percentage of glycerol in methanol-glycerol mixture	131
4.1	(a) Representative plot for the determination of <i>cmc</i> by Carpena's method by using experimental conductivity data for Gemini-1 + CTAB mixed systems at bulk mole fraction of CTAB, $\alpha_{\text{CTAB}} = 0.0$, (Inset shows the determination of <i>cmc</i> without Carpena's method), (b) Plot of experimental conductivity data for Gemini-1 + CTAB mixed system at different bulk mole fraction of CTAB (α_{CTAB}) using Carpena's method	137
4.2	(a) Representative plot for the determination of <i>cmc</i> by Carpena's method by using experimental conductivity data for Gemini-1 + TTAB mixed systems at bulk mole fraction of TTAB, $\alpha_{\text{TTAB}} = 1.0$, (Inset shows the determination of <i>cmc</i> without Carpena's method), (b) Plot of experimental conductivity data for Gemini-1 + TTAB mixed system at different bulk mole fraction of TTAB (α_{TTAB}) using Carpena's method	138
4.3	(a) Representative plot for the determination of <i>cmc</i> by Carpena's method by using experimental conductivity data for Gemini-1 + DTAB mixed systems at bulk mole fraction of DTAB, $\alpha_{\text{DTAB}} = 1.0$, (Inset shows the determination of <i>cmc</i> without Carpena's method), (b) Plot of experimental conductivity data for Gemini-1 + DTAB mixed system at different bulk mole fraction of DTAB (α_{DTAB}) using Carpena's method	139
4.4	(a) Representative plot for the determination of <i>cmc</i> by Carpena's method by using experimental conductivity data for Gemini-2 + CTAB mixed systems at bulk mole fraction of CTAB, $\alpha_{\text{CTAB}} = 1.0$, (Inset shows the determination of <i>cmc</i> without Carpena's method), (b) Plot of experimental conductivity data for Gemini-2 + CTAB mixed system at different bulk mole fraction of CTAB (α_{CTAB}) using Carpena's method	140
4.5	(a) Representative plot for the determination of <i>cmc</i> by Carpena's method by using experimental conductivity data for Gemini-2 + TTAB mixed systems at bulk mole fraction of TTAB, $\alpha_{\text{TTAB}} = 0.0$, (Inset shows the determination of <i>cmc</i> without Carpena's method), (b) Plot of experimental conductivity data for Gemini-2 + TTAB mixed system at different bulk mole fraction of TTAB (α_{TTAB}) using Carpena's method	141
4.6	Plot of experimental conductivity data for Gemini-2 + DTAB mixed system at different bulk mole fraction of DTAB (α_{DTAB}) using Carpena's method	142

Figure No.	Caption	Page No.
4.7	Fluorescence spectra of DMACA in presence of various mixed systems in aqueous solution. $\lambda_{ex} = 378$ nm	142
4.8	Plots of fluorescence intensities of DMACA as a function of total surfactants concentration of various mixed systems. $\lambda_{ex} = 378$ nm	143
4.9	Critical micelle concentrations (<i>cmc</i> and <i>cmc*</i>) versus bulk mole fraction, α_1 for monomeric + Gemini-1 systems	147
4.10	Critical micelle concentrations (<i>cmc</i> and <i>cmc*</i>) and mole fraction, α_1 for monomeric + Gemini-2 systems	148
4.11	Micellar mole fractions, X_1 calculated using Rubhing's method and X_1^{ideal} versus bulk mole fraction, α_1 for monomeric + Gemini-1 systems	152
4.12	Micellar mole fractions, X_1 calculated using Motomura's method and X_1^{ideal} versus bulk mole fraction, α_1 for monomeric + Gemini-1 systems	152
4.13	Micellar mole fractions, X_1 calculated using Rodena's method and X_1^{ideal} versus bulk mole fraction, α_1 for monomeric + Gemini-1 systems	153
4.14	Micellar mole fractions, X_1 calculated using Rubhing's method and X_1^{ideal} , vs, solution mole fraction α_1 of monomeric + Gemini-2	154
4.15	Micellar mole fractions, X_1 calculated using Motomura's method and X_1^{ideal} , vs, solution mole fraction α_1 of monomeric + Gemini-2	155
4.16	Micellar mole fractions, X_1 calculated using Rodena's method and X_1^{ideal} , vs, solution mole fraction α_1 of monomeric + Gemini-2	155
4.17	Emission peak maxima (cm^{-1}) of DMACA in different % of dioxane-water mixture versus solvent polarity parameter ($E_T(30)$)	160
4.18	Plot of anisotropy (r) of DMACA in different % of glycerol-water mixtures	162
4.19	Plot of viscosity (cP) of different % of glycerol-water mixtures	162
4.20	Plot of $(F - F_o) / ([S]_{TOTAL} - cmc)$ vs F in (a) DTAB + Gemini-1 and (b) DTAB + Gemini-2 mixed system at $\alpha_{DTAB} = 0.2$	163
5.1	Absorption and fluorescence spectra of C-153 in pure water and in aqueous solutions of 12-s-12, 2Br ⁻ . $\lambda_{ex} = 375$ nm	168
5.2	Plots of specific conductivity (κ) versus concentration of aqueous solutions of gemini surfactants at 298.15 K	168
5.3	Variation of the fluorescence energy at peak maximum of C-153 in dioxane-water mixture with $E_T(30)$ of dioxane-water mixture at 298.15 K	170
5.4	Time resolved fluorescence decay of C-153 at 445 nm in 12-3-12 micelles along with the best fit and residuals. [12-3-12] = 10 mM. $\lambda_{ex} = 375$ nm	171
5.5	Plot of $(I_i - I_o) / (I_C - I_o)$ against $[M]^{-1}$ for 12-3-12 micelles	174
5.6	Time-resolved fluorescence decays of C-153 in 12-3-12, 2Br ⁻ micelles at (1) 655 nm, (2) 520 nm, (3) 460 nm, and (4) for instrument response function	175
5.7	Time-resolved emission spectra (TRES) of C-153 in the micelles of (a) 12-3-12, 2Br ⁻ (b) 12-4-12, 2Br ⁻ (c) 12-6-12, 2Br ⁻ (d) 12-8-12, 2Br ⁻ (e) 12-12-12, 2Br ⁻ surfactants of concentration 10mM	176

Figure No.	Caption	Page No.
5.8	Decays of solvent correlation function, $C(t)$ of C-153 in the micelles of gemini surfactants, 12-s-12, 2Br ⁻ of concentration of 10mM	177
5.9	Degree of counter ion dissociation (α) versus spacer chain, s of 12-s-12, 2Br ⁻	178
5.10	Fluorescence anisotropy decays of C-153 in pure water and in micelles of 12-s-12, 2Br ⁻ surfactants	180
5.11	The size distribution graph for the micelles of gemini surfactants obtained from DLS measurement	181
6.1	Absorption spectra of C-153 in presence of pure and mixed surfactant systems of TX-100 and 12-6-12	188
6.2	Fluorescence spectra of C-153 in presence of pure and mixed surfactant systems of TX-100 and 12-6-12. $\lambda_{ex} = 375$ nm	189
6.3	Fluorescence spectra of C-153 with increasing concentration (from bottom to top) of 12-6-12. Inset shows the plot of fluorescence intensity with concentration of 12-6-12, ($\lambda_{exc} = 375$ nm)	189
6.4	Plot of fluorescence energy at peak maxima (ϵ_{max}^{fl}) of C-153 versus $E_T(30)$ of different percentage of dioxane-water mixture $\lambda_{ex} = 375$ nm	191
6.5	Plot of microviscosity (η_m) versus bulk mole fraction of gemini surfactants, 12-s-12. [TX-100+12-s-12] = 10 mM	192
6.6	The size distribution graph for the micelles of TX-100 + 12-s-12 obtained from DLS measurement (a) $s = 3$, (b) $s = 6$, (c) $s = 8$, and (d) $s = 12$	194
6.7	Time-resolved fluorescence decays of C-153 in TX-100+12-6-12 micelles at 0.8 bulk mole fraction of 12-6-12. 1 to 4 at 620 nm, 565 nm, 520 nm, 445 nm, respectively and 5 for instrument response function	196
6.8	Time resolved emission spectra of C-153 in TX-100 + 12-s-12 at 0.8 bulk mole fraction (a) TX-100 + 12-3-12, (b) TX-100 + 12-6-12, (c) TX-100 + 12-8-12, and (d) TX-100 + 12-12-12, (from right to left) 200ps, 500ps, 2000ps, and 10000 ps	197
6.9	Decay of solvent correlation function, $C(t)$ of C-153 in pure and mixed surfactant systems of TX100+12-s-12 with (a) $s = 3$, (b) $s = 6$, (c) $s = 8$ and (d) $s = 12$ at different bulk mole fractions of gemini surfactants. [TX-100+12-s-12] = 10 mM	197
6.10	Plot of average solvation time, $\langle \tau_s \rangle$ versus bulk mole fraction of gemini surfactant in the mixture, TX-100+12-s-12 with $s = 3, 6, 8, 12$	199
6.11	Anisotropy decays of C-153 in pure surfactants and in mixed surfactant systems of TX-100 and 12-s-12 with (a) $s = 3$, (b) $s = 6$, (c) $s = 8$ and (d) $s = 12$ at various bulk mole fractions of 12-s-12	204
6.12	Variation of average rotational relaxation time, $\langle \tau_r \rangle$ with bulk mole fraction of a gemini surfactant in the mixed micelles of TX-100 and 12-s-12 with $s = 3, 6, 8$ and 12	204
7.1	Fluorescence spectra of DMACA in presence of increasing concentration (bottom to top) of pure 12-4-12. $\lambda_{ex} = 378$ nm, [DMACA] = 5 μ M	212
7.2	Plot of fluorescence intensity of DMACA with increasing concentration of pure 12-4-12	213

Figure No.	Caption	Page No.
7.3	Absorption spectra of C-480 in presence of 10 mM of pure 12-4-12 and 10 mM of 12-4-12 + urea at different concentrations. [C-480] = 5 μ M	214
7.4	Fluorescence spectra of C-480 in presence of water, pure 10 mM of pure 12-4-12 and 10 mM of 12-4-12 + 5 M urea concentration. [C-480] = 5 μ M. λ_{ex} = 375 nm	215
7.5	Variation of the fluorescence energy at peak maximum (ϵ_{max}^{fl}) of C-480 in dioxane-water mixture with E_T (30) of dioxane-water mixture. [C-480] = 5 μ M. λ_{ex} = 375 nm	216
7.6	Fluorescence spectra of DMACA in presence of 10 mM of 12-4-12 and 10 mM of 12-4-12 in presence of various concentrations of urea. λ_{ex} = 378 nm, [DMACA] = 5 μ M	217
7.7	Size distribution graph for the micelles of 10 mM of pure 12-4-12 and 10 mM 12-4-12 in presence of various concentration of urea	219
7.8	Decays of fluorescence anisotropy of C-480 in the pure water, 10 mM of pure 12-4-12 and 10 mM of 12-4-12 in presence of various concentration of urea. λ_{ex} = 375 nm, λ_{em} = 475 nm	221
7.9	Time-resolved fluorescence decays of C-480 in 12-4-12 ([12-4-12] = 10 mM) +5 M urea concentration. 1 to 3 at 565 nm, 515 nm, 455 nm, respectively and 4 for instrument response function	223
7.10	Time resolved emission spectra of C-480 in 12-4-12 + urea ([12-4-12] = 10 mM, [Urea] = 5 M) (from right to left) 0 ps, 500 ps, 5000 ps, and 10000 ps	224
7.11	Decays of solvent correlation function, $C(t)$ of C-480 in the micelles of 12-4-12 in presence of various concentration of urea	225
8.1	UV-Visible absorption spectra of C-490 in water, CHX + n-pentanol (2.4%) mixed solvent (bulk solvent) and in RMs systems	230
8.2(a)	Steady-state fluorescence spectra of C-490 in water, bulk solvent and in RMs systems. λ_{exc} = 375 nm	232
8.2(b)	Steady-state fluorescence spectra of C-490 in water, bulk solvent and in RMs systems. λ_{exc} = 412 nm	232
8.3	Excitation spectra of C-490 recorded in $w_o = 30$ and monitored at (a) $\lambda_{ems} = 435$ nm, (b) 550 nm and absorption spectra of C-490 in (c) bulk solvent and (d) $w_o = 30$	233
8.4	Plot of fluorescence peak maxima of C-490 in different percentage of dioxane-water mixture	234
8.5	Steady-state fluorescence anisotropy (r) of C-490 vs w_o . Inset (a) plot for average rotational correlation times (τ_c) vs w_o and (b) non-radiative rate constant (k_{nr}) vs w_o . $\lambda_{exc} = 375$ nm	235
8.6	Time-resolved fluorescence anisotropy decay of C-490 in RMs of 12-4-12	238
8.7	Time-resolved fluorescence decay of C-490 in 12-4-12 RMs for (a) $w_o = 0$ and (b) $w_o = 2$. 1 to 4 at 560 nm, 470 nm, 455 nm, 425 nm, respectively and 5 for instrument response function	239

Figure No.	Caption	Page No.
8.8	RES of C-490 in RMs for (a) $w_o = 0$, (b) $w_o = 2$, (c) $w_o = 25$, and (d) $w_o = 30$	240
8.9	Decays of solvent correlation function, $C(t)$ of C-490 in RMs at (■) $w_o = 0$, (●) $w_o = 2$, (▼) $w_o = 30$	240
9.1	Absorption spectra of BSA at different concentrations of 12-4-12. [BSA] = 5 μ M	248
9.2	Variation of absorption peak maximum and absorbance of BSA with the concentration of gemini surfactant, 12-4-12	248
9.3	(a) Steady-state fluorescence spectra and (b) $\lambda_{\max}^{\text{fl}}$ of BSA in presence of various concentration of 12-4-12. $\lambda_{\text{ex}} = 295$ nm. [BSA] = 5 μ M	250
9.4	Plot of fluorescence intensity of BSA with concentration of gemini surfactant	251
9.5	Synchronous fluorescence spectra of BSA at $\Delta\lambda = 60$ nm in presence of (a) 12-4-12 and (b) 12-4(OH)-12. [BSA] = 5 μ M	252
9.6	Synchronous fluorescence spectra of BSA at $\Delta\lambda = 15$ nm in presence of (a) 12-4-12 and (b) 12-4(OH)-12. [BSA] = 5 μ M	253
9.7	Binding isotherm of 12-4-12 and 12-4(OH)-12 with BSA	254
9.8	Variation of excited state average lifetime of BSA with the concentration of gemini surfactants. $\lambda_{\text{ex}} = 300$ nm, λ_{em} is the fluorescence peak maximum in respective system, [BSA] = 5 μ M	258
9.9	Stern -Volmer plot of BSA and BSA -12-4-12/12-4(OH)-12 systems. [BSA] = 5 μ M . [12-4-12] = [12-4(OH)-12] = 5 mM	259
9.10	Variation of excited state lifetime of BSA in presence of GdHCl. [BSA] = 5 μ M, $\lambda_{\text{ex}} = 300$ nm	260
9.11	Fluorescence spectra of unfolded BSA to demonstrate interaction process in presence of (a) 12-4-12 and (b) 12-4(OH)-12. $\lambda_{\text{exc}} = 295$ nm	261
9.12	Time resolved fluorescence spectra of unfolded BSA in presence of different concentrations of 12-4-12 to show interaction process. $\lambda_{\text{ex}} = 300$ nm, λ_{em} is the fluorescence maxima in respective system, [BSA] = 5 μ M	262
9.13	Average excited state lifetime of BSA for surfactant interaction process in presence of 12-4-12 and 12-4(OH)-12. $\lambda_{\text{ex}} = 300$ nm, λ_{em} is the fluorescence maxima in respective system, [BSA] = 5 μ M	262

List of schemes

S.No.	Caption	Page No.
1.1	Structure of betaine dye	31
1.2	DMABN and other similar model compounds	36
1.3	Structure of Coumarin derivatives	48
2.1	Molecular structures of fluorescence probes	74
2.2	Molecular structures of conventional and gemini surfactants	76
2.3	Block diagram of a steady-state spectrofluorimeter	98
2.4	Block diagram of time-resolved spectrofluorimeter	100
3.1	(a) Molecular structure and (b) model of trans-2-[4-(N,N-dimethylaminostyryl)]pyridine (2-DMASP)	106
3.2	Dication-monocation and monocation-neutral equilibria of 2-DMASP in aqueous solution at ground and excited states	118
3.3	Structures of (a) E – and (b) Z – forms of 2-DMASP	122
3.4	Representation of (a) CTA ion, (b) bromide ion, (c) sulphate ion, (d) nitrate ion, and (e) p-toluene sulphonate ion	127
9.1	Representation of binding of gemini surfactant with BSA in different concentration range of the former	255
9.2	Rotational conformers of Tryptophan (Trp)	255

List of tables

Table No.	Caption	Page No.
2.1	Empirical formula, molar mass, and ¹ H-NMR data of synthesized gemini surfactants	77
3.1	Solvent polarity parameter ($E_T(30)$), Absorption peak maxima (λ_{\max}^{ab}), fluorescence peak maxima (λ_{\max}^{fl}), Stokes shift ($\Delta\bar{\nu}$) and fluorescence quantum yields (ϕ_f) of 2-DMASP in different solvents	108
3.2	Excited singlet state lifetimes (τ_i) ^{a,b} , average singlet state lifetimes ($\langle\tau\rangle$), pre-exponential factors (a_i), quantum yields (ϕ), radiative (k_r) and non-radiative (k_{nr}) rate constants of 2-DMASP in different pure solvents	116
3.3	Optimized geometry of 2-DMASP at the ground state (S_0) in vacuuo at DFT ((B3LYP/6-31+G(d,p)) level	122
3.4	Comparison between the experimental and computed energy values in vacuuo and MeCN solvent	125
3.5	Critical micelle concentration (cmc), absorption peak maxima (λ_{\max}^{ab}), fluorescence maxima (λ_{\max}^{flu}), $E_T(30)$, steady-state anisotropy (r), and microviscosity values of cetyltrimethylammonium surfactants with different counterions (concentration of surfactant = 10 mM)	128
4.1	Values of cmc of monomeric + Gemini-1/Gemini-2 from conductivity and fluorescence measurements at 303.15 K	144
4.2	Values of interaction parameter (β), for monomeric + Gemini-1/Gemini-2 mixed micellar systems	148
4.3	Various mixed micellar parameters for monomeric + Gemini-1 mixed systems based on conductivity measurement	150
4.4	Various mixed micelles parameters for monomeric + Gemini-2 surfactants based on conductivity measurement at 303.15K	151
4.5	Excess Gibbs free energy of micelle, G^E , counter ions dissociation, g and standard Gibbs free energy of micellization, ΔG_m^o for monomeric + Gemini-1 systems at 303.15 K	157
4.6	Excess Gibbs energy of micelle formation, G^E , counter ions dissociation, g and standard Gibbs energy of micellization, ΔG_m^o for monomeric + Gemini-2 at 303.15K	158
4.7	Microenvironmental properties of monomeric + Gemini-1 mixed systems	160
4.8	Microenvironmental properties of monomeric + Gemini-2 mixed systems	161
5.1	Absorption (λ_{\max}^{abs}) and steady-state fluorescence peak maxima (λ_{\max}^{fl}) of C-153 in pure solvents and the micelles of gemini surfactants, cmc of surfactants and aggregation number of micelles (N)	169
5.2	Excited singlet state lifetime (τ) ^a , pre-exponential factors (a), fluorescence quantum yield (ϕ_f), radiative (k_r) and non-radiative (k_{nr}) rate constants of C-153 in various homogeneous and micellar media	172

Table No.	Caption	Page No.
5.3	Fluorescence anisotropy (r) ^a , excited singlet state lifetime (τ_f) ^b , rotational correlation time (τ_r) of DPH ^c , microviscosities (η_m) of micelles, binding constant (K) and standard gibbs free energy of binding (ΔG^0) of C-153 at 298.15 K	173
5.4	Decay characteristics of $C(t)$ of C-153 in different micellar systems	177
5.5	Rotational relaxation parameters for C-153 in micelles of 12- s -12, 2Br ⁻ gemini surfactants	182
5.6	Hydrodynamic radius, wobbling motion time (τ_w), lateral diffusion time (τ_D), time for overall rotational motion of the micelle (τ_m), lateral diffusion coefficient (D_L), wobbling diffusion coefficient (D_w), cone angle (θ_o) and order parameter ($ S $) obtained from the anisotropy decays of C-153 in different 12- s -12, 2Br ⁻ micelles	182
6.1(a)	UV-visible absorption peak maxima (λ_{max}^{ab}) and fluorescence peak maxima ^a (λ_{max}^f) of C-153 in mixed systems, TX-100+12- s -12 ($s = 3$ and 6), cmc and $E_T(30)$ values of pure and mixed systems, TX-100+12- s -12 ($s = 3$ and 6)	190
6.1(b)	UV-visible absorption peak maxima (λ_{max}^{ab}) and fluorescence peak maxima ^a (λ_{max}^f) of C-153 in mixed systems, TX-100+12- s -12 ($s = 8$ and 12), cmc and $E_T(30)$ values of mixed systems, TX-100+12- s -12 ($s = 8$ and 12)	190
6.2(a)	Fluorescence anisotropy (r) ^a , excited singlet state lifetime (τ_f) ^b , rotational correlation time (τ_R) of DPH, microviscosities (η_m) of micelles of pure and mixed surfactant systems of TX-100 + 12-3-12 and TX-100 + 12-6-12. Total concentration of surfactants = 10 mM	193
6.2(b)	Fluorescence anisotropy (r) ^a , excited singlet state lifetime (τ_f) ^b , rotational correlation time (τ_R) of DPH, microviscosities (η_m) of micelles of pure and mixed surfactant systems of TX-100+12-8-12 and TX-100+12-12-12. Total concentration of surfactants = 10 mM	193
6.3(a)	Decay characteristic of solvent correlation function, $C(t)$ of C-153 in presence of pure and mixed surfactants systems. [TX-100+ 12- s -12, $s = 3,6$] =10 mM	198
6.3(b)	Decay characteristic of solvent correlation function, $C(t)$ of C-153 in presence of pure and mixed surfactants systems. [TX-100+ 12- s -12, $s = 8,12$] =10 mM	198
6.4(a)	Rotational relaxation parameters for C-153 in the mixed micelles of TX-100+12- s -12, 2Br ⁻ with $s = 3$ and 6	203
6.4(b)	Rotational relaxation parameters for C-153 in the mixed micelles of TX-100+12- s -12, 2Br ⁻ with $s = 8$ and 12	203
6.5(a)	Hydrodynamic radius (r_h) ^a , lateral diffusion time (τ_D), time for overall rotational motion of the micelle (τ_m), wobbling motion time (τ_w), wobbling diffusion coefficient (D_w), cone angle (θ_o) and order parameter ($ S $) obtained from the anisotropy decays of C-153 in different micelles of TX-100+12- s -12, 2Br ⁻ with $s = 3$ and 6	206

Table No.	Caption	Page No.
6.5(b)	Hydrodynamic radius (r_h) ^a , lateral diffusion time (τ_D), time for overall rotational motion of the micelle (τ_m), wobbling motion time (τ_w), wobbling diffusion coefficient (D_w), cone angle (θ_0) and order parameter ($ S $) obtained from the anisotropy decays of C-153 in different micelles of TX-100+12- <i>s</i> -12, 2Br ⁻ with <i>s</i> = 8 and 12	206
7.1	Critical micelles concentration (<i>cmc</i>), mole fraction partition coefficient (K^{mic}), standard molar Gibbs free energy ($\Delta G^{o, mic}$), absorption peak maxima (λ_{max}^{ab}) ^a , fluorescence peak maxima (λ_{max}^f) ^b of C-480, in aqueous solution of pure 12-4-12 and 12-4-12 with various concentrations of urea	213
7.2	Fluorescence anisotropy (<i>r</i>) ^a , excited singlet state lifetime (τ_f) ^b , rotational correlation time (τ) of DPH, microviscosities (η_m) of micelles of 10 mM of pure 12-4-12 and 10 mM of 12-4-12 + urea at various concentrations	217
7.3	Excited singlet state life times (τ_i) ^a of C-480 in aqueous solutions of pure 12-4-12 and 12-4-12+ urea	219
7.4	Rotational relaxation times of C-480 in aqueous solution of 10 mM 12-4-12 and 10 mM 12-4-12 + urea at various concentrations	221
7.5	Hydrodynamic radius (r_h), lateral diffusion time (τ_D), time for rotational motion of the micelle as a whole (τ_m), wobbling motion time (τ_w), wobbling diffusion coefficient (D_w), cone angle (θ_0) and order parameter ($ S $) obtained from the anisotropy decays of C-480 in different systems	222
7.6	Decay characteristic of solvent correlation function, $C(t)$ of C-480 in presence of various systems	224
8.1	Absorption and fluorescence peak maxima of C-490 in pure solvents, mixed solvent and in RMs systems, and $E_T(30)$	231
8.2	Fluorescence quantum yield (ϕ_f), excited singlet state lifetimes (τ_i), radiative (k_r) and non-radiative (k_{nr}) rate constants of C-490 in different systems	236
8.3	Rotational relaxation time of C-490 in pure solvents and RMs of gemini surfactant (12-4-12)	237
8.4	Decay characteristic of $C(t)$ of C-490 in RMs of gemini surfactant	241
9.1	Excited state lifetimes ^{a,b} of BSA in presence of 12-4-12	256
9.2	Excited state lifetimes ^{a,b} of BSA in presence of 12-4(OH)-12	257

List of abbreviations and symbols

Symbol	Abbreviation
$\lambda_{\max}^{\text{ab}}$	Absorption peak maximum
A	Acceptor
f	Activity coefficient
AOS	Alfa-olefinic sulfonate
4-AP	4-aminophthalimide
ADC	Analog-to-digital converter
Å	Angstrom
AM1	Austin model 1
$\langle \tau \rangle$	Average fluorescence lifetime
$\langle \tau_s \rangle$	Average solvation time
V_m	Average molar volume
N	Aggregation number
K_s	Binding constant
Gemini-1	1,3-bis(dodecyl- <i>N,N</i> -dimethylammonium bromide)-2-propanol
Gemini-2	1,4-bis(dodecyl- <i>N,N</i> -dimethylammonium bromide)-2,3-butanediol
BSA	Bovine serum albumin
CPC	Cetylpyridinium chloride
CTAB	Cetyltrimethyl ammonium bromide
CT	Charge transfer
ΔH_m^*	Chemical part of enthalpy
C-153	Coumarin 153
C-480	Coumarin 480
C-490	Coumarin 490
θ_o	Cone angle
C_{mc}	Critical micellar concentration

Symbol	Abbreviation
DSE	Debye–Stokes–Einstein
DFT	Density functional theory
α	Degree of counter ion dissociation
DAS	Decay analysis software
ϵ	Dielectric constant
DO	1,4-dioxane
9-DMA	9-(<i>N,N</i> -Dimethylamino)anthracene
DMACA	4-(<i>N,N</i> -dimethylamino) cinnamaldehyde
DMF	Dimethyl formamide
DMSO	Dimethyl sulfoxide
DMABN	Dimethylaminobenzonitrile
DPH	1,6-diphenyl-1,3,5-hexatriene
D	Donor
D-A	Donor-Acceptor
DTAB	Dodecyltrimethylammonium bromide
DLS	Dynamic light scattering
$E_T(30)$	Empirical solvent polarity parameter
EG	Ethylene glycol
pK_a^*	Excited state acidity constant
μ_e	Excited state dipole moment
λ_{em}	Emission wavelength
λ_{ex}	Excitation wavelength
G^E	Excess Gibbs free energy of micelle formation
r	Fluorescence anisotropies
F_0/F	Fluorescence intensity ratio
$I(t)$	Fluorescence intensity decay
λ_{max}^{fl}	Fluorescence peak maxima
ϕ	Fluorescence quantum yields

Symbol	Abbreviation
$\epsilon_{\max}^{\text{fl}}$	Fluorescence energy peak maxima
τ	Fluorescence lifetime
FT-IR	Fourier transform infrared spectroscopy
FCE state	Frank-Condon excited state
FCG state	Frank-Condon ground state
FMO	Frontier molecular orbitals
pK_a	Ground state acidity constant
μ_g	Ground state dipole moment
cmc^*	Ideal critical micellar concentration
IC	Internal conversion
ISC	Intersystem crossing
ICT	Intramolecular charge transfer
τ_e	Internal motion of the probe
β	Interaction parameter
τ_D	Lateral diffusion of the fluorophores
LE	Locally excited
r_h	Mean hydrodynamic radius
Λ	Molar Conductivity
X_1	Micellar mole fraction
k_{nr}	Non-radiative rate constant
NMR	Nuclear magnetic resonance
ORD	Optical rotatory dispersion
S	Order parameter
PMT	Photomultiplier tube
PICT	Planar intramolecular charge transfer
PCM	Polarized continuum model
w_o	[polar solvent] / [surfactant]
Brij 58	Polyoxyethylene-(20)-cetyl-ether

Symbol	Abbreviation
Brij 35	Polyoxyethylene-(23)-lauryl-ether
Tween 80	Polyoxyethylene-sorbitan monooleate
PESs	Potential energy surfaces
a	Pre-exponential factor
PJT	Pseudo-Jahn Teller
Q	Quencher
k_r	Radiative rate constant
n	Refractive index
R	Regression coefficient
RICT	Rehybridization by intramolecular charge transfer
RMs	Reverse micelles
τ_{ir}	Rotational correlation times
τ_m	Rotational motion of the micelle
SHG	Second harmonic generation
SDS	Sodium dodecyl sulfate
AOT	Sodium salt of dioctyl sulfosuccinic acid
NaBr	Sodium bromide
NaCl	Sodium chloride
SCM	Solvatochromic comparison method
TX-100	t-octylphenoxypolyethoxyethanol
$C(t)$	Solvent correlation function
K	Specific conductivity
μ_m^o	Standard chemical potential
ΔG_m^o	Standard Gibbs free energy of micellization
ΔH_m^o	Standard enthalpy of micellization
ΔS_m^o	Standard entropy of micellization
K_{SV}	Stern-Volmer quenching constant

Symbol	Abbreviation
$(\nu_{ab}-\nu_{\eta})$ or (ν_{ss})	Stokes shift
THF	Tetrahydrofuran
TTAB	Tetradecyltrimethylammonium bromide
TLC	Thin layer chromatography
TDDFT	Time dependent density functional theory
TCSPC	Time-correlated single photon counting
$r(t)$	Time-resolved fluorescence anisotropy
TRES	Time-resolved emission spectra
TAC	Time-to-amplitude converter
DMASBT	Trans-2-[4-(dimethylamino)styryl]benzothiazole
TICT	Twisted intramolecular charge transfer
η	Viscosity
WICT	Wagged intramolecular charge transfer
WR	Water
D_w	Wobbling diffusion coefficient
τ_w	Wobbling motion time

Chapter 1

Introduction

1.1 Surfactants

Surfactants are wetting agents that lower the surface tension of a liquid, allowing easier spreading, and can also lower the interfacial tension between two liquids. Surfactant is an abbreviation for surface active agent, which means active at surface. Surfactants are usually organic molecules. The name amphiphile is sometimes used synonymously with surfactant. A surfactant molecule consists of two parts; a non-polar hydrophobic tail and a polar hydrophilic headgroup (Figure 1.1). The unusual properties of surfactants are due to the presence of a hydrophilic headgroup and hydrophobic tail of the surfactant molecule. The polar headgroup of the surfactant molecule interacts with the polar solvents via dipole-dipole or ion-dipole interactions. A small quantity of surfactant molecules rests upon the water-air interface and decreases the surface tension of water.

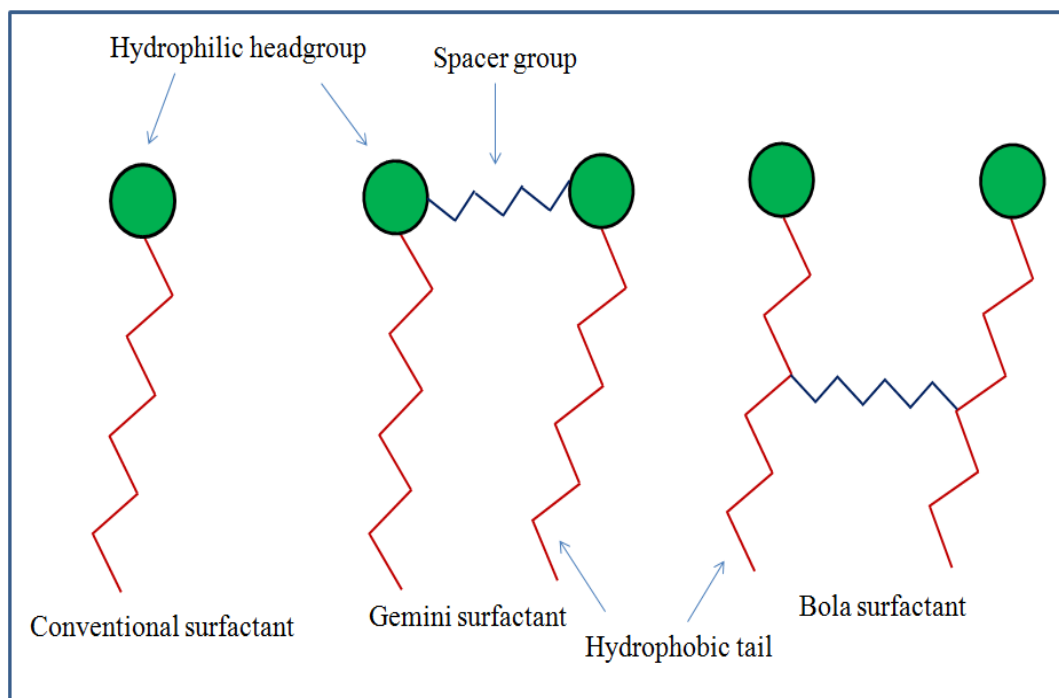


Figure 1.1: Structures of various types of surfactants

Solution properties of molecular assemblies are of great importance in colloid and interface sciences. The term “colloid” was used for glue-like materials, which appeared to consist of only one phase when viewed under the microscope. Boundary between the two phases is termed as “interface”. Molecular assemblies of surfactant molecules are gaining much attention since the last century. Generally, most of the natural and biological processes occur at the interface or in confined systems, e.g. biomembranes, vesicles and proteins. The physicochemical properties of surfactant assemblies can act as a model system for biological membranes. Surfactant assemblies like micelles, reverse micelles etc. can mimic some of the physicochemical properties of biological systems. Surfactants, because of their high ability to solubilize the membrane proteins, are extremely important in simulating the complex environmental condition present in larger bioaggregates such as biological membranes. Many of the newly developed active pharmaceutical drugs are rejected because of their poor solubility in water. Different efforts to improve the solubility of drugs using a capable vehicle to enclose hydrophobic drugs, such as inclusion complexes with cyclodextrins, microemulsions, dendrimers or liposome formulations have been established so far. However, all these systems exhibit disadvantages¹⁻³. The micelles are well explored as drug carriers for water-insoluble drugs, nanocarriers for efficient drug delivery, and found to have applications in cultural heritage conservation, oil fields and thickeners for personal and home care products.⁴⁻⁷

1.1.1 Classification of surfactants

In fact, it is the nature of the polar headgroup which is used to classify surfactants into different categories.

(a) Cationic surfactants: These are the surfactants having a positively charge headgroup. Nitrogen based compounds are constituted the vast majority of cationic surfactants. Sulfonium, phosphonium and sulfoxonium surfactant also exist. The general formula of cationic surfactant is $R_nX^+Y^-$, where R represents one or more hydrophobic chains, X is headgroup and Y is counterion. For example, cetyltrimethyl ammonium bromide (CTAB) $[C_{16}H_{33}N^+(CH_3)_3Br^-]$, cetylpyridinium chloride (CPC) $[C_6H_5N^+C_{16}H_{33}Cl^-]$, will fall under this category.

(b) Anionic surfactants: These are the surfactants having a negatively charged headgroup. They are by far the largest surfactant class. Carboxylate, sulfate, sulfonate

and phosphate are the polar groups found in anionic surfactants. The counterions commonly used are sodium, potassium, ammonium, calcium and various protonated alkyl amines. Sodium and potassium impart water solubility, whereas calcium and magnesium promote oil solubility of surfactants. Examples include sodium dodecyl sulfate (SDS) $[\text{C}_{12}\text{H}_{25}\text{SO}_4^-\text{Na}^+]$, alfa-olefinic sulfonate (AOS) $[\text{CH}_3(\text{CH}_2)_9\text{C}_2\text{H}_4\text{SO}_3^-\text{Na}^+]$. Anionic surfactants are used in greater amount than any other class of surfactants.

(c) Nonionic surfactants: The headgroup of this class of surfactants does not have any charge. The hydrophilic part contains the polyoxyethylene, polyoxypropylene or polyol derivatives. The hydrophobic part contains saturated or unsaturated fatty acids or fatty alcohols. The nonionic surfactants can be classified as polyol esters, polyoxyethylene esters poloxamers. The polyol esters include glycol and glycerol esters and sorbitan derivatives. Polyoxyethylene esters includes polyethylene glycol. The most commonly used nonionic surfactants are ethers of fatty alcohols. Examples: Triton X-100, Tweens, Brijis, PEGs etc.

(d) Zwitterionic surfactants: These surfactants possess both anionic and cationic groups on the hydrophobic moiety. These surfactants can be anionic (negatively charged), cationic (positively charged) or non-ionic (no charge) in solution, depending on the acidity or pH of the solution. In these surfactants, the positive charge is almost due to ammonium group, but the source of the negative charge may vary (carboxylate, sulphate, sulphonate). The more common zwitterionic surfactants include N-alkyl and C-alkyl betains and sultains as well as phosphatidyl amino alcohols and acids, e.g., 3-(dimethyldodecylamino)-propane-1-sulphonate $[\text{CH}_3(\text{CH}_2)_{11}\text{N}^+(\text{CH}_3)_2\text{CH}_2\text{CH}_2\text{CH}_2\text{SO}_3^-]$, [(dodecyldimethylammonio)alkyl] phenyl phosphinates $[\text{C}_{12}\text{H}_{25}\text{N}^+(\text{CH}_3)_2(\text{CH}_2)_n \text{C}_6\text{H}_5\text{PO}_2^-]$.

There are some surfactants having a single ionic headgroup and two hydrophobic tail attached to it, e.g., sodium salt of dioctyl sulfosuccinic acid (anionic surfactant) commonly known as Aerosol OT or AOT and dioctadecyldimethylammonium chloride (cationic surfactant). Ionic surfactants with three hydrophobic chains are also known⁸. In gemini surfactant, the surfactant monomer units are attached by a flexible or rigid spacer at the headgroups⁹ (Figure 1.1), whereas surfactant molecules with two surfactant monomers attached by a spacer at the hydrophobic tails are called bola surfactants¹⁰ (Figure 1.1).

Further, both the head and tail groups can be polymeric in nature, as in the case of block copolymers.

Besides these synthetic surfactants, there are some surfactants which are naturally occurring e.g. simple lipids (carboxylic acid esters), complex lipids (fatty acid esters containing phosphorous, nitrogen bases, and or/sugars), bile acids such as cholic and deoxycholic acid.

1.1.2 Gemini surfactants

Gemini surfactants are a special class of surfactants which have two hydrophobic tails and two polar headgroups covalently linked through a spacer at their headgroups (Figure 1.1). Gemini surfactants, therefore, have three structural elements, a hydrophilic group, a hydrophobic group, and the spacer part. The spacer part can be hydrophilic or hydrophobic, rigid or flexible in nature. The polar headgroups can be neutral, positively or negatively charged. These novel surfactants attract considerable attention because of their unique properties which are superior to their conventional counterpart. The expression gemini surfactant was first used by Menger *et al.*⁹ to denote *bis*-surfactants made up of two amphiphilic moieties connected to the headgroups by the rigid spacers benzene and stilbene. However, in 1971, these kinds of surfactants were first studied by Bunton *et al.*⁶ investigating their catalytic effects on nucleophilic substitutions reactions. Devinsky *et al.*⁷ who synthesized bisquaternary ammonium gemini surfactants with a great variety of structures, and that of Okahara *et al.*^{11,12} who synthesized a large number of anionic gemini surfactants.

The pioneering and extensive works from the research groups of Zana,^{13,14} Menger,^{15,16} Rosen,^{17,18} Okahara,^{11,12} Oda,^{19,20} Engberts,^{21,22} *et al.* have greatly promoted advancements of gemini surfactants and inspired tremendous interest in this field. The variety of gemini surfactants have been synthesized and investigated which include anionic, cationic, zwitterionic, and non-ionic gemini surfactants with different kinds of spacer groups and a variety of structural types: alkylglucoside-based²³, arginine-based²⁴, glucamide-based²⁵, sugar-based²⁶, with unsaturated linkages^{27,28}, hydrolyzable²⁹, and with nonidentical headgroups³⁰. Cationic gemini surfactants with ammonium headgroups and bromide ions as counterions have been extensively studied. These gemini surfactants are denoted by *m-s-m*, m and s respectively represent the number of carbons atoms within the hydrocarbon tail and the spacer, respectively. Gemini surfactants are superior

to their conventional surfactants in number of ways such as remarkably low critical micellar concentration (CMC), unusual rheological properties, better wetting ability, low Krafft temperature, and so on. Owing to these unique properties, gemini surfactants have shown great promise in various fields. Many surfactant-producing companies now have ongoing research programs on gemini surfactants. One company, Sasol (formerly Condea, located in Marl, Germany), is already offering formulations (Ceralution®) based on anionic gemini surfactants, which can be used as dispersing or emulsifying agents for foam production and so forth. Of course, the discovery of the very interesting and unexpected properties of gemini surfactants led to the synthesis and investigation of the properties of even longer homologs that are referred as trimeric or tetrameric surfactant. A limited number of trimeric and tetrameric surfactants have been synthesized³¹. Gemini surfactants also have potential applications in various biological fields. Conventional cationic surfactants are highly chemically stable, but have poor chemical and biological degradability, which limits their use. Furthermore, due to their strong interactions with negatively charged surfaces, including the lipid membranes of cells, cationic surfactants are toxic to aquatic organisms and show hemolytic activity. They show great promise in various areas, such as gene transfection³², drug entrapment and release³³, and vitamin solubilization³⁴, and as components of body care products³⁵ and antibacterial and antifungal formulations³⁶. Gemini surfactants can easily be adsorbed at interfaces, and can interact with the cellular membranes of microorganisms, giving them high antimicrobial activity³⁷. Gemini surfactants also show various types of interaction with conventional surfactants³⁸, cyclodextrins³⁹, DNAs⁴⁰, proteins⁴¹, room temperature ionic liquids⁴² and nanoparticles⁴³.

1.1.3 Micelles formation by surfactant

Surfactants are the amphiphilic molecules. They have distinct hydrophobic tail and hydrophilic head. In aqueous solution, surfactants at low concentration act much as normal electrolytes, but at higher concentration surfactants behave very differently. At low concentration the surfactant molecules partitions between the surface and solution. On the surface of the liquid the tail of surfactant molecules remain out of water. Increasing the concentration of surfactant, the surface of the liquid becomes crowded. Further increasing the concentration, the surfactant will start to self assemble again try to keep the hydrophobic tails out of contact with water. The concentration above which

surfactant start aggregating or micelles start forming is known as the critical micelle concentration (cmc) (Figure 1.2).

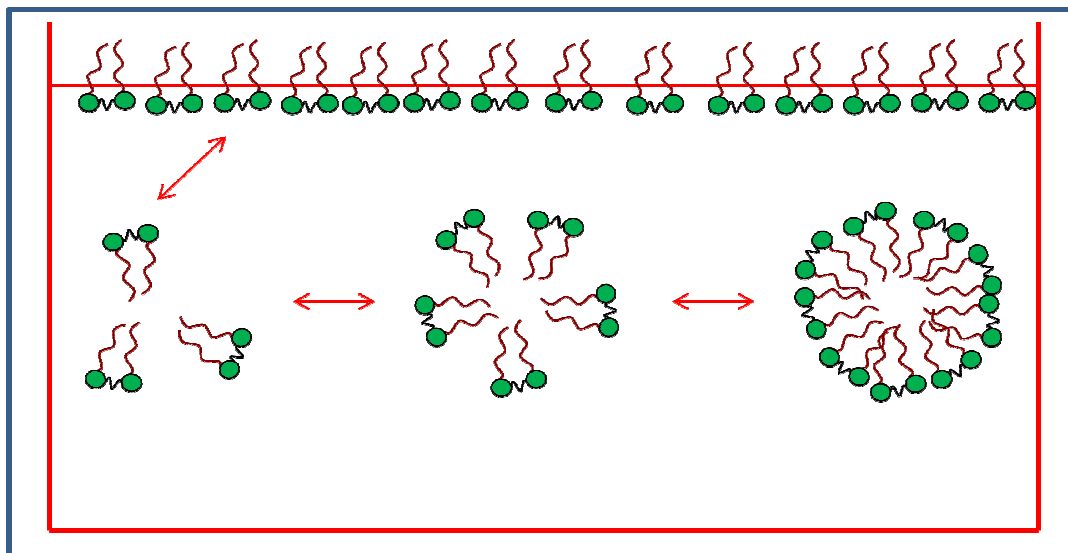


Figure 1.2: Schematic representation of formation of micelle

The formation of micelles in aqueous solution is viewed as a process involving the tendency for alkyl chains to avoid energetically unfavorable contacts with water, and the desire for the polar parts to maintain contact with the aqueous environment. Various methods have been used for the determination of cmc . Surface tension, fluorescence, conductance, viscosity, dynamic light scattering, sound velocity, calorimetry, dye solubilization etc. are the few methods used for the determination of cmc value. Conductometric techniques are not suitable for non-ionic or zwitterionic surfactants. For obtaining the cmc value of surfactants an appropriate physico-chemical property is plotted with the surfactant concentration. A break point in the plot gives the cmc value. In some cases the formation of micelles is not a single step process. In these cases the formation of micelles is initiated by formation of pre-micellar aggregates. Pre-micellar aggregates are formed below the concentration of cmc . For conventional surfactants, pre-micellar aggregates are formed in solution for surfactant molecules having at least 14 carbon atoms in the hydrophobic tail. Gemini surfactants also form pre-micellar aggregates⁹. Various methods are used for the detection of pre-micellar aggregates⁴⁴⁻⁴⁷. The pronounced maxima observed in the plot of the square root of the concentration of surfactant with their corresponding molar conductivity, is strong evidence for the formation of pre-micellar aggregates⁴⁸.

1.1.4 Factors affecting micellization

There are various factors which affect the micellization process of surfactant in aqueous medium. The factors on which the micellization of different types of surfactant significantly depends are:

1. The structure of surfactants
2. Presence of electrolytes
3. Presence of organic additives
4. Temperature

1.1.4.1 The structure of surfactant

Cmc of the surfactants depends on the hydrophobic tails, headgroups, counterions and the spacer groups (in case of gemini surfactant) as discussed below:

1.1.4.1.1 Effect of hydrophobic chain length

The increase in number of carbon atoms in unbranched hydrocarbon chain length of surfactants leads to decrease in cmc . However, for the chain greater than 16, this rule is no longer holds possibly due to coiling of chains in solutions.⁴⁹ The value of cmc usually becomes one half on addition of each methylene group to straight hydrophobic chain attached to single terminal hydrophilic group. However, in nonionic surfactants each methylene group reduces cmc to one-tenth of its original value. A phenyl group, being part of hydrophobic group, is considered equivalent to about three and half-methylene group. If hydrocarbon chain is branched, the carbon atom on which branching occurs appears to exhibit one half of effect than that on straight chain. The presence of sp^2 hybridized carbon (in case of C=C bond) causes cmc to increase.^{49,50} In case of symmetric gemini surfactants, $m-s-m$, the variation in cmc with m is linear upto $m = 16$ for the $s = 2, 3, 5$ and 6 and upto $m = 18$ for $s = 4$, but the series, $m-8-m$ shows a departure from linearity starting at $m = 14$, as presented in the review of Zana.⁵¹ In case of dissymmetric gemini surfactants the hydrophobic chains influences the diversity of aggregation behavior. Oda and co-workers studied the $m-2-n$ series with equal $m + n$ values and indicated that these dissymmetric gemini surfactants have similar cmc values.⁵²⁻⁵⁵ Han *et al.*⁵⁶ observed that as the m/n ratio increases, the cmc of the $m-s-n$ series decreases linearly.

1.1.4.1.2 Effect of headgroups

The surfactants having same hydrophobic chain length but different headgroups have pronounced difference between their *cmc* values.⁴⁹ The aqueous solution of nonionic surfactants has much lower *cmc* than that of ionics with same number of carbon atoms. The effect of variation of headgroup on *cmc* is more in gemini surfactants than that in conventional surfactants. Okhara *et al.*⁵⁷⁻⁵⁹ synthesized a very large number of anionic gemini surfactants with sodium sulfate, sulfonate, phosphate or carboxylate headgroups. Engbert's *et al.*⁶⁰ synthesized bisphosphate gemini surfactants and they observed very low *cmc* values. The *cmc* value of gemini surfactant does not vary by substitution of CH₃-group by CH₃CH₂- in the headgroup.⁶¹ Through substitution of CH₃- with HOCH₂CH₂-, a series of cationic gemini surfactants have been synthesized.⁶² These surfactants start to form dimers at concentrations well below their *cmc*. Above the *cmc*, these surfactants form both micelles and vesicles spontaneously with a micelle-to-vesicle transition. The hydrogen bonding among the -OH groups of headgroups and water molecules as well as the strong hydrophobic interaction among the hydrocarbon side chains should be the main origins for the unique aggregation behavior of these gemini surfactants.⁶³

1.1.4.1.3 Effect of spacer (in case of gemini surfactants)

The effect of the spacer of gemini surfactants usually discussed with respect to its conformation and location in aggregates. The length of the spacer plays important role in aggregation.^{64,51} As reported,^{65,66} the *cmc* values of gemini surfactants, *m-s-m* go through a maximum at $s = 5$ or 6 for the surfactants with a hydrophobic polymethylene spacer and increase slowly and monotonously with the number of ethylene oxide units for the surfactants with a hydrophilic poly(ethylene oxide) spacer. It is believed that the increase of *cmc* with s observed for $s \leq 6$ for *m-s-m* surfactants is due to a conformational change in the surfactant molecule.⁶⁵ Gemini surfactant with spacer group of short chain length (12-2-12, 2Br⁻) shows concentration dependent micellar growth forming worm-like micelles. 12-3-12, 2Br⁻ gemini surfactant molecules form spheroidal micelles at a concentration of 30 mM. The drastic decrease of *cmc* with increasing s at $s \geq 10$ is attributed to a progressive penetration of the spacer in the micelle hydrophobic core. The change in conformation of gemini surfactant molecule followed by progressive penetration of the spacer with increasing s is expected to affect the number of water

molecules per spacer group at the Stern layer or micelle-water interface. It has been observed that a hydrophilic, flexible spacer prompts micelle formation, which leads to smaller *cmc* values.⁶⁷ The aggregation behavior of the gemini surfactants with a partially fluorinated spacer has also been investigated.⁶⁸ Interestingly, the *cmc* does not increase monotonously with the substitution of fluorine atom in the spacer, but the hydrophobicity and rigidity of the spacer enhanced and became less soluble in water. In addition, the spacer of gemini surfactants generates a great tendency to form a variety of aggregate structures, such as worm-like micelles and tubule aggregates in aqueous solution of gemini surfactants.⁶⁵ Zana *et al.*¹⁰ have investigated the microstructure of the aggregate of the dimeric surfactant with $m = 12$ and $s = 2, 3$ and 4 in aqueous medium, using cryogenic transmission electron microscopy. It was found that the dimeric surfactants with a short spacer ($s = 2, 3$) form long, threadlike and entangled micelles even at low concentration, while surfactants with $s = 4$ form spherical micelles. These observations reveal that the length of a spacer affects the morphology of the aggregates formed by the dimeric surfactant molecules and that short spacers promote lower spontaneous curvature in the self-assemblies.

1.1.4.1.4 Effect of counterion binding

The increase in degree of counterion binding in aqueous solution causes *cmc* to decrease generally. The extent of binding of counterion increases with increase in polarizability and charge of the counter ion, while it decreases with increase in hydrated radius. Oda *et al.*^{19,20} studied a series of gelators based gemini surfactants, 16-2-16, X_2 , with $X_2 = 2Br^-$, L-malate, D-glucarate, 2D-gluconate, and L-, D- and meso-tartarates and found that covalent interactions between the charged headgroups and chirality in the counterions are critical factors for determining the morphologies of aggregates. The nature of the counterion significantly affects the micellization process. Both *cmc* and counterion dissociation increase in the sequence $SO_4^{2-} < NO_3^- < Br^- < Ac^- < Cl^- < F^-$. The results are related to the different hydration situation of these counterions and match with the extent of the bare ions to the dimensions of the gemini headgroup region.⁵⁶

1.1.4.2 Presence of electrolytes

In aqueous solution the presence of electrolyte causes a change in the *cmc*, the effect being more pronounced for anionic and cationic than for zwitterionic surfactants and more pronounced for zwitterionics than for non-ionics. The change in the *cmc* of

non-ionics and zwitterionics on the addition of electrolyte has been attributed mainly to the “salting-out” or “salting-in” of the hydrophobic groups in the aqueous solvent by the electrolyte, rather than the effect of the latter on the hydrophilic groups of the surfactant.^{69,70} Salting-in or salting-out by an ion depends upon whether the ion is a water structure breaker or a water structure maker. Ions with a large ionic charge/radius ratio, such as F^- , are highly hydrated and are water structure makers. They salt out the hydrophobic groups of the monomeric form of the surfactant and decrease the *cmc*. Ions with a small ionic charge/radius ratio, such as CNS^- , are water structure breakers; they salt in the hydrophobic groups of the monomeric form of the surfactant and increase the *cmc*.⁵⁰ Han *et al.*⁵⁶ studied the effect of sodium bromide (NaBr) on the complex formation between gemini surfactant 12-12-12 and oppositely charged polyelectrolyte sodium carboxymethylcellulose and they observed that NaBr barely affects the *cmc* for this system. This was explained in terms of the counter action of the increase of the interaction and the screening of the interaction resulting from the added salt. Rabinovich *et al.*⁷¹ have investigated the effect of sodium chloride (NaCl) on the micellization properties of conventional and gemini surfactant. They observed that the extent of decrease in *cmc* is more pronounced in case of gemini surfactants than conventional surfactants.

1.1.4.3 Effect of organic additives

Organic material present with surfactant in small amount produce marked changes in the *cmc* value in aqueous medium. There are two class of organic material which affects the *cmc* value.

Class I material: They are polar organic molecule such as alcohols and amides. These materials affect the *cmc* at lower concentration. These compounds reduce the *cmc* value. Shorter-chain members of Class I material are adsorbed mainly in the outer portion of the micelle close to the water-micelle “interface”. The longer-chain members of this class are probably adsorbed mainly in the outer portion of the core, between the surfactant molecules. Adsorption of the additives in these fashions decreases the work required for micellization, in the case of ionic surfactants probably by decreasing the mutual repulsion of the ionic heads in the micelle. Straight chain compounds reduce the *cmc* to greater extent than branched chain compounds. Very short-chain polar compounds, (dioxane and ethanol) at low concentrations also reduce the *cmc*. But the

effect is very small.⁷² In these compounds, adsorption probably occurs on the surface of the micelle, near to the hydrophilic headgroup.

Class II material: Compounds of this class change the cmc of the surfactant at high bulk concentration. Urea, formamide, N-methylacetamide, guanidinium salts, short-chain alcohols, water-soluble esters, dioxane, ethylene glycol, and other polyhydric alcohols such as fructose and xylose etc are the few members of this class. These compounds modify the structure of water, its dielectric constant, or its solubility parameter (cohesive energy density). Urea, formamide, and guanidinium salts are believed to increase the *cmc* because of disruption of the water structure.⁷³ This disruption of the water structure may increase the degree of hydration of the hydrophilic group, and since hydration of the hydrophilic group opposes micellization, may cause an increase in the cmc. These water structure breakers may also increase the cmc by decreasing the entropy effect accompanying micellization. Xylose or fructose are the water structure maker, decrease the CMC of the surfactant.⁷⁴

Dioxane, ethylene glycol, water-soluble esters, and short-chain alcohols at high bulk phase concentrations may increase the cmc because they decrease the cohesive energy density, or solubility parameter, of the water, thus increasing the solubility of the surfactant and hence the *cmc*.⁷³ Moreover, these compounds decrease the dielectric constant of water, this increases the mutual repulsion between headgroup of the surfactants thus opposing micellization and increasing the *cmc*.

1.1.4.4 Effect of temperature

The effect of temperature on *cmc* is complex. The *cmc* first decreases with temperature to a minimum value and then increases. According to Rosen⁵⁰ the increase in temperature causes decreased hydration of hydrophilic heads, which favors micellization. Increase in temperature also causes disruption of structured water around hydrophobic ends, an effect that disfavors micellization. However, according to Akhtar *et al.*⁷⁵ for ionic surfactants, increase in temperature increases the degree of hydrophobic dehydration which favors micellization and the degree of hydrophilic hydration decreases which disfavors micellization. Partial dehydration of polar heads cause gradual increase in repulsion between them thus making micellization difficult and increasing the *cmc*. Disruption in structured water around hydrophobic groups also increases with temperature. The relative magnitudes of two opposing factors will decide whether *cmc*

will increase or decrease in particular temperature range. For ionics, the minimum in *cmc* appears at around 298 K, while for non-ionic at 323 K. For bivalent metal alkyl sulphate *cmc* is independent of temperature.⁴² Several groups have studied the effect of temperature on the micellization behavior of gemini surfactants.⁷⁶⁻⁷⁸

1.1.5 Aggregation number

The number of surfactant molecules in a micelle is called aggregation number. It is decided by the dissimilarity between surfactant and solvent. It, thus, increases with increase in hydrophobic character of surfactants. The addition of neutral electrolyte to ionic surfactant solution causes aggregation number to increase, which is probably due to the compression of electrical double layer surrounding the ionic heads and decreasing repulsion between them. In this way more surfactant molecules are permitted to be present in micelle.⁵⁰ Micellar solutions are assumed to be monodisperse (all micelles having same size and same aggregation numbers) so that unnecessary complications may be avoided. The aggregation number can be calculated using steady-state fluorescence quenching and time-resolved fluorescence quenching methods.

1.1.6 Structure and shape of the micelles

According to the first model proposed by Hartely⁷⁹, micelles are considered as globular structures having a hydrocarbon core surrounded by a highly hydrophilic region formed by the surfactant headgroups, counterions and water molecules (Figure 1.3). It follows spherical aggregate containing 50-200 monomer units. It may be less than 50 also, especially in case of gemini surfactant. The radius of the sphere is approximately equal to the extended length of the hydrocarbon chain of the surfactant. The ionic headgroups of the surfactants and a portion of the counterions form a compact “Stern” layer at the micellar surface, in which about 60-75% of the micellar charge is believed to be neutralized.⁸⁰ The remaining counterions form a diffused Gouy-Chapman layer where they are dissociated from the micellar region and are free to exchange with ions distributed in the bulk aqueous phase. On the macroscopic scale, a micellar medium could be described as a mixed aqueous-organic solvent.⁸¹ The hydrocarbon portion of the micelle cannot have an open space at the center and consequently, micelle size does not exceed the maximum (stretched out) length of the hydrocarbon chain.⁸² Experimental evidence has been produced supporting the view that water cannot rigorously be excluded from the micellar core. Further, it is also supported by ¹H NMR, ¹³C NMR and

by other spectroscopic studies.⁸⁰ Menger's model proposed that micelles are open structures containing a series of microchannels allowing deeper water penetration.⁸³ According to the “Reef” model, water does not penetrate beyond the ionic group, whereas “Fjord” model states that, water percolates nearly to the center of the micelle. Menger *et al.*⁸⁴ proposed that water cannot reach the very centre of the micellar core, but can penetrate as far as seven carbon atoms away from the headgroup. They also proposed the “porous cluster” model using ¹³C NMR, optical rotatory dispersion (ORD) and molecular models.⁸⁵

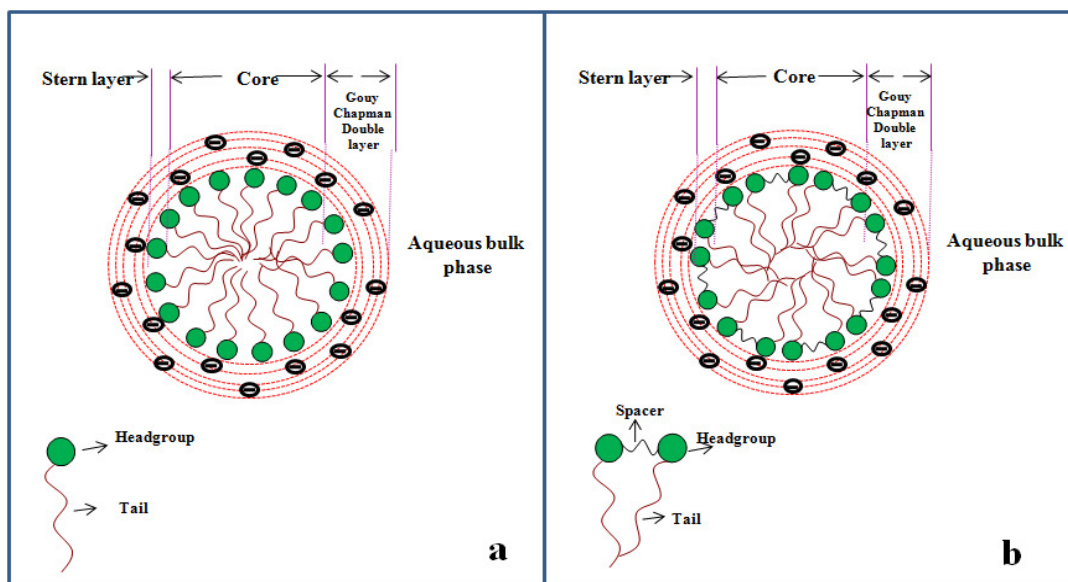


Figure 1.3: Spherical cross section of idealized micelles of (a) cationic conventional surfactant and (b) cationic gemini surfactant

Micelle structures are dynamic in nature and in equilibrium with monomers and other forms of aggregates in solution. Depending on the temperature, concentration, and other experimental variables, the micelles may be roughly spherical, ellipsoidal, disk like or rod-shaped and bilayers. Depending on the headgroup structure, ionic micelles have been found to be either (a) spherical at all concentrations, (b) rod shaped at all concentrations, (c) spherical at low concentrations and rod shaped at high concentrations.

Depending on the structure of the surfactant, headgroup, and charge on the headgroup the micelle shape can vary. Micellar shape depends on the relative values of tail length (l), headgroup area (a) and the molecular volume (v) of the molecule.⁸⁶ Israelachvili *et al.*⁸⁷ reported that depending on the value of packing parameter $p (= v/al)$, the surfactant aggregates could acquire different shapes (Figure 1.4). They showed that,

micelles are spherical for $p < 1/3$ and ellipsoidal and cylindrical for $1/3 < p < 1/2$. The surfactant aggregates tend to be bilayers for $p > 1/2$ and in suitable cases this results in formation of vesicles⁸⁶ and if $p > 1$ it will form reverse micelles.


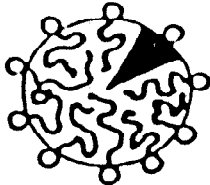
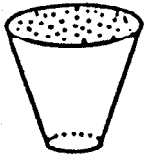


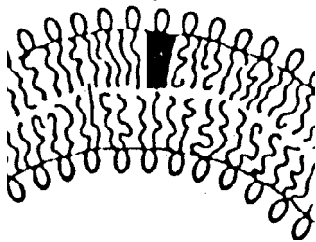

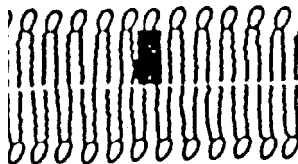
Critical packing parameter (v/al)	Critical packing shape	Structure of the micelle
$< 1/3$	Cone 	Spherical micelles 
$1/3 - 1/2$	Truncated Cone 	Cylindrical micelles 
$1/2 - 1$	Truncated Cone 	Flexible bilayers, Vesicles 
~ 1	Cylinder 	Planar bilayers 

Figure 1.4: Different shapes of micelle based on critical packing parameter

In case of gemini surfactant, the spacer group plays a very significant role. Hence, the properties of gemini surfactants cannot be explained only in terms of packing parameters, because the link between headgroups can modify both the spontaneous curvature and the bending modulus. Actually, for a given tail length, the morphology in aqueous solutions depends strongly on the spacer. For example, it was observed for the

series with $m = 12$ and $2 \leq s \leq 16$, that the surfactant aggregates into spherical micelles, cylindrical micelles or vesicles, depending on the value of s . Measurement of a at the air/water interface shows that this parameter varies in non-monotonic manner. It increases rapidly for short spacers, reaches a maximum for medium spacers (containing 10 to 12 methylene groups), and decreases for even larger spacers. As for the two parameters (a and l) involved to determine p , l is supposed to remain unchanged as the spacer carbon number is increased and is expected to have a slow monotonic increase, except for very long spacers ($s \geq 14$). So the change in the morphology of gemini surfactant are mostly influenced by the spacer on the surface area.⁸⁸

Micelles can be classified into two types, depending upon the kind of solvent used:

1. Normal or aqueous micelles

The structure of the aggregates in water as solvent is such that interior of the micelles consists of the hydrophobic core and the hydrophilic residues are located on the surface and are in contact with water.

2. Inverted or reverse micelles (discussed later).

1.1.7 Thermodynamics of micellization

The main concern of thermodynamics applied to micellar systems is the behavior of the chemical potentials (or activities) of the various solute species when the temperature and composition of the solution are altered. Basically there are two approaches that have been made to explain the thermodynamics of micelle formations (i) Phase separation model⁸¹⁻⁸⁶ (ii) Mass action model.⁸⁹

1.1.7.1 Phase separation model

This approach treats micelle as a separate, but a soluble phase, which begins to form at the *cmc*. This model could be formulated by assuming that the chemical potential of the surfactant in the micellar state is a constant at a given temperature and may be adopted as the standard chemical potential, μ_m^o analogues to the standard chemical potential of a pure liquid or solid. Equilibrium with the surfactant in solution is then represented by Equation 1.1

$$\mu_m^o = \mu_1^o + RT \ln a_1 \quad (1.1)$$

where R is the gas constant, T is the absolute temperature, μ_1^o is the standard chemical potential in solution and a_1 is the activity of surfactant monomer in solution. Putting $a_1 = X_1 f_1$, the standard Gibbs free energy of micellization per mole of monomer, ΔG_m^o is given by Equation 1.2:

$$\Delta G_m^o = \mu_m^o - \mu_1^o = RT \ln X_1 \quad (1.2)$$

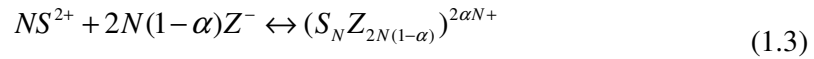
where X_1 is the mole fraction of monomers and the activity coefficient, f_1 is taken as unity. The *cmc* may be denoted as X_1 . This expression is only applicable for nonionic conventional surfactant.

1.1.7.2 Mass action model

This approach is consistent with the fact that the properties of the solutions change continuously at the *cmc* and predicts correctly that the activity of the monomer changes above the *cmc* and enables bond counterions to be included in the case of ionic surfactants.

The brief derivation of the ΔG_m^o for all types of conventional and gemini surfactants can be found in the article by Zana.⁹⁰ Since the present research work focus on the gemini surfactant, this model is discussed here in detail for gemini surfactant:

One can apply the mass action model to the monomer \leftrightarrow micelles equilibrium in the micellar solutions for gemini surfactants. After assuming that the gemini surfactant molecules are 2:1 electrolytes, the ionization process of gemini surfactant in water may be presented as Equation 1.3:



where, S^{2+} and Z^- denote the gemini surfactant monomer cation and counter anion, respectively, N is the aggregation number of micelle, and α is the degree of counter ion dissociation. If activity coefficients are neglected, the equilibrium constant is given by the Equation 1.4:

$$K = \frac{\left[(S_N Z_{2N(1-\alpha)})^{2\alpha N+} \right]}{\left[S^{2+} \right]^N \times \left[Z^- \right]^{2N(1-\alpha)}} \quad (1.4)$$

Since the standard Gibbs free energy change, $\Delta G^\circ = -RT \ln K$, the Gibbs free energy of micellization per monomer for the above equilibrium system may be given as:

$$\Delta G_m^\circ = \frac{-RT \ln K}{N} \quad (1.5)$$

or,

$$\Delta G_m^\circ = -RT \left\{ \frac{\ln \left[\left(S_N Z_{2N(1-\alpha)} \right)^{2\alpha N+} \right]}{N} - \ln [S^{2+}] - 2(1-\alpha) \ln [Z^-] \right\} \quad (1.6)$$

when the aggregation number (N) is large, the contribution of the first term will be negligible.

So, Gibbs free energy will become:

$$\Delta G_m^\circ = RT \left\{ \ln [S^{2+}] + 2(1-\alpha) \ln [Z^-] \right\} \quad (1.7)$$

If the concentration is very close to the cmc , one can assume $[S^{2+}] \approx [Z^-] \approx cmc$. Therefore, the Gibbs free energy of micellization per monomer may be written as:

$$\Delta G_m^\circ = RT(3-2\alpha) \ln cmc \quad (1.8)$$

This relation can also be written as given below, where cmc is on the molar scale:

$$\Delta G_m^\circ = RT(3-2\alpha) \ln X_{cmc} \quad (1.9)$$

The term $(3-2\alpha)$ accounted for the partial dissociation of counter ions from the micelles.

The standard enthalpy of micellization, ΔH_m° can be obtained from the temperature variation of cmc by applying the Gibbs-Helmholtz relationship (Equation 1.10):

$$\Delta H_m^\circ = \frac{\delta(\Delta G_m^\circ/T)}{\delta(1/T)} \quad (1.10)$$

The expression for standard enthalpy of micellization, ΔH_m° obtained from Equations 1.9 and 1.10 is (Equation 1.11):

$$\Delta H_m^\circ = -RT^2 (3-2\alpha) \left(\frac{\delta \ln X_{cmc}}{\delta T} \right)_p - \ln X_{cmc} \left(\frac{\delta \alpha}{\delta T} \right) \quad (1.11)$$

In case α is not significantly dependent on temperature, the second term in the right hand side of Equation 1.11 can be neglected and an average value of α i.e. α_{avg} can be used in place of α in the remaining term of same equation. Therefore, the final expression to be used to calculate ΔH_m^o becomes as Equation 1.12:

$$\Delta H_m^o = -RT^2(3 - 2\alpha_{avg}) \left(\frac{\delta \ln X_{cmc}}{\delta T} \right) \quad (1.12)$$

The standard entropy of micellization, ΔS_m^o can be determined by using the Equation 1.13:

$$\Delta S_m^o = \frac{(\Delta H_m^o - \Delta G_m^o)}{T} \quad (1.13)$$

The Gibbs free energy of micellization for conventional ionic surfactant (1:1 electrolyte) can be calculated using Equation 1.14:

$$\Delta G_m^o = RT(2 - \alpha) \ln X_{cmc} \quad (1.14)$$

1.1.8 Mixed micelles

Micellar systems consisting of mixtures of surfactants of variable structure are known as mixed micelle system (Figure 1.5). Mixed micelles have received increasing attention since the early 1980s. Mixed micellar systems serve as good models for the study of molecular interactions on complex supramolecular aggregates⁹¹⁻⁹³ to mimic the behavior of biological systems and functions (ion transport, drug delivery, and so forth)⁴⁹ and to provide better performance characteristics in their technological applications (pharmaceutical, food, detergency and cosmetic industries, micellar solubilization)⁹⁴ than those consisting of only one type of surfactant. Some of the surfactants have very high surface activity but at the same time they are costly. A large scale application of a single surfactant is not economical from the industry point of view due to the high cost of their mass production and purification. Therefore, to get almost equal activity, mixing of a more surface active and expensive surfactant with a comparatively less surface active and cheaper surfactant in different proportions, is one of the shortest ways. To meet these requirements, gemini and conventional mixed surfactant systems would be the best choice. Because of this, there has been a considerable research on the molecular interactions between different surfactants in their binary mixtures.^{92,95-99} Various types of

molecular interactions are possible in surfactant systems e.g.: (1) electrostatic interaction between ionic hydrophilic groups, (2) ion–dipole interaction between ionic and nonionic hydrophilic groups, (3) steric interactions between bulky groups, (4) van der Waals interactions between hydrophobic groups, and (5) hydrogen bonding among constituent surfactant molecules. Surfactants system show ideal behavior if there is no interaction between surfactants molecules. If the interaction between surfactants are attractive, it is sometimes called synergism and if repulsive, called antagonism. Zana *et al.*^{100,101} worked on mixed systems of cationic gemini surfactants and conventional surfactants. To study the properties of mixed micelles, different methods are developed over the period of time. These methods are briefly explained in Section 2.2.13 (material and methods). Now-a-days, many groups are involved in investigating the interactions between different types of gemini surfactants and conventional surfactants in their mixed micellization processes.^{92,96,97-106}

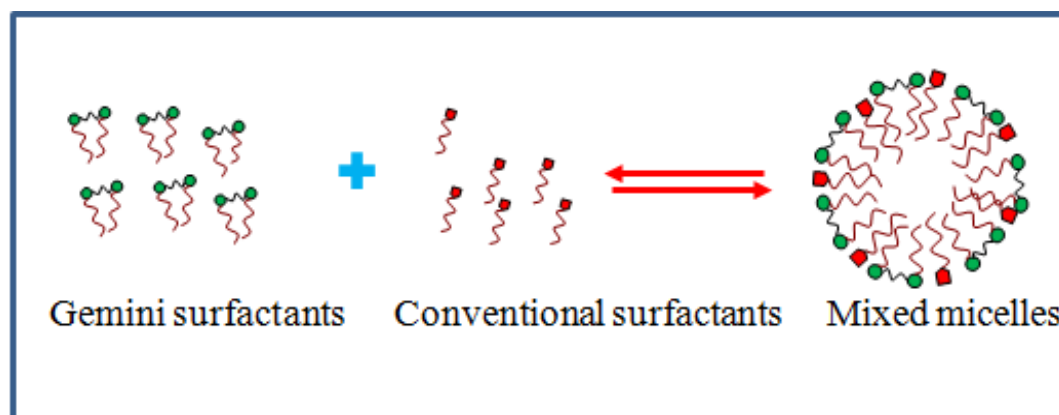


Figure 1.5: Formation of mixed micelles of a conventional surfactant with a gemini surfactant

1.2 Reverse micelles

It is discussed that surfactant molecules dispersed in polar solvents form micelles. Reverse micelles (RMs) are formed when surfactant molecules are dispersed in nonpolar solvents (hexane, heptane, benzene etc.) (Figure 1.6). In RMs, the polar headgroups of surfactant molecules are pointed toward the nanoscale droplet of polar solvent. The hydrophobic tail of surfactant molecules projected outward into the nonpolar solvent phase.¹⁰⁷ Usually water is considered as a polar solvent in RMs.¹⁰⁸ Some other polar solvents (acetonitrile, propylene glycol (PG), ethylene glycol (EG), and formamide (FA)) which are immiscible with nonpolar solvents also form RMs. RMs made from water are

known as aqueous RMs and RMs made from other polar solvents are known as nonaqueous RMs.¹⁰⁸ Reverse micelle have been used for many different applications including modeling biological reactions,¹⁰⁹⁻¹¹² nanoreactors,^{113,114} templates for nanoparticle syntheses,¹¹⁵⁻¹¹⁸ drug delivery vessels,¹¹⁹⁻¹²¹ size-controlling microreactors for a variety of aqueous chemical reactions,¹²² vehicles for drug delivery,¹²³ membrane mimetic systems,¹⁰⁷ and also in separation and extraction processes of both metal ions and proteins.¹²⁴⁻¹²⁶ Generally, RMs are defined by the ratio of the polar solvent (usually water) to the amount of surfactant present, ($w_o = [\text{polar solvent}]/[\text{surfactant}]$). Size of RMs depends upon w_o values. Shape and size of RMs have been characterized using various methods including scattering techniques such as SANS,¹²⁷⁻¹²⁹ small-angle X-ray scattering (SAXS),^{130,131} and both dynamic and static light scattering.¹³²⁻¹³⁴ Reverse micelles can be made from a variety of different surfactants viz anionic, cationic, nonionic, and zwitterionic surfactants. Most commonly used anionic surfactant is AOT. This surfactant is the most widely employed, due to the fact that it readily forms well characterized reverse micelles over a wide range of water/surfactant mole ratios. To form RMs, cationic surfactant requires a co-surfactant, typically a short chain alcohol. Cationic surfactant cetyltrimethylammoniumbromide (CTAB) has been used for the preparation of RMs.¹⁰⁸ Cationic gemini surfactants also form RMs in presence of co-surfactant.¹³⁵⁻¹³⁷ Zhao *et al.* have studied the various physical properties of RMs of gemini surfactants.¹³⁵⁻¹³⁷ Xu *et al.*¹³⁸ prepared uniform silver nanoparticles in reverse micelles of gemini surfactant.

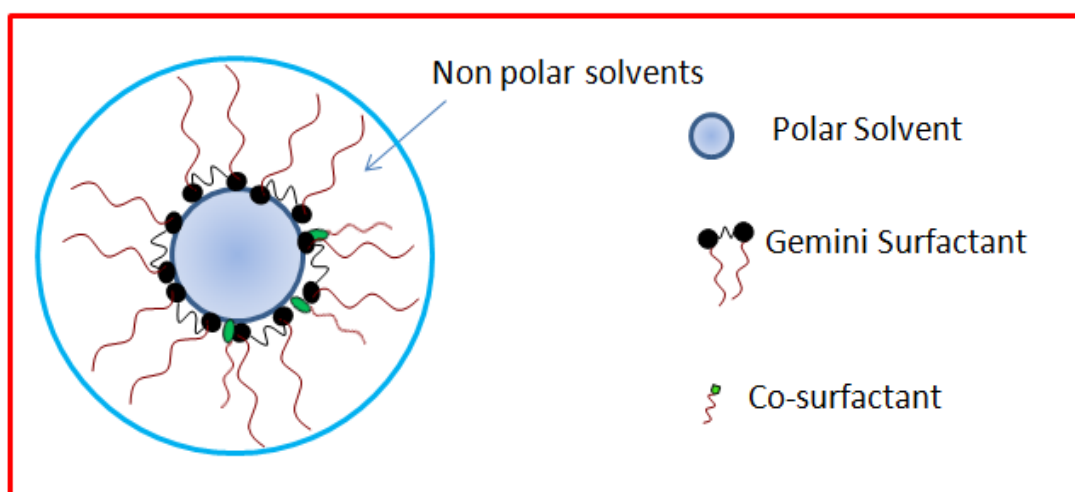


Figure 1.6: Diagrammatic representation of reverse micelles formed by gemini surfactants and co-surfactants

Water present in natural systems is often found in conditions very different from those of the bulk liquid.¹³⁹ RMs having water as polar solvent can provide a good model of specific water in living organisms, which plays an important role in biological functions.¹⁴⁰ Douhal *et al.*¹⁴¹ observed three regions in the behavior of confined water molecules within the RM. The nature of the water inside the reverse micelles of conventional surfactants has been well explored through various steady-state and time-resolved spectroscopies.¹⁴²⁻¹⁴⁵ Zhao *et al.*¹³⁵ reported various states of water in RMs of gemini surfactant using FTIR technique.

1.3 Proteins

Proteins are the most versatile and abundant macromolecule in living systems. Proteins are polymers of 20 different amino acids joined by peptide bonds. Out of four levels of protein structure the primary structure of protein is determined by the sequence different of amino acids. Secondary structure of proteins are formed by regular hydrogen bonding interactions between N-H and C=O groups in the invariant parts of the amino acids in the polypeptide backbone or main chain. It is of two types the alpha helices and beta sheet. The tertiary structure of a protein is the three dimensional structure of the protein. The tertiary structure is maintained by four types of interaction between side chain groups of amino acid residues: (1) hydrogen bonding, (2) ionic interactions between oppositely charged groups (salt bridges), (3) hydrophobic interactions, and (4) disulfide cross-linkages. The covalent linkage (4) is much stronger than the noncovalent interactions (1-3).¹⁴⁶ Multiple polypeptide chains of protein interact with each other and arrange themselves to form a larger aggregate protein complex that is referred as quaternary structure of protein. Among a variety of proteins available serum albumins are well known and extensively studied because of its great importance in biological functions.

1.3.1 Significance of serum albumins

Albumins are broadly used as a model protein for various biophysical, biochemical and physicochemical studies.¹⁴⁷ They are the most copious of the proteins in blood plasma, accounting for about 60% of the total protein corresponding to a concentration of 42 g/l and provide about 80% of the osmotic pressure of blood. Principal function of serum albumin is to transport fatty acids, a great variety of metabolites and drugs such as anti-coagulants, tranquilizers and general anesthetics.¹⁴⁸ Albumin proteins have the interesting properties of binding with a variety of

hydrophobic ligands such as fatty acids, bilirubin, warfarin, tryptophan, steroids, anaesthetics and several dyes.¹⁴⁷ In recent years, recombinant proteins and antibodies are widely used in treatment and prevention of diseases.¹⁴⁹ Hence, there is a need of analytical techniques to detect and analyze the protein samples apart from characterization techniques to monitor the conformational variants. These changes in conformation of proteins can be due to environmental stress, chemical changes of protein such as oxidation due to environmental and various types of aggregate formation etc.^{150,151} Fluorescence spectroscopy can be applied to characterize the protein conformation. Among serum albumins, bovine serum albumin (BSA) is used in this research work and the structure of BSA is discussed below.

1.3.2 Structure of BSA

BSA is a globular serum protein with high water solubility. In a single polypeptide chain (primary structure) BSA contains 583 amino acids. Primary structure of BSA consists of nine loops which are held together by 17 disulfide bonds. The secondary structure is composed of 67% of helix of six turns. The tertiary structure consists of three domains, I, II and III with each domain constituted by subdomains IA, IB, IIA, IIB, IIIA and IIIB. Domains II and III share a common interface, binding of a probe with domain III results in the conformation changes to domain II also. BSA contains two tryptophan residues, Trp-134 is located near the surface of the albumin molecule in the second helix of subdomain IB, whereas Trp-212 in a hydrophobic subdomain IIA.¹⁵² The molecular weight of BSA is 66 kD.¹⁵²

1.3.3 Intrinsic fluorescence of BSA

Structural changes in the native structure of BSA can be studied by fluorescence spectroscopy (Discussed in detail in the next section). Proteins contain three aromatic amino acid residues tryptophan (Trp), tyrosine (Try), and phenylalanine (Phe). The intrinsic fluorescence of BSA is largely attributed to tryptophan (Trp) residues, with only a minor contribution by the numerous tyrosines (Try). Trp has much stronger fluorescence and higher quantum yield than the other two aromatic amino acids. The intensity, quantum yield, and wavelength of maximum fluorescence emission of Trp depend on environment of Trp. Hence, alterations in the fluorescence properties of Trp are used to study any structural change of BSA by any external substance.¹⁵³⁻¹⁵⁵ Fluorescence emissions of Try and Phe are not sensitive to great extent.

1.3.4 Interaction of BSA with surfactant

Amino acid residues of BSA have hydrophobic and hydrophilic properties. Due to this dualism, surfactant molecules interact with BSA. Interactions of proteins with surfactants have studied extensively.¹⁵³⁻¹⁵⁶ Interactions of proteins with surfactants are of great importance not only in vivo but also in wide variety of industrial, biological, pharmaceutical, and cosmetic systems.¹⁵⁷⁻¹⁶³ In general, ionic surfactants are chosen for the study of protein-surfactant interactions in view of their application in the area of membrane study.¹⁶⁴

Additions of ionic surfactants lead to the denaturation and conformational change of protein. The nature of the protein-surfactant interaction can be well understood in terms of the binding isotherms. With increasing the surfactant concentration the binding isotherms display four characteristic regions. These regions include (A) Specific binding, (B) Non-cooperative binding, (C) Cooperative binding and (D) Saturation of binding. In specific binding region, at lowest concentration of surfactant, surfactant binds to the specific high energy sites of protein and these interactions are predominately electrostatic in nature. In non-cooperative binding region binding of surfactant with protein is very gradual. In cooperative binding region the binding affinity of surfactant to protein increases drastically. It has been suggested that the protein unfolds in the cooperative binding region and significant number of hydrophobic binding sites previously buried in the interior of BSA are exposed.¹⁶⁵ In saturation binding region, binding of the surfactant on the protein does not occur and there will be a formation of normal micelle as excess of surfactant is added. A variety of models have been proposed to mimic how surfactant interacts with protein.¹⁶⁶⁻¹⁶⁹ In a rodlike-particle model upon binding with surfactant, protein expands into a highly prolate ellipsoid. In a flexible cylindrical micelle model, protein wraps around the surface of cylindrical surfactant micelles. In a necklace-bead model (most commonly accepted model), surfactant micelles are arranged along a flexible polypeptide chain.

Interactions of protein with single chain surfactants have been extensively studied.^{154,155,168-170} Study on interaction of gemini surfactant with protein is an area that demands a thorough investigation. Liu *et al.*¹⁷¹ have studied the interaction of cationic gemini surfactants with BSA. Xu *et al.*¹⁵³ have studied the interaction of gemini surfactant with BSA and gelatin. They reported that binding of gemini

surfactant induces changes of the microenvironment around the aromatic amino acid residues and disulfide bonds of BSA at high surfactant concentration. Gao *et al.*¹⁷² have studied the effect of tail length of anionic gemini surfactant on interaction with BSA. Faustino *et al.*¹⁷³ have reported the effect of pH, temperature and surfactant stereochemistry on gemini surfactant-protein interaction. Rather *et al.*¹⁷⁴ have studied the refolding of BSA by using gemini surfactant and reported that gemini surfactant refold the denatured BSA by very low concentration of gemini at which the conventional surfactant remain ineffective.

1.4 Fluorescence spectroscopy

Now-a-days, many advanced spectroscopic analytical techniques are available. Fluorescence spectroscopy is one of the most fashionable techniques due to their high sensitivity and selectivity. Fluorescence spectroscopy has evolved rapidly during the past decades. The increased interest in this spectroscopy is due to advances in time resolution, methods of data analysis, and improved instrumentation. Fluorescence spectroscopy is having applications in various areas such as biochemistry, biophysics, environmental sciences, nuclear chemistry, cell biology, forensic sciences, medical diagnostics etc. Fluorescence spectroscopy has become a very potential technique in DNA sequencing, immunoassays, flow cytometry and genetic analysis.^{175, 176}

The phenomenon of fluorescence occurs due to photophysical processes in excited electronic state. Any molecule which has been electronically excited after absorbing the light of suitable quanta comes back to its ground state either by radiative mechanism or by non-radiative mechanism. The process in which molecule comes to the ground state from the excited state by radiative mechanism and emit photons is called fluorescence emission. The fluorescence photons have several informations at a given wavelength such as energy (wavelength), intensity (number of photons), time and polarization. These parameters of the fluorescence photons give the information about the local environment surrounding the fluorophore under investigation. So fluorescence intensity, spectrum, polarization and their time dependence are important parameters that can be used for the characterization.¹⁷⁶

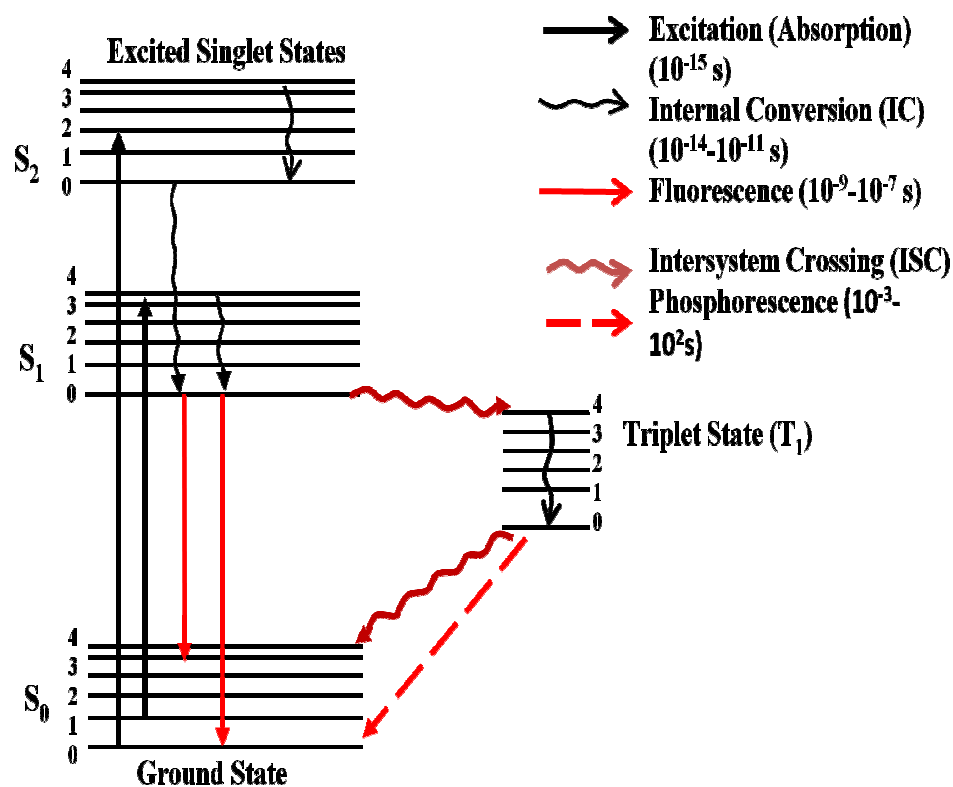


Figure 1.7: Jablonski diagram showing fates of polyatomic molecules upon photoexcitation

The mechanisms by which electronically excited molecules come to ground state are given by the Jablonski diagram as shown in Figure 1.7.¹⁷⁷. At room temperature mainly molecules populate the lowest electronic state, which can be explained by Boltzmann distribution. S_0 denote the lowest singlet electronic ground state with multiplicity one. S_1 and S_2 denote the first and second singlet electronic excited states, respectively. Upon interacting with incident light in UV-range molecules undergo electronic transition in $\sim 10^{-15}$ seconds from ground state (S_0) to a higher excited state (say S_2) accompanied with a vibrational transition. Molecule present in higher vibrational level of the higher excited electronic state (say S_2) dissipates its excess vibrational energy as thermal energy and goes to zero vibrational level ($v = 0$) of the S_2 state. The energy gap between the higher electronic states is generally smaller than the energy gap between S_1 state and S_0 state. For this reason molecule arrives at S_1 state quickly by internal conversion (IC) or quantum mechanical tunnelling, followed by vibrational relaxation to $v = 0$ level of S_1 state. Now, if there is an overlap between the zero vibrational level of S_1 state and higher vibrational level of

S_0 state, molecule comes back to the S_0 state by internal conversion. The molecule can also release its excitation energy as photon. This radiative deactivation process of molecule from S_1 state to S_0 state is called as fluorescence. Sometimes the zero vibrational level of S_1 state couples with the higher vibrational levels of the triplet state say, T_1 . In such cases, the molecule in the S_1 state can also undergo a spin-conversion to the first triplet state T_1 . This process is called intersystem crossing (ISC). The molecule at higher vibrational level of T_1 state quickly loses its vibrational energy and arrives at $v = 0$ level of T_1 state. From T_1 state also molecule can return to S_0 state either by non-radiative process, i.e. intersystem crossing or by radiative process i.e. phosphorescence. Transition from T_1 to the singlet ground state (S_0) is forbidden and as a result the rate constants for triplet emission are several orders of magnitude smaller than those of fluorescence. Both radiative processes leave the molecule to the Frank-Condon ground (FCG) state, from where molecule goes to zero vibrational level of S_0 state by collisional deactivation process. Phosphorescence spectrometry lacks sensitivity when applied in liquid solution at ambient room temperature. Phosphorescence is either seldom observed or observed with weak signal, because of the forbidden character of the phosphorescence triplet-to-singlet transition. Phosphorescence is a very slow process usually occurring in microseconds to milliseconds. In contrast, fluorescence is a relatively fast process occurring in picoseconds to nanoseconds. An electronic spectrum is generally affected by the factors such as substituents, pH, nature of solvents etc.

1.4.1 Effect of substituent

Absorption and fluorescence spectra of the molecule depend upon the substituent on the molecule. The absorption and fluorescence maxima shifted towards longer wavelength with increasing the conjugation e.g. benzene, naphthalene and anthracene. According to Kasha's rule fluorescence occurs if the $\pi \rightarrow \pi^*$ is the lowest energy transition, and phosphorescence is possible if $n \rightarrow \pi^*$ is the lowest energy transition.¹⁷⁸ Substitution of alkyl group on the aromatic ring has little effect which results in the small red shifts in absorption and fluorescence spectra. Substitution by alkyl side chain increases the vibrational degrees of freedom and thereby increases internal conversion, so the fluorescence quantum yield decreases. Fluorescence quantum yield thus depends upon the rate of non-radiative processes with respect to the rate of radiative process. Substitution of electron donating group, e.g. $-\text{OH}$, $-\text{NH}_2$, $-\text{N}(\text{CH}_3)_2$, $-\text{OCH}_3$ on benzene

ring results in the large red shift, whereas the presence of halogen atoms on aromatic molecule decreases the fluorescence quantum yield with increase in atomic number of the halogen atom, due to the heavy atom effect.¹⁷⁹ These heavy atoms actually increase the spin-orbit coupling and thus the rate of intersystem crossing. The introduction of hetero atom sometimes increases the rate of non-radiative process which results in the decrease in fluorescence quantum yield.^{180, 181} Pyrrole, furan and thiophene are non-fluorescent, carbazole and dibenzofuran show fluorescence.¹⁸² Mixed nitrogen-oxygen or nitrogen-sulphur heterocycles are often highly fluorescent compared to simple monocyclic heterocycles of oxygen and sulphur.¹⁸³

1.4.2 Solvent effect

Environment around the probe molecule affects the position and intensity of absorption and fluorescence spectra of the probe. Characterization of various different systems using a certain probe molecule requires the photophysical study of the probe molecule in different solvents of varying polarity. Generally, an absorption and emission spectrum of a probe in a variety of solvents (nonpolar, polar aprotic and protic) are recorded at reasonable probe concentration. This will involve both solute-solute and solute-solvent interactions. Thus the spectral characteristics of the molecules depend on the nature of the solvent as well as on the solute. So, the effect of solvents on the spectral properties of the solute molecules is discussed in two parts in this section.

1.4.2.1 Dispersive or general solvent interactions

These interactions basically involve the electrostatic forces, and the spectral shifts can be correlated with the refractive index (n) and dielectric constant (ϵ) of the solvents. General interactions can be divided into following types:-

- I. **Dipole-Dipole interaction:** Here both solute and solvent molecules have permanent dipole moment.
- II. **Dipole-Induced dipole interaction:** Here one is having permanent dipole moment which induces a dipole to the other.
- III. **Induced Dipole-Induced Dipole interaction (London Dispersion forces):** Here both solute and solvent molecules do not have permanent dipole moment.

The magnitude of these interactions follow the order I > II > III.

1.4.2.2 Specific interactions

Specific interactions include hydrogen bonding, complex formation between solute and solvent. These interactions which are comparatively more stronger than non-specific interaction between solute and solvent can result in drastic changes in absorption and fluorescence spectra of probe molecules.

The electronic transitions can be divided into three different kinds, (i) $\pi \rightarrow \pi^*$, (ii) charge transfer and, (iii) $n \rightarrow \pi^*$. In all these transitions, the dipole moment of the molecule is altered and thus interactions with the solvent molecules depend upon the change in this dipole moment. The hydrogen bond interaction changes the spectral characteristics of molecules to a great extent. The hydrogen bonding properties between solvent and solute in the ground state are often different from that in the first singlet excited state.

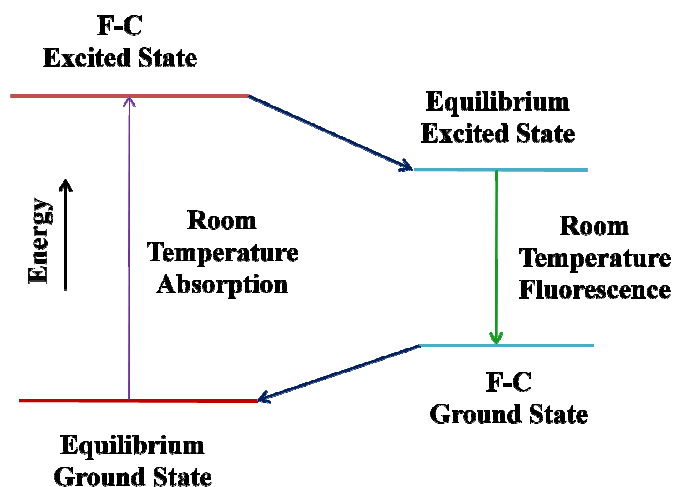


Figure 1.8: Schematic representations of equilibrium and Frank-Condon (F-C) electronic states

According to Frank-Condon principle, absorption of light occurs within 10^{-15} s, is too short compared with the period of nuclear motion. At the instant of its formation of Frank-Condon excited state (FCE) (Figure 1.8), the excited solute molecule is momentarily surrounded by a solvent cage whose size and orientation is similar to those that are present in the ground state.

The molecule in the FCE state relaxes vibrationally to the lowest vibrational level of the first excited singlet state within the time scale of 10^{-13} s. Subsequent to excitation and vibrational relaxation, the solvent cage reorganizes accordingly in the new

environment due to the change in charge distribution and thus the dipole moment upon excitation, within the time scale of 10^{-11} and 10^{-12} s. This solvent reorganization or reorientation is commonly called as “solvent relaxation”. The combined effect of vibrational, solvent and geometry relaxations is termed as thermal relaxation. By these processes, an equilibrium excited state is formed in which solvent configuration is optimal for the geometry and electron distribution of the excited molecule. Emission occurs from the equilibrium excited state to the metastable Frank-Condon ground (FCG) state. The molecule in the FCG state is still in the environments which are similar to that in the excited state due to rapid transition. Vibrational and solvent relaxation further brings it to equilibrium ground state. Since the thermally relaxed excited state is lower in energy than FCE state and FCG state is higher in energy than thermally relaxed ground state, fluorescence occurs at longer wavelength than absorption. This loss in energy between absorption and fluorescence is called the Stokes-shift and is denoted by $(\bar{\nu}_{ab} - \bar{\nu}_{fl})$, where $\bar{\nu}_{ab}$ and $\bar{\nu}_{fl}$ are the reciprocal of wavelength of absorption and fluorescence spectral maximum, respectively.

The distinction between various kinds of transitions can be made on the basis of molar extinction coefficient, effect of solvents on spectral characteristics and emission properties. In general, $n \rightarrow \pi^*$ transitions are very weak and get blue shifted in the presence of protic solvents and phosphorescence is the major pathway for the deactivation of excited state energy. On the other hand, both $\pi \rightarrow \pi^*$ and charge transfer (CT) bands are strong and band maxima get red shifted with the increase in polarity or proton donor capacity of solvent and fluorescence is generally observed as compared to phosphorescence. The solvatochromic shift is more in case of CT transition than $\pi \rightarrow \pi^*$ transition.

The issue on the interactions (specific or non-specific) between the probe molecules and solvent attracted the attention of many researchers. There are several reports that the emission maxima which is approximately linearly dependent on the solvent polarity function of various forms, is satisfactorily correlated with the solvatochromic plots.¹⁸⁴ In some cases for strongly hydrogen-bonding protic solvents, e.g., alcohols or water, deviation from the correlation has been reported.¹⁸⁵⁻¹⁸⁷ Pringsheim¹⁸⁸ and Forster¹⁸⁹ systematically studied the effects of solvents on

fluorescence spectra of aromatic molecules. The significance of hydrogen bonding in the solvent effect has been reported by Pimental,¹⁹⁰ Mataga and Tsumo.¹⁸¹

Lippert,^{191,192} McRae¹⁹³ and Suppan¹⁹⁴ have carried out the quantitative treatment of the effect of solvents on the absorption and fluorescence spectra. Oshika,¹⁹⁵ Lippert^{196,192} and Mataga *et al.*¹⁹⁷ were the first to derive equations relating changes in the dipole moments on excitation with spectral changes. These equations were modified by Liptay,¹⁹⁸ Bilot and Kawaski¹⁹⁹ and Bhakshiev²⁰⁰ by including polarizability of the fluorophores and dispersive interactions. Later, Lippert and Mataga^{191,192,197} modified the equation by neglecting the polarizability effects of the fluorophore. Lippert-Mataga equation is widely reported²⁰¹⁻²⁰⁵ to analyse the solvatochromic effect using the Equation 1.15:

$$\left(\bar{\nu}_{ab} - \bar{\nu}_{fl}\right) = \left[\frac{2(\mu_e - \mu_g)^2}{hca^3} \right] \Delta f + \text{constant} \quad (1.15)$$

$$\text{where, } \Delta f = \frac{(\varepsilon - 1)}{(2\varepsilon + 1)} - \frac{(n^2 - 1)}{(2n^2 + 1)}$$

ε is dielectric constant of a particular solvent,

n is refractive index of a particular solvent,

μ_g and μ_e are the ground state and excited state dipole moments of fluorophore, respectively,

h is Planck's constant,

c is the velocity of light,

a is the Onsager cavity radius.

The excited state dipole moment of the fluorophore can be calculated using this equation.

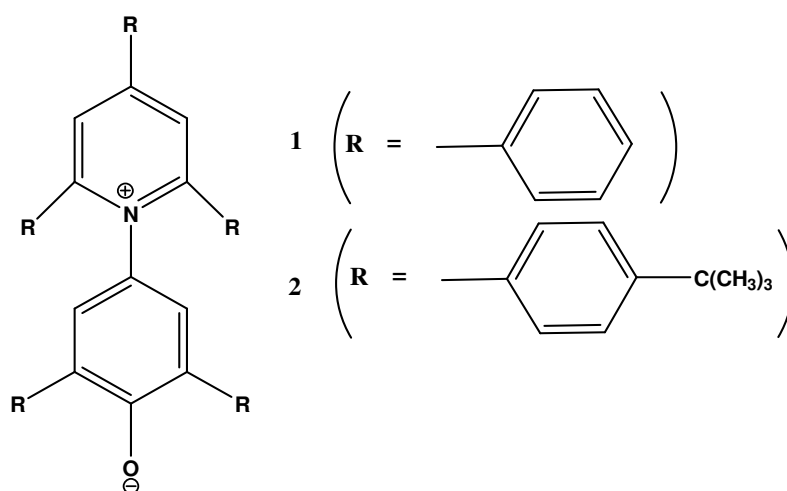
Similar to the other equations derived by different researchers, Lippert-Mataga equation also considers only the non-specific interactions between the fluorophore and solvent and not the specific interactions. Hence, it can be applicable only for the fluorophore in nonpolar and polar aprotic solvents. But the term polarity is loosely used to describe both non-specific and specific interactions. Hence, different polarity scales were also reported for fluorescent probes where all types of interactions are considered. The number of dyes designed and studied for different polarity scales are available in the

literature.²⁰⁶ For instance, Reichardt's empirical scale of solvent polarity, which includes upto 360 solvents namely, $E_T(30)$ scale is widely used for many compounds. This scale is similar to Kosower's Z-values.^{207,208}

$E_T(30)$ values are based on the negatively solvatochromic pyridinium N-phenolate betaine dye (**1**) (Scheme 1.1) as probe molecule and defined as the molar electronic transition energies (E_T) of dissolved **1**, measured in kilocalories per mole (kcal/mol) at room temperature (25°C) and normal pressure (1 bar) according to the following Equation 1.16:

$$\begin{aligned} E_T(30)(\text{kcalmol}^{-1}) &= hc\bar{\nu}_{\max} N_A = (2.8591 \times 10^{-3}) \bar{\nu}_{\max} (\text{cm}^{-1}) \\ &= 28591 / \lambda_{\max} (\text{nm}) \end{aligned} \quad (1.16)$$

where $\bar{\nu}_{\max}$ is the frequency of maximum absorption and λ_{\max} is the corresponding wavelength of the maximum of the longest wavelength band. This is the intramolecular charge-transfer $\pi \rightarrow \pi^*$ absorption band of dye **1**. In the first publication,²⁰⁹ the betaine dye **1** had, by chance, the formula number 30. Therefore, the number 30 was added in order to avoid confusion with ' E_T ', often used in photochemistry as abbreviation for triplet energy. This betaine dye **1** exhibits an unusually high solvatochromic band shift. Its negatively solvatochromic, intramolecular charge transfer absorption band is hypsochromically shifted by 357 nm on moving from diphenyl ether ($\lambda_{\max} = 810$ nm) to water ($\lambda_{\max} = 453$ nm).²⁰⁶



Scheme 1.1: Structure of betaine dye

In addition, normalized E_T^N scale²¹⁰ also can be used for charge transfer fluorescent probes.²⁰⁴ They are dimensionless numbers, which can be obtained based on Equation.1.17 using water and tetramethylsilane (TMS) as extreme polar and nonpolar reference solvents, respectively. Hence E_T^N scale ranges from 0 for TMS, the least polar solvent to 1.0 for water, the most polar solvent. As this scale needs a dye which should be sufficiently soluble for solvatochromic measurements in nonpolar and polar solvents, the dye **2** (Scheme 1.1) is used for this purpose.

$$E_T^N = \frac{E_T(\text{solvent}) - E_T(\text{TMS})}{E_T(\text{water}) - E_T(\text{TMS})} = \frac{E_T(\text{solvent}) - 30.7}{32.4} \quad (1.17)$$

The $E_T(30)$ and E_T^N polarity scales include the effects of specific as well as non-specific interactions. However, the disadvantages of such scales are that the information about the individual contribution of different solvent effects is lost. To overcome this, Taft *et al.*²¹¹ have proposed the solvatochromic comparison method (SCM). This is a multiparameter approach which separates the effects of general solvent polarity (π^*), hydrogen bond donor ability (α) and hydrogen bond acceptor ability (β) of the solvents on the spectral properties. The equation describing these effects is shown below:

$$E = E^o + c\pi^* + a\alpha + b\beta \quad (1.18)$$

where a , b and c are the coefficients and E^o is the spectral maxima independent of solvent effects. A negative value of coefficient indicates the stabilization, whereas a positive value indicates the destabilization.

1.4.3 Excited state dipole moment

To infer the charge separation of the probe molecule in the presence of polar solvents, in the excited state, the excited state dipole moments can be calculated experimentally as well as theoretically. The experimental calculations can be done by measuring the solvatochromism either from the solvent polarity effect on the Stokes shift²¹²⁻²¹⁴ or from the fluorescence shift alone, which is advisable if the absorption and emission transitions have different orbital origins. This can also be calculated theoretically by performing quantum chemical calculations. In addition to fluorescence spectroscopic techniques, time-resolved microwave conductivity (TRMC) is also used to calculate the singlet excited-state dipole moments of number of aminobenzonitriles in

cyclohexane, benzene and 1,4-dioxane.²¹⁵ On the other hand, Samanta and Fessender determined the excited state dipole moment of PRODAN from transient dielectric loss measurements.²¹⁶ Saha *et al.*²⁰⁴ reported the excited state dipole moment of a charge transfer probe by performing solvatochromic study. In addition Saha *et al.*²⁰⁵ calculated the excited state dipole moment of the same charge transfer probe theoretically using Semi-empirical Austin Model 1 (AM1) calculations, which was in very good agreement with the value calculated experimentally. Guchhait *et al.*²¹⁷ calculated the excited state dipole moment using time dependent density functional theory (TD-DFT).

1.4.4 Dual fluorescence by charge transfer systems

In 1962, Lippert *et al.*²¹⁸ reported that *p*-*N,N*-dimethylamino benzonitrile (DMABN) (Figure 1.9) shows dual fluorescence consisting of two bands in polar solvents. Among the two bands, one being “normal” for closely related benzene derivatives, the other, at considerably lower energy, being an “anomalous” one. Lippert *et al.*²¹⁹ proposed a solvent-induced reversal of excited states. The anomalous band was assigned to fluorescence from the polar 1L_a type state (Figure 1.9), which is preferentially stabilized by solvation. This anomalous band corresponding to the emission from 1L_a state was called as A band, whereas the normal short-wavelength band for emission from 1L_b state was called as B band. The emitting states, also called A* and B* states, could be in thermal equilibrium. Lippert *et al.*²¹⁹ proposed the excited state inversion of $^1L_b \rightarrow ^1L_a$ (Figure 1.9).

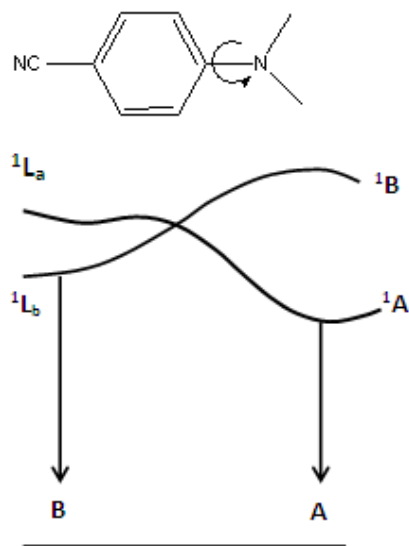


Figure 1.9: Excited state reversal of DMABN

To assign the origin of this new fluorescence band different groups have proposed different hypothesis, which are listed below:

1. Emission from excimer²¹⁹⁻²²²
2. Proton transfer and hydrogen bonding²²³⁻²²⁵
3. Exciplex with solvent^{226,227}
4. Pseudo-John Teller (PJT) Effect: Rehybridization of the donor^{228,229}
5. Rehybridization by Intramolecular Charge Transfer (RICT)^{230, 231}
6. Planar Intramolecular Charge Transfer (PICT)²³²⁻²³⁵
7. Twisted Intramolecular Charge Transfer (TICT)²³⁶

The brief discussion of all models can be found in the review article by Grabowski *et al.*²³⁶ Since in the present research TICT model has been used for some charge-transfer probes, it is discussed in detail below:

1.4.5 Twisted intramolecular charge transfer (TICT)

In 1973, Rotkiewicz, Grellmann and Grabowski²³⁷ suggested a dynamic relaxation of DMABN with internal twisting of the dimethylamino group, coupled with an electron transfer from the amino nitrogen to the far-away in-plane π_y^* orbital of the cyano or, in better agreement with later experiments, to the π_z^* orbital extending over the entire benzonitrile group. According to this hypothesis, the B band is assigned to a fluorescence, F_B originated from an approximately coplanar structure at the excited state, whereas the A band is assigned to a fluorescence, F_A originated from a charge transfer excited-state conformation with a highly twisted NMe_2 group, possibly perpendicular to the aromatic ring as shown in Figure 1.11. Figure 1.10 shows schematically the two fluorescing species, the B^* and the TICT state. A full electron transfer can appear in such an orthogonal conformation (Figure 1.10), because the system is decoupled with a zero overlap of the orbitals involved. Similar behavior was observed in numerous other Donor-Acceptor (D-A) compounds, which are structurally different from DMABN and the rotamerism accompanying the intramolecular separation of charges was assumed to be a rather widespread phenomenon.^{236,238} Thus, the term twisted intramolecular charge-transfer state was coined, abbreviated as TICT.

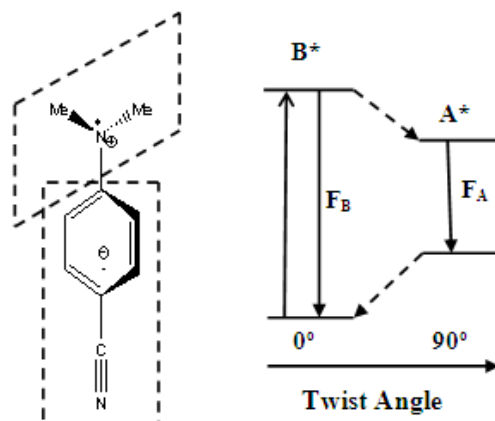


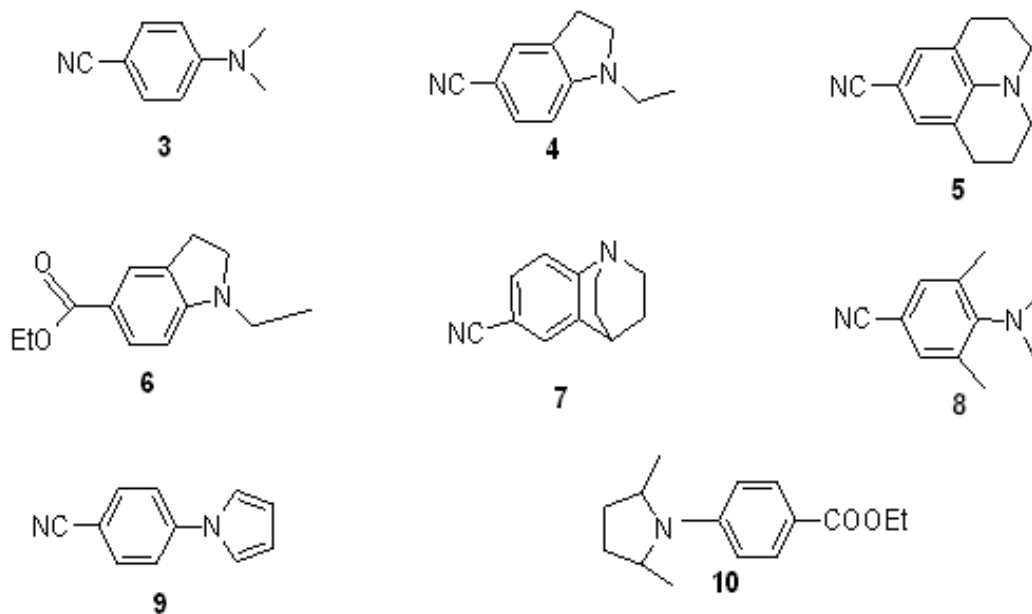
Figure 1.10: TICT model of DMABN



Figure 1.11: Model of a TICT excited state for a D-A molecule²³¹

Further, to support the hypothesis of twisted state, Grabowski, Rotkiewicz, & co-workers^{238,239} synthesized model compounds for DMABN where the dimethylamino group was rigidly held in the planar or perpendicular position, or where the planar arrangement of the dimethylamino group was increasingly hindered by ortho substituents in the benzene ring (Scheme 1.2). The bridged nitriles **4** and **5** as well as the ester **6** did not exhibit the A band in the fluorescence spectrum²⁴⁰ although they showed very similar absorption spectra. The fully perpendicular benzoquinuclidine **7**, on the other hand, showed the A band, but lacked the B band altogether. Visser *et al.*²³⁹⁻²⁴¹ synthesised similar compounds with more flexible bridges. From these experiments, Visser *et al.*²³⁹⁻²⁴¹ concluded that possibility of reaching an orthogonal conformation of the dimethylamino group is a must for the occurrence of the A band. Later, it was reported by different researchers²⁴²⁻²⁴⁵ that the B band of **3** was strongly quenched with the increase in the amount of polar solvent constituent in a mixture. In a highly polar medium, quenching of B band can be due to the greater stabilization of the TICT state giving A band. But certain exceptions were also reported. TICT emission in the gas phase is observed for **8** and **9**. The compound, **10** show TICT emission even in aliphatic

hydrocarbon solvents supporting the fact that exciplex formation is not responsible for highly Stokes-shifted fluorescence band.^{246,247}



Scheme 1.2: DMABN and other similar model compounds

1.4.6 Twisted geometry

The interesting feature of TICT state is twisted geometry.^{248,249} Flexible molecules spontaneously relax to a conformation with minimum interaction between locally excited (LE) and charge-transfer state while leads to full charge separation. This is called as “minimum overlap rule” supported by valence bond model.^{250, 251} This spontaneous twisting of planar molecules to the perpendicular conformation in the excited state is generally supported with different quantum chemical calculations. Soujanya *et al.*²⁵² reported the TICT phenomenon of DMABN using AM1 semi-empirical calculations. Later, a series of N,N-heterocyclic 4-aminobenzonitriles is investigated theoretically by a combination of density functional theory and multi-reference configuration interaction (DFT/MRCI).²⁵³ The different conformers of 9-(N,N-dimethylamino)anthracene (9-DMA) corresponding to the dual fluorescence have been reported by performing AM1 calculations.²⁵⁴ The fully twisted conformer is responsible for large Stokes-shifted CT type fluorescence, whereas they predicted an angle of 56° for the conformer responsible for normal Stokes-shifted fluorescence.²⁵⁴ Chakraborty *et al.*²⁵⁵ reported the potential energy curves along the two possible twisting coordinates (donor twisting and acceptor twisting) for the ground and excited states both in vacuo

and in polar aprotic solvent using time dependent density functional theory (TDDFT) and time dependent density functional theory including polarized continuum (TDDFT-PCM) model, respectively for the compound *N,N*-dimethylaminonaphthyl-(acrylo)-nitrile. They found that both the twisted paths, i.e., along the donor and acceptor groups, favor the formation of stable twisted excited state, but the twisting through acceptor path is energetically favourable than the donor path. Further, they have used the frontier molecular orbitals (FMO) to support the donor twisting rather than the acceptor twisting. The S_1 state is shown to be responsible for the TICT emission in these cases. Recently, Saha and co-workers¹⁹⁹ have reported the TICT fluorescence properties of trans-2-[4-(dimethylamino)styryl]benzothiazole (DMASBT). From their study, they have showed that S_1 state is responsible for the LE fluorescence, whereas S_3 state is responsible for the TICT fluorescence in DMASBT. Bangal *et al.*²⁵⁶ have reported the TICT fluorescence properties of 4-*N,N*-dimethylamino cinnamaldehyde (DMACA). They performed the AM1 calculation which is corroborated well with the large dipole moment change and the charge transfer in orthogonal position as found from experimental observations.

1.4.7 Kinetics of TICT

The following are the important factors which influence the rate of TICT formation.

(I) Effect of temperature: Lippert *et al.*²¹⁸ reported the effect of temperature on the stationary dual fluorescence intensities of DMABN. They have proposed a simple steady-state approximation results in the quantum yields as follows:

$$\frac{\phi_A}{\phi_B} = \frac{k_{fA} \bar{k}}{k_{fB} (k_A + \bar{k})} \quad (1.19)$$

where ϕ_A and ϕ_B are the quantum yields of A band and B band respectively,

k_{fA} and k_{fB} are the rates of radiative processes from A^* and B^* state, respectively

k_A is the rate of non-radiative process from A^* state,

\bar{k} is the rate for $B^* \rightarrow A^*$,

\bar{k} is the rate for $A^* \rightarrow B^*$

The ϕ_A/ϕ_B values were found to increase with increase in the temperature upto T_{\max} for compounds **9** and **10** (Scheme 1.2) in a polar solvent, n-butyl chloride.²⁵⁷ T_{\max} , is the point at which ϕ_A/ϕ_B ratio is maximum; dynamic equilibrium $B^* \rightleftharpoons A^*$ is established during the excited state lifetime. At temperatures less than T_{\max} , only the irreversible transition $B^* \rightarrow A^*$ takes place. In addition, increase in k_{fA} at 298 K compared to at very low temperature for DMABN and its analogues in different polar solvents are also reported.^{236,258} This increase in rate of TICT emission can be due to the thermal activation is linked with the strongly forbidden character of the emission from the zero vibrational level of the TICT state. At increased temperatures, the thermal population should lead to a more allowed emission from higher, non-totally symmetric vibrational levels vibronically mixed with other electronic states.²³⁶

(II) Effect of solvent: The extensively studied compound **3** possesses dual fluorescence in polar solvents. In addition to the derivatives of **3**, different compounds are also reported for dual fluorescence.^{254,259-261} The normal emission is vibronically resolved (structured), whereas the large Stokes-shifted band (F_A) is broad and structureless. The long wavelength fluorescence band (CT emission) generally undergoes a strong red shift with an increase of the polarity of the solvent.^{254,262} Chakraborty *et al.*,²¹⁷ Bangal *et al.*²⁶³ and Saha *et al.*²⁰⁴ reported the decrease in the quantum yield of TICT band in presence of protic solvents. This phenomenon is because of huge stabilization of TICT state in presence of protic solvents opens the non-radiative pathways for energy transfer.

(III) Effect of viscosity: The increase in the emission intensity of compound **3** and different TICT molecules in presence of viscous solvents are reported in literature.^{264,254} Mielniczak *et al.*²⁶⁵ have also reported the enhancement of emission intensity in TICT fluorescence of 4-(4-dimethylaminostyryl)pyridinium (DMASP) derivative. They explained that the enhancement of the TICT fluorescence intensity with the increase in the viscosity of the medium surrounding the fluorophore is due to the reduction of the non-radiative transitions induced by intramolecular reorientation and diffusional collisions with the solvent molecules.²⁶⁵ Further, they have used Debye–Stokes–Einstein (DSE) hydrodynamic model to justify their conclusion. Saha *et al.*²⁶⁶ noticed the enhancement of TICT fluorescence of DMASBT associated with bathochromic shift. They argued that the restricted rotation of already twisted group, $-N(CH_3)_2$ of DMASBT causes greater extent of donation of charge towards acceptor, thereby stabilizing the

TICT state, which results in large Stokes-shifted fluorescence. Saha *et al.*²⁶⁶ used the free-volume model to explain the high quantum yield of DMASBT in the highly viscous solvents at low temperature.

1.4.8 Intermolecular proton transfer reaction

Reorganization of electronic charge densities at different atoms of a molecule takes place during electronic transitions. In the ground and excited states the electronic charge densities at different atoms of the molecule may vary. Thus acidity or basicity of a molecule in the ground state may be different from that in the excited state. Protonation or deprotonation of a molecule is an extreme case of hydrogen bond donating or hydrogen bond accepting nature of a solvent. So the effect of protonation or deprotonation is similar as hydrogen bonding but greater in magnitude. Ground state acidity constant (pK_a) value can be estimated accurately from absorption spectroscopy.

Excited state acidity constant (pK_a^*) can be determined by the following three methods:

- Fluorometric titration method²⁶⁷
- Förster cycle method^{268, 269}
- Time-dependent fluorescence method²⁷⁰

In the present work, the Förster cycle method has been used, and discussed in method section of the next chapter.

1.4.9 Fluorescence intensity decay and lifetime

Time-resolved fluorescence spectroscopic methods give the information regarding the kinetics of the various processes involved in the deactivation of the excited state.¹⁷⁶ The fluorescence intensity decay is a plot of fluorescence intensity as a function of time. Fluorescence intensity decay, $I(t)$, for a system having single fluorophore is a single exponential and is given as Equation 1.20:¹⁷⁶

$$I(t) = I_0 e^{-t/\tau} \quad (1.20)$$

where, I_0 is the initial intensity and τ is the fluorescence lifetime. Some systems may have more than one fluorescent species and hence the fluorescence intensity decay has to be fitted with multi-exponential function instead of single exponential function. For multi-exponential function the fluorescence intensity decay equation will be such as:

$$I(t) = \sum_{i=0}^n a_i e^{-t/\tau_i} \quad (1.21)$$

where a_i and τ_i are i th pre-exponential factor (amplitude) and the lifetime in the multiexponential decay, respectively. The average lifetime $\langle \tau \rangle$ of the multiexponential decays is defined as in the Equation 1.22:

$$\langle \tau \rangle = \sum_i a_i \tau_i \quad (1.22)$$

The fluorescence lifetime is related to the radiative and the nonradiative rates. The relation between the fluorescence quantum yield (Φ) and fluorescence lifetime (τ) is given as Equation 1.23:

$$\tau = \frac{1}{k_r + k_{nr}} = \frac{\phi}{k_r} \quad (1.23)$$

where k_r and k_{nr} are the rate constants for radiative and non-radiative processes, respectively. The fluorescence quantum yield (Φ) is defined as the ratio of the number of photons emitted to the number of photons absorbed.

1.4.10 Fluorescence quenching

The process in which fluorescence intensity of the fluorophore decreases is known as fluorescence quenching.¹⁷⁶ The variety of processes e.g. excited state reactions, energy transfer, complex formation, collisions with similar and different molecules can lead to decrease in fluorescence intensity.

In general, fluorescence quenching is referred to a process where the electronic energy of the excited molecule is transferred to the translational energy of the quencher molecule. The fluorescence quenching can take place by two mechanisms:

1.4.10.1 Dynamic quenching

In dynamic quenching the quencher must diffuse to the fluorophore during its excited state lifetime. Upon contact, the fluorophore returns to the ground state, without emission of photon. It is described by the Stern-Volmer expression as given in Equation 1.24:

$$\frac{F_o}{F} = 1 + k_q \tau_o [Q] = 1 + K_{sv} [Q] \quad (1.24)$$

where F_o and F are the fluorescence intensities in the absence and in the presence of quencher, respectively. The concentration of quencher is given by $[Q]$, k_q is bimolecular

quenching rate constant, τ_o is the lifetime of the fluorophore in the absence of quenchers. K_{SV} is the Stern-Volmer quenching constant. In dynamic quenching since:

$$\frac{F_o}{F} = \frac{\tau_o}{\tau} \quad (1.25)$$

Stern-Volmer relation (Equation 1.24) can also be written as:

$$\frac{F_o}{F} = \frac{\tau_o}{\tau} = 1 + k_q \tau_o [Q] \quad (1.26)$$

where τ is the life time in the presence of quencher. A plot of $\frac{F_o}{F}$ or $\frac{\tau_o}{\tau}$ versus $[Q]$ yields a straight line passing through 1. From slope, one can calculate the value of Stern-Volmer quenching constant. k_q can be calculated from $\frac{K_{SV}}{\tau_o}$. Dynamic quenching is also called collisional quenching.

1.4.10.2 Static quenching

In case of static quenching a non-fluorescent complex is formed between the fluorophore and the quencher in the ground state. Because of this the concentration of the free emitting fluorophore decreases and thereby decreasing the fluorescence intensity. In this case¹⁷⁶ the Stern-Volmer equation is:

$$\frac{F_o}{F} = 1 + K_s [Q] \quad (1.27)$$

where K_s is the association constant of complex formation in the ground state. From the plot of $\frac{F_o}{F}$ versus $[Q]$, the slope gives the value of K_s . In either event the primary requirement is that the quencher and fluorophore must come in contact with each other.

Static and dynamic quenching can be distinguished (Figure 1.12). In the case of dynamic quenching, the excited state lifetime decreases with the increase of quencher concentration and $\frac{F_o}{F} = \frac{\tau_o}{\tau}$, whereas in the case of static quenching lifetime does not depend upon quencher concentration and $\frac{\tau_o}{\tau} = 1$. Moreover, dynamic quenching is diffusion controlled. With the increase of temperature the value of diffusion coefficient increases, thereby increasing the bimolecular quenching rate constant. On the other hand, increased temperature is likely to result in decreased stability of complexes, and thus decreasing the rate of static quenching.

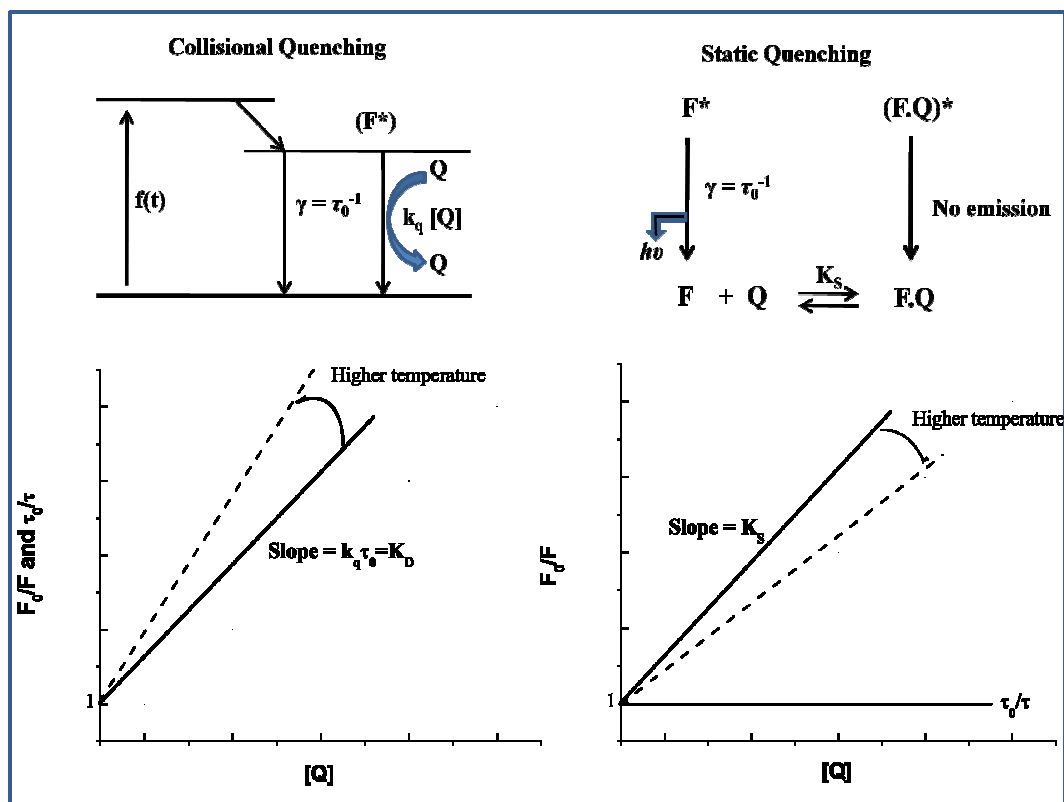


Figure 1.12: Comparison of dynamic and static quenching¹⁷¹

1.4.11 Fluorescence anisotropy

When fluorophore molecules are exposed to the polarized light, some of the fluorophores molecules are preferentially excited. The fluorescence emission from the excited fluorophores is also polarized. The extent of polarization of the fluorescence emission is described in terms of anisotropy (r). Fluorescence anisotropy measurement is important in biophysical and biochemical research in the sense that any factor which is responsible for change in size, shape, or segmental flexibility of a molecule will also change the observed anisotropy^{271,272} Fluorescence anisotropy measurements have been used to quantify protein denaturation and also for measurement of dynamics of proteins. Fluorescence anisotropy helps to find out the probable location of the probe in the microheterogeneous environment.^{176,273} Saha and co-workers found the steady-state fluorescence anisotropy measurement a very useful tool to monitor premicellar aggregates formation of conventional and gemini surfactants.^{274,275}

1.4.11.1 Steady-state fluorescence anisotropy

The steady-state fluorescence anisotropy¹⁷⁵ is defined as in Equation 1.28:

$$r = \frac{I_{VV} - GI_{VH}}{I_{VV} + 2GI_{VH}} \quad (1.28)$$

where I_{VV} and I_{VH} are the intensities obtained from the excitation polarizer oriented vertically and the emission polarizer oriented in vertical and horizontal orientations, respectively. The correction factor G is defined as:

$$G = \frac{I_{HV}}{I_{HH}} \quad (1.29)$$

where I terms refer to parameters same as mentioned above for the horizontal position of the excitation polarizer.

1.4.11.2 Time-resolved fluorescence anisotropy

In molecular assemblies the measurement of time dependent fluorescence anisotropy gives additional information about rotational relaxation of the fluorophores. In time domain, the sample is excited by a short pulse of polarized light and the time dependent parallel ($I_{\parallel}(t)$) and perpendicular ($I_{\perp}(t)$) components of the fluorescence are used to form the time-resolved fluorescence anisotropy, $r(t)$:

$$r(t) = \frac{I_{\parallel}(t) - I_{\perp}(t)}{I_{\parallel}(t) + 2I_{\perp}(t)} \quad (1.30)$$

To compensate the polarization biased of the detection system and monochromator efficiency, the above equation modified to Equation 1.31:

$$r(t) = \frac{I_{\parallel}(t) - GI_{\perp}(t)}{I_{\parallel}(t) + 2GI_{\perp}(t)} \quad (1.31)$$

where G represents the correction factor for the detector sensitivity to the polarization detection of emission.

For a single isotropic rotor, $r(t)$ decays with a single rotational correlation time (τ_r)¹⁷⁵

$$r(t) = r_o \exp\left(-\frac{t}{\tau_r}\right) \quad (1.32)$$

For more complicated system, $r(t)$ becomes multi-exponential:

$$r(t) = r_o \sum_i a_{ir} \exp\left(-\frac{t}{\tau_{ir}}\right) \quad (1.33)$$

where a_{ir} and τ_{ir} are the fractional contribution of total depolarization and rotational correlation times attributed to reorientational motion i , respectively. r_o is the fundamental anisotropy. In terms of Stoke-Einstein theory, τ_r is related to the medium by,

$$\tau_r = \frac{\eta V}{kT} = \frac{1}{6D} \quad (1.34)$$

where η is the viscosity of the medium, V is the molecular volume, k is the Boltzmann's constant, T is the absolute temperature and D is the rotation diffusion coefficient.

1.4.12 Solvation dynamics

A probe molecule whose dipole moment increases in the electronically excited state gives solvent polarity dependent fluorescence emission spectra. An instant dipole can be created by exciting such a molecule with light radiation. In the ground state the polar solvent molecules are randomly oriented around the weakly polar probe molecule. After photoexcitation the polar solvent molecules remain randomly oriented around the dipole because the solvent relaxation process is very much slower than the photoexcitation process. Subsequently the polar solvent molecules reorient around the newly created dipole. The process of reorientation of polar solvent molecules around the instantly created dipole after photoexcitation referred as solvation dynamics (Figure 1.13).

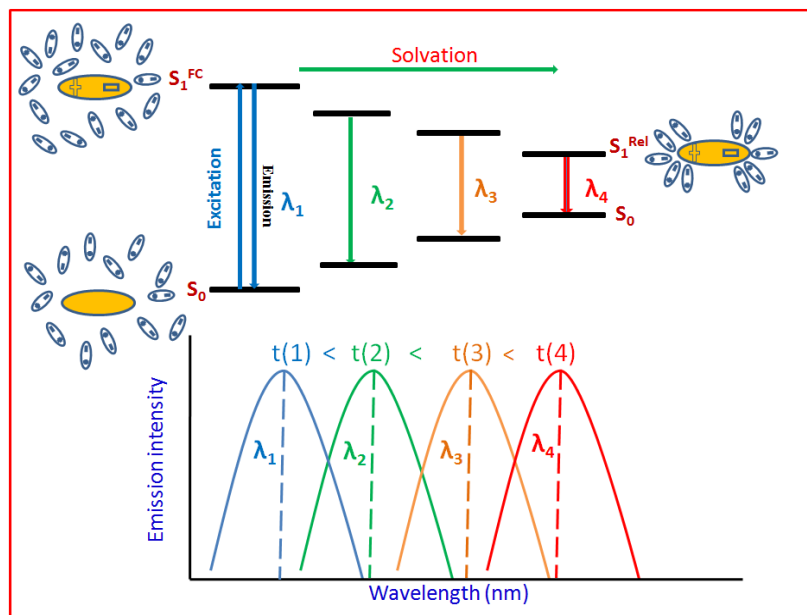


Figure 1.13: Schematic diagram showing mechanism of solvation dynamics

The solvation dynamics study is now a well known technique to get the idea about the response of the solvent molecule at the molecular level. The time taken for the solvent molecules on going from the Frank-Condon (F-C) excited state to relaxed excited state (R) is defined as the average solvation time $\langle\tau_s\rangle$. With increase in time the energy of the solute dipole decreases and the fluorescence maxima shifted towards longer wavelength. This phenomenon is termed as time dependent Stokes shift (TDSS).

In solvation dynamics process emission wavelength dependent decays has been observed. At shorter wavelength the fluorescence decays from the unsolvated dipole. At longer wavelength time resolved fluorescence spectra shows a growth in the decay followed by a slow decay with a negative pre-exponential factor. Thus the most fashionable evidences of solvation dynamics are TDSS and emission wavelength dependent time resolved fluorescence spectra (TRES). Time is needed for the F-state molecules to reach the R state. Even if the F and R states have the same intrinsic decay time, the long-wavelength decay will appear to be slower. Also, at the moment of excitation all the molecules are assumed to be in the F state. No molecules are in the R state until some relaxation has occurred. If the emission spectrum was observed immediately after excitation, then a blue-shifted or unrelaxed emission will be observed. If the time of observation is later, then more of the molecules will have relaxed to longer wavelengths, resulting in emission spectra that are progressively shifts to longer wavelengths at longer times. These emission spectra, representing discrete times following excitation, are called the time-resolved emission spectra (TRES). The solvation dynamics is monitored by the decay of solvent correlation function $C(t)$ and given in Equation 1.35:

$$C(t) = \frac{\nu(t) - \nu(\infty)}{\nu(0) - \nu(\infty)} \quad (1.35)$$

where, $\nu(t)$, $\nu(\infty)$ and $\nu(0)$ are the peak frequencies at time t , infinity and zero, respectively obtained from TRES.

1.4.12.1 Application of solvation dynamics

Water is an essential part for all living organism. In the biological assemblies, water molecule shows different characteristics than water in the bulk. Biological water differs markedly than bulk water in ultra slow and ultra fast time scale. Ultra slow

component of biological water is few orders of magnitude slower than fast component. Solvation dynamics technique has advantage over other techniques. Solvation dynamics study gives dynamics in the immediate vicinity of fluorescent probe. The application of solvation dynamics in presence of pure solvents and in different soft matter systems are discussed below.

1.4.12.1.1 Solvation dynamics in presence of pure solvents

Solvation dynamics of fluorescence active probe molecules in pure solvent have been studied by many research groups by using several techniques such as fluorescence up-conversion,^{276,277-280} three photon echo peak shift^{281,282} and Optical Kerr effect.^{283,284} Among all these techniques fluorescence up-conversion method is one of the most popular method to study the solvation dynamics in pure solvents. The solvation dynamics in case of pure water is very fast as compared to other polar solvents. Jimenez *et al.*²⁷⁶ reported a gaussian component of time constant of less than 50 fs and a slower biexponential decay with time constant 126 and 880 fs. The observed solvation process was bimodal in nature for pure water with time constant of 160 fs (33%) and 1200 fs (67%) using the probe 7-(dimethylamino) coumarin-4-acetate and 250 fs (50%) and 960 fs (50%) using the probe Coumarin 343.^{285,286} Vajda *et al.*²⁸⁷ also reported the bimodal nature of water using Coumarin 102 as a probe and the observed solvation time was 310 fs (74%) and 50 ps (26%). Fleming *et al.*²⁸¹ reported that the major part of the solvation occurs within 30 fs using three photon echo peak shift method. The solvent relaxation time of tryptophan in pure water is bimodal with time constant of 180 fs (20%) and 1.1 ps (80%).²⁸⁸ Solvent relaxation time of 1-anilinonaphthalene-8-sulfonate is bimodal with time constants 185 fs (22%) and 1.2 ps (78%).^{289,290}

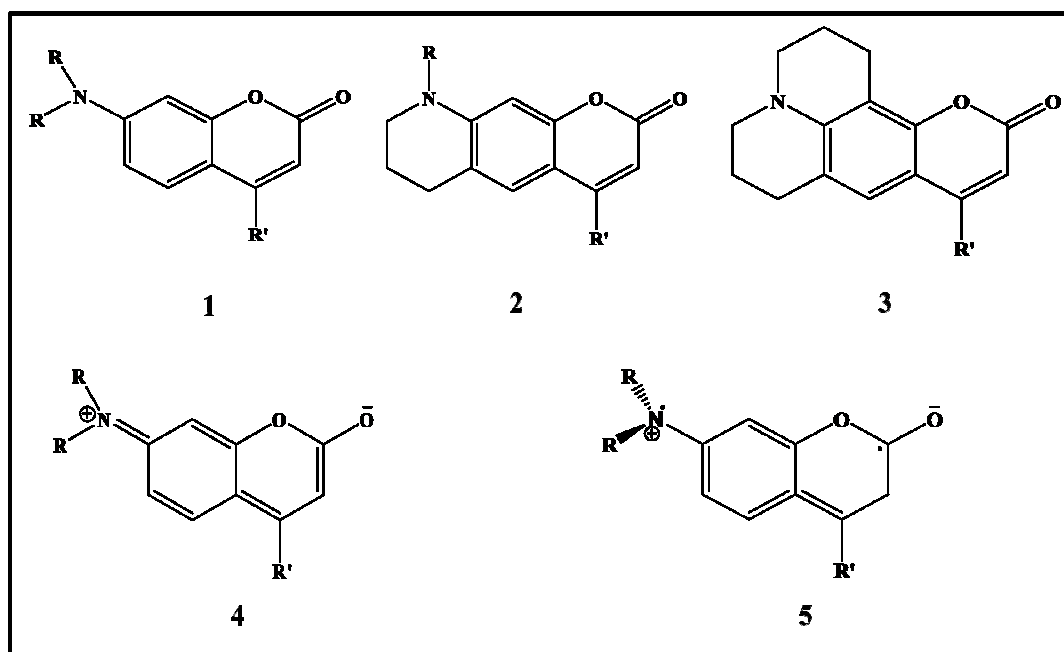
Horng *et al.*²⁹¹ reported the solvation time of Coumarin-153 in methanol was within 280 fs. The average solvation time of Coumarin-152 and anionic form of Coumarin-343 were 6.2 and 8.3 ps, respectively.^{292,293} Solvation time in methanol was also reported using the probes, 2-(p-dimethylaminostyryl) pyridylmethyl iodide and 4-dicyanomethylene-2-methyl-6-(p-dimethylamino) styryl)-4H-pyran.^{294,295} The solvation dynamics study has also been carried out in acetonitrile using several fluorescence probes such as Coumarin-480, Coumarin-311, Coumarin-153, LDS-750, thiopyrilium dye, IR 1061, cyanine dye, and IR 1048.²⁹⁶⁻³⁰⁰

1.4.12.1.2 Solvation dynamics in microheterogeneous systems

Solvation dynamics have been studied in various microheterogeneous systems like micelles, mixed micelles, RMs, vesicles etc. These self organized molecular assemblies have resemblance with biological lipid membranes. Solvation dynamics in these systems is found to be many folds slower than that in pure solvents. Solvation dynamics in presence of some conventional surfactants has been studied by Bhattacharyya and co-workers.³⁰¹ They reported the bimodal nature of solvation dynamics. To explain the bimodal behavior of solvation dynamics in presence of microheterogeneous systems, Bagchi *et al.*³⁰² proposed a dynamic exchange model based on free and bound water species and the strength of the hydrogen bonds. According to them dynamic equilibrium between the “free” and “bound” water molecules are responsible for the bimodal solvation dynamics. The “bound” water molecules are responsible for slower component. However, comparatively “free” water molecules are responsible for fast solvation. Sarkar and co-workers have studied the solvation dynamics in various systems e.g., micelles of Brij 35 and Brij 58,³⁰³ CTAB micelles,³⁰⁴ the mixed micelles of surfactants (TX-100, Tween 80 and CTAB) with bile salt,^{305,306} and also the mixed micelles of different cationic conventional surfactants,³⁰⁷ and ionic liquids.³⁰⁸ Samanta and co-workers have reported the dynamics of different types of Coumarins in various types of room temperature ionic liquids.^{309,310} Shirota *et al.*^{311,312} have demonstrated the effect of surfactant concentration and the effect of solvent isotope on the dynamics of Coumarin-102 and Coumarin-153. They have also reported the solvation dynamics in the micelles of cationic and anionic surfactants. They have found that the solvation dynamics in the aqueous micelles of anionic surfactant is slower than that in the aqueous micelles of cationic surfactant. The slow solvation dynamics in anionic micelles as compared to that in cationic micelles is due to stronger hydrogen bonding interaction between the water molecule and headgroup the former than that in the latter. Saha *et al.* studied the solvation dynamics in presence of gemini surfactants.³¹³ Effect of hydroxyl group present at spacer group of gemini surfactant on solvation dynamics has been monitored. Solvation dynamics becomes slow with increasing the number of hydroxyl group in the spacer part of gemini surfactant. The increase in the solvation time could be due to the formation of hydrogen bonds between water molecules and hydroxyl group(s) of spacer group which results in protection of the probe molecule from its contact with some of the water molecules. Moreover, hydrogen bonding interactions between hydroxyl group(s) of the spacer group and water molecules may restrict the mobility of water molecules as well.

Levinger *et al.*³¹⁴ studied the solvation dynamics in RMs of AOT and conventional surfactants. Sarkar *et al.*^{315,316} studied the solvation dynamics in aqueous and nonaqueous RMs. They reported that the solvation dynamics depends upon the water and methanol content in RMs but very less depends upon the amount of acetonitrile. Dependency of solvation dynamics on water and methanol contents in RMs is due to the presence of hydrogen bonding network.

For the study of solvation dynamics selection of fluorescence active probe is very important. For this purpose various 7-amino coumarin probe molecules are used. Coumarin dyes are the well known laser dyes which emit a strong fluorescence with significant charge transfer (CT) character.^{317,318} Coumarins are the derivatives of 1,2-benzopyrone. Chemical structure of some coumarin molecules are shown by scheme 1.3.



Scheme 1.3: Structure of Coumarin derivatives

One of the basic requirements for the study of solvation dynamics by using fluorescence molecules is that these molecules should have nonpolar or weakly polar ground state and highly polar excited state. 7-amino coumarin dyes meet all these basic requirements and hence they are efficient probe for such study. Coumarin-153 is an ideal solvation probe. The ground state of Coumarin-153 is polar with a measured dipole moment of 6.55 ± 0.01 D.³¹⁹ The $S_0 \rightarrow S_1$ transition leads to the S_1 dipole

moment between 14.2 D and 16.0 D, depending on solvents.³²⁰ Furthermore, its S_1 state is well separated from other excited singlet states and there is no report of occurrence of any excited state reaction in most of the solvents. Due to such properties, Coumarins are used for solvation dynamics studies.

1.5 Scope of the present research work

Intramolecular charge transfer (ICT) fluorescence molecules have many applications in photoelectronic devices, chemical sensor, nonlinear optical properties, probing molecule induced nanotubular suprastructures, and photobiological process. The fluorescence properties of these types of molecules change with changing the surrounding environment. These molecules are very sensitive towards the polarity and viscosity of the environment. Surfactant assemblies (micelles) are the simple biomimicking system. Characterization of micelles in terms of determination of micropolarity and microviscosity of the environment around drug or probe molecules deserve obvious importance. Many cellular functions are related to the viscosity of the environment, and the alteration in cell membrane viscosity is well known to be responsible for several diseases. The precise measurements of viscosity in biological systems, and in particular real-time measurements of viscosity changes on a microscopic scale, require the development of methods that are applicable at the molecular level. Therefore, determination of viscosity changes on a microscopic scale is a challenge. Although, some fluorescent probe molecules have been used for this purpose, their fluorescence properties are not that much sensitive to the microviscosity and sometimes they are insensitive to the polarity change of the environment. Therefore, it is imperative to find out probe molecules, whose fluorescence properties will be dependent on both viscosity and polarity of medium. TICT probes are expected to serve this purpose very well. Saha *et al.*³²¹⁻³²³ have studied the microenvironmental properties of various systems using ICT properties of *trans*-2-[4-(dimethylamino)styryl]benzothiazole DMASBT. It has been found that their fluorescence properties are very much sensitive towards the polarity and viscosity of microenvironment around them.^{324, 325} In the present thesis, we have explored TICT fluorescence properties of *para*-N,N-dimethylaminocinnamaldehyde (DMACA) and another TICT molecule *trans*-2-[4-(N,N-dimethylaminostyryl)]pyridine (2- DMASP).

Moreover, working with DMACA with its very simple linear and small structure is expected to have low possibility of perturbation of native size and shape of micelles.

Gemini surfactants are special class of surfactants in which a molecule composed of two hydrophobic tail groups and two hydrophilic headgroups covalently connected by a spacer group. These surfactants have attracted the attention of various academic research and industrial applications for their number of surface-active properties better than those of corresponding conventional surfactants have. They have much lower *cmc*, a high efficiency in reducing the surface/interfacial tension, and very unusual aggregation morphologies. The micellar systems (of gemini surfactants) have similarity to bilayer lipid membrane, enzymes and other biomimicking systems, and have applications in synthesis of nanoparticles, pharmaceuticals, food industries and also in cosmetic science. A detailed study on the aggregation behaviour of available as well as newly synthesised gemini surfactants are very important. The spacer group of the gemini surfactant plays very important role in the formation of micelles. The nature of the spacer group may provoke to the formation of premicellar aggregates e.g., hydroxyl group substituted spacer group. Although lot of research has been done on the effect of spacer group on the aggregation behaviour of gemini surfactants, but still such study is mysterious for colloid science researchers.

Mixed micellar systems have received a lot of attention because of their capacity to serve as good models for the study of molecular interactions in complex supramolecular aggregates to mimic the behavior of biological systems and functions. These systems also provide better performance characteristics in their technological applications than those consisting of only one type of surfactant. The synergistic effect of surfactant mixtures is used in detergent industries and in health-care industries.^{50,326,327} For example, it is found that the critical micelle concentration (*cmc*) for surfactant mixtures is often lower than that of one of the individual components, which exhibits lower skin irritation than that exhibited by neat surfactants.³²⁸

Some of the surfactants have very high surface activity but at the same time they are costly. A large scale application of a single surfactant is not economical from the industry point of view due to the high cost of their mass production and purification. Therefore, to get almost equal activity, mixing of a more surface active and expensive surfactant with a comparatively less surface active and cheaper surfactant in different

proportions, is one of the shortest ways. To meet these requirements, gemini and conventional mixed surfactant systems would be the best choice. Mixed micellization behavior of gemini surfactants with the conventional surfactants strongly dependent on the nature of the spacer group of the gemini surfactants and the chain lengths of gemini as well as conventional surfactants. The change in mixed micellization behavior with the variation of chain length of simple alkyl chain of the spacer groups of gemini surfactants are reported in the literature. Work with the substituted spacer and the variation in the substitution of the spacer of gemini surfactants are rare.

Micellar and RMs systems are found to have resemblance with biological systems as lipid membranes. The functions performed by the biological membranes have encouraged the researchers to look for a simple biologically mimicking systems, which can mimic, at least some of the physicochemical properties of the biological membrane architecture. In many man made and naturally occurring systems water is not present as a pure bulk liquid. In these systems usually water interacts with the interface. Micelles and RMs provided a simple model system in which to study how the interfacial complexity affects the properties of water near an interface. The water molecule plays a central role in biological systems. The properties of water molecules in presence of self-organized assemblies and macromolecules (also known as bound water) are found to be different from that of ordinary bulk water (free water). Studies have showed that water molecules present inside the pool of the RMs not only behave like bulk water, but also behave like bound water molecules. There are several techniques such as NMR relaxation dispersion,³²⁹ dielectric relaxation³³⁰ and solvation dynamics available to study the properties of free and bound water molecules in various systems of molecular assemblies. Due to higher sensitivity towards time and length scale, solvation dynamics has been found to be one of the best techniques. So there are several reports on the study of solvation dynamics in the micelles of conventional surfactants. After having a vast survey of literature, we realized that the micelles and mixed micelles of gemini surfactants with conventional surfactants are equally very interesting systems to study the solvation dynamics of water molecules. Moreover, the effect of spacer chain length of gemini surfactant on solvation dynamics enhanced the interesting features of gemini surfactants. Effect of protein denaturing substance on solvation dynamics in presence of gemini surfactant also very important. The mechanism of protein denaturation by urea is still debatable topic. Two different mechanisms are offered regarding urea induced denaturation of protein. Some of the

studies show that urea act as a water structure breaker and some other studies show that urea act as a water structure maker. Considering the importance of urea in protein denaturation process and as a non linear optical material it would be worth to elucidate the dynamical feature of urea.

Nearly all aspects of biological processes are dependent on the three dimensional structure of protein. Interaction of surfactants with protein can lead to denaturation and conformational change of protein. These interactions are important in a wide variety of industrial, biological, pharmaceutical, and cosmetic systems and also contribute to the understanding of the action of surfactants as solubilizing agents to recover proteins from inclusion bodies and in the renaturation of the proteins produced in the genetically engineered cells via the artificial chaperone protocol. Denaturing effect of surfactant on protein happened at very low concentration as compare to other denaturing agents like urea, guanidine hydrochloride etc. The binding behavior surfactant and protein depends upon the features of surfactant. Many investigations have been focused on the interaction between monomeric surfactants and protein. Few reports are available on the unique behavior of the interaction between protein and gemini surfactants.¹⁷¹⁻¹⁷⁴ It is well known that variation in the spacer part of gemini surfactants leads to great differences in the surfactants properties. Study on interaction of gemini surfactants with difference in the spacer group with BSA is expected to be quite interesting.

Chapter 2 deals with the materials and methods used in the present research work.

Chapter 3 describes the photophysical characterization of trans-2-[4-(N,N-dimethylamino)styryl]pyridine (2-DMASP). Effects of various polar and nonpolar solvents on ground and excited states have been reported. Prototropic equilibria of 2-DMASP at ground and excited state have been studied. The different possible pathways for the twisting of 2-DMASP such as donor twisting and acceptor twisting are carried out with the help of time dependent density functional theory (TD-DFT) and the possible pathway responsible for TICT fluorescence has been identified. The photophysical characterization of the dye, 2-DMASP shows that TICT emission properties of 2-DMASP is highly sensitive to the polarity of the environment around it. Hence, it is useful to probe aggregation behavior of surfactants. Various physical properties of

surfactant aggregates depend upon the counterion of the surfactant molecules. Wang *et al.*³³¹ studied the various thermodynamics properties of hexadecyltrimethylammonium surfactants. Microenvironmental properties (microviscosity and micropolarity) of micelles of CTAX (X= Br⁻, SO₄²⁻, NO₃⁻, and PTSA) have not been studied so far. 2-DMASP is chosen to characterize micellar systems due to the following features of it:

- 2-DMASP is neutral and hydrophobic. The absence of permanent charge eliminates the ionic interaction of the probe with the surrounding environment.
- 2-DMASP is potential in comparison to other neutral probe as pyrenes because of its dual fluorescence properties are very much sensitive to the polarity and the viscosity of the medium.
- Stokes shift of 2-DMASP correlate very well with static polarity of the environment, in terms of an empirical solvent polarity parameter, $E_T(30)$.
- 2-DMASP exhibits measurable fluorescence intensities in both polar and non-polar solvents which make it a potential polarity sensor.
- 2-DMASP is also sensitive to the viscosity of its environment. The steady-state anisotropy of the 2-DMASP correlates very well with varying compositions of glycerol-water mixture.

Hence, it is observed that 2-DMASP is highly sensitive to probe the change in polarity as well as viscosity of the microenvironments and it can be a potential microsensor for biomimicking as well as real biological systems.

Chapter 4 deals with the the study of mixed micellization behavior of conventional surfactants (CTAB/TTAB and DTAB) with two gemini surfactants, Gemini-1 and Gemini-2 in pure water. Mixed surfactant systems have various industrial applications. The aim of this study is to reveal the effect of hydrocarbon tail length of conventional surfactants and spacer group of gemini surfactants on the mixed micelle formation. The study has been carried out by conductivity measurements and these results are further compared with the data obtained from fluorescence method. The experimental data have been analyzed by different theoretical models proposed by Clint,³³² Rubingh,³³³ Rodenas³³⁴ and Motomura.³³⁵ Various thermodynamic properties have been calculated for the pure and mixed surfactants systems. Conductivity measurements have been done to determine the cmc of all the mixed surfactant systems at different bulk compositions. The cmc values were also determined by fluorescence

method to avoid the criticism. In almost all the reported studies, pyrene fluorescent probe molecule is used for the determination of the cmc and the micropolarity of microheterogeneous systems.³³⁶ In the present study, we have used as an alternate a fluorescent probe molecule DMACA. The fluorescence properties of DMACA are very much sensitive to the polarity and the viscosity of microenvironment around it.³²⁴ The micropolarity and microviscosity of mixed micellar systems as well as cmc have been estimated probing DMACA. Instead of using two different probes, pyrene and DPH for the determination of micropolarity and microviscosity, respectively, in the present work a single probe molecule has been explored for both the purposes. Moreover, DMACA having a small, linear structure as compared to that of pyrene is expected to impose less perturbation of native size and shape of micelles. Knowing the fact that the fluorescence properties of DMACA, are very much sensitive to the polarity and viscosity of microenvironment around it,^{324, 325} the micropolarity and the microviscosity of mixed micelles have been estimated probing DMACA. Binding constants of DMACA with micelles have been determined.

Chapter 5 demonstrates the solvation dynamics and rotational relaxation of Coumarin 153 (C-153) in the micelles of a series of cationic gemini surfactants, 12-*s*-12, 2Br⁻ (*s* = 3, 4, 6, 8, 12) containing a hydrophobic polymethylene spacer with different chain length. The motivation of this study with these gemini surfactants is to understand how the time constant of solvation process is affected with varying the chain length in the spacer group. Present work also demonstrates the effect of chain length of spacer group of gemini surfactants on the bi-modal behavior of rotational relaxations of C-153. This study provides with better picture about the microenvironment around the probe. To our knowledge, this kind of study on the effects of chain length of spacer groups of gemini surfactants on solvation dynamics and rotational relaxation at the Stern layer has not been reported. Micelles having resemblance with biological lipid membranes, and in particular gemini surfactants being more surface active than their counterpart conventional surfactants, the present work has obvious importance. Spacer chain length has also effect on counter ion binding, we want to see the effect of this phenomenon on solvation dynamics because counter ions also contribute to the solvation dynamics. Since the aggregation behavior of gemini surfactants can be tuned by changing the chemical nature of spacer group, the study of dynamics of water molecules and rotational

relaxation of a molecule at the Stern layer or micelle-water interface has practical and fundamental importance.

Chapter 6 deals with the study on solvation dynamics and rotational relaxation of C-153 in mixed micelles of non-ionic surfactant, Triton X-100 and a series of cationic gemini surfactants, 12-*s*-12,2Br⁻ with varying polymethylene spacer chain length (*s* = 3, 6, 8, 12) at different bulk mole fractions of a surfactant. Mixture of surfactants has many fundamental and industrial applications. Mixed surfactants have been received much more attention because mixed surfactant systems provide better performance characteristics than those consisting of only one type of surfactant. Mixed surfactant systems of cationic gemini surfactants and nonionic conventional surfactants show better performance properties than the micelles of individual surfactants. Owing to ubiquitous applications of mixed surfactant systems of gemini surfactant and nonionic monomeric surfactant, the study to find new insight of the properties of these mixed surfactant systems is very essential for practical and fundamental importance. Importance of the present study is to demonstrate simultaneously how the solvation dynamics and rotational relaxation in a nonionic micelles change with increasing composition of a gemini surfactant and how this change depends on chain length of spacer group of gemini surfactants. Results obtained from the present study demonstrate the physicochemical properties of mixed micelles which could be useful for potential applications of mixed micelles in biology and industry.

Chapter 7 deals with the study of effect of urea on solvation dynamics and rotational relaxation of C-480 in aqueous micelles of gemini surfactant, 12-4-12. The hydrogen bonding network of water molecules originate many unusual behavior of liquid water. Presence of urea in water urea mixture affects the hydrogen bonding structure of water. Frank model suggests that urea act as a structure breaker of water.³³⁷ Neutron scattering study does not show any evidence of breakup of the pure water cluster with the addition of urea.³³⁸ Two different mechanisms have been proposed to explain the urea action on aqueous solvent: (a) an indirect mechanism in which urea acts as a water “structure breaker” facilitating the solvation of nonpolar solutes, (b) a direct mechanism whereby urea participates in the solvation of hydrophobic solutes in water by replacing some water molecules in the hydration shell of solute.³³⁹⁻³⁴² In the present work effect of urea on water dynamics in presence of a cationic gemini surfactant has been investigated.

Cmc of gemini surfactant increased in presence of urea. Micropolarity around C-480 has no effect in presence of urea. Microviscosity value decreased in presence of urea.

Chapter 8 explains the study on solvation and rotational relaxation with some photophysical properties of coumarin 490 (C-490) in the presence of (12-4-12)/cyclohexane/*n*-pentanol/water reverse micelles (RMs). RMs are one of the simplest biological membrane mimetic systems. Reverse micelles afford the opportunity of examining molecules with various states of hydration, simulating situations present in water restricted environments prevailing the self-reproduction in supramolecular systems. Such model systems are able to capture a number of essential features of the biological membranes avoiding much of their complexities. Zhao *et al.*¹³⁵⁻¹³⁷ reported some physical properties of gemini surfactant RMs. Photophysical properties of C-490 are explored in the RMs of gemini surfactant. Probe molecule, C-490 resides in the water pool of RMs. A lesser extent of hydrogen bonding interactions between –OH group of pentanol and C-490 molecule takes place at the interface of present RMs as compared to RMs of reported conventional cationic surfactants. C-490 migrates to the water pool with increasing content of water molecules. As a result of this, the steady-state fluorescence properties, rotational relaxation and solvation dynamics results depend on the water loading of RMs unlike RMs of conventional cationic surfactants. Because of the same reason, the solvation dynamics in gemini surfactant RMs is one order of magnitude faster as compared to RMs of conventional cationic surfactants. The faster solvation dynamics in gemini surfactant RMs as compared to reported AOT RMs is due to the absence of hydrogen bonding interaction between water molecules and quaternary ammonium headgroups of gemini surfactant. The polarity of the surrounding microenvironment is found to have very little effect on the rates of non-radiative processes in the water pool of gemini surfactant RMs. The rates of non-radiative processes in the present RMs are found to be higher than that in reported AOT RMs.

Chapter 9 deals with the study of interaction of cationic gemini surfactants (12-4-12 and 12-4(OH)-12) with BSA. Proteins are very important in living organism and take part in almost all life processes. Proteins can bind with various types of molecules. Interactions of protein with surfactants have been studied for many years because mixtures of protein and surfactant have many important applications in biosciences, food and cosmetics, detergents and biotechnological processes. Interaction of conventional

surfactant with BSA has been reported. Gemini surfactant has many superior properties than a conventional surfactant. In this study, we have demonstrated the effect of spacer group of gemini surfactant on interaction with BSA. Gemini surfactant 12-4(OH)-12 unfolds the BSA more efficiently than 12-4-12. The binding isotherm of the gemini surfactants on BSA has been constructed. The binding isotherm display characteristic regions with increasing gemini surfactants concentration. The excited singlet state life time of tryptophan residue of BSA vary with the concentration of the gemini surfactants. It shows a systematic binding of gemini surfactant with BSA. Interaction of unfolded BSA with gemini surfactants also has been studied. Gemini surfactant 12-4-12 interacted with the unfolded BSA to greater extent than 12-4(OH)-12.

References:

- (1) M. Jones, J. Leroux, *Eur. J. Pharm. Biopharm.* **1999**, *48*, 101.
- (2) V.P. Torchilin, *J. Controlled Release* **2001**, *73*, 137.
- (3) A.N. Lukyanov, V.P. *Adv. Drug Deliv. Rev.* **2004**, *56*, 1273.
- (4) J. Zeng, X. Xu, X. Chen, Q. Liang, X. Bian, L. Yang, X. Jing, *J. Controlled Release* **2003**, *92*, 227.
- (5) E. Carretti, L. Dei, P. Baglioni, *Langmuir* **2003**, *19*, 7867.
- (6) C.A. Bunton, L. Robinson, J. Schaak, M.F. Stam, *J. Org. Chem.* **1971**, *36*, 2346.
- (7) F. Devinsky, L. Masarova, I. Lacko, *J. Colloid Interface Sci.* **1985**, *105*, 235.
- (8) H. N. Patrick, G. G. Warr, in *Specialist Surfactants*, Ed. I. D. Robb, Blackie Academic & Professional, New York, 1997.
- (9) F.M. Menger, C.A. Littau, *J. Am. Chem. Soc.* **1991**, *113*, 1451.
- (10) R. Zana, Y. Talmon, *Nature* **1993**, *362*, 228.
- (11) Y. Zhu, A. Masuyama, M. Okahara, *J. Am. Oil Chem. Soc.* **1991**, *68*, 268.
- (12) Y.P. Zhu, A. Masuyama, Y. Kobata, Y. Nakatsuji, M. Okahara, M. J. Rose, *J. Colloid Interface Sci.* **1993**, *158*, 40.
- (13) R. Zana, M. Benrraou, R. Rueff, *Langmuir* **1991**, *7*, 072.
- (14) R. Zana, *J. Colloid Interface Sci.* **2002**, *246*, 182.
- (15) F.M. Menger, V.A. Migulin, *J. Org. Chem.* **1999**, *64*, 8916.

-
- (16) F.M. Menger, B.N.A. Mbadugha, *J. Am. Chem. Soc.* **2001**, *123*, 875.
- (17) L.D. Song, M.J. Rosen, *Langmuir* **1996**, *12*, 1149.
- (18) J.H. Mathias, M.J. Rosen, L. Davenport, *Langmuir* **2001**, *17*, 6148.
- (19) R. Oda, I. Huc, S.J. Candau, *Chem. Commun.* **1997**, 2105.
- (20) R. Oda, I. Huc, M. Schmutz, S.J. Candau, F.C. MacKintosh, *Nature* **1999**, *399*, 566.
- (21) F.L. Duivenvoorde, M.C. Feiters, S.J. van der Gaast, J.B.F.N. Engberts, *Langmuir* **1997**, *13*, 3737.
- (22) M. Johnsson, A. Wagenaar, J.B.F.N. Engberts, *J. Am. Chem. Soc.* **2002**, *125*, 757.
- (23) M. J. L Castro, J. Kovensky, A. F. Cirelli, *Langmuir* **2002**, *18*, 2477.
- (24) A. X. Pinazo, W. L. Perez, M. R. Infante, E. I. Frances, *Langmuir* **1999**, *15*, 3134.
- (25) J. Eastoe, P. Rogueda, A. M. Howe, A. R. Pitt, R. K. Heenan, *Langmuir* **1996**, *12*, 2701.
- (26) M. Johnsson, A. Waganaer, M.C.A. Stuart, J. F. N. Engberts, *Langmuir* **2003**, *19*, 4609.
- (27) F. M Menger, J. S. Keiper, V. Azov, *Langmuir* **2000**, *16*, 2062.
- (28) T. Tatsumi, W. Zhang, T. Kida, Y. Nakatsuji, D. Ono, T. Takeda, I. Ikeda, *J. Surfactants Detgts.* **2001**, *4*, 279.
- (29) T. Tatsumi, W. Zhang, T. Kida, Y. Nakatsuji, D. Ono, T. Takeda, I. Ikeda, *J. Surfactants Detgts.* **2000**, *3*, 167.
- (30) Alami, E., K. Holmberg, and J. Eastoe, *J. Colloid Interface Sci.* **2002**, *247*, 447.
- (31) D. Jurasin, I. Habus, N.F. Vincekovic, *Colloids and Surfaces A: Physicochem. Eng. Aspects* **2010**, *368*, 119.
- (32) M.A. Llies, W.A. Seitz, B.H. Johnson, E.L. Ezell, A.L. Miller, Thompson, E.B. A.T. Balaban, *J. Med. Chem.* **2006**, *49*, 3872.
- (33) B.C. Stephenson, C.O. Rangel-Yagui, A. Pessoa, L.C. Tavares, K. Beers, D. Blankschtein, *Langmuir* **2006**, *22*, 1514.
- (34) E.N.K. Sakai, Y. Takamatsu, S.C. Sharma, K. Torigoe, T. Yoshimura, K. Esumi, H. Sakai, M. Abe, *J. Oleo Sci.* **2008**, *57*, 423.

-
- (35) M. Macian, J. Seguer, M. R. Infante, C. Selve, M. P. Vinardell, *Toxicology* **1996**, *106*, 1.
- (36) E. Oblak, A. Gamian, R. Adamski, S. Ulaszewski, *Cell. Mol. Biol. Lett.* **2010**, *15* 215.
- (37) J. Luczynski, R. Frackowiak, A. Wloch, H. Kleszczynska, S. Witek, *Cell. Mol. Biol. Lett.* **2013**, *18*, 89.
- (38) N. Azum, M.A. Rub, A.M. Asiri, A.A.P. Khan, A. Khan, *J. Surfact. Deterg.* **2013**, *16*, 77.
- (39) W. Wang, Y. Han, M. Gao, Y. Wang, *Cryst. Eng. Comm.* **2013**, *15*, 2648.
- (40) S.D. Wettig, A.O. Kamel, *J. Thermodyn. Catal.* **2013**, *4*, 1.
- (41) L. Liu, X. Fei, S. Zhu, L. Yu, B. Zhang, *Langmuir* **2013**, *29*, 5132.
- (42) J. Luczak, C. Jungnickel, M. Markiewicz, J. Hupka, *J. Phys. Chem. B* **2013**, *117*, 5653.
- (43) M. Li, C. Zhang, X.L. Yang, H.B. Xu, *RSC Advances*, **2013**, *3*, 16304.
- (44) F.M. Menger, C.A. Littau, *J. Am. Chem. Soc.* **1993**, *115*, 10083.
- (45) A. Pinazzo, X. Wen, L. P´erez, M.R. Infante, E.I. Franses, *Langmuir* **1999**, *15*, 3134.
- (46) N. Hattori, H. Hirata, H. Okabayashi, C.J. O’Connor, *Colloid Polym. Sci.* **1999**, *277*. 361.
- (47) L. Grosmaire, M. Chorro, C. Chorro, S. Partyka, R. Zana, *Colloid Polym. Sci.* **2000**, *115*, 31.
- (48) R. Zana, *Adv. Colloids Interface Sci.* **2002**, *97*, 205.
- (49) D. Attwood, A.T. Florence, *Surfactant systems*, Chapman and Hall, London, **1985**.
- (50) M.J. Rosen, *Surfactants and Interfacial Phenomenon*, Wiley Interscience, New York, **1978**.
- (51) R. Zana, in *Gemini Surfactants: Synthesis, Interfacial and Solution-Phase Behavior and Applications*, Marcel Dekker, Inc, New York, **2004**.
- (52) R. Oda, I. Huc, S. J. Candau, *Chem. Commun.* **1997**, 2105.
- (53) R. Oda, I. Huc, J.C. Homo, B. Heinrich, M. Schmutz, S. Candau, *Langmuir* **1999**, *15*, 2384.

-
- (54) R. Oda, I. Huc, D. Danino, Y. Talmon, *Langmuir* **2000**, *16*, 9759.
- (55) I. Huc, R. Oda, *Chem. Commun.* **1999**, 2025.
- (56) Y. Han, Y. Wang, *Phys. Chem. Chem. Phys.* **2011**, *13*, 1939.
- (57) Y.P. Zhu, A. Masuyama, M. Okahara, *J. Am. Oil Chem. Soc.* **1990**, *67*, 459.
- (58) Y.P. Zhu, A. Masuyama, Y.I. Kirito, M. Okahara, *J. Am. Oil Chem. Soc.* **1991**, *68*, 539.
- (59) Y.P. Zhu, A. Masuyama, Y.I. Kirito, M. Okahara, M. Rosen, *J. Am. Oil Chem. Soc.* **1992**, *69*, 626.
- (60) F.L. Duivenvoorde, M.C. Feiters, S.J.V. Gaast, J.B.F.N. Engberts, *Langmuir* **1997**, *13*, 3737.
- (61) T. Lu, F. Han, G. Mao, G. Lin, J. Huang, X. Huang, Y. Wang and H. Fu, *Langmuir* **2007**, *23*, 2932.
- (62) X. Huang, Y. Han, Y. Wang, M. Cao, Y. Wang, *Colloids Surf. A: Physicochem. Eng. Aspects* **2008**, *325*, 26.
- (63) Y. Han, Y. Wang, *Phys. Chem. Chem. Phys.* **2011**, *13*, 1939.
- (64) D. Ke, Q. Yang, M. Yang, Y. Wu, J. Li, H. Zhou, X. Wang, *Colloids Surf. A: Physicochem. Eng. Aspects* **2013**, *436*, 80.
- (65) R. Zana, *J. Colloid Interface Sci.* **2002**, *248*, 203.
- (66) T. Okano, N. Egawa, M. Fujiwara, M. Fukuda, *J. Am. Oil Chem. Soc.* **1996**, *73*, 31.
- (67) N. Azum, M.A. Rub, A.M. Asiri, A.A.P. Khan, A. Khan, *J. Surfact. Deterg.* **2013**, *16*, 77.
- (68) Y. Li, P. Li, C. Dong, X. Wang, Y. Wang, H. Yan, R.K. Thomas, *Langmuir* **2006**, *22*, 42.
- (69) P. Mukerjee, *Adv. Colloid Interface Sci.* **1967**, *1*, 241.
- (70) A. Ray, *Nature* **1971**, *231*, 313.
- (71) Y.I. Rabinovich, J.R. Kanicky, S. Pandey, H. Oskarsson, K. Holmberg, B.M. Moudgil, D.O. Shah, *J. Colloids Interface Sci.* **2005**, *288*, 583.
- (72) K. Shirahama, R. Matuura, *Bull. Chem. Soc. Japan*, **1965** *38*, 373.
- (73) M. J. Schick, A. H. Gilbert, *J. Colloid Sci.* **1965** *20*, 464.

- (74) M. J. Schwuger, B. Bunsenes, *Ges. Phys. Chem.* **1971**, *75*, 167.
- (75) F. Akhtar, M.A. Hoque, M.A. Khan, *J. Chem. Thermodyn.* **2008**, *40*, 1082.
- (76) S. Manet, Y. Karpichev, D. Dedovets, R. Oda, *Langmuir* **2013**, *29*, 3518.
- (77) P.A. Koya, Kabir-ud-din, K. Ismail, *J. Solution Chem.* **2012**, *41*, 1271.
- (78) B. Kumar, D. Tikariha, K.K. Ghosh, N. Barbero, P. Quagliotto, *J. Chem. Thermo.* **2013**, *62*, 178.
- (79) G.S. Hartley, *Aqueous solution of paraffin chain salts*, Herman, Paris, **1936**.
- (80) K. Kalyanasundaram, *Photochemistry in microheterogeneous systems*, Academic Press, Orlando, FI, **1987**.
- (81) M.E.D. Garcia, A. Sanz-Medel, *Talanta*, **1986**, *33*, 255.
- (82) H.V. Tartar, *J. Phys. Chem.* **1955**, *59*, 1195.
- (83) F.M. Menger, *Acc. Chem. Res.* **1979**, *12*, 111.
- (84) F.M. Menger, H. Yoshinaga, K.S. Venkatasubban, A.R. Das, *J. Org. Chem.* **1981**, *46*, 415.
- (85) F.M. Menger, B.J. Boyer, *J. Am. Chem. Soc.* **1980**, *102*, 5936.
- (86) P.S. Goyal, V.K. Aswal, *Curr. Sci.* **2001**, 80.
- (87) J.N. Israelachvili, D.J. Mitchell, B.W. Ninham, *J. Chem. Soc., Faraday Trans. 2* **1976**, *72*, 1525.
- (88) E. Buhler, E. Mendes, P. Boltenhagen, J.P. Munch, R. Zana, S.J. Candau, *Langmuir*, **1997**, *13*, 3096.
- (89) J.N. Philips, *Trans. Faraday. Soc.* **1955**, *51*, 561.
- (90) R. Zana, *Langmuir* **1996**, *12*, 1208.
- (91) R. Sharma, S. Mahajan, R.K. Mahajan, *Colloids and Surfaces A: Physicochem. Eng. Aspects* **2013**, *427*, 62.
- (92) R. Sanan, R.K. Mahajan, *Ind. Eng. Chem. Res.* **2011**, *50*, 7319.
- (93) M.S. Bakshi, I. Kaur, R. Sood, J. Singh, K. Singh, S. Sacher, K.J. Singh, G. Kaur, *J. Colloid Interface Sci.* **2004**, *271*, 227.
- (94) S.D. Christian, J.F. Scamehorn, *Solubilization in Surfactant Aggregates*, Marcel Dekker: New York, **1995**

-
- (95) Y. Jiang, X. Lu, H. Chen, S. Mao, M.Liu, P. Luo, Y. Du, *J. Phys. Chem. B* **2009**, *113*, 8357.
- (96) P.A. Koya, Kabir-ud-din, *J. Colloid Interface Sci.* **2011**, *360*, 175.
- (97) E. Junquera, E. Aicart, *Langmuir* **2002**, *18*, 9250.
- (98) X. Yang, J. Wang, Y. Wang, J. Ye, H. Yan, R.K. Thomas, *J. Colloid Interface Sci.* **2005**, *286*, 739.
- (99) A. Rodriguez, M.M. Graciani, A.J.M. Vargas, M.L. Moya, *J. Phys. Chem. B* **2008**, *112*, 11942.
- (100) R.G. Alargova, I.I. Kochijashky, M.L. Sierra, K. Kwetkat, R. Zana, *J. Colloid Interface Sci.* **2001**, *235*, 119.
- (101) F. Schosseler, A. Anthony, G. Beinert, R. Zana, *Langmuir* **1995**, *11*, 3347.
- (102) Kabir-ud-Din, M. S. Sheikh, M. A. Mir, A. A. Dar, *J. Colloid Interface Sci.* **2010**, *344*, 75.
- (103) N. Azum, A. Z. Naqvi, M. A, Kabir-ud-Din, *J. Colloid Interface Sci.* **2008**, *328*, 429.
- (104) Kabir-ud-Din, M. S. Sheikh, A. A. Dar, *J. Colloid Interface Sci.* **2009**, *333*, 605.
- (105) R. K. Mahajan, R. Kaur, V. K. Aswal, *Colloid Surf. A Physicochem. Eng. Asp.* **2013**, *419*, 61.
- (106) M. S. Bakshi, K. Singh, *J. Colloid Interface Sci.* **2005**, *287*, 288.
- (107) J.H. Fendler, *Membrane Mimetic Chemistry*, Wiley Interscience, NewYork, **1982**, Chapter 3
- (108) N. M. Correa, J. J. Silber, R. E. Riter, Nancy E. Levinger, *Chem. Rev.* **2012**, *112*, 4569.
- (109) R .D. Falcone, M. A. Biasutti, N. M. Correa, J. J. Silber, E. Lissi, E. Abuin, *Langmuir*, **2004**, *20*, 5732.
- (110) C. N. Durfor, R. J. Bolin, R. J. Sugawara, R. J. Massey, J. Jacobs, P. G. Schultz, *J. Am. Chem. Soc.* **1988**, *110*, 8713.
- (111) F. M. Menger, K. Yamada, *J. Am. Chem. Soc.*, **1979**, *101*, 6731.
- (112) J. H. Fendler, *Chem. Rev.* **1987**, *87*, 877.

-
- (113) M. D. Johnson, B. B. Lorenz, P. C. Wilkins, B. G. Lemons, B. Baruah, N. Lamborn, M. Stahla, P. B. Chatterjee, D. T. Richens, D. C. Crans, *Inor. Chem.*, **2012**, *51*, 2757.
- (114) K. R. Kumar, D. E. Brooks, *Macro. Rapid Comm.* **2005**, *26*, 155.
- (115) B. L. Cushing, V. L. Kolesnichenko, C. J. O'Connor, *Chem. Rev.* **2004**, *104*, 3893.
- (116) H. Colfen, S. Mann, *Angew. Chem. Int. Edit.* **2003**, *42*, 2350.
- (117) M. P. Pileni, *Nat. Mater.* **2003**, *2*, 145.
- (118) Y. Xia, P. Yang, Y. Sun, Y. Wu, B. Mayers, B. Gates, Y. Yin, F. Kim, H. Yan, *Adv. Mater* **2003**, *15*, 353.
- (119) C. C. M. Goymann, *Eur. J. Pharma and Biopharma*, **2004**, *58*, 343.
- (120) M. J. Lawrence, G. D. Rees, *Adv. Drug Delivery Rev.*, **2000**, *45*, 89.
- (121) M. J. Lawrence, *Eur. J. Drug Metabolism and Pharm.*, **1994**, *19*, 257.
- (122) M. P. Pileni, *Structure and Reactivity in Reverse Micelles*, Elsevier, Amsterdam, **1989**.
- (123) M. J. Lawrence, *Curr. Opin. Colloid Interface Sci.*, **1996**, *1*, 826.
- (124) K. O. Asare, *Adv. Colloid Interface Sci.*, **1991**, *37*, 123.
- (125) K. O. Asare, *Colloid Sci.*, **1990**, *50*, 373.
- (126) T. A. Hatton, in *Surfactant-based Processes*, ed. J. M. Scamehorn and J. H. Horwell, Marcel Dekker, New York, **1989**, *33*, 558
- (127) B. H. Robinson, C. Toprakcioglu, J. C. Dore, P. J. Chieux, *Chem. Soc.-Faraday Trans* **1984**, *80*, 13.
- (128) J. Eastoe, T. F. Towey, B. H. Robinson, J. Williams, R. K. Heenan, *J. Phys. Chem.*, **1993**, *97*, 1459.
- (129) B. Svensson, U. Olsson, P. Alexandridis, K. Mortensen, *Macromolecules*, **1999**, *32*, 6725.
- (130) L. K. Shrestha, T. Sato, K. Aramaki, *Phys. Chem. Chem. Phys.*, **2009**, *11*, 4251.
- (131) B. A. Simmons, C. E. Taylor, F. A. Landis, V. T. John, G. L. Mcpherson, D. K. Schwartz, R. Moore, *J. Am. Chem. Soc.* **2001**, *123*, 2414.
- (132) M. Zulauf, H. F. Eicke, *J. Phys. Chem.* **1979**, *83*, 480.

- (133) H. B. Bohidar, M. Behboudnia, *Colloid Surf. A Physicochem. Eng. Asp.* **2001**, 178, 313.
- (134) M. A. Michaels, S. Sherwood, M. Kidwell, M. J. Allsbrook, S. A. Morrison, S. C. Rutan, E.E. Carpenter, *J. Colloid Interface Sci.* **2007**, 311, 70.
- (135) J. Zhao, S. Deng, J. Liu, C. Lin, and O. Zheng, *J. Colloid Interface Sci.*, 2007, **311**, 237.
- (136) O. Zheng, J. Zhao, X. Fu, *Langmuir*, 2006, **22**, 3528.
- (137) O. Zheng, J. X. Zhao, and X. M. Fu, *J. Colloid Interface Sci.*, 2006, **300**, 310.
- (138) J. Xu, X. Han, H. Liu, Y. Hu, *Colloid Surf. A Physicochem. Eng. Asp.* **2006**, 273, 179.
- (139) T. K. Jain, M. Varshney, A. Maitra, *J. Phys. Chem.* **1989**, 93, 7409.
- (140) D. Zhong, S.K. Pal, A. H. Zewail, *Chem. Phys. Lett.* **2011**, 503, 1.
- (141) A. Douhal, G. Angulo, M. Gil, J. A. Organero, M. Sanz, L. Tormo, *J. Phys. Chem. B* **2007**, 111, 5487.
- (142) A. Sengupta, R. V. Khade, P. Hazra, *J. Phys. Chem. A* **2011**, 115, 10398.
- (143) P. Hazra, N. Sarkar, *Chem. Phys. Lett.*, 2001, **342**, 303.
- (144) P. Hazra, D. Chakrabarty, A. Chakraborty, N. Sarkar, *Chem. Phys. Lett.*, 2003, **382**, 71.
- (145) P. Hazra, N. Sarkar, *Phys. Chem. Chem. Phys.*, **2002**, 4, 1040.
- (146) C. Branden, J. Tooze, *Introduction to protein structure*, second ed., Garland, New York, **1999**.
- (147) D. Carter, J.X. Ho, *Advances in protein chemistry*, Academic Press, New York, **1994**.
- (148) S. Curry, H. Mandelkow, P. Brick, N. Franks, *Nat. Struct. Biol.*, **1998**, 5, 827.
- (149) G. Walsh, *Nat. Biotech.* **2006**, 24, 769.
- (150) W. Wang, S. Singh, D.L. Zeng, K. King, S. Nema, *J. Pharm. Sci.*, **2007**, 96, 1.
- (151) A. Hawe, M. Sutter, W. Jiskoot, *Pharm. Res.* **2008**, 25, 1487.
- (152) A. Chakrabarty, A. Mallick, B. Halder, P. Das, N. Chattopadhyay *Biomacromolecules* **2007**, 8, 920.

- (153) D. Wu, G. Xu, Y. Sun, H. Zhang, H. Mao, Y. Feng, *Biomacromolecules*, **2007**, 8, 708
- (154) E.L. Gelamo, C.H.T.P. Silva, H. Imasato, M. Tabak, *Biochimica et Biophysica Acta*, **2002**, 84, 1594.
- (155) S. De, A. Girigoswami, S. Das, *J. Colloid Inter. Science*, **2005**, 285, 562.
- (156) N. Gull, P. Sen, R. H. Khan, Kabir-ud-Din, *Langmuir*, **2009**, 25, 11686.
- (157) M. Vasilescu, D. Angelescu, M. Almgren, A. Valstar, *Langmuir* **1999**, 15, 2635.
- (158) B. P. Kamat, J. Seetharamappa, *J. Pharm. Biomed. Anal.* **2004**, 35, 655.
- (159) F. Khodaghali, B. Eftekharezadeh, R. Yazdanparast, *Protein*, **2008**, 27,123.
- (160) A. Sulkowska, *J. Mol. Struct.* **2002**, 614, 227.
- (161) D. Kelley, D. McClements, *J. Food Hydrocolloids* **2003**, 17, 73.
- (162) C. Sun, J. Yang, X. Wu, X. Huang, F. Wang, S. Liu, *J. Biophys.* **2005**, 88, 3518.
- (163) C. L. Mesa, *J. Colloid Interface Sci.* **2005**, 286, 148.
- (164) A. Helenius, K. Simons, *Biochim. Biophys. Acta*, **1975**, 415, 29.
- (165) R. Das, D. Guha, S. Mitra, S. Kar, S. Lahiri, S. Mukherjee, *J. Phys. Chem. A* **1997**, 101, 4042.
- (166) K. Ibel, R. P. May, K. Kirschner, H. Szadkowski, E. Mascher, P. Lundahl, *Eur. J. Biochem.*, **1990**, 190, 311.
- (167) K. P. Ananthapadmanabhan, E.D. Goddard, In *Interaction of Surfactants with Polymers and Proteins*; CRC Press: Boca Raton, FL **1993**, 319.
- (168) N. J. Turro, X. G. Lei, K. P. Ananthapadmanabhan, M. Aronson, *Langmuir*, **1995**, 11, 2525.
- (169) E.L. Gelamo, M. Tabak, *Spectrochimica Acta Part A*, **2000**, 56, 2255.
- (170) C. C. Ruiz, J. M. Hierrezuelo, J. Aguiar, J. M. P. Garcia, *Biomacromolecules*, **2007**, 8, 2497.
- (171) Y. Pi, Y. Shang, C. Peng, H. Liu, Y. Hu, J. Jiang, *Biopolymers*, **2006**, 83, 243.
- (172) Y. S. Ge, S. X. Tai, Z.Q. Xu, L. Lai, F. F. Tian, D. W. Li, F. L. J. Y. Liu, Z.N. Gao, *Langmuir* **2012**, 28, 5913.
- (173) C. M. C. Faustino, R. T. C. Antonio, L. G. Rio, *Biomacromolecules*, **2009**, 10, 2508.

- (174) N. Gull, M. A. Mir, J. M. Khan, R. H. Khan, G. M. Rather, A. A. Dar, *J. Colloid Inter. Science*, **2011**, *364*, 157.
- (175) B. Valeur, *Molecular Fluorescence: Principles and Applications*, Wiley-VCH Verlag GmbH, **2001**.
- (176) J.R. Lakowicz, *Principles of Fluorescence Spectroscopy*, Springer, New York, 2006.
- (177) A. Jablonski, *Z. Physik* **1935**, *94*, 38.
- (178) M. Kasha, *Disc. Faraday Soc.* **1950**, *9*, 14.
- (179) S.G. Schulman, *Fluorescence and phosphorescence spectroscopy: Physicochemical principles and practice*, Pergamon Press, Oxford, **1977**.
- (180) N. Mataga, T. Okada, N. Yamamoto, *Chem. Phys. Lett.* **1967**, *1*, 119.
- (181) N. Mataga, S. Tsumo, *Bull. Chem. Soc. Jpn.* **1957**, *30*, 367.
- (182) R.C. Heckman, *J. Mol. Spectrosc.* **1958**, *2*, 27.
- (183) S.G. Schulman, *In Physical methods in heterocyclic chemistry*, A.R. Katritzky (Ed.), Academic Press, New York, **1974**.
- (184) W. Rettig, *J. Mol. Struct.* **1982**, *84*, 303.
- (185) P. Suppan, *Chem. Phys. Lett.* **1986**, *128*, 160.
- (186) D. Pilloud, P. Suppan, L. Van Haelst, *Chem. Phys. Lett.* **1987**, *137*, 130.
- (187) W. Baumann, H. Bischof, J.C. Fröhling, C. Brittinger, W. Rettig, K. Rotkiewicz, *J. Photochem. Photobiol. A: Chem.* **1992**, *64*, 49.
- (188) P. Pringsheim, *Fluorescence and phosphorescence*, Inter-Science, New York, **1949**.
- (189) T. Forster, *Fluorescenz organischer verbindungen*, Vanderhock and Ruprecht, Gottingen, **1951**.
- (190) G.C. Pimentel, *J. Am. Chem. Soc.* **1957**, *79*, 3323.
- (191) E. Lippert, *Z. Naturforsch* **1955**, *10A*, 541.
- (192) E. Lippert, *Z. Naturforsch, Teil A* **1962**, *17*, 621.
- (193) E.G. McRae, *J. Phys. Chem.* **1957**, *61*, 562.
- (194) P. Suppan, *J. Chem. Soc. A* **1968**, 3125.
- (195) Y. Oshika, *J. Phys. Soc. Japan* **1954**, *9*, 594

- (196) E. Lippert, *Z. Naturforsch* **1955**, 10A, 541.
- (197) N. Mataga, Y. Kaifu, M. Koizumi, *Bull. Chem. Soc. Jpn.* **1955**, 28, 690.
- (198) W. Liptay, *Z. Naturforsch* **1965**, 20A, 1441.
- (199) L. Bilot, A. Kawaski, *Z. Naturforsch* **1962**, 18A, 621.
- (200) N.G. Bhakhshiev, *Opt. Spektroskopiya* **1962**, 10, 717.
- (201) M. Shaikh, J. Mohanty, P.K. Singh, A.C. Bhasikuttan, R.N. Rajule, V.S. Satam, S.R. Bendre, V.R. Kanetkar, H. Pal, *J. Phys. Chem. A* **2010**, 114, 4507.
- (202) N. Dash, F.A.S. Chipem, R. Swaminathan, G. Krishnamoorthy, *Chem. Phys. Lett.* **2008**, 460, 119.
- (203) G. Krishnamoorthy, S.K. Dogra, *Spectrochim. Acta, Part A* **1999**, 55, 2647.
- (204) S.K. Saha, P. Purkayastha, A.B. Das, *J. Photochem. Photobiol. A: Chem.* **2008**, 195, 368.
- (205) A. Demeter, V. Mile, T. Bérces, *J. Phys. Chem. A* **2007**, 111, 8942.
- (206) C. Reichardt, *Chem. Rev.* **1994**, 94, 2319.
- (207) E.M. Kosower, *J. Am. Chem. Soc.* **1958**, 80, 3253.
- (208) E.M. Kosower, J.A. Skorcz, W.M. Schwarz, J.W. Patton, *J. Am. Chem. Soc.* **1960**, 82, 2188.
- (209) K. Dimroth, C. Reichardt, T. Siepmann, F. Bohlmann, *Liebigs Ann. Chem.* **1963**, 661, 1.
- (210) C. Reichardt, E. Harbusch-Gornert, *Liebigs Ann. Chem.* **1983**, 721.
- (211) M.J. Kamlet, J.L.M. Abboud, M.H. Abraham, R.W. Taft, *J. Org. Chem.* **1983**, 48, 2877.
- (212) K. Sivakumar, T. Stalin, N. Rajendiran, *Spectrochim. Acta, Part A* **2005**, 62, 991.
- (213) A. Chakraborty, S. Kar, N. Guchhait, *J. Photochem. Photobiol. A: Chem.* **2006**, 181, 246.
- (214) W. Schuddeboom, S.A. Jonker, J.M. Warman, U. Leinhos, W. Kuehnle, K.A. Zachariasse, *J. Phys. Chem.* **1992**, 96, 10809.
- (215) W. Schuddeboom, S.A. Jonker, J.M. Warman, U. Leinhos, W. Kuehnle, K.A. Zachariasse, *J. Phys. Chem.* **1992**, 96, 10809.

- (216) A. Samanta, R.W. Fessenden, *J. Phys. Chem. A* **2000**, *104*, 8972.
- (217) A. Chakraborty, S. Kar, N. Guchhait, *Chemical Physics*, **2006**, *324*, 733.
- (218) E. Lippert, W. Luder, H. Boos, In *Advances in molecular spectroscopy*, A. Mangini (Ed.), Pergamon Press, Oxford, **1962**.
- (219) O.S. Khalil, R.H. Hofeldt, S.P. MCGlynn, *Chem. Phys. Lett.* **1972**, *17*, 479.
- (220) O.S. Khalil, R.H. Hofeldt, S.P. MCGlynn, *J. Lumin.*, **1973**, *6*, 229.
- (221) O.S. Khalil, R.H. Hofeldt, S.P. MCGlynn, *Spectrosc. Lett.* **1973**, *6*, 147.
- (222) O.S. Khalil, *Chem. Phys. Lett.* **1975**, 172.
- (223) E.M. Kosower, H. Dodiuk, *J. Am. Chem. Soc.* **1976**, *98*, 924.
- (224) C. C. Dubroca, A. Peirigua, S.A. Lyazidi, G. Nouchi, *Chem. Phys. Lett.* **1983**, *98*, 511.
- (225) C. C. Dubroca, S.A. Lyazidi, G. Nouchi, A. Peirigua, *Nouv. J. Chim.* **1986**, *10*, 337.
- (226) E.A. Chandross, In *The exciplex*, M. Gordon, W.R. Ware (Eds.), Academic Press, New York, **1975**.
- (227) E.A. Chandross, H.T. Thomas, *Chem. Phys. Lett.* **1971**, *9*, 397.
- (228) K.A. Zachariasse, T. Von der Haar, A. Hebecker, U. Leinhos, W. Kuhnle, *Pure Appl. Chem.* **1993**, *65*, 1745.
- (229) U. Leinhos, W. Kuehnle, K.A. Zachariasse, *J. Phys. Chem.* **1991**, *95*, 2013.
- (230) F.D. Lewis, B. Holman, *J. Phys. Chem.* **1980**, *84*, 2328.
- (231) K.T. Huang, J.R. Lombardi, *J. Chem. Phys.* **1971**, *55*, 4072.
- (232) K.A. Zachariasse, *Chem. Phys. Lett.* **2000**, *320*, 8.
- (233) Y.V. Ichev, W. Kühnle, K.A. Zachariasse, *J. Phys. Chem. A* **1998**, *102*, 5670.
- (234) K.A. Zachariasse, M. Grobys, E. Tauer, *Chem. Phys. Lett.* **1997**, *274*, 372.
- (235) K.A. Zachariasse, M. Grobys, T. von der Haar, A. Hebecker, Y.V. Il'ichev, O. Morawski, I. Rückert, W. Kühnle, *J. Photochem. Photobiol. A: Chem.* **1997**, *105*, 373.
- (236) Z.R. Grabowski, K. Rotkiewicz, W. Rettig, *Chem. Rev.* **2003**, *103*, 3899.
- (237) K. Rotkiewicz, K.H. Grellmann, Z.R. Grabowski, *Chem. Phys. Lett.* **1973**, *19*, 315.
- (238) Z.R. Grabowski, K. Rotkiewicz, A. Siemiarz, *J. Lumin.* **1979**, *18*, 420.
- (239) K. Rotkiewicz, W. Rubaszewska, *Chem. Phys. Lett.* **1980**, *70*, 444.

- (240) R.J. Visser, C.A.G.O. Varma, *J. Chem. Soc., Faraday Trans. 2* **1980**, 76, 453.
- (241) R.J. Visser, P.C.M. Weisenborn, C.A.G.O. Varma, *Chem. Phys. Lett.* **1985**, 113, 330.
- (242) R.J. Visser, C.A.G.O. Varma, J. Konijnenberg, P.C.M. Weisenborn, *J. Mol. Struct.* **1984**, 114, 105.
- (243) R.J. Visser, C.A.G.O. Varma, J. Konijnenberg, P. Bergwerf, *J. Chem. Soc., Faraday Trans. 2* **1983**, 79, 347.
- (244) R.J. Visser, P.C.M. Weisenborn, C.A.G.O. Varma, M.P. De Haas, J.M. Warman, *Chem. Phys. Lett.* **1984**, 104, 38.
- (245) Y. Wang, M. McAuliffe, F. Novak, K.B. Eisenthal, *J. Phys. Chem.* **1981**, 85, 3736.
- (246) K. Rotkiewicz, W. Rubaszewska, *J. Lumin.* **1982**, 27, 221.
- (247) H. Bischof, W. Baumann, N. Detzer, K. Rotkiewicz, *Chem. Phys. Lett.* **1985**, 116, 180.
- (248) T. Taniguchi, J. Wang, S. Irle, S. Yamaguchi, *Dalton Trans.*, **2013**, 42, 620.
- (249) A. Mishra, S. Chatterjee, G. Krishnamoorthy, *J. Photochem. Photobiol. A: Chem.* **2013**, 260, 50.
- (250) V. Bonacic-Koutecky, J. Michl, *J. Am. Chem. Soc.* **1985**, 107, 1765.
- (251) V. Bonacic-Koutecký, J. Köhler, J. Michl, *Chem. Phys. Lett.* **1984**, 104, 440.
- (252) T. Soujanya, G. Saroja, A. Samanta, *Chem. Phys. Lett.* **1995**, 236, 503.
- (253) A.B.J. Parusel, *Chem. Phys. Lett.* **2001**, 340, 531.
- (254) J. Dey, I.M. Warner, *J. Phys. Chem. A* **1997**, 101, 4872.
- (255) A. Chakraborty, S. Kar, N. Guchhait, *J. Photochem. Photobiol. A: Chem.* **2006**, 181, 246.
- (256) P.R. Bangal, S. Panja, S. Chakravorti, *J. Photochem. Photobiol. A: Chem.* **2001**, 139, 5.
- (257) W. Rettig, G. Wermuth, *J. Photochem.* **1985**, 28, 351.
- (258) M. Van der Auweraer, Z.R. Grabowski, W. Rettig, *J. Phys. Chem.* **1991**, 95, 2083.
- (259) N. Dash, F.A.S. Chipem, R. Swaminathan, G. Krishnamoorthy, *Chem. Phys. Lett.* **2008**, 460, 119.

- (260) S. Murali, W. Rettig, *J. Phys. Chem. A* **2005**, *110*, 28.
- (261) S.I. Druzhinin, A. Demeter, K.A. Zachariasse, *Chem. Phys. Lett.* **2001**, *347*, 421.
- (262) S. Murali, W. Rettig, *J. Phys. Chem. A* **2005**, *110*, 28.
- (263) P.R. Bangal, S. Panja, S. Chakravorti, *J. Photochem. Photobiol. A: Chem.* **2001**, *139*, 5.
- (264) M.A. Haidekker, T.P. Brady, D. Lichlyter, E.A. Theodorakis, *Bioorg. Chem.* **2005**, *33*, 415.
- (265) A. Mielniczak, B. Wandelt, S. Wysocki, *Mater. Sci.* **2002**, *20*, 59.
- (266) S.K. Saha, P. Purkayastha, A.B. Das, S. Dhara, *J. Photochem. Photobiol. A: Chem.* **2008**, *199*, 179.
- (267) A. Weller, *Z. Elektrochem.* **1952**, *56*, 662.
- (268) T. Forster, *Naturwis* **1949**, *36*, 186.
- (269) T. Forster, *Z. Electrochem.* **1950**, *54*, 531.
- (270) A. Weller, *Progress in reaction kinetics*, Pergamon Press, London, **1961**.
- (271) B. Sengupta, P.K. Sengupta, *Biochem. Biophys. Res. Commun.* **2002**, *299*, 400.
- (272) S. Muthusubramanian, S.K. Saha, *J. Luminescence* **2012**, *132*, 2166.
- (273) A. Mallick, B. Haldar, S. Maiti, N. Chattopadhyay, *J. Colloid Interface Sci.* **2004**, *278*, 215.
- (274) M. Sowmiya, A.K. Tiwari, S.K. Saha, *J. Colloid Interface Sci.* **2010**, *344*, 97.
- (275) S.S. Jaffer, M. Sowmiya, S.K. Saha, P. Purkayastha, *J. Colloid Interface Sci.* **2008**, *325*, 236.
- (276) R. Jimenez, G.R. Fleming, P.V. Kumar, M. Maroncelli, *Nature* **1994**, *369*, 471.
- (277) P.F. Barbara, W. Jarzeba, *Adv. Photochem.* **1990**, *15*, 1.
- (278) A. Vajda, R. Jimenez,; S.J. Rosenthal, V. Fidler, G.R. Fleming, E.W. Castner, *J. Chem. Soc. Faraday Trans.* **1995**, *91*, 867.
- (279) M. Maroncelli, *J. Mol. Liq.* **1993**, *57*, 1.
- (280) A.S. Hojniak, I. Deperasinska, K. Oberda, Y. Erez, D. Huppert, Y.P. Nizhnik, *Phys. Chem. Chem. Phys.* **2013**, *15*, 9914.
- (281) M.J. Lang, X.J. Jordanides, X. Song, G.R. Fleming, *J. Chem. Phys.* **1999**, *110*, 5884.

- (282) T. Joo, Y. Jia, J.-Y. Yu, M.J. Lang, G.R. Fleming, *J. Chem. Phys.* **1996**, *104*, 6089.
- (283) B. Zolotov, A. Gan, B.D. Fainberg, D. Huppert, *Chem. Phys. Lett.* **1997**, *265*, 418.
- (284) M. Cho, S.J. Rosenthal, N.F. Scherer, L.D. Ziegler, G.R. Fleming, *J. Chem. Phys.* **1992**, *96*, 5033.
- (285) M. Glasbeek, H. Zhang, *Chem. Rev.* **2004**, *104*, 1929.
- (286) W. Jarzeba, G.C. Walker, A.E. Johnson, M.A. Kahlow, P.F. Barbara, *J. Phys. Chem.* **1988**, *92*, 7039.
- (287) A. Vajda, R. Jimenez,; S.J. Rosenthal, V. Fidler, G.R. Fleming, E.W. Castner, *J. Chem. Soc. Faraday Trans.* **1995**, *91*, 867.
- (288) S.K. Pal, J. Peon, A.H. Zewail, *Proc. Natl. Acad. Sci. USA* **2002**, *99*, 1763.
- (289) S.K. Pal, J. Peon, A.H. Zewail, *Proc. Natl. Acad. Sci. USA* **2002**, *99*, 15297.
- (290) S.K. Pal, J. Peon, A.H. Zewail, *Chem. Phys. Lett.* **2002**, *363*, 57.
- (291) M.L. Horng, J.A. Gardecki, A. Papazyan, M. Maroncelli, *J. Phys. Chem.* **1995**, *99*, 17311.
- (292) M.A. Kahlow, W. Jarzeba, T.J. Kang, P.F. Barbara, *J. Chem. Phys.* **1989**, *90*, 151.
- (293) K. Tominaga, G.C. Walker, *J. Photochem. Photobiol. A* **1995**, *87*, 127.
- (294) S.A. Kovalenko, N.P. Ernsting, Ruthmann, *J. Chem. Phys. Lett.* **1996**, *258*, 445.
- (295) A.M. Jonkman, P. van der Meulen, H. Zhang, M. Glassbeek, *Chem. Phys. Lett.* **1996**, *256*, 21.
- (296) E.W.Jr. Castner, M. Maroncelli, G.R. Fleming, *J. Chem. Phys.* **1987**, *86*, 1090.
- (297) S.A. Kovalenko, N.P. Ernsting, Ruthmann, *J. Chem. Phys.* **1997**, *106*, 3504.
- (298) M.A. Kahlow, T.J. Kang, P.F. Barbara, *J. Chem. Phys.* **1988**, *88*, 2372.
- (299) P. van der Meulen, H. Zhang, A.M. Jonkman, M. Glassbeek, *J. Phys. Chem.* **1996**, *100*, 5367.
- (300) P. Proposito, M. Casalboni, F.de Matteis, M. Glassbeek, A. Quatela, E. van Veldhoven, H. Zhang, *J. Lumin.* **2001**, *94*, 641.
- (301) N. Sarkar, A. Datta, S. Das, K. Bhattacharyya, *J. Phys. Chem.* **1996**, *100*, 15483.

- (302) N. Nandi, B. Bagchi, *J. Phys. Chem. B* **1997**, *101*, 10954.
- (303) D. Chakrabarty, P. Hazra, A. Chakraborty, N. Sarkar, *Chem. Phys. Lett.* **2004**, *392*, 340.
- (304) A. Chakraborty, D. Chakrabarty, P. Hazra, D. Seth, N. Sarkar, *Chem. Phys. Lett.* **2003**, *382*, 508.
- (305) D. Chakrabarty, P. Hazra, A. Chakraborty, N. Sarkar, *J. Phys. Chem. B* **2003**, *107*, 13643.
- (306) D. Chakrabarty, P. Hazra, N. Sarkar, *J. Phys. Chem. A* **2003**, *107*, 5887.
- (307) D. Chakrabarty, A. Chakraborty, D. Seth, P. Hazra, N. Sarkar, *J. Chem. Phys.* **2005**, *122*, 184516.
- (308) A. Chakraborty, D. Seth, D. Chakrabarty, P. Setua, N. Sarkar, *J. Phys. Chem. A* **2005**, *109*, 11110.
- (309) R. Karmakar, A. Samanta, *J. Phys. Chem. A* **2002**, *106*, 4447.
- (310) R. Karmakar, A. Samanta, *J. Phys. Chem. A* **2003**, *107*, 7340.
- (311) H. Shirota, Y. Tamoto, H. Segawa, *J. Phys. Chem. A* **2004**, *108*, 3244.
- (312) Y. Tamoto, H. Segawa, H. Shirota, *Langmuir* **2005**, *21*, 3757.
- (313) Amit K. Tiwari, Sonu, and Subit K. Saha, *J. Phys. Chem. B* **2014**, *118*, 3582.
- (314) E. M. Corbeil, N. E. Levinger, *Langmuir* **2003**, *19*, 7264.
- (315) P. Hazra, N. Sarkar, *Phys. Chem. Chem. Phys.* **2002**, *4*, 1040.
- (316) P. Hazra, D. Chakrabarty, N. Sarkar, *Chem. Phys. Lett.* **2003**, *371*, 553.
- (317) X. Liu, J. M. Cole, K. S. Low, *J. Phys. Chem. C*, **2013**, *117*, 14723.
- (318) K. Khemakhem, H. Ammar, S. Abid, R.E. Gharibi, S.F. Forgues, *Dyes and Pigments*, **2013**, *99*, 594.
- (319) C.R. Moyland, *J. Phys. Chem.* **1994**, *98*, 13513.
- (320) K. Recthaler, G. Kohler, *Chem. Phys.* **1994**, *189*, 99.
- (321) S. Muthusubramanian, S.K. Saha, *J. Luminescence* **2012**, *132*, 2166.
- (322) M. Sowmiya, A.K. Tiwari, S.K. Saha, *J. Colloid Interface Sci.* **2010**, *344*, 97.
- (323) S.S. Jaffer, M. Sowmiya, S.K. Saha, P. Purkayastha, *J. Colloid Interface Sci.* **2008**, *325*, 236.

- (324) P. R. Bangal, S. Panja, S. Chakravorti, *J. Photochem. Photobiol. A* **2001**, *139*, 5.
- (325) S. Panja, P. Chowdhury, S. Chakravorti, *Chem. Phys. Lett.* **2003**, *368*, 654.
- (326) E.G. Lomax, *Amphoteric surfactants*; Marcel Dekker: New York, **1996**, Chapter 1, p. 1.
- (327) X. Domingo, In: E.G. Lomax (Ed.), *Amphoteric surfactants*; Marcel Dekker: New York, **1996**, Chapter 3, p. 75.
- (328) T. J. H. Manning, G. H. Holland, G. Rennie, P. Revell, J. Hines, M. D. Barratt, D. A. Basketter, *Food and Chemical Toxicology* **1998**, *36*, 233.
- (329) V.P. Denisov, J. Peters, H. D. Horlein, B. Halle, *Nature Struct. Biol.* **1996**, *3*, 505.
- (330) T. Telgmann, U. Kaatze, *J. Phys. Chem. A* **2000**, *104*, 1085.
- (331) N. Jiang, P. Li, Y. Wang, J. Wang, H. Yan, R. K. Thomas, *J. Colloid and Interface Science* **2005**, *286*, 755.
- (332) J.H. Clint, *J. Chem. Soc. Faraday Trans.* **1975**, *171*, 1327.
- (333) D.N. Rubingh, K.L. Mittal, *Solution Chemistry Surfactants*, Plenum Press, New York, **1979**.
- (334) E. Rodenas, M. Valiente, M. del Sol Villafuella, *J. Phys. Chem. B* **1999**, *103*, 4549.
- (335) K. Motomura, M. Yamanaka, M. Aratono, *Colloid Polym. Sci.* **1984**, *262*, 948
- (336) J. M. Hierrezuelo, J. Aguiar, C. C. Ruiz, *Colloids and Surfaces A: Physicochem. Eng. Aspects* **2005**, *264*, 29.
- (337) H. S. Frank, F. J. Franks, *Chem. Phys.* **1968**, *48*, 4746.
- (338) A. K. Soper, E. W. Castner, A. Luzar, *Biophys. Chem.* **2003**, *105*, 649.
- (339) T. Yamazaki, A. Kovalenko, V. V. Murashov, G. N. J. Patey, *J. Phys. Chem. B* **2010**, *114*, 613.
- (340) A. Das, C. Mukhopadhyay, *J. Phys. Chem. B* **2009**, *113*, 12816.
- (341) M. C. Stumpe, H. J. Grubmuller, *J. Phys. Chem. B* **2007**, *111*, 6220.
- (342) M. E. Lee, N. F. A. van der Vegt, *J. Am. Chem. Soc.* **2006**, *128*, 4948.

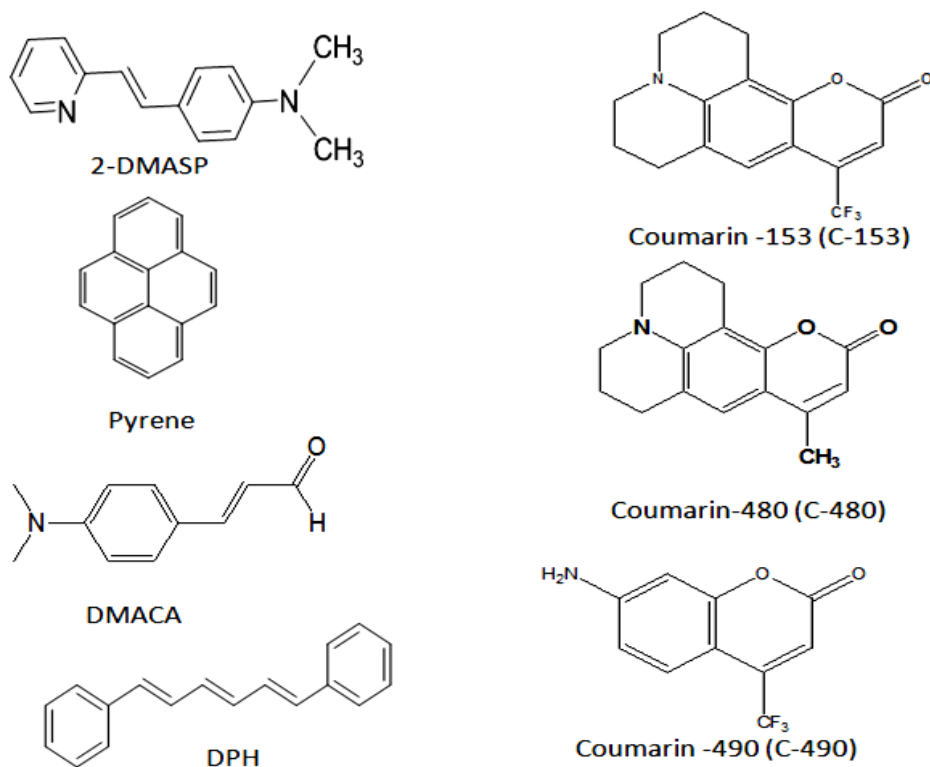
Chapter 2

Materials, methods and instrumentation

2.1 Materials

2.1.1 Fluorescence probes

Trans-2-[4-(*N,N*-dimethylamino)styryl]pyridine (2-DMASP), 4-(*N,N*-dimethylamino) cinnamaldehyde (DMACA), 1,6-diphenyl-1,3,5-hexatriene (DPH), pyrene, and Coumarin-490 (C-490) were procured from Sigma Chemical Company WI, USA. 2-DMASP, DMACA and pyrene were recrystallized from a mixture of water and a small percentage (10%) of ethanol. A single spot was noticed for the recrystallized compound in thin layer chromatography (TLC) plate. DPH and C-490 were of highest purity grade and used as received. Coumarin-153 (C-153) and Coumarin-480 (C-80) were obtained from the Exciton (laser grade), Ohio, USA and was used as received. The molecular structures of these compounds are shown below as Scheme 2.1.



Scheme 2.1: Molecular structures of fluorescence probes

2.1.2 Surfactants (conventional and gemini surfactants)

2.1.2.1 Conventional surfactants

Surfactants dodecyltrimethylammoniumbromide (DTAB), and tetradecyltrimethylammoniumbromide (TTAB) were procured from Alfa-Aesar Chemical Company, USA. Cetyltrimethylammoniumbromide (CTAB), and t-octylphenoxypolyethoxyethanol (TX-100) were purchased from Sigma Chemical Company WI, USA. All these surfactants were used as received.

Counterions Br⁻ of CTAB were exchanged by SO₄²⁻, NO₃⁻, and *p*-toluenesulphonic acid (PTSA) by following the reported procedure¹. Briefly, CTAB was dissolved in water and then strongly anion exchange resin Amberlyst A26OH (purchased from Sd-fine Chemical Company, India) was added to replace Br⁻ by OH⁻ ions. The mixture was stirred for two hours. After that the solution was filtered and neutralized by the appropriate acid. The resulting solution was then freeze dried to give the corresponding salt. Surfactants with different counter ions are denoted as CTABr, CTA1/2SO₄, CTANO₃, CTAPTSA.

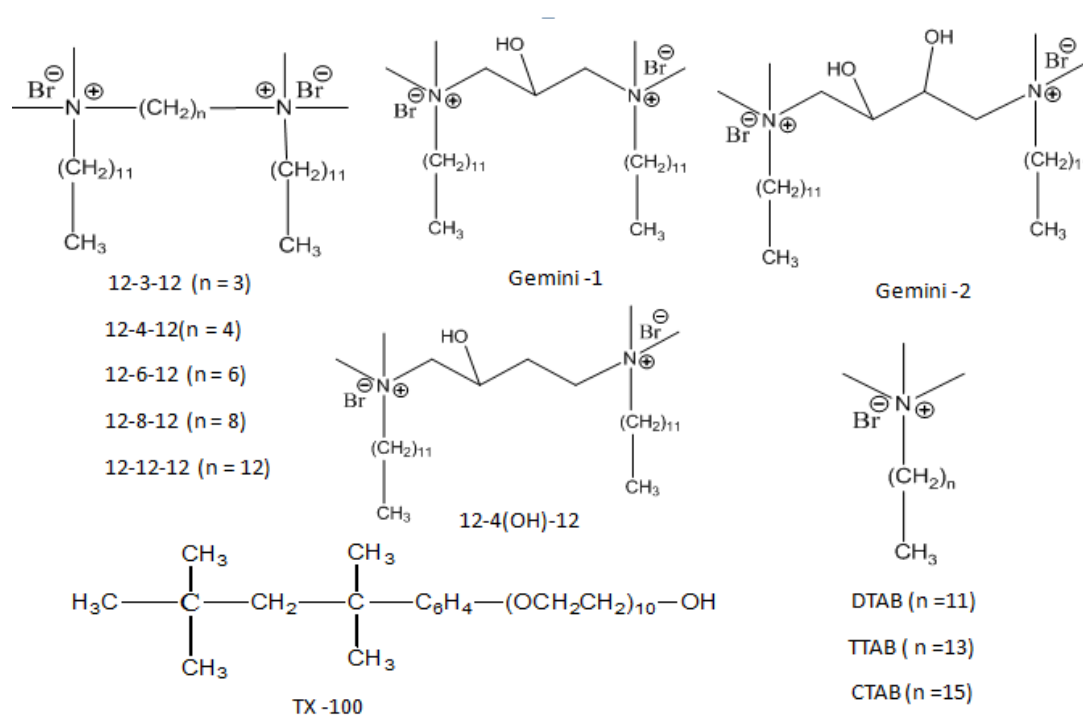
2.1.2.2 Gemini surfactants

2.1.2.2.1 Synthesis of gemini surfactants

1,3-dibromopropane, 1,4-dibromobutane, 1,5-dibromopentane, 1,6-dibromohexane, 1,8-dibromooctane, 1,12-dibromododecane are purchased from Spectrochem Company, India. 1,3-dibromo-2-propanol, 1,4-dibromo-2,3-butanediol, 1,4-dibromo-2-butanol are purchased from Sigma Chemical Company, WI, USA and *N,N*-dimethyldodecylamine, were procured from Alfa Aesar, USA.

The molecular structures of the synthesized gemini surfactants are given by Scheme 2.2. The procedures for the synthesis of gemini surfactants are reported elsewhere². Brief procedure of the synthesis is explained here. To synthesise gemini surfactants, 1,3-bis(dodecyl-*N,N*-dimethylammonium bromide)-2-propanol or 12-3(OH)-12 (Gemini-1) and 1,4-bis(dodecyl-*N,N*-dimethylammoniumbromide)-2,3-butanediol or 12-4(OH)₂-12 (Gemini-2), 1,4-bis(dodecyl-*N,N*-dimethylammoniumbromide)-2-butanol or 12-4(OH)-12 required amounts of 1,3-dibromo-2-propanol, 1,4-dibromo-2,3-butanediol, and 1,4-dibromo-2-butanol, respectively were mixed with 2 molar equivalent

(plus a 10% excess) of *N,N*-dimethyldodecyl amine. The mixture was refluxed in dry ethanol for 72 h and then cooled at the end of the reaction. The solid material obtained from the reaction was recovered by filtration and recrystallized several times from a mixture of ethylacetate/methanol (10:1 v/v). Gemini surfactants, 1,3-bis(dodecyl-*N,N*-dimethylammoniumbromide)-propane or 12-3-12, 1,4-bis(dodecyl-*N,N*-dimethylammoniumbromide)-butane or 12-4-12, 1,6-bis(dodecyl-*N,N*-dimethylammoniumbromide)-hexane or 12-6-12, 1,8-bis(dodecyl-*N,N*-dimethylammoniumbromide)-octane or 12-8-12, 1,12-bis(dodecyl-*N,N*-dimethylammoniumbromide)-dodecane or 12-12-12 have been synthesized by mixing the required amounts of 1,3-dibromopropane, 1,4-dibromobutane, 1,5-dibromopentane, 1,6-dibromohexane, 1,8-dibromooctane, 1,12-dibromododecane, respectively with 2 molar equivalent (plus a 10% excess) of *N,N*-dimethyldodecylamine. The workup (purification) procedures for these geminis are same as mentioned above for other gemini surfactants. The structures of synthesized compounds were confirmed by nuclear magnetic resonance ($^1\text{H-NMR}$) spectroscopy data. The data are listed in Table 2.1 and $^1\text{H-NMR}$ spectra of all synthesized gemini surfactants are given in Appendix A. $^1\text{H-NMR}$ spectrum of Gemini-12-4-12 is shown by Figure 2.1 as a representative one.



Scheme 2.2: Molecular structures of conventional and gemini surfactants

Table 2.1: Empirical formula, molar mass, and ¹H-NMR data of synthesized gemini surfactants

Compounds	Empirical formula	Molar mass	¹ H-NMR
Gemini-1	C ₃₁ H ₆₈ N ₂ Br ₂ O	644.70	(400MHz, DMSO) δ: 0.860 (t, 6H, CH ₃), 1.239-1.234 (m, 44H, CH ₂), 1.719-1.629 (m, 4H, CH ₂), 3.147 (s, 12H, CH ₃), 4.737 (s, 1H, OH), 6.192-6.172 (t, 1H, CH).
Gemini-2	C ₃₂ H ₇₀ N ₂ O ₂ Br ₂	674.73	(400MHz, DMSO) δ: 0.861(t, 6H, CH ₃), 1.239-1.237 (m, 44H, CH ₂), 1.706-1.676 (t, 4H, CH ₂), 3.081 (s, 12H, CH ₃), 4.117 (s, 2H, OH), 5.794-5.781 (t, 2H, CH).
12-4(OH)-12	C ₃₂ H ₇₀ N ₂ Br ₂ O	658.73	(500 MHz, CDCl ₃) δ: 0.85 (t, 6H, CH ₃), 1.31-1.23 (m, 36H, CH ₂), 1.74 (t, 4H, CH ₂), 2.57 (t, 4H, CH ₂), 3.26(s, 6H, N-CH ₂), 3.33(s, 6H, N-CH ₂), 3.49-3.43(m, 2H, CH), 3.61-3.60 (m, 1H, CH), 3.75-3.73 (m, 1H, CH), 3.90 (t, 1H, CH), 4.17 (t, 1H, CH), 4.59 (s, 1H, O-CH), 5.72 (s, 1H, OH).
12-3-12	C ₃₁ H ₆₈ N ₂ Br ₂	628.73	(400 MHz, CDCl ₃) δ: 0.85 (t, J = 6.9 Hz, 6H, CH ₃), 1.35 – 1.19 (m, 36H, CH ₂), 1.80 – 1.69 (m, 4H, CH ₂), 2.72 – 2.58 (m, 2H, CH ₂), 3.39 (s, 12H, CH ₃), 3.56 – 3.45 (m, 4H, CH ₂), 3.85 – 3.72 (m, 4H, CH ₂).
12-4-12	C ₃₂ H ₇₀ N ₂ Br ₂	642.73	(500 MHz, CDCl ₃) δ: 0.86 (t, 6H, CH ₃), 1.27 – 1.18 (m, 24H, CH ₂), 1.38 – 1.32 (m, 8H, CH ₂), 1.77 – 1.69 (m, 4H, CH ₂), 2.13 – 2.07 (m, 4H, CH ₂), 2.66-2.59 (s, 4H, CH ₂), 3.31 (s, 12H, N-CH ₃), 3.45 – 3.42 (m, 4H, N-CH ₂), 3.91 (t, 4H, N-CH ₂).
12-6-12	C ₃₄ H ₇₄ N ₂ Br ₂	670.73	(400 MHz, CDCl ₃) δ: 0.84 (t, J = 6.8 Hz, 6H, CH ₃), 1.34 – 1.18 (m, 36H, CH ₂), 1.57 – 1.45 (m, 4H, CH ₂), 1.73 - 1.62 (m, 4H, CH ₂), 2.00 – 1.89 (m, 4H, CH ₂), 3.36 (s, 12H, CH ₃), 3.50 – 3.43 (m, 4H, CH ₂), 3.72 – 3.60 (m, 4H, CH ₂).
12-8-12	C ₃₆ H ₇₈ N ₂ Br ₂	698.73	(400 MHz, CDCl ₃) δ: 0.80 (t, J = 6.8 Hz, 6H, CH ₃), 1.37 – 1.16 (m, 44H, CH ₂), 1.69 – 1.58 (m, 4H, CH ₂), 1.85 – 1.69 (m, 4H, CH ₂), 3.28 (s, 12H, CH ₃), 3.47 – 3.37 (m, 4H, CH ₂), 3.61 – 3.48 (m, 4H, CH ₂).
12-12-12	C ₄₀ H ₈₆ N ₂ Br ₂	754.73	(400 MHz, CDCl ₃) δ: 0.82 (t, J = 6.8 Hz, 6H, CH ₃), 1.36 – 1.17 (m, 52H, CH ₂), 1.74 – 1.59 (m, 8H, CH ₂), 3.32 (s, 12H, CH ₃), 3.51 – 3.44 (m, 4H, CH ₂), 3.58 – 3.51 (m, 4H, CH ₂).

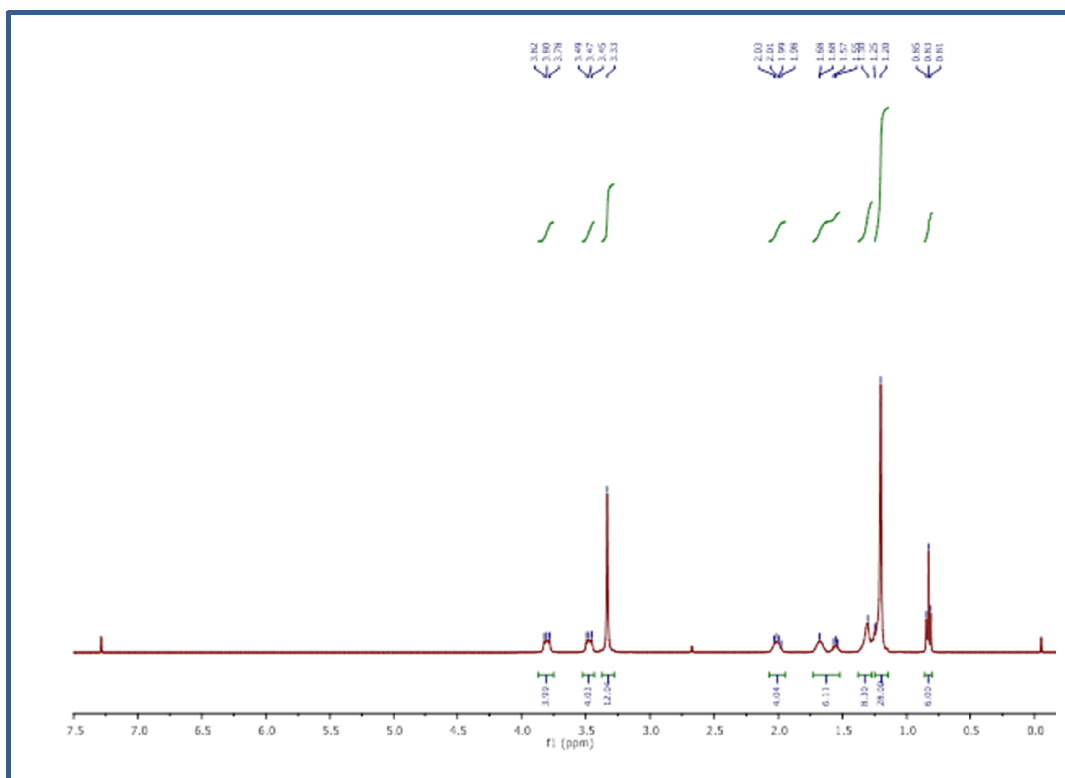


Figure 2.1: ^1H -NMR spectrum of gemini 12-4-12

2.1.3 Solvents and other materials

Solvents such as *n*-hexane, cyclohexane, diethylether, 1,4-dioxane, ethylacetate, tetrahydrofuran (THF), dimethyl formamide (DMF), dimethyl sulfoxide (DMSO), acetonitrile, *n*-butanol, isopropanol, *n*-pentanol, and methanol are procured from Spectrochem Company, India. All solvents were of spectroscopy grade and used as received. Ethanol was purchased from Changshu Yangyuan Chemical Company, China. Ludox as scatterer and quinine sulphate were procured from Aldrich Chemical Company, WI, USA and were used as received. Standard KCl solution of specific conductivity $1413 \mu\text{S}\cdot\text{cm}^{-1}$ for calibration of conductometer was procured from Merck, India. Glycerol was purchased from Alfa Aesar, USA. NaOH and H_2SO_4 used for the adjustment of pH of the solutions were procured from Spectrochem Company, India. Bovine serum albumin (BSA) purchased from Sigma Chemical Company, WI, USA used as received. Urea, guanidine hydrochloride, disodium hydrogen orthophosphate (Na_2HPO_4), phosphoric acid (H_3PO_4) and acrylamide were purchased from Sd-fine Company, India. Na_2HPO_4 was used to prepare buffer solution. H_3PO_4 used to adjust the pH of buffer solution. Triple distilled water was used for the preparation of aqueous and aqueous buffer solutions.

2.2 Methods

2.2.1 Preparation of different solutions

Stock solution of 2-DMASP (0.5 mM) was prepared in pure methanol to record the UV-Visible absorption and fluorescence spectra of it in pure solvents. 0.1 mL of this solution was poured in a 10 mL volumetric flask and left for a few hours for complete evaporation of methanol and then the compound was dissolved in respective solvents to make final volume of 10 mL. The final concentration of 2-DMASP in all the experimental solutions used for spectroscopic measurements was 5 μ M.

For the preparation of the solutions of different concentrations of hexadecyltrimethylammonium, CTAX (X= Br⁻, SO₄²⁻, NO₃⁻, and PTSA) with different counterions in water with constant concentration of 2-DMASP, 0.015 mL of 2-DMASP solution in methanol was added in a vial and left till the evaporation of methanol. After the evaporation of methanol, required volume of aqueous solution of surfactants was added and the final volume of it was adjusted to 1.5 mL. The final concentration of 2-DMASP in all the solutions was 5 μ M.

Stock solution of DMACA (0.5 mM) was prepared in pure methanol. For the preparation of solutions of different concentrations of gemini surfactants, conventional surfactant and their mixture (mixed surfactant) in water with constant concentration of DMACA, 0.015 mL of DMACA solution in methanol was added in a vial and left till the evaporation of methanol. Methanol was evaporated because of good solubility of DMACA in water at this concentration. After the evaporation of methanol, required volume of aqueous solution of gemini surfactants, conventional surfactants and their mixture were added and the final volume of it was adjusted to 1.5 mL. The final concentration of DMACA in all the solutions was 5 μ M. Similar method was opted for the preparation of solutions of different concentrations of gemini surfactants, conventional surfactants and their mixture (mixed surfactant) in water with constant concentration of pyrene (2 μ M).

To study the solvation dynamics and rotational relaxation of C-153 in aqueous solution of 12-3-12, 12-4-12, 12-6-12, 12-8-12, 12-12-12, TX-100 and in mixed surfactant systems of TX-100 and 12-s-12 (s = 3, 6, 8, and 12) a constant concentration of C-153 (5Mm) was used. The stock solution of C-153 (0.5 mM) was prepared in pure

methanol and 0.05 mL of C-153 was added in a test tube and left till the evaporation of methanol. Then required volume of gemini surfactants and TX-100 (in case of mixed surfactants systems) was added and the final volume of it was adjusted to 5 mL. For the study of effect of urea concentration on solvation and rotational relaxation of C-480 in presence of fixed concentration of 12-4-12 constant concentration (5 μM) of C-480 was used. DPH solution was prepared in THF. After preparation of surfactants solutions in presence of DPH in test tubes, the test tubes were kept in dark before measuring absorption and fluorescence.

For the preparation of reverse micelles (RMs) of gemini surfactant (12-4-12), calculated amount of 12-4-12 was dissolved in cyclohexane and *n*-pentanol mixed solution. A calculated amount of this solution was transferred into a 20 ml stopper test tube which already contains C-490. Calculated amount of triple distilled water was added into the same test tube to make a water pool. The volume was made up to 10 ml by adding extra cyclohexane and *n*-pentanol solvents. Final concentration of *n*-pentanol in the all the solutions was kept at 2.4%. Many solutions were prepared in the same way by varying the values of w_o . All the solutions were sonicated until they were optically transparent. Final concentrations of C-490 and 12-4-12 in all the solutions were 0.01 mM and 20 mM, respectively.

Sodium-phosphate buffer of 25mM was prepared in triple distilled water, adjusted to pH 7.4 and BSA (5 μM) solutions were prepared in sodium-phosphate buffer solution. Gemini surfactants, acrylamide, and guanidine hydrochloride solutions with varying concentrations were prepared in sodium-phosphate buffer.

For measuring the specific conductance, concentrated stock solutions of gemini surfactants were prepared by dissolving required amounts of surfactants in triple distilled water. Stock solution was then added progressively using a micropipette to a container containing water kept in a thermostat (Julabo, F25) with a temperature accuracy of $\pm 0.01^\circ\text{C}$. Before the measurement of specific conductance (κ), proper mixing and equilibration of solutions were ensured. In a similar way, the aqueous solutions with a given mole fraction of conventional surfactant in the solution but varying total concentration of conventional-gemini mixed surfactants were prepared. All the solutions were then kept for 5–6 h to achieve equilibrium.

2.2.2 Determination of dissociation constant

2.2.2.1 Ground state dissociation constant (pK_a)

The dissociation of an acid can be represented as



The ground state dissociation constant (pK_a) in dilute solution can be related to pH by the Equation 2.2

$$pH = pK_a + \log \left(\frac{[B]}{[BH^+]} \right) \quad (2.2)$$

where [B] and [BH⁺] are the concentration of base and its conjugate acid, respectively.

The plot of pH versus log ([B]/[BH⁺]) is a straight line with a slope = 1. pK_a value was calculated from the intercept of this plot.

If the absorption spectra of the conjugate acid-base species are not overlapped then ([B]/[BH⁺]) is given by

$$\frac{[B]}{[BH^+]} = \frac{\varepsilon_{BH^+} - \varepsilon}{\varepsilon - \varepsilon_B} = \frac{A_{BH^+} - A}{A - A_B} \quad (2.3)$$

where ε_{BH^+} , A_{BH^+} and ε_B , A_B are molar extinction coefficient and absorbance of conjugate acid and base, respectively. If at a selected wavelength absorbance due to conjugate acid is zero, then Equation 2.3 becomes,

$$\frac{[B]}{[BH^+]} = \frac{\varepsilon}{\varepsilon_B - \varepsilon} = \frac{A}{A_B - A} \quad (2.4)$$

where ε and A are molar extinction coefficient and absorbance of base respectively in a solution of intermediate pH .

If the absorption spectra of the conjugate acid-base species overlap with each other, the concentration of the respective species can be determined using following equations:

$$[B] = \frac{A_{\lambda_1} \varepsilon_{\lambda_2}(BH^+) - A_{\lambda_2} \varepsilon_{\lambda_1}(BH^+)}{\varepsilon_{\lambda_1}(B) \varepsilon_{\lambda_2}(BH^+) - \varepsilon_{\lambda_2}(B) \varepsilon_{\lambda_1}(BH^+)} \quad (2.5)$$

$$[BH^+] = \frac{A_{\lambda_1} \varepsilon_{\lambda_2}(B) - A_{\lambda_2} \varepsilon_{\lambda_1}(B)}{\varepsilon_{\lambda_1}(BH^+) \varepsilon_{\lambda_2}(B) - \varepsilon_{\lambda_2}(BH^+) \varepsilon_{\lambda_1}(B)} \quad (2.5)$$

where A_{λ_1} and A_{λ_2} are the absorbances of the solutions at the wavelengths λ_1 and λ_2 respectively. $\varepsilon_{\lambda_1}(B)$, $\varepsilon_{\lambda_2}(B)$, $\varepsilon_{\lambda_1}(BH^+)$, $\varepsilon_{\lambda_2}(BH^+)$ are the molar extinction coefficients of species B and BH^+ at wavelengths λ_1 and λ_2 , respectively. The values of $\varepsilon_{\lambda_1}(B)$, $\varepsilon_{\lambda_2}(B)$, $\varepsilon_{\lambda_1}(BH^+)$, $\varepsilon_{\lambda_2}(BH^+)$ were calculated from the absorbance at the respective λ 's when the pH values were such that only acid or base forms was present in the solution.

2.2.2.2 Excited state dissociation constant

The respective solution at a given pH was excited at the isosbestic wavelength or isosbestic point. The excited state dissociation constant (pK_a^*) was calculated by using Förster cycle method³

$$pK_a - pK_a^* = \frac{E_{HX} - E_X}{2.303RT} \quad (2.7)$$

where E_{HX} and E_X are the energies of electronic transitions for the conjugate acid and base, respectively. These are estimated by averaging the energies corresponding to the absorption and fluorescence maxima of both acid and base forms:

$$E_{HX} = Nhc \left(\frac{\nu_{HX}^a + \nu_{HX}^f}{2} \right) \quad (2.8)$$

$$E_X = Nhc \left(\frac{\nu_X^a + \nu_X^f}{2} \right) \quad (2.9)$$

where the terms in parentheses refer to the wavenumbers for the maxima of absorption and fluorescence.

2.2.3 Solvatochromic comparison method (SCM)

A well known multiparametric approach, solvatochromic comparison method (SCM) proposed by Kamlet *et al.*⁴, has been used to know the information about the individual contribution of different solvent effects. This multiparametric approach method separates the dielectric effect of the solvents (π^*), hydrogen-bond donor ability (α), and hydrogen-bond acceptor ability (β) of the solvent on the spectral properties. The equation describing these effects is:

$$E = E^0 + c\pi^* + a\alpha + b\beta \quad (2.10)$$

where a , b and c are the coefficients and E° is the spectral maxima independent of solvent effects. The values of, π^* , α and β of different solvents have taken from the report of Kamlet *et al.*⁴ The values of E are absorption/fluorescence band maxima in terms of cm^{-1} .

2.2.4 Quantum chemical calculations

All the theoretical calculations of 2-DMASP have been performed using Gaussian 03W suite of programs. The global minimum structures 2-DMASP has been obtained by optimizing the geometry at DFT level using B3LYP hybrid functional and 6-31+G(d,p) basis set. The theoretical potential energy surfaces (PESs) at the ground and first two excited singlet states have been calculated following TICT model as proposed by Grabowski *et al.*^{5,6} The PESs of the first and second excited states in vacuo have been obtained by TDDFT method employing the above mentioned basis set. The TDDFT-PCM model has been used for the construction of PESs in acetonitrile (MeCN) as solvent. The use of TDDFT method for the calculation of excited states has been limited to single point calculations because of unavailability of analytical gradients in this method. Highest occupied molecular orbitals (HOMO) and lowest unoccupied molecular orbital (LUMO) diagrams have also been constructed from the optimized structure and twisted form of 2-DMASP in vacuo and acetonitrile as solvent.

2.2.5 Determination of micropolarity of environment around 2-DMASP, DMACA, C-490, C-153, and pyrene

The micropolarity is expressed in equivalent scale of $E_T(30)$ which is an empirical solvent polarity parameter comparing the fluorescence behavior of probe molecule in microheterogeneous systems to that in a mixture of homogeneous solvents of varying composition.⁷⁻¹⁰ We have followed the same procedure reported by Saha *et al.*¹¹ to calculate the micropolarity in equivalent scale of $E_T(30)$ of the environment surrounding the 2-DMASP, DMACA, C-490, and C-153 in a microheterogeneous system. The emission spectra of 2-DMASP, DMACA, C-490, and C-153 in dioxane-water mixtures were recorded, and then the emission maxima (in terms of wavenumbers) were plotted against $E_T(30)$. The plots have been provided in the respective chapters.

For the calculation of micropolarity around pyrene in presence of solutions of different concentrations of gemini surfactants, conventional surfactant and their mixture (mixed surfactant) in water, the ratio of first (I_1) and third (I_3) vibronic peaks (I_1/I_3) of pyrene has been calculated and compare the same in presence of pure solvents.

2.2.6 Determination of microviscosity of environment around, 2-DMASP, DMACA, and DPH

The steady-state fluorescence anisotropy measurement is important in biophysical and biochemical research in the sense that any factor which is responsible for change in size, shape, or segmental flexibility of a molecule will also change the observed anisotropy.¹² The extent of restrictions imposed by the microenvironment on the dynamic properties of the molecule is directly manifested through the values of fluorescence anisotropy. Fluorescence anisotropy of a fluorescent probe molecule is intimately connected with the viscosity of the microenvironment around it. Hence, microviscosity is estimated from a comparison of the fluorescence anisotropy of a fluorescent probe in an environment with those of the probe in different environments of known viscosities.^{8, 13-15}

The fluorescence anisotropy of 2-DMASP in different percentages (v/v) of glycerol in glycerol-water mixtures have been measured. Fluorescence anisotropy of 2-DMASP in presence of surfactant has been measured. The anisotropy values of 2-DMASP in presence of surfactants and glycerol-water mixtures are correlated. Microviscosity value determined from the plot of variation of viscosity for different percentages of glycerol in glycerol-water mixtures. Similar method also used for the determination of microviscosity around DMACA in pure and mixed surfactant systems.

In case of DPH microviscosity has been determined by using Debye–Stokes–Einstein relation¹⁶

$$\eta_m = kT \tau_r / V_h \quad (2.11)$$

where V_h is the hydrodynamic volume of DPH (313 \AA^3)¹⁶ and τ_r is rotational correlation time of DPH. The rotational correlation time, τ_r , can be obtained from Perrin equation

$$\tau_r = \tau(r_o / r - 1)^{-1} \quad (2.12)$$

where r_o is the steady-state fluorescence anisotropy in a highly viscous solvent and is taken to be 0.362¹⁶, r and τ are steady state fluorescence anisotropy and excited singlet state lifetime in surfactant solution, respectively.

2.2.7 Steady state fluorescence anisotropy measurements

The steady state fluorescence anisotropy, r can be represented as¹²

$$r = \frac{I_{VV} - GI_{VH}}{I_{VV} + 2GI_{VH}} \quad (2.13)$$

where I_{VH} and I_{VV} are the intensities obtained from the excitation polarizer oriented vertically and the emission polarizer oriented in horizontal and vertical positions, respectively. The factor G is defined as:

$$G = \frac{I_{HV}}{I_{HH}} \quad (2.14)$$

where I_{HV} and I_{HH} are the intensities obtained from the excitation polarizer oriented in horizontal position and emission polarizer oriented in vertical and horizontal positions, respectively.

2.2.8 Fluorescence quantum yield, radiative and non-radiative rate constants calculations

The fluorescence quantum yields (ϕ) of the compounds were calculated with reference to quinine sulphate¹⁷ ($\phi = 0.55$) in 0.1N H₂SO₄, the commonly used fluorescence standard. Corrected fluorescence spectra were recorded for solutions of absorbance less than 0.1 at the excitation wavelength. Generally, the longest wavelength band maximum was chosen for excitation. In case of a system with an isosbestic point in the absorption spectra, the excitation was carried out at isosbestic wavelength. Quantum yield of the samples were calculated using the Equation 2.15.

$$\phi_{\text{unknown}} = \phi_{\text{standard}} \times \frac{F_{\text{unknown}}}{F_{\text{standard}}} \times \frac{A_{\text{standard}}}{A_{\text{unknown}}} \quad (2.15)$$

ϕ is fluorescence quantum yield, F is area under the curve of corrected fluorescence spectra, A is absorbance at excitation wavelength.

The rates of radiative and non-radiative processes have been calculated by using the following equations:

$$k_r = \frac{\Phi}{\tau} \quad (2.16)$$

$$k_{nr} = \frac{k_r}{\Phi} - k_r \quad (2.17)$$

τ is the excited singlet state lifetime and k_r and k_{nr} are the radiative and non-radiative decay rate constants, respectively.

2.2.9 Binding constant of probe to micelles

According to the model proposed by Sepulveda and coworkers,¹⁸ the binding constant of the probe molecule (DMACA) to micelles can be determined by the use of the equation:

$$\frac{F - F_o}{[\text{Sur}] - cmc} = K_S F_m - K_S F \quad (2.18)$$

where F , F_o , and F_m are fluorescence intensities of probes at intermediate concentrations of surfactant, in water and when it is completely bound to the micelle. $[\text{Sur}]$ is the concentration of surfactant, cmc is the critical micelle concentration and K_S is binding constant. From the slope of the plot $(F - F_o) / ([\text{Sur}] - cmc)$ versus fluorescence intensity, F , the binding constant, K_S can be calculated.

Binding constant (K_S) of C-153 with different gemini surfactants has been calculated by using the method of Almgren *et al.*¹⁹ (Equation 2.19):

$$(I_i - I_o) / (I_C - I_o) = 1 + (K_S [M])^{-1} \quad (2.19)$$

where I_o , I_C , and I_i are the fluorescence intensities of C-153 in the absence of gemini surfactants, at an intermediate concentration and at saturation condition. The micellar concentration $[M]$ is given by

$$[M] = \frac{([\text{Sur}] - cmc)}{N} \quad (2.20)$$

where $[\text{Sur}]$ is the gemini surfactant concentration and N is the aggregation number.

The standard free energy change for the binding of C-153 with the micelles of gemini surfactants has been calculated by using equation 2.21.

$$\Delta G^o = -RT \ln K \quad (2.21)$$

2.2.10 Determination of aggregation number

Aggregation numbers of micelles were determined by the method of steady-state fluorescence quenching of micellized probe molecules. If the quenching mechanism is static in nature in that case, the measured ratio of the fluorescence intensity (F/F_o) in the presence of quencher to that in the absence of quencher is related to the micellar ($[M]$) and quencher ($[Q]$) concentrations by the Equation 2.22:

$$\frac{F}{F_o} = \exp\left(-\frac{[Q]}{[M]}\right) \quad (2.22)$$

On the basis of pseudophase model, the effective micellar concentrations:

$$[M] = \frac{[Det] - cmc}{N} \quad (2.23)$$

where $[Det]$ is the concentration of surfactants and N is the aggregation number. From the Equations 2.22 and 2.23, one can obtain

$$\ln\left(\frac{F_o}{F}\right) = \frac{N[Q]}{[Det] - cmc} \quad (2.24)$$

Since $[Det] \gg cmc$, neglecting the latter term, Equation 2.24 becomes:

$$\ln\left(\frac{F_o}{F}\right) = \frac{N[Q]}{[Det]} \quad (2.25)$$

For the determination of N , $[Det]$ is kept constant and $[Q]$ is varied. $\ln(F_o/F)$ is plotted against $[Q]$ to determine N from the slopes of the linear curves passing through the origin. In the present work pyrene has been used as probe, since the pyrene fluorescence quenching by cetylpyridinium chloride as a quencher in the micelles of cationic surfactants is known to be static in nature.²⁰

2.2.11 Solvation dynamics

The solvation dynamics is monitored by the decay of the solvent response function (SRF), $C(t)$, which is defined as:

$$C(t) = \frac{\nu(t) - \nu(\infty)}{\nu(0) - \nu(\infty)} \quad (2.26)$$

$\nu(0)$ is the frequency at “zero-time”, as calculated by the method of Fleming and Maroncelli,²¹ $\nu(\infty)$ is the frequency at “infinite time”, which may be taken as the maximum of the steady-state fluorescence spectrum if solvation is more rapid than the population decay of the probe and $\nu(t)$ is the frequency at time t , which can be determined by taking the maximum from the log-normal fits as the emission maximum.^{21,22} The $C(t)$ function can be determined using “spectral reconstruction” method. This method involves reconstruction of time-resolved emission spectra (TRES) from wavelength dependent time-resolved decay data.¹⁸ For this purpose the fluorescence decays are collected at 10/15 nm intervals spanning the fluorescence spectrum. All decays are fitted to be/tri-exponential. The TRES were constructed by following the procedure of Fleming and Maroncelli.²¹ The impulse response function, $I(\lambda, t)$ is defined as in Equation 2.27:

$$I(\lambda, t) = \sum a_i(\lambda) \exp\left[\frac{-t}{\tau_i(\lambda)}\right] \quad (2.27)$$

where $a_i(\lambda)$ is the pre-exponential factor, and $\tau_i(\lambda)$ is the decay time at that wavelength with $\sum a_i(\lambda) = 1$.

A TRES is constructed after calculating a set of $H(\lambda)$ values, which is defined as in Equation 2.28:

$$H(\lambda) = \frac{F(\lambda)}{\sum a_i(\lambda)\tau_i(\lambda)} \quad (2.28)$$

where $F(\lambda)$ is the steady-state intensity. The TRES at different times were constructed from the appropriately normalized intensity decay functions, $I'(\lambda, t)$ for various wavelengths and at various times using Equation 2.29:

$$I'(\lambda, t) = H(\lambda) \times I(\lambda, t) = H(\lambda) \sum a_i(\lambda) \exp\left[\frac{-t}{\tau_i(\lambda)}\right] \quad (2.29)$$

Each time-resolved emission spectrum (TRES) was fitted by “log-normal line shape function”, which is defined as:

$$g(\nu) = g_o \exp\left[-\ln 2 \left(\frac{\ln[1 + 2b(\nu - \nu_p) / \Delta]}{b}\right)^2\right] \quad (2.30)$$

where, g_o , b , ν_p and Δ are the peak height, asymmetric parameter, peak frequency, and width parameter, respectively. The peak frequency evaluated from this log-normal fitting

of TRES was then used to construct the decay of the solvent correlation function $C(t)$. In generating $C(t)$, the first point was obtained from the zero time spectrum. The second point was taken at the maximum of the instrument response function. Finally the time dependence of the calculated $C(t)$ values were fitted by bi/tri-exponential function (Equation 2.31).

$$C(t) = \sum_i a_{is} \exp\left(-\frac{t}{\tau_{is}}\right) \quad (2.31)$$

Then the average solvation time is given by:

$$\langle \tau_s \rangle = \sum_i a_{is} \tau_{is} \quad (2.32)$$

where a_{is} is the relative contribution of the solvation component, τ_{is} .

2.2.12 Time-resolved fluorescence anisotropy

The time-resolved fluorescence anisotropy, $r(t)$ ¹² has been calculated using Equation 2.33:

$$r(t) = \frac{I_{\parallel}(t) - GI_{\perp}(t)}{I_{\parallel}(t) + 2GI_{\perp}(t)} \quad (2.33)$$

where G represents the correction factor for the detector sensitivity to the polarization detection of emission, $I_{\parallel}(t)$ and $I_{\perp}(t)$ are fluorescence decays polarized parallel and perpendicular to the polarization of the excitation light, respectively. G factor for our instrument is ~0.6.

Generally, the fluorescence anisotropy decay of the fluorescence probe molecule residing in micelles, mixed micelles or reverse micelles is having two components, fast and slow components. This bi-exponential fluorescence anisotropy decay is generally not because of its different locations, but due to its various kinds of rotational motions.²³ For detailed explanation of the bi-exponential behavior of anisotropy decay as a result of different types of rotational motions, the theoretical model often used is the two-step and wobbling-in-a-cone model.²⁴ These models are applicable for spherical micelles.

2.2.12.1 Two-step model

According to the two-step model the fast and slow motions are assumed to be separable. If two motions are independent, the total rotational anisotropy function will be biexponential as:

$$r(t) = r_o [a_{1r} e^{-t/\tau_{1r}} + a_{2r} e^{-t/\tau_{2r}}] \quad (2.34)$$

where r_o is the limiting anisotropy to represent the inherent depolarization of the probe molecule, τ_{1r} and τ_{2r} are the fast and slow rotational relaxation components of the probe molecule in various media i.e. in the present case micellar media, respectively, and a_{1r} and a_{2r} are the relative amplitudes of two components, respectively. Based on the two-step model, both lateral diffusion of the fluorophore along the surface of micelles (τ_D) and rotational motion of the micelle as a whole (τ_m) contribute to the slow rotational relaxation time (τ_{2r}). τ_{2r} is related to the relaxation time corresponding to the τ_m and the relaxation time corresponding to the τ_D as follows (Equation 2.35):

$$\frac{1}{\tau_{2r}} = \frac{1}{\tau_D} + \frac{1}{\tau_m} \quad (2.35)$$

To compute the τ_m , Debye-Stokes-Einstein (DSE) equation is used assuming that the spherical micelle is rotating in the solvent (in our case water) with sticking boundary conditions²⁵ as follows:

$$\tau_m = \frac{4\pi\eta r_h^3}{3kT} \quad (2.36)$$

where r_h is the hydrodynamic radius of the micelle, η is the shear viscosity of water, k is the Boltzmann constant and T is the temperature in Kelvin scale. Knowing the values of τ_{2r} and τ_m , τ_D can be calculated using Equation 2.35.

2.2.12.2 Wobbling in a cone model

The restricted motion of a rodlike rotor with the transition moment parallel to the long axis is described by the wobbling-in-a-cone model.²³ This model describes the internal motion of the probe (τ_e) in terms of a cone angle (θ_o) and wobbling diffusion coefficient (D_w). The schematic representation of wobbling-in-a-cone model is shown in Figure 2.2. To measure the spatial restrictions of the motion of the probe molecule in its surroundings, the order parameter, S is often computed. The value of the order parameter

ranges from 0 to 1, where a value of 0 indicates no restriction and 1 means complete restriction of the rotational motion of the probe molecule. The order parameter is related to the recovery decay of anisotropy by:

$$r(t) = r_o \left[S^2 \exp\left(-\frac{t}{\tau_{2r}}\right) + (1 - S^2) \exp\left(-\frac{t}{\tau_{1r}}\right) \right] \quad (2.37)$$

After comparing Equations 2.28 and 2.31 one can calculate S as, $S^2 = a_{2r}$.

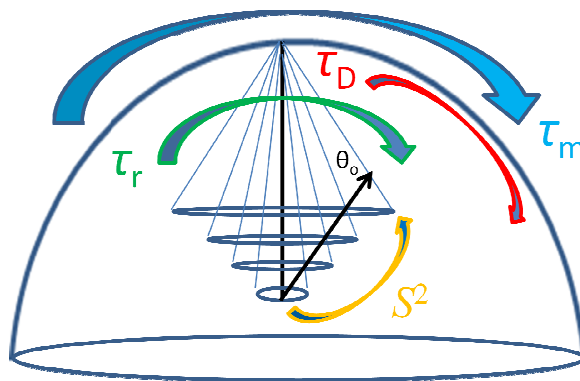


Figure 2.2: Schematic representation of wobbling-in-a-cone model of rotational dynamics

The order parameter is a measure of the equilibrium orientational distribution of the fluorophore. The order parameter is zero if the fluorophore tumbles freely and the equilibrium orientational distribution is completely random. For the micellar solution the value of order parameter generally lies in the range of 0.55-0.88, indicating that the equilibrium orientational distribution is highly constrained because of the aqueous or non-aqueous interface in the micelles or reverse micelles. If the order parameter value is less than 0.5 in micelles then it can be explained on the basis of spinning-in-equatorial-band model.²⁶ The order parameter does not contain any information about the dynamical properties of the fluorophore. The dynamics are instead reflected in the faster rotational correlation time, which can be described by the wobbling motion of the fluorophore. According to the wobbling-in-a-cone model, the order parameter is related to the cone angle, θ_o as in Equation 2.38.

$$\theta_o = \cos^{-1} \left[\frac{1}{2} \left((1 + 8S)^{1/2} - 1 \right) \right] \quad (2.38)$$

According to the spinning-in-equatorial-band, the order parameter is related to the cone angle, θ_0 as in Equation 2.39.

$$S^2 = \left[\frac{1}{2} (1 - \cos^2 \theta_0) \right]^2 \quad (2.39)$$

Wobbling motion time (τ_w) corresponding to the restricted rotational diffusion is related to the fast relaxation time (τ_{1r}) and slow relaxation time (τ_{2r}) as in Equation 2.40:

$$\frac{1}{\tau_{1r}} = \frac{1}{\tau_w} + \frac{1}{\tau_{2r}} \quad (2.40)$$

The wobbling diffusion coefficient, D_w is calculated using Equation 2.41:

$$D_w = \frac{7\theta^2}{24\tau_e} \quad (2.41)$$

where θ is the cone angle in radian. The lateral diffusion coefficient (D_L) is calculated using Equation 2.42.

$$D_L = r_h^2 / 4 \tau_D \quad (2.42)$$

where r_h is hydrodynamic radius of the micelle.

2.2.13 Conductivity measurement

The conductance or specific conductance of an electrolyte solution is the measurement of its ability to conduct electricity. The reciprocal of electric resistance (R) is called electrical conductivity and that of specific resistance (ρ) is called specific conductivity (κ):

$$\kappa = \frac{1}{\rho} = \frac{1}{R} \times \frac{l}{A} \quad (2.43)$$

where, l/A is known as cell constant. Cell constant of the present conductometer is 1.0 cm^{-1} . The SI unit of specific conductance is Siemens per meter (Sm^{-1}). The conductivity dip cell was calibrated with a standard KCl solution of specific conductivity $1413 \mu\text{S}\cdot\text{cm}^{-1}$ procured from Merck, India. The experimental determination of specific conductance of surfactant solution helps to calculate their *cmc* and the degree of counter ion dissociation (α). The following parameters have been calculated from conductivity measurement:

(i) Critical Micellar concentration (cmc): Conductivity method can be applied to measure the *cmc* of only ionic surfactants. The change in the specific conductance of

ionic surfactant solutions at the *cmc* is due to the different degree of surfactant ionization below (surfactant monomers behave as strong electrolytes) and above (micelles are partially ionized) the *cmc*. Below the *cmc*, the conductivity of ionic surfactant solutions is made up of independent contributions of cations and anions and increases rapidly, whereas above the *cmc* (due to the formation of micelles) the conductivity of ionic surfactants decreases usually. According to William *et al.*²⁷ the *cmc* of ionic surfactants can be determined by the break point of two straight lines of specific conductivity (κ) versus surfactant concentration plot in pre-micellar and post-micellar region. Some times the determination of the *cmc* using William's method seems to be difficult because it is a tedious task to choose the exact break point in the plot of specific conductance (κ) versus surfactant concentration. So to overcome this problem, Carpena²⁸ proposed a method to calculate the *cmc* value using the plot of specific conductance (κ) versus surfactant concentration. This method is based on the fitting of the experimental raw data to a non-linear function (Equation 2.44) obtained by direct integration of a Boltzmann type sigmoidal function:

$$y = A0 + (A1 * x) + A3 * (A2 - A1) * \ln \left[\frac{\left(1 + \exp\left(\frac{(x - A4)}{A3}\right) \right)}{\left(1 + \exp\left(\frac{-A4}{A3}\right) \right)} \right] \quad (2.44)$$

where $A0$ is the initial conductivity of water, $A1$ and $A2$ are the limiting slopes for low and high concentrations, respectively (or pre- and post-micellar slopes, respectively), $A4$ is the central point of the transition, i.e. the *cmc* and $A3$ is the width of the transition.

(ii) The degree of counter ion dissociation: The degree of counter ion dissociation (α) can be calculated from the ratios of post-micellar and pre-micellar slopes of the plot of specific conductance (κ) versus surfactant concentration using Williams' method. The α can also be determined by Carpena method by taking the ratio of $A2$ and $A1$, which are obtained after using Equation 2.44 on the plot of specific conductance (κ) versus surfactant concentration.

2.2.14 Methods to study thermodynamics of mixed micelles

To study the thermodynamic properties of mixed micelles various methods proposed in literature are explained below:

2.2.14.1 Clint's method

Based on the phase separation model, Clint²⁹ proposed a method to calculate the ideal cmc values (cmc^*) for the mixed surfactant systems. The cmc^* can be calculated using Equation 2.38 for a binary mixed surfactant system:

$$\frac{1}{cmc^*} = \frac{\alpha_1}{cmc_1} + \frac{(1-\alpha_1)}{cmc_2} \quad (2.45)$$

where α_1 is the bulk mole fraction of the first surfactant in mixed system, cmc_1 and cmc_2 are the cmc values of first and second surfactants in pure states, respectively.

2.2.14.2 Rubingh's method

On the basis of regular solution theory, Rubingh *et al.*³⁰ proposed one simplest model for the treatment of non-ideal mixed surfactant systems. This theory allows for the calculation of the micellar mole fractions, X_1^{Rub} by solving Equation 2.46 by iterative method, and also the interaction parameter, β using Equation 2.47:

$$\frac{[X_1^2 \ln(cmc\alpha_1/cmc_1X_1)]}{(1-X_1)^2 \ln[cmc(1-\alpha_1)/cmc_2(1-X_1)]} = 1 \quad (2.46)$$

$$\beta = \frac{\ln(cmc\alpha_1/cmc_1X_1)}{(1-X_1)^2} \quad (2.47)$$

The magnitude of interaction between the two different amphiphiles in the mixed micelle state has been indicated by β . Ideally the values of β should remain constant for the whole composition range. The positive, negative or zero values of β indicate the repulsive, attractive or no interactions, respectively. The attractive interactions in mixed micelles can be called 'synergism' if it follows the conditions which are (i) $\beta < 0$, and (ii) $|\beta| > |\ln(cmc_1/cmc_2)|$ and the repulsive interactions can be called 'antagonism' if it follows the conditions which are (i) $\beta > 0$, and (ii) $|\beta| > |\ln(cmc_1/cmc_2)|$. The activity coefficients of first (f_1) and second (f_2) surfactants within micelles can be calculated by following Equations 2.49 and 2.50, respectively using the micelle mole fraction (X_1^{Rub}) obtained by Rubingh's method.

$$f_1 = \exp[\beta(1-X_1)^2] \quad (2.48)$$

$$f_2 = \exp[\beta(X_1)^2] \quad (2.49)$$

2.2.14.3 Rodenas method

Based on Lange's model,³¹ Rodenas *et al.*³² recently proposed a new method to study the mixed micellar systems. It uses the Gibbs-Duhem equation to relate the activity coefficients of the surfactant in the mixed micelles. It does not introduce any restrictions on the activity coefficients of the surfactants in the mixed micelles and the micelle mole fraction of the surfactant, X_1^{Rod} can be obtained by using Equation 2.50:

$$X_1 = -(1 - \alpha_1) \alpha_1 \left(\frac{\partial \ln cmc}{\partial \alpha_1} \right) + \alpha_1 \quad (2.50)$$

2.2.14.4 Motomura method

Motomura *et al.*³³ have explained the process of mixed micellization on the basis of thermodynamics and takes into account dissociation of ionic surfactants.^{34,35} According to this approach, micellization is considered to be similar to a macroscopic bulk phase, and the energetic parameters associated with the process are expressed by excess thermodynamic quantities. Composition of mixed micelles (\bar{X}_1) can be determined by using the Equation 2.51:

$$\bar{X}_1 = \bar{\alpha}_1 - \left(\frac{\bar{\alpha}_1 \bar{\alpha}_2}{\delta cmc} \right) \left(\frac{\delta cmc}{\delta \bar{\alpha}_1} \right) \times \left[1 - \frac{\delta v_1 v_2}{v_1 v_2 (1 - \bar{\alpha}_1) + v_2 v_1 \bar{\alpha}_1} \right] \quad (2.51)$$

$$\bar{cmc} = (v_1 \bar{\alpha}_1 + v_2 \bar{\alpha}_2) cmc_{\text{exp}} \quad (2.52)$$

where \bar{X}_1 is the micelle mole fraction of the monomeric surfactant, $\bar{\alpha}_1$ is the bulk mole fraction, and δ is the Kronecker delta. $\bar{\alpha}_1$ is given by the following Equation 2.53:

$$\bar{\alpha}_1 = \frac{\alpha_1 v_1}{\alpha_1 v_1 + \alpha_2 v_2} \quad (2.53)$$

where v_1 and v_2 are the number of ions produced by the surfactant upon dissociation. The variable v_1 is given by 1 for non-ionic surfactants, by 2 for monomeric ionic surfactants, and by 3 for dimeric ionic surfactants.

The micellar mole fraction in the ideal state can be calculated by using Equation 2.54:

$$X_1^{\text{ideal}} = \left[\frac{\alpha_1 cmc_2}{\alpha_1 cmc_2 + (1 - \alpha_1) cmc_1} \right] \quad (2.54)$$

The excess Gibbs energy of micelle (G^E) is calculated by the equation:

$$G^E = RT[X_1 \ln f_1 + (1 - X_1) \ln f_2] \quad (2.55)$$

The standard Gibbs free energy of mixed micelle formation (ΔG_m^o) is calculated by the equation:

$$\Delta G_m^o = (3 - 2g)RT \ln X_{cmc} \quad (2.56)$$

where g is the counterion dissociation constant, R is the gas constant, T is the temperature, and X_{cmc} is the cmc in mole fraction.

2.3 Instrumentation

2.3.1 UV-Visible spectrophotometer

UV-Visible absorption spectroscopy is the most widely used spectroscopic tool which provides useful information about the sample under studied. It refers to spectroscopic tool that measures the absorption of UV-Visible radiation, as a function of frequency or wavelength, due to its interaction with a sample. The environmental effects alter the relative energy of ground and excited states, and this alteration causes spectral shifts. The absorbance (A) of an absorber (concentration C) having a molar extinction coefficient ϵ_λ at wavelength λ is given by the Equation 2.57.

$$A = \log \left(\frac{I_o}{I} \right) = \epsilon_\lambda Cl \quad (2.57)$$

where A is absorbance (optical density), I_o and I represent the intensity of the incident and transmitted light, C is the concentration of the light absorbing species and l is the path length of the light absorbing medium. The absorption spectra were collected using Shimadzu UV-1800 (for work explained in Chapter 5, 6, 7, and 9) and Jasco V-630 (for work explained in Chapter 3, and 8) UV-Visible spectrophotometer at room temperature (Figure 2.3). A matched pair of 1 cm quartz cuvettes (Hellma, 1 cm light path, capacity 3.5 ml, Model: 100-QS) was used for absorption measurements.



(a)



(b)

Figure 2.3: Photograph of the (a) Shimadzu UV-1800 and (b) Jasco V-630 UV-Visible spectrophotometers

2.3.2 Steady-state spectrofluorimeter

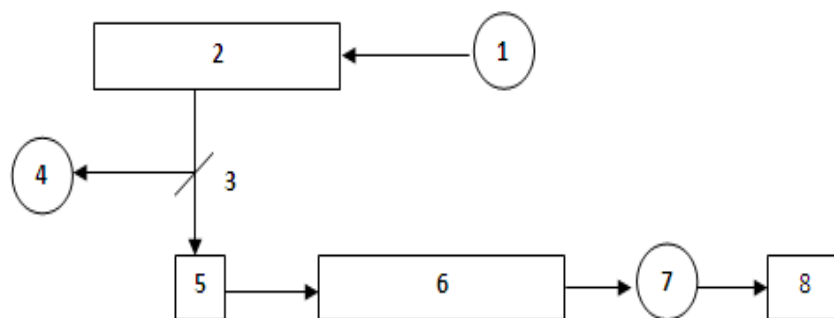
Fluorescence measurements were performed using a Horiba Jobin Yvon Fluoromax-4 scanning spectrofluorimeter and the photograph of this instrument is shown in Figure 2.4. The spectrofluorimeter irradiates a sample with excitation light and measures the fluorescence emitted from the irradiated sample to perform a qualitative or quantitative analysis. The block diagram of the instrument is shown in Scheme 2.3. The brief description of its components is given below.



Figure 2.4: Photograph of the steady-state spectrofluorimeter

This instrument is equipped with the light source of 1905-OFR 150-W Xenon lamp. The lamp housing is provided with ozone self-decomposition. This instrument contains Czerny-Turner monochromators for excitation and emission. The important part of monochromator is a reflection grating. A grating disperses the incident light by means of its vertical grooves. The gratings in this instrument contain $1200 \text{ grooves mm}^{-1}$, and are blazed at 330 nm (excitation) and 500 nm (emission). Blazing is etching the grooves at a particular angle, to optimize the grating's reflectivity in a particular spectral region. This instrument uses a direct drive for each grating to scan the spectrum up to 200 nm s^{-1} , with accuracy better than 0.5 nm, and repeatability of 0.3 nm. The scan range of this instrument is 240-850 nm. The cell holder holds a cell filled with sample.

The emission monochromator selectively receives fluorescence emitted from the sample and the photomultiplier tube (PMT) measures the intensity of the fluorescence. The monochromator has a diffraction grating whose size is the same as that of the excitation monochromator to collect the greatest possible amount of light. The detector in this system consists of photomultiplier tube for both photometry and monitor sides. Generally, the Xenon lamps used in spectrofluorimeter are characterized by very high emission intensity and an uninterrupted radiation spectrum. However, their tendency to unstable light emission will result in greater signal to noise ratio if no counter measure is incorporated. In addition, the non-uniformity in the radiation spectrum of the Xenon lamp and in the spectral sensitivity characteristics of the photomultiplier tube (these criteria are generally called instrument functions) causes distortion in the spectrum. To overcome these factors, the photomultiplier tube monitors a portion of excitation light and feeds the resultant signal back to the photomultiplier tube for fluorescence scanning. This scheme is called the light-source compensation system. The slits widths are adjustable from the computer in units of bandpass or millimeters. This preserves maximum resolution and instant reproducibility. The steady-state fluorescence anisotropy measurements were performed with the same steady-state spectrofluorimeter fitted with a polarizer attachment (105UV polarizers), manufactured by POLACOAT Co., USA. The measurement was obtained by placing one polarizer on each of excitation and emission sides. The sample was taken in a Quartz cuvette (Hellma, 1 cm light path, capacity 3.5 ml, Model: 101-QS) with four walls transparent to measure the excitation and emission spectra.



(1) 1905-OFR 150-W Xenon Lamp, (2) Excitation monochromator, (3) Beam splitter, (4) Monitor side photomultiplier tube, (5) Cell holder, (6) Emission monochromator, (7) Fluorescence side photomultiplier tube, and (8) Recorder

Scheme 2.3: Block diagram of a steady-state spectrofluorimeter

2.3.3 Time-resolved spectrofluorimeter

The excited singlet state lifetimes were estimated from intensity decays using Horiba Jobin Yvon Fluorocube-01-NL picosecond time-correlated single-photon counting (TCSPC) experimental setup. Photograph of this instrument is shown in Figure 2.5. A picosecond diode laser of 375 nm (NanoLED 375L, IBH, UK), and 300 nm and 370 nm nanoled ((NanoLED 300 nm, 370 nm, IBH, UK) were used as a light sources. The fluorescence signals were detected at magic angle (54.7°) polarization using a TBX photon detection module (TBX-07C). The instrument response function of this laser system is ~ 165 ps. A simplified block diagram of the instrument is shown in Scheme 2.4.

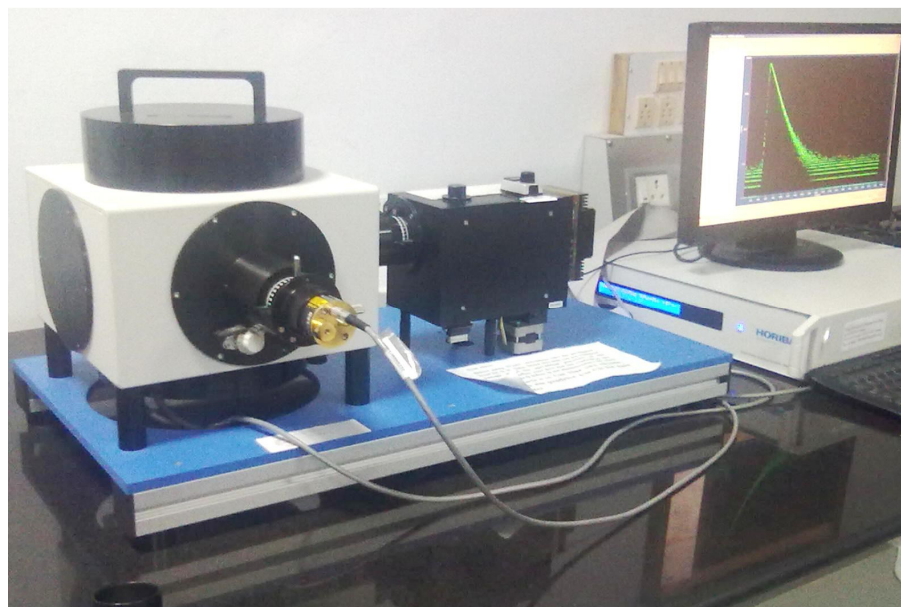
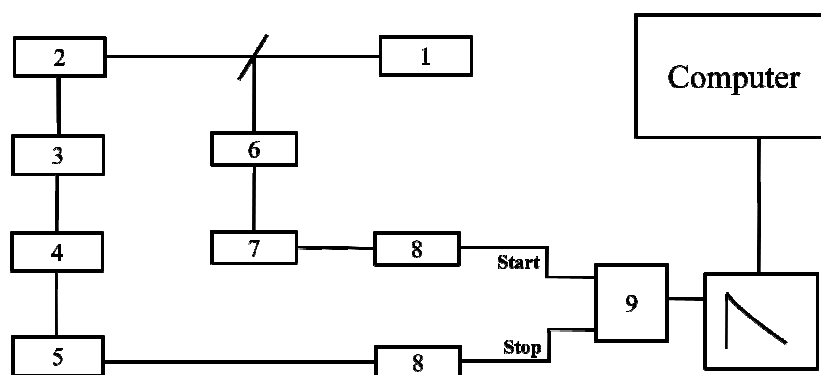


Figure 2.5: Photograph of the time-resolved spectrofluorimeter

2.3.3.1 Time-Correlated Single Photon Counting (TCSPC) technique

TCSPC is based on the detection of single photons of a periodical light signal. It is a statistical sampling technique with single photon detection sensitivity, capable of picosecond timing resolution. The TCSPC technique relies on the concept that the probability distribution for emission of a single photon after an excitation event yields the actual intensity versus time distribution of all the photons emitted as a result of the excitation. By sampling, the single photon emission following a large number of excitation events, the experiment constructs the probability distributions.

Time-to-amplitude converter (TAC) is the heart of this technique. The elapsed time between the initial rise in intensity of the pulse light source and the detection of an emitted photon from the sample is measured by it. In operation, an electrical pulse is generated at a time exactly correlated with the time of generation of the optical pulse by the trigger. After receiving the trigger pulse, the TAC then initiates the charging of a capacitor plate, which is routed to the TAC start input via a discriminator. The same optical pulses (which trigger the TAC) excite the fluorescent sample. Now only one stop photon is detected for every 100-200 excitations. The signal resulting from the detected photon stops the charging ramp in the TAC, which transmits a pulse. The amplitude of this pulse is proportional to the charge in the capacitor, and hence to the time difference between the start and stop pulses.



(1) Diode laser, (2) Sample holder, (3) Fluorescence, (4) Monochromator, (5) Micro-channel plate-photomultiplier tube, (6) Photodiode, (7) Delay, (8) Constant fraction discriminator, and (9) Time-to-amplitude converter

Scheme 2.4: Block diagram of time-resolved spectrofluorimeter

The TAC output pulse is given a numerical value within the analog-to-digital converter (ADC) and a count is stored in the data storage in an address corresponding to that number. Excitation and data storage are repeated again and again in this way until the decay curve of the sample is not obtained.

2.3.3.2 Deconvolution procedure

If the sample is excited with an infinitely short pulse of light, the time domain decay profile will be obtained. But in most of the cases, the excitation pulses are on the same timescale as the fluorescence process. So the fluorescence response become the convolution of the measured instrumental prompt response $P(t')$ and the theoretical fluorescence response function $F(t)$ of the form:

$$R(t) = \int_0^t P(t')F(t-t')dt' \quad (2.58)$$

where t' defines the variable time delays or channel numbers of the infinitesimally small widths dt' (i.e. channel widths) of which the $P(t')$ is composed. There are number of methods available to extract $P(t')$ from $F(t)$ but the most commonly used method is least-square method in concert with an iterative reconvolution scheme. The convolution integral is then calculated by the test model (Equation 2.59)

$$F(t) = \sum_i a_i e^{t/\tau_i} \quad (2.59)$$

and using initial set of a_i and τ_i values and the measured instrument response function. The calculated data is compared with the observed data, and a_i and τ_i terms are adjusted until best fit is obtained. The quality of the fit is tested by the chi-square value (χ^2):

$$\chi^2 = \sum_{i=1}^n \omega_i [R(t) - R_c(t)]^2 \quad (2.60)$$

where $R_c(t)$ is calculated values by assuming the functional form of $F(t)$, ω_i is the weighting factor [$\omega_i = 1/R(t)$], i is the number of data points in the decay file. ω_i follows the Poisson statistics. The χ^2 value close to 1.0 indicates goodness of the fit. The goodness of fit was also checked by weighted residuals. For a good fit the weighted residuals should be randomly distributed around zero.

2.3.3.3 Analysis of fluorescence decays

In all the cases the analysis of fluorescence decays were performed using the commercially available global lifetime analysis software i.e. decay analysis software (DAS 6) of IBH (UK).

2.3.4 Other instruments

The zeta potential and the dynamic light scattering (DLS) measurements of the aggregates of gemini surfactants were carried out in Zeta Sizer, model Nano ZS (ZEN 3600, Malvern Instruments, UK). Photograph of the Zeta Sizer instrument is shown in Figure 2.6. Samples were filtered prior to the measurements with 0.22- μ M filter (Durapore, PVDF). The wavelength of the laser light was 6328 Å, and the scattering angle was 173°.



Figure 2.6: Photograph of the Zeta Sizer instrument

At least five set of measurements were carried out for each sample at ambient conditions. The scattering intensity signal of the sample is passed to a digital signal processing board called a correlator, which compares the scattering intensity at successive time intervals to derive the rate at which the intensity is varying. This correlator information is then passed to a computer and the data was analyzed with the Zetasizer software to derive size information.

To perform conductivity measurements direct reading Eutech Instruments combined pH and conductometer, model PC 510 has been used. The same instrument has been used to adjust the pH of aqueous solutions. Photograph of the conductometer is shown in Figure 2.7. A thermostat, model Julabo, F25 with a temperature accuracy of ± 0.01 °C was used as temperature controller.



Figure 2.7: Photograph of the conductometer

The FT-IR spectra were recorded in ABB Boman MB 3000 instrument. The surfactants were mixed with dry potassium bromide (KBr) powder and pellets were prepared. The pellets have been used to record FT-IR.

¹H-NMR spectra were recorded in deuterated chloroform (CDCl₃) and dimethylsulfoxide (DMSO) solution with a Bruker-avance instrument at SAIF, Punjab University, Chandigarh and at AIRF, Jawaharlal Nehru University, New Delhi, and Department of Chemistry, BITS, Pilani, Pilani Campus.

References:

- (1) N. Jiang, P. Li, Y. Wang, J. Wang, H. Yan, R. K. Thomas, *J. Colloid Interface Sci.* **2004**, 286, 755.
- (2) M. Rosen, L. Liu, *J. Am. Oil. Chem. Soc.* **1996**, 76, 885.
- (3) T. Forster, *Elektrochemie* **1950**, 54, 42.
- (4) M.J. Kamlet, J. L. M. Abboud, M. H. Abraham, R.W. Taft, *J. Org. Chem.* **1983**, 48, 2877.
- (5) Z. R. Grabowski, *Pure Appl Chem* **1992**, 64, 1249.
- (6) Z.R. Grabowski, K. Rotkiewicz, A. Siemiarzczuk, D.J. Cowley, W. Baumann, *Nouv J Chim* **1979**, 3,443.
- (7) R. Das, D. Guha, S. Mitra, S. Kar, S. Lahiri, S. Mukherjee, *J. Phys. Chem. A* **1997**, 101, 4042.
- (8) A. Mallick, B. Haldar, S. Maiti, N. Chattopadhyay, *J. Colloid Interface Sci.* **2004**, 278, 215.
- (9) R.B. Macgregor, G. Weber, *Nature* **1986**, 319, 70.
- (10) S.M. Dennison, J. Guharay, P.K. Sengupta, *Spectrochim. Acta, Part A* **1999**, 55, 1127.
- (11) S.K. Saha, P. Purkayastha, A.B. Das, *J. Photochem. Photobiol. A: Chem.* **2008**, 195, 368.
- (12) J.R. Lakowicz, Principles of fluorescence spectroscopy, Kluwer Academic, New York, 1999.
- (13) A. Mallick, B. Haldar, N. Chattopadhyay, *J. Phys. Chem. B* **2005**, 109, 14683.

-
- (14) A. Mallick, B. Haldar, S. Maiti, S.C. Bera, N. Chattopadhyay, *J. Phys. Chem. B* **2005**, *109*, 14675.
- (15) X. Wang, J. Wang, Y. Wang, H. Yan, P. Li, R.K. Thomas, *Langmuir* **2004**, *20*, 53.
- (16) S. Roy, A. Mohanty, J. Dey, *Chem. Phys. Lett.* **2005**, *414*, 23.
- (17) G.G. Guilbault, *Practical fluorescence*, Marcel Dekker Inc., New York, 1973.
- (18) C. Hirose, L. Sepulveda, *J. Phys. Chem.* **1981**, *85*, 3689.
- (19) M. Almgren, F. Grieser, J. K., Thomas, *J. Am. Chem. Soc.* **1979**, *101*, 279.
- (20) R.G. Alargova, I.I. Kochijashky, M.L. Sierra, R. Zana, *Langmuir* **1998**, *14*, 5412.
- (21) M. Maroncelli, G.R. Fleming, *J. Chem. Phys.* **1987**, *86*, 6221.
- (22) A. Maciejewski, J. Kubicki, K. Dobek, *J. Phys. Chem. B* **2003**, *107*, 13986.
- (23) J. Kinoshita, S. Kawato, A. Ikegami, *J. Biophys.* **1977**, *20*, 289.
- (24) N.C. Maiti, M.M.G. Krishna, P.J. Britto, N. Periasamy, *J. Phys. Chem. B* **1997**, *101*, 11051.
- (25) E.L. Quitevis, A.H. Marcus, M.D. Fayer, *J. Phys. Chem.* **1993**, *97*, 5762.
- (26) L.B.-A. Johansson, A. Niemi, *J. Phys. Chem.* **1987**, *91*, 3020.
- (27) R. Williams, J.N. Phillips, K. Mysels, *J. Trans. Faraday Soc.* **1955**, *51*, 728.
- (28) P. Carpena, J. Aguiar, P.B. Galvan, C.C. Ruiz, *Langmuir* **2002**, *18*, 6054.
- (29) J.H. Clint, *J. Chem. Soc., Faraday Trans. 1* **1975**, *71*, 1327.
- (30) D.N. Rubingh, K.L. Mittal, *Solution Chemistry Surfactants*; Plenum Press: New York, 1979.
- (31) H. Lange, K.H. Beck, *Kolloid Z. Z. Polym.* **1973**, *251*, 424.
- (32) E. Rodenas, M. Valiente, M.S. Villafruela, *J. Phys. Chem. B* **1999**, *103*, 4549.
- (33) K. Motomura, M. Yamanka, M. Aratono, *Colloid Polym. Sci.* **1984**, *262*, 948.
- (34) M. Aratono, M. Villeneuve, T. Takiue, N. Ikeda, H. Iyoto, *J. Colloid Interface Sci.* **1998**, *200*, 161.
- (35) A. Rodriguez, M.M. Graciani, A.J.M. Vargas, M.L. Moya, *J. Phys. Chem. B* **2008**, *112*, 11942.

Chapter 3

Study on intramolecular charge transfer fluorescence properties of trans-2-[4-(N,N-dimethylaminostyryl)]pyridine in homogeneous and micellar media

This chapter is divided into two sections. The photophysical properties and prototropic equilibria of trans-2-[4-(N,N-dimethylaminostyryl)]pyridine (2-DMASP, scheme 3.1) have been discussed experimentally and theoretically in section 3.1. The aggregation behavior of CTAB with various counterions has been demonstrated using change in photophysical properties of 2-DMASP in section 3.2

3.1 Study on photophysical properties and prototropic equilibria of trans-2-[4-(N,N-dimethylaminostyryl)]pyridine*

This section describes the photophysical characterization of a “push-pull” molecule 2DMASP using UV-Visible absorption, steady-state fluorescence and time-resolved fluorescence measurements. 2-DMASP exhibits fluorescence from a locally excited (LE) state in non-polar solvents. However, in polar solvents, fluorescence occurs from an intramolecular charge transfer state (ICT) with high dipole moment obtained not only through the rapid relaxation of LE state upon a single excitation, but also by the excitation of ground ICT state. The twisting of the donor moiety with respect to the acceptor moiety results in a complete charge transfer giving highly Stokes-shifted fluorescence in polar solvents. The potential energy surfaces along the donor and acceptor twist coordinates for the ground and first two singlet excited states have been evaluated at density functional theory (DFT) and time dependent density functional theory (TD-DFT) levels, respectively using B3LYP hybrid functional and 6-31+G(d,p) basis set. Monocation-neutral and dication-monocation equilibria of 2-DMASP at both ground and excited states have been studied.

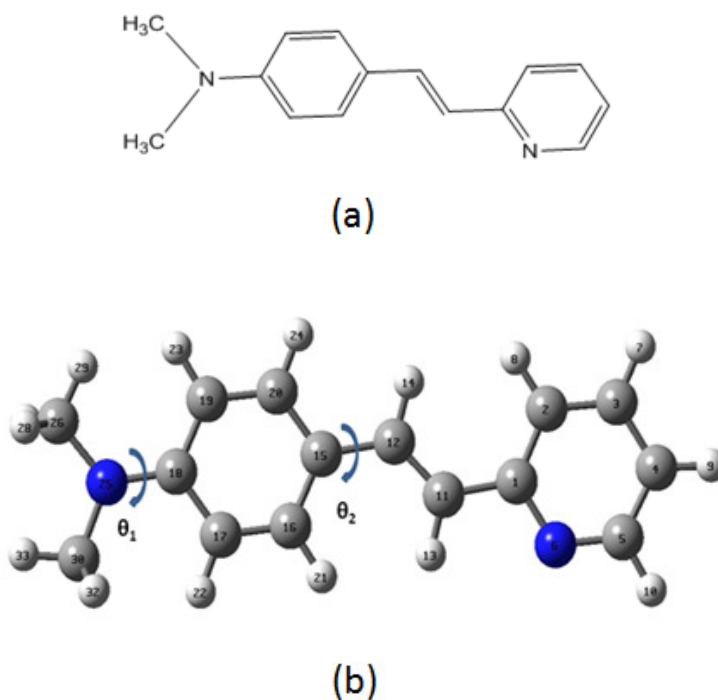
* Sonu, Amit K. Tiwari, Amrit Sarmah, Ram Kinkar Roy, Subit K. Saha, *Dyes and Pigments* **2014**, 102, 114

3.1.1 Results and discussions

3.1.1.1 UV-Visible absorption spectra of 2-DMASP

The UV-Visible absorption spectra of 2-DMASP recorded in different pure solvents of various properties (non-polar, polar aprotic and polar protic) are shown in Figure. 3.1. Absorption spectra of 2-DMASP in these solvents exhibit absorption bands at ~348-370 nm range with a shoulder at ~330 nm (Fig. 3.1). A red-shift is observed for the absorption band with increasing the polarity of the medium (Table 3.1)

This is due to the larger extent of stabilization of the excited state than that of the ground state in the polar environments upon photoexcitation. This phenomenon also indicates that the excited state is more polar than the ground state. This finding is in the agreement with the ICT as a result of transfer of electron from the donor group, -N(CH₃)₂ to the acceptor part of 2-DMASP.^{1,2}



Scheme 3.1: (a) Molecular structure and (b) model of trans-2-[4-(N,N-dimethylaminostyryl)]pyridine (2-DMASP)

It is noteworthy that a concomitant blue shift of the absorption band is observed in water with respect to that in other protic solvents (Figure. 3.1 inset). Similar observation has been reported by Jana *et al.*³ and Paul *et al.*⁴ This could be because of the

presence of intermolecular hydrogen bonding interactions between 2-DMASP and water molecules forming hydrogen bonded solvated clusters.³⁻⁶ This is justified with the fact that the hydrogen bonding efficiency of water is greater than that of other protic solvents. The blue shift of the absorption band is due to the higher stability of the ground state than that of the excited state as a result of hydrogen bonding interactions between solute and solvent molecules. It is pertinent to note that in addition to invoke the solvent polarity effect, the specific solute-solvent interactions are also needed to be considered to account for the photophysical properties of molecular systems with ICT emission.⁷ No significant shift of shoulder of the absorption bands has been observed with increasing polarity of the solvents.

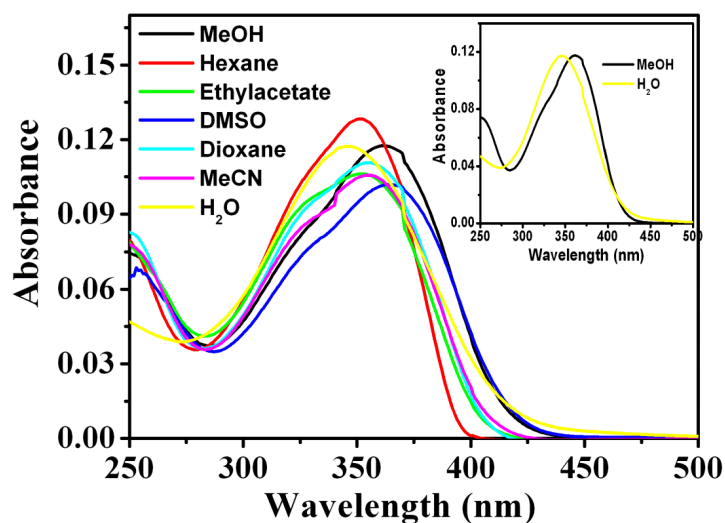


Figure 3.1: Absorption spectra of 2-DMASP in different pure solvents. [2-DMASP] = 5 μ M. Inset shows the absorption spectra in H₂O and MeOH

There are different modes of solute-solvent interactions and these solute-solvent interactions control the solvent induced spectral properties of the solute. To scrutinize the different modes of solute-solvent interactions, a multiparametric approach, solvatochromic comparison method (SCM) has been used (Chapter 2, Section 2.2.3). Excluding the data in water⁸, the equation obtained from this approach with regression coefficient (*r*) value of 0.94 is as follows:

$$E = 28308 - 243.37\pi^* - 1021.28\alpha + 765.28\beta \quad (3.1)$$

The negative values of '*c*' and '*a*' indicate stabilization, whereas positive value of '*b*' indicates destabilization. The negative value of '*a*' means that the lone pair of

electrons on pyridine nitrogen atom is offered to hydrogen-bonding solvents that favors the pulling of electrons from the donor part, $-N(CH_3)_2$ of 2-DMASP. This pulling of electrons is resulting in the greater delocalization of lone pair of electrons of nitrogen atom of donor group with the cloud of the ring.^{1,9,10} The stabilization in the protic solvents also indicates that the basicity of pyridine nitrogen atom is higher than the basicity of nitrogen atom of $-N(CH_3)_2$, because the effect of protonation is the extreme case of hydrogen bonding.⁹

Table 3.1: Solvent polarity parameter ($E_T(30)$), Absorption peak maxima (λ_{\max}^{ab}), fluorescence peak maxima (λ_{\max}^{fl}), Stokes shift ($\Delta\bar{\nu}$) and fluorescence quantum yields (ϕ_f) of 2-DMASP in different solvents

Solvent	$E_T(30)$ (kcal mol ⁻¹)	λ_{\max}^{ab} (nm)	λ_{\max}^{fl} (nm) ^a	$\Delta\bar{\nu}$ (cm ⁻¹)	$\phi_f^{b,c}$
Cyclohexane	30.9	(329),352	418	4485	0.017
<i>n</i> -Heptane	31.1	(329),352	417	4428	0.017
<i>n</i> -Hexane	32.2	(328),352	416	4370	0.016
Diethylether	34.5	(328),350	429	5261	0.022
1,4-Dioxane	36.0	(328),355	438	5337	0.031
THF ^d	37.4	(331),355	453	6093	0.042
Ethylacetate	38.1	(328),352	449	6137	0.030
DMF ^e	43.6	(330),367	469	5925	0.051
DMSO ^f	44.8	(332),370	478	6106	0.054
MeCN ^g	45.6	(330),355	473	7027	0.048
<i>i</i> PrOH ^h	48.4	(330),355	465	6663	0.024
<i>n</i> -BuOH ⁱ	49.7	(329),357	465	6505	0.026
EtOH ^j	51.9	(329),357	476	7002	0.032
MeOH ^k	55.5	(330),362	482	6790	0.019
Water	63.1	348	512	9287	0.015

λ values in parenthesis are for shoulder. ^a $\lambda_{\text{ex}} = 356$ nm, ^b $\lambda_{\text{ex}} = 356$ nm ^cStandard deviation (SD) = ± 0.001 ^dTetrahydrofuran, ^eDimethylformamide, ^fDimethylsulfoxide, ^gAcetonitrile, ^hIsopropanol, ⁱ*n*-Butanol, ^jEthanol, ^kMethanol

To further support this observation, the charge density on both nitrogen atoms in the ground state has been calculated theoretically after optimization the structure using theoretical parameters mentioned in chapter 2 (Sec.2.2.4). The charge densities on the pyridine nitrogen atom and the nitrogen atom of $-N(CH_3)_2$ group are found to be -0.18

and -0.11, respectively. These values are in accordance with the fact that the basicity of pyridine nitrogen atom is higher than that of nitrogen atom of $-N(CH_3)_2$ group in the ground state. The negative value of 'c' is a sign of stabilization due to dipolar interactions which attributes to the red shift of absorption band with increasing polarity of the solvents as also observed in our previous work.^{1,10} It is noteworthy that the dipolar interactions offer minor contribution as compared to hydrogen bonding interactions since the magnitude of 'c' is lesser than that of 'a'.

3.1.1.2 Fluorescence study of 2-DMASP

The fluorescence spectra of 2-DMASP have been recorded in different pure solvents of varying polarities and hydrogen bonding capabilities at $\lambda_{ex} = 356$ nm and are displayed in Figure 3.2. The related spectroscopic parameters (fluorescence peak maximum, Stokes shift and quantum yield) are summarized in Table 3.1. As can be seen from Figure 3.2, the fluorescence band is structured in a nonpolar solvent. This indicates that in a nonpolar solvent fluorescence is originated from the LE state. However, broad structureless fluorescence bands are appeared in polar protic and polar aprotic solvents. The fluorescence spectra of 2-DMASP shifted towards red with increasing the solvent polarity which depicts that fluorescence originates from highly polar excited state of ICT character.^{7,11} These results imply that there are two kinds of emitting states, a nonpolar LE state and a polar ICT state. In a non-polar solvent fluorescence occurs from the LE state while in a polar solvent ICT state becomes responsible for emission. It is reported that increasing the hydrogen bonding ability of the solvent favors red shifted ICT emission^{1,3-5,7,12-14} We also observed the same red shifted ICT emission in polar protic solvents (Figure 3.2). It is to be noted that the fluorescence spectra show no dependence on the excitation wavelength.

The excitation spectra of 2-DMASP in different solvents have been recorded. It has been observed that the excitation spectra are emission wavelength dependent in polar aprotic and polar protic solvents. Figure 3.3 represents the excitation spectra of 2-DMASP in MeOH as solvent at different emission wavelengths as a representative figure. An excitation spectrum found at ~ 353 nm is gradually red shifted with increasing the emission wavelength and finally the bands appear with fixed wavelength maximum at ~ 366 nm. The excitation spectra with a peak maximum at ~ 353 nm match with an absorption spectrum in a non-polar solvent, whereas

excitation spectra with a peak maximum at ~ 366 nm is similar to an absorption spectrum in polar aprotic as well as polar protic solvents.

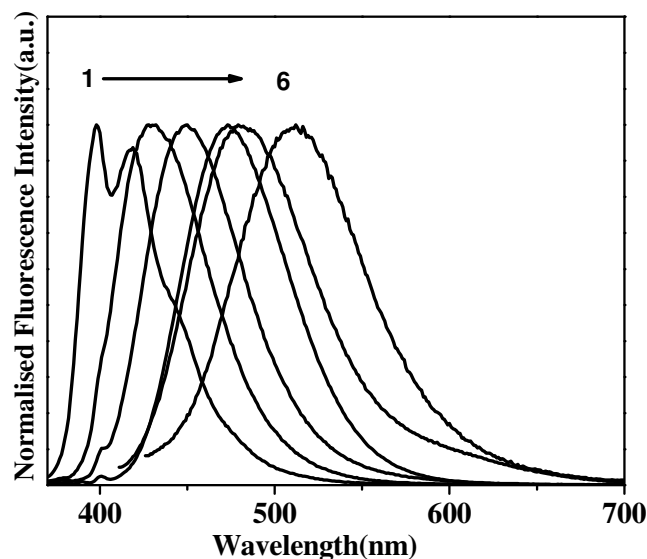


Figure 3.2: Emission spectra of 2-DMASP in different pure solvents at $[2\text{-DMASP}] = 5\mu\text{M}$. Spectra 1 to 6 correspond to cyclohexane, diethylether, ethylacetate, MeCN, MeOH, and H_2O , respectively. $\lambda_{\text{ex}} = 356$ nm

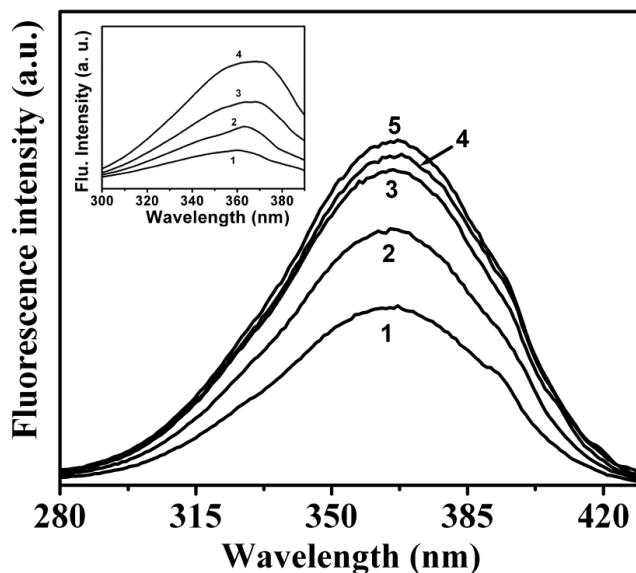


Figure 3.3: Excitation spectra of 2-DMASP in MeOH at different emission wavelengths. 445(1), 455(2), 465(3), 490(4), and 480(5). Inset represents clear change in excitation spectra with respect to emission wavelength 410(1), 415(2), 420(3), and 425(4)

Thus emission wavelength dependent excitation spectra in polar solvents suggest that different excited species are responsible for emission, although intensity of LE state fluorescence is very low in the present case. However, emission wavelength independent excitation spectra in non-polar solvents imply that fluorescence emission occurs only from LE state. Unlike the results reported by Chakraborty et al.⁷, in the present case the ICT state of 2-DMASP may not be created only through singly LE species, but also by excitation of ground state ICT species as well. This ground state ICT species could be created as a result of formation of complex between 2-DMASP and solvent because of interactions between solute and solvent shell.¹⁵⁻¹⁹ Similar results were also obtained in our previous study with 4-DMASP.¹

To further study the existence of two different emitting states, fluorescence spectra of 2-DMASP have been recorded in dioxane-water mixtures of varying compositions and are shown by Figure 3.4. There is a continuous red shift of emission maxima with increasing the percentage of water. The intensity of the band continuously increased up to ~30% of water in the mixture and then starts decreasing with further increasing the percentage of water (Inset of Figure 3.4). These observations suggest that ICT excited state is generated through the LE state. The initial increase in fluorescence intensity with concomitant red shift in fluorescence band with increasing percentage of water is due to progressive increase in the population of ICT state. The fluorescence intensity then starts decreasing with further increase in the amount of water in the mixture is because of the stabilization of ICT state. At this stage the quenching of fluorescence is because of opening of non-radiative paths as a result of stabilization of ICT state making the state energetically closer to the triplet as well as ground twisted states.^{1,4,5,20} Excitation spectra of 2-DMASP in non-polar solvents have been recorded and found to be independent of the emission wavelength which is contrary to the excitation spectra of same in polar protic and polar aprotic solvents. Figure 3.5 represents the excitation spectrum of 2-DMASP in cyclohexane which is almost matching with the absorption spectrum of same in cyclohexane. Absorption spectrum of 2-DMASP in cyclohexane is also matching with the lower emission wavelength excitation spectrum of 2-DMASP in MeOH. This phenomenon indicates that the LE state is responsible for the fluorescence band of 2-DMASP in higher energy region. However, matching of excitation spectrum in MeOH at higher emission wavelength with the absorption spectrum in the same solvent indicates that the band is due to ICT fluorescence.

Although fluorescence originates from two different emitting states, LE and ICT in polar protic and polar aprotic solvents, but the quantum yield of LE fluorescence is very low in these solvents. This low quantum yield of LE fluorescence could be because of rapid relaxation of the initially formed LE state to ICT state and is in excellent harmony with literature report on various amino stilbenes.²¹

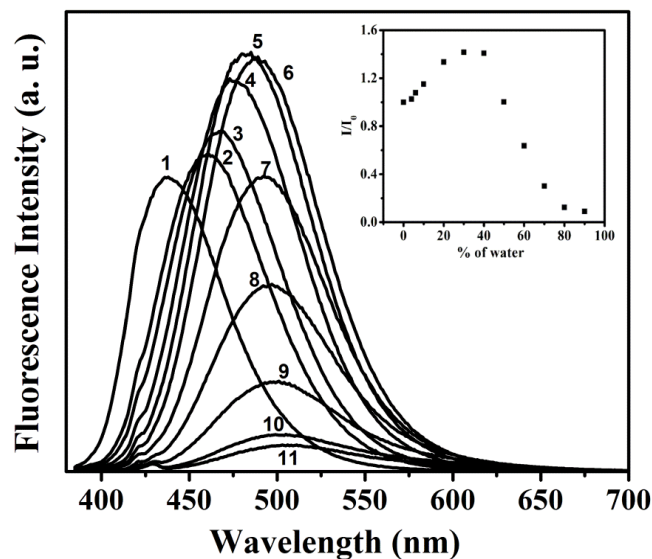


Figure 3.4: Fluorescence spectra of 2-DMASP in different percentages of dioxane-water mixtures, From 1 to 11, % of dioxane is 100, 94, 90, 80, 70, 60, 50, 40, 30, 20 and 10 respectively. Inset shows the fluorescence intensity ratio of 2-DMASP in different percentages of dioxane-water mixtures. $\lambda_{ex}=374$ nm

Kamlet's SCM has also been used to analyze the fluorescence data. The equation obtained by this method with good regression coefficient ($r = 0.99$) is as follow:

$$E = 23854.303 - 3483.021\pi^* - 1357.585\alpha + 434.822\beta \quad (3.2)$$

The higher magnitudes of 'c' as well as 'a' for excited state as compared to that for ground state indicate that both dipole-dipole interactions and hydrogen bond acceptor ability of 2-DMASP contribute more to the stabilization of excited state than that of ground state. The higher magnitude of 'c' at the excited state than that in ground state is attributed to the greater extent of dipole-dipole interaction at the former state because the excited state dipole moment of 2-DMASP (15.23 Debye, discussed later) is much higher than the ground state dipole moment (4.96 Debye). Moreover, higher magnitude of 'a' in the excited state than that in the ground state supports the fact that there is a greater extent of transfer of charge from the donor to the acceptor part of 2-DMASP at the

former state than that in the later state. It is also noteworthy that the dipole-dipole interactions has major contribution towards the stabilization of excited state as compared to that by hydrogen bond acceptor ability of 2-DMASP. However, this is appeared in reversed manner as far as the contribution towards the stabilization of ground state is concerned as discussed above.

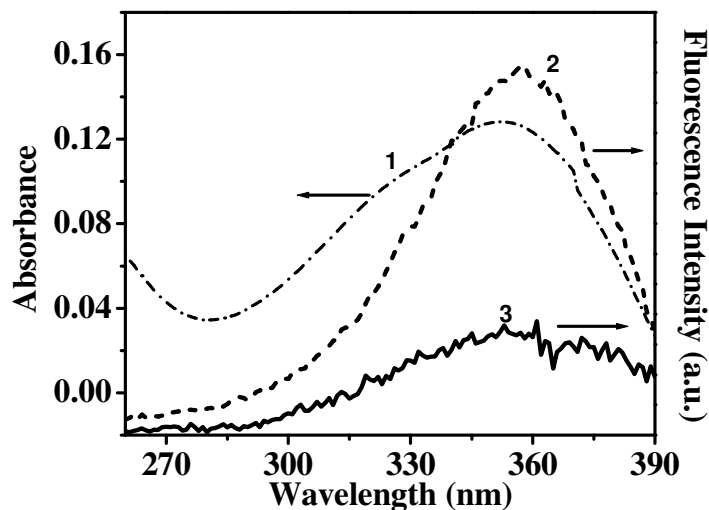


Figure 3.5: Absorption (1) and excitation (2) spectrum ($\lambda_{em} = 470$ nm) of 2-DMASP in cyclohexane and excitation (3) spectrum of 2-DMASP in MeOH ($\lambda_{em} = 410$ nm)

The polarity sensitive emission properties of 2-DMASP are assessed through implementation of Lippert-Mataga equation (Chapter 1, Section 1.4.2.2). The cavity radius and ground state dipole moment of global minimum structure of 2-DMASP have been calculated respectively as 5.05 Å and 4.96 Debye at DFT level using B3LYP functional and 631G+(d,p) basis set by Gaussian 03W suite of programs. Using the slope of Lippert-Mataga plot (Figure 3.6), the excited state dipole moment is found to be 15.23 Debye. This enormous change in the dipole moment of 2-DMASP from ground to excited state is indicating a great extent of redistribution of atomic charge from donor part to acceptor part⁴ in the excited state. The huge difference between the dipole moments of 2-DMASP at ground and excited states is consistent with the higher extent of contribution of dipole-dipole interaction towards the stability of excited state than that of ground state as discussed above. The found dipole moment of 2-DMASP (15.23 Debye) is lower than that of 4-DMASP (16.98 Debye) studied by us earlier.¹ This could be because of larger charge separation in the latter than that in the former as expected from the different placement of nitrogen atom in these two molecules.

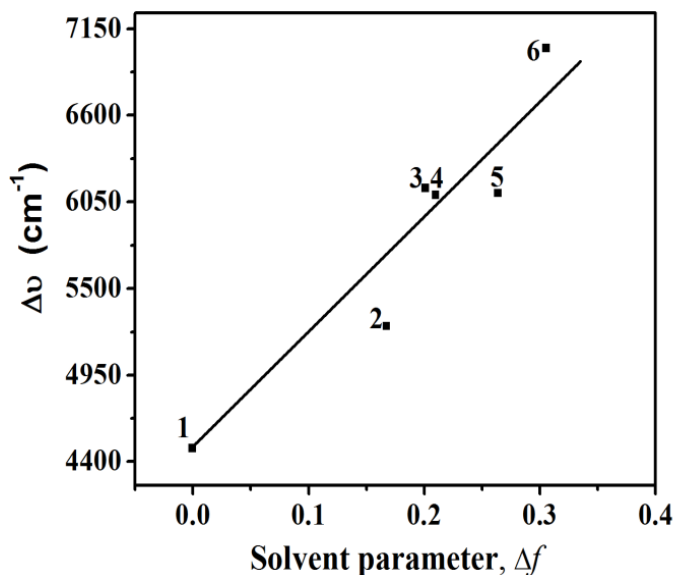


Figure 3.6: Plot of Stokes shift, $\Delta\nu$ (cm^{-1}) of 2-DMASP vs. solvent parameter, Δf in (1) cyclohexane, (2) diethylether, (3) ethylacetate, (4) THF, (5) DMF and (6) MeCN

The Stokes shifts of 2-DMASP in different solvents have been plotted against solvent polarity parameter, $E_T(30)$ (Figure 3.7). The plot of Stokes shift vs $E_T(30)$ produced two separate lines with different slopes, one for non-polar and polar aprotic solvents and the other for polar protic solvents. This observation clearly shows that two types of interactions are present. In case of polar aprotic solvents only dipolar interaction is effective, however for polar protic solvents both dipolar and hydrogen-bonding interactions are present.^{3,4,12,14}

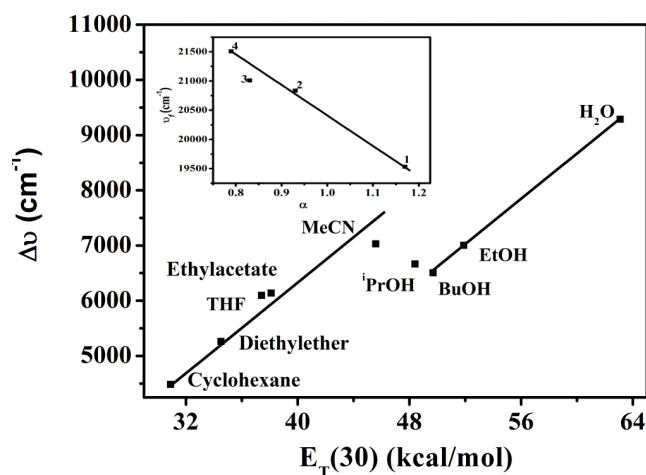


Figure 3.7: Plot of Stokes shift, $\Delta\nu$ (cm^{-1}) versus solvent polarity parameter, $E_T(30)$ (kcal mol^{-1}) for 2-DMASP in different polar aprotic and polar protic solvents. Inset shows the plot of emission maxima in terms of wavenumber, $\bar{\nu}_f$ (cm^{-1}) versus hydrogen bonding parameter, α . H_2O (1), MeOH(2), EtOH(3), *i*PrOH(4)

Inset of Figure 3.7 displays the plot of emission maxima, $\bar{\nu}_f$ (in cm^{-1}) of 2-DMASP versus hydrogen-bonding parameter, α in polar protic solvents and the emission maxima varies linearly with α . The linearity of the plot again indicates that the ICT fluorescence characteristics in polar protic solvents are affected by the hydrogen-bonding interaction.^{3,4}

3.1.1.3 Effect of nature of solvents on excited singlet state lifetime

The excited singlet state lifetimes of 2-DMASP in different pure solvents have been recorded (Table 3.2). The average singlet state lifetime for a biexponential iterative fitting has been calculated from the pre-exponential factors (a_i) and decay times (τ_i) using the following equation¹:

$$\langle \tau \rangle = a_1 \tau_1 + a_2 \tau_2 \quad (3.5)$$

Depending on the nature of solvents different kinds of species of 2-DMASP exist in the excited state and as a result of that the decay profiles vary. The monoexponential decay in a nonpolar solvent (dioxane) is due to the LE species and the same in a highly polar solvent (MeOH) is due to the ICT species. However, both LE and ICT species are responsible for the biexponential decay in the solvent of intermediate polarity. The lifetime of the fast component (τ_1) corresponds to the ICT species, but the slower component (τ_2) belongs to the LE species.¹³ In DMSO, MeCN and *n*-BuOH decays are biexponential correspond to LE and ICT species. The two components are almost equally populated in DMSO. The comparatively higher average lifetime in DMSO as compared to that in other solvents could be because of restricted motions in 2-DMASP in this viscous solvent. The restricted motions cause slower rate of non-radiative processes resulting in comparatively higher quantum yield (0.054). Data in Table 3.2 show that with increasing the polarity and/or hydrogen bond donor ability of the solvents, there is a decreasing tendency of the average lifetimes and also the lifetimes of ICT species. It is also noteworthy that with increasing the polarity of the solvents, the weightage of the fast component increases with concomitant decrease in the weightage of the slower component which is in consistent with the decrease in fluorescence quantum yield. These results rationalize the fact that there would be progressive increase in the population and stabilization of the ICT species with increasing polarity of the solvent. Time-correlated single photon counting (TCSPC) fluorescence intensity decay profiles of 2-DMASP in some selected solvents are shown by Figure 3.8.

Table 3.2: Excited singlet state lifetimes (τ_i)^{a,b}, average singlet state lifetimes ($\langle\tau\rangle$), pre-exponential factors (a_i), quantum yields (ϕ), radiative (k_r) and non-radiative (k_{nr}) rate constants of 2-DMASP in different pure solvents

Solvent	$E_T(30)$ (kcal mol ⁻¹)	ϕ	τ_1 (ps)	a_1	τ_2 (ps)	a_2	$\langle\tau\rangle$ (ps)	$k_r \times 10^{-8}$ (s ⁻¹)	$k_{nr} \times 10^{-9}$ (s ⁻¹)	χ^2
1,4-Dioxane	36.0	0.031	-	-	98	1.00	98	0.32	0.99	1.03
DMSO	44.8	0.054	157	0.48	405	0.52	287	1.88	3.30	1.02
MeCN	45.6	0.048	178	0.86	353	0.14	202	2.38	4.71	1.02
n-BuOH	49.7	0.026	88	0.88	324	0.12	116	2.24	8.40	1.08
MeOH	55.5	0.019	75	1.00	-	-	75	2.53	13.1	1.03

^a $\lambda_{ex} = 375$ nm. ^b λ_{em} are peak maxima in respective solvents

The radiative (k_r) and non-radiative (k_{nr}) rate constants of 2-DMASP in different solvents have been calculated using Equation 2.16 and 2.17, respectively (Chapter 2, Section 2.2.8). The results show that with increasing the polarity of the solvents, the rate of non-radiative processes increases. The lifetime of 2-DMASP in MeOH is significantly shorter than that in a polar aprotic solvents. MeOH being a highly polar protic solvent induces high degree of stabilization of the ICT state of 2-DMASP producing a single exponential fast decay component of only ICT character. This phenomenon is attributed to the high rate of non-radiative processes and low fluorescence quantum yield of 2-DMASP in MeOH (Table 3.2) as a result of not only intersystem crossing from excited ICT state to the triplet state, but also internal conversion from excited ICT state to the ground ICT state.¹

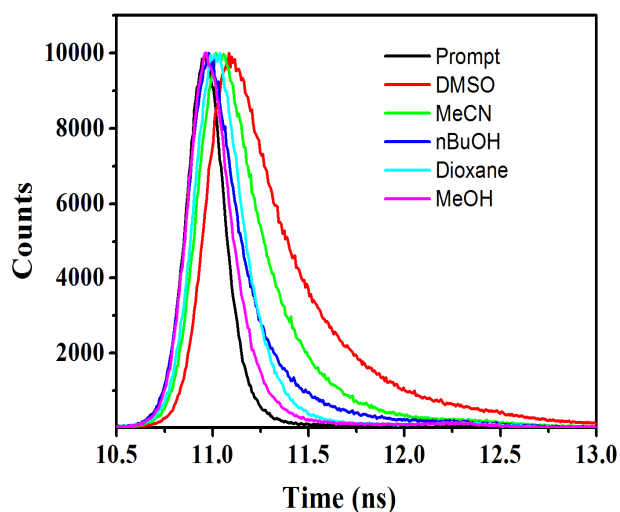
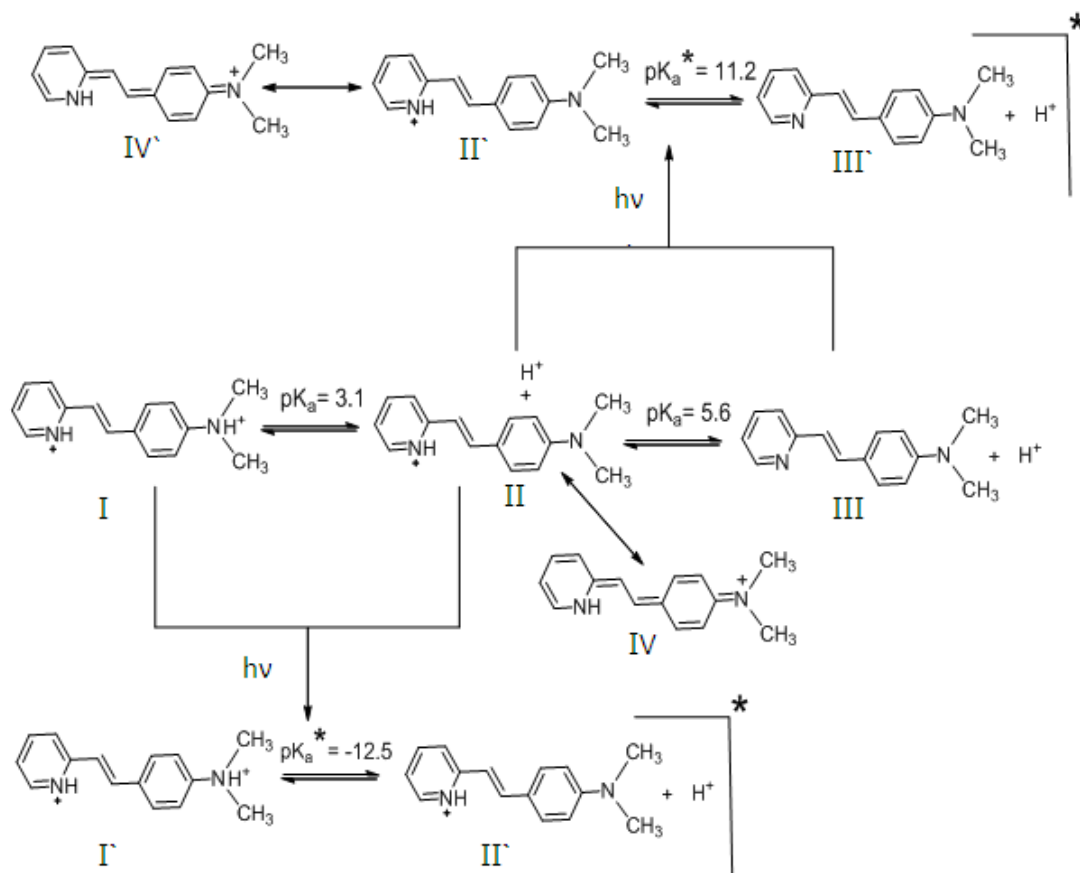


Figure 3.8: TCSPC fluorescence intensity decay profiles of 2-DMASP in some selected solvents, $\lambda_{ex} = 375$ nm. λ_{em} are peak maxima in respective solvents

3.1.1.4 Effect of pH on absorption and fluorescence spectra of 2-DMASP

Effect of pH on absorption and fluorescence spectra of 2-DMASP has been studied. Scheme 3.2 shows the equilibrium between dication and monocation, and also between monocation and neutral species in the ground and excited states. Figure 3.9 displays the absorption spectra of monocation II and neutral III species of 2-DMASP in equilibrium at various pH in aqueous medium. It has been shown in the absorption spectra in Figure. 3.1 that 2-DMASP has a band maximum at 347 nm in water at pH 7.4. As the pH of the solution goes below 7.3, the absorption band of monocation II with band maximum at 425 nm starts emerging at the expense of the band of neutral III species at 347 nm. An isosbestic point for this equilibrium (species II and III) is observed at ~374 nm. It is already mentioned that in the ground state, the charge density on pyridine nitrogen atom is more than that on the nitrogen atom of $-N(CH_3)_2$ group. So, with lowering the pH of the solution below 7.3, the protonation preferentially occurs at pyridine nitrogen atom. Protonation at pyridine nitrogen atom leads to the greater extent of pulling of charge from the donor to the acceptor part and the band maximum shift towards longer wavelength. Very large red shift of the spectrum of monocation II can also be due the occurrence of resonance interaction of the lone pair of electrons of $-N(CH_3)_2$ group with the π -cloud of acceptor part leading to the resonating structure IV.

Further decrease in the pH of the solution below 4.65 the absorbance of monocation II species starts decreasing and simultaneously a new band starts appearing at 325 nm (Figure. 3.10). The band at 325 nm is due to the formation of dication I of 2-DMASP and it is blue shifted with respect to neutral III species as well. Absorbance of dication I species continuously increases with further decrease in the pH of the solution. A clear isosbestic point is observed at 353 nm and it reveals that equilibrium exists between dication I and monocation II. The dication I species is blue shifted with respect to neutral III species, since the lone pair of nitrogen atom of $-N(CH_3)_2$ group engaged with proton and no more available for transfer of charge from the donor site.



Scheme 3.2: Dication-monocation and monocation-neutral equilibria of 2-DMASP in aqueous solution at ground and excited states

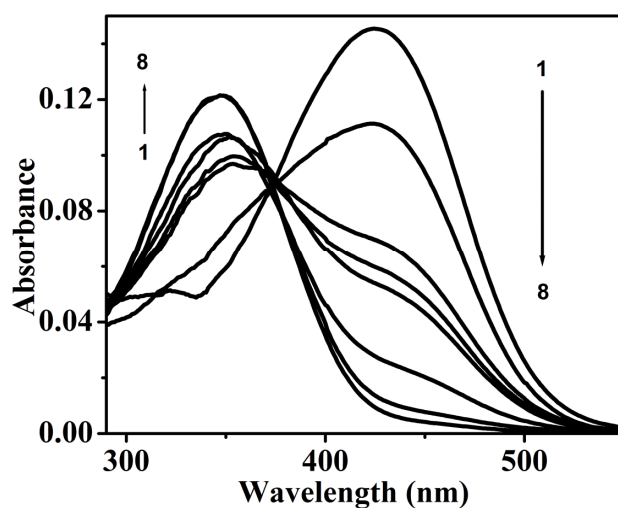


Figure 3.9: Absorption spectra of neutral-III and monocation-II species of 2-DMASP (Scheme 3.2) in equilibrium in aqueous solutions at different pH. Spectra from 1 to 8 correspond to the pH 4.65, 5.21, 5.46, 5.58, 5.70, 6.23, 7.25, and 7.89, respectively

The ground state pK_a of dication-monocation (species I and II) and monocation-neutral (species II and III) equilibria have been calculated using Henderson equation and found to be 3.1 and 5.6, respectively. In our earlier study, the pK_a value of dication-monocation equilibrium of 4-DMASP was also found to be same as 2-DMASP.¹

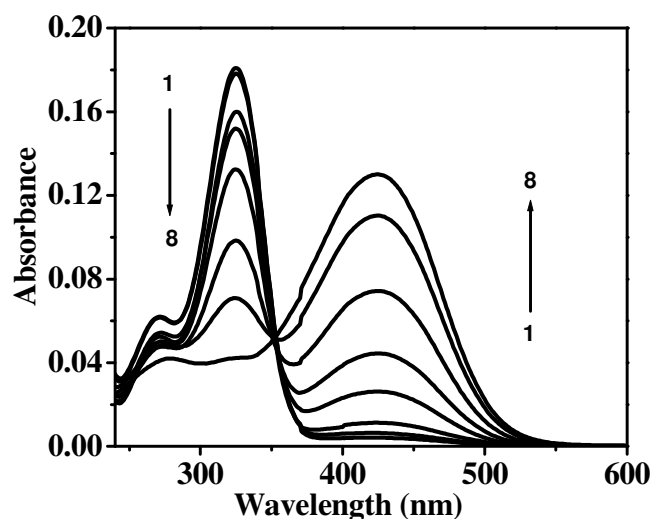


Figure 3.10: Absorption spectra of monocation-II and dication-I (Scheme 3.2) in equilibrium in aqueous solutions at different pH. Spectra from 1 to 8 correspond to the pH 1.92, 2.11, 2.43, 2.74, 2.97, 3.28, 3.61, and 3.88, respectively

The fluorescence spectra of various species involved in both the said equilibria have also been recorded to study the equilibria at the excited state. To study the equilibrium between the excited state monocation and neutral species (species II' and III', respectively), the fluorescence spectra were recorded between pH 7.65 to 3.91 (Figure. 3.11). In water at pH 7.65, the fluorescence band appears at 512 nm. Initially with decreasing the pH of the solution the fluorescence intensity decreases without giving any band for monocation species. A fluorescence spectrum with mixed bands appears only at pH 4.37. At a pH of 3.91, a broad band with peak maximum at ~578 nm was observed. This band is apparently for monocation species II'. Appearance of no clear band corresponding to the monocation species II' could be because of the fact that the monocation species has got two resonating structures (II' and IV'). As compared to ground state the resonating structure, IV' might be easily accessible at the excited state. The excited state acidity constant (pK_a^*) of this monocation neutral equilibrium, has been calculated using Förster cycle (Chapter 2, Section 2.2.2.2). The pK_a is the ground state

acidity constant = 5.6. The pK_a^* is found to be 11.2. However, pK_a^* value calculated is not accurate as the fluorescence band maximum of the monocation species could not be calculated precisely.

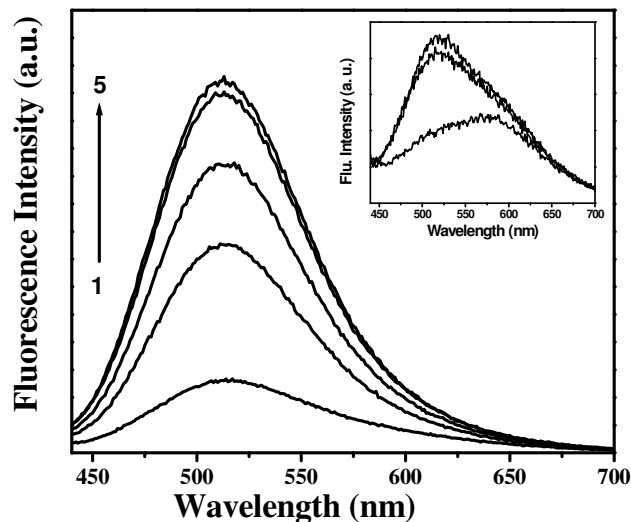


Figure 3.11: Fluorescence spectra of 2-DMASP in aqueous solution at different pH. Spectra from 1 to 5 correspond to the pH 4.59, 4.91, 5.31, 5.66, and 7.65, respectively. Inset shows the emission spectra of 2-DMASP in aqueous solution at pH 3.91, 4.27, and 4.37 (bottom to top)

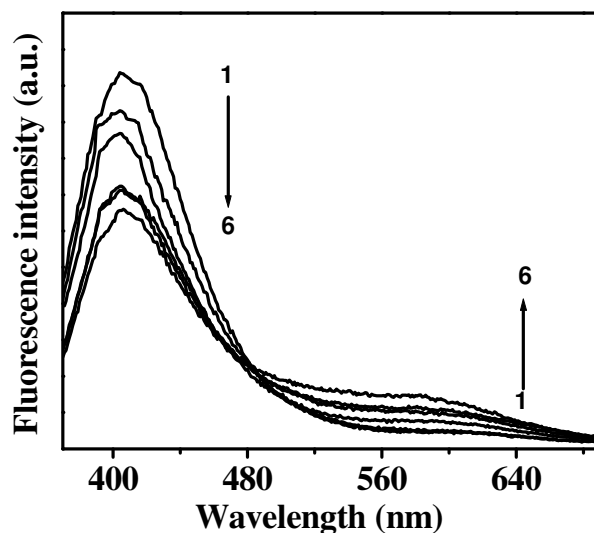


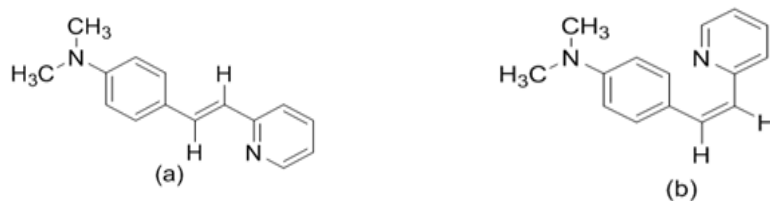
Figure 3.12: Fluorescence spectra of 2-DMASP in aqueous solution at different pH. Spectra from 1 to 6 correspond to the pH 2.11, 2.58, 2.74, 2.97, 3.28, and 3.61, respectively

Figure 3.12 shows the fluorescence spectra of dication I' and monocation II' in equilibrium in the pH range 2.11 to 3.61. The fluorescence peak maximum of dication I' is 403 nm which is blue shifted with respect to the neutral species of peak maximum 512 nm and with respect to the monocation species of peak maximum 578 nm. The acidity constant for this equilibrium at the excited state (pK_a^*) has also been calculated using Förster cycle as mentioned above. The difference between the ground and excited states dication-monocation acidity constants is found to be 15.6 which is in well agreement with that reported by Wang et al.²² So, the ground state dication-monocation acidity constant (pK_a) value being 3.1, the excited state acidity constant of dication I' and monocation II' equilibrium is calculated to be -12.5. This value is also not accurate because of the same reason mentioned above. This indicates that there is a very strong tendency of the dication species to undergo deprotonation and form monocation upon photoexcitation.²³ Because in the ICT excited state, the acceptor group efficiently pulls electron towards it from the donor group which leads to the cleavage of the bond between the proton and the positively charged nitrogen atom of $-N(CH_3)_2$ group and finally the dication of 2-DMASP is changed into the monocation easily. The absorption peak maximum (325 nm) of dication species is close to that of shoulder of absorption band of 2-DMASP in any solvent. The fluorescence band (peak maximum, 403 nm) of the same species appears in the range of fluorescence of 2-DMASP in a nonpolar solvent. These results support that the excitation and emission properties of the dication species resemble with that of 2-DMASP with planar geometry. The absence of absorption band at ~ 350 nm for dication species indicates that the ICT state of 2-DMASP exists in the ground state as well.

3.1.1.5 Theoretical calculations

The experimentally observed ICT reaction of 2-DMASP at the excited state has been supported by performing theoretical calculations using DFT. In the ground state, the global minimum structure shows the E-form of 2-DMASP (Scheme 3.3) with respect to C12-C11 bond while the corresponding Z-form has comparatively higher energy due to the presence of steric interaction. According to the global minimum structure of 2-DMASP in the ground state, the donor group $-N(CH_3)_2$ [C30-N25-C18-C17 = -1.53 (θ_1)] and the acceptor group, $-CH=CH-C_5H_4N$ [C16-C15-C12-C11 = -0.480 (θ_2)] are almost coplanar with the benzene ring. The possibility of resonance delocalization in the ground state is confirmed by almost coplanarity of donor and acceptor group. Geometries

of 2-DMASP in vacuo and MeCN as solvent have been optimized using the above mentioned hybrid functional and basis set. The relevant computational parameters of optimized structure of 2-DMASP in vacuo are tabulated in Table 3.3.



Scheme 3.3: Structures of (a) E – and (b) Z – forms of 2-DMASP

To understand the phenomenon of photoinduced ICT reaction in 2-DMASP in the light of TICT model, the potential energies of the molecule at the ground and first two excited singlet states have been obtained by the rotation of the donor (θ_1) and the acceptor (θ_2) groups separately around the benzene ring plane both in vacuo and MeCN solvent. The PESs at ground and at the first two excited singlet states (S_1 and S_2) along the donor rotation were constructed in vacuo and MeCN solvent and are displayed in Figure 3.13 and same for the acceptor rotation are displayed in Figure 3.14. The potential energies at the singlet ground state in vacuo and MeCN solvent increases with increasing both the donor and the acceptor twist angles starting from $\theta_1 = \theta_2 = 0^\circ$ and reach a maximum at $\theta_1 = \theta_2 = 90^\circ$. Along the donor twisting coordinate (θ_1), the excited state, S_1 gets stabilized at a perpendicular orientation ($\theta_1 = 90^\circ$) both in vacuo and MeCN solvent. It depicts the formation of a stabilized twisted geometry in the excited state. Moreover, the twisting along the donor path is energetically favorable over the acceptor path.

Table 3.3: Optimized geometry of 2-DMASP at the ground state (S_0) in vacuo at DFT ((B3LYP/6-31+G(d,p)) level

Bond	Calculated value (Å)	Angle/dihedral angle	Calculated value (degree)
N25-C18	1.384	N25-C26-C30	115.70
N25-C30	1.450	C26-C25-C18	123.98
C18-C19	1.410	C11-C1-C2	124.00
C20-C15	1.400	C11-C1-N6	114.90
C16-C17	1.380	C15-C12-C11	127.34
C19-C20	1.390	C12-C11-C1	126.67
C17-C18	1.410	C30-N25-C18-C17	-1.53
C15-C12	1.450	C16-C15-C12-C11	-0.48
C12-C11	1.350	C20-C15-C12-C11	179.56
C1-C11	1.460	C12-C11-C1-N6	-179.94
C1-C2	1.410	C12-C11-C1-C2	0.12

Various spectroscopic parameters have been extracted from the theoretical calculations and compared with those obtained from experiments and are listed in Table 3.4. Experimentally obtained absorption spectra consist of a band with a shoulder in all the solvents except in water. The actual band corresponds to transition from S_0 state to S_1 state. It has been observed experimentally that the molecule absorbs at 352 nm (3.52 eV) in hexane (calculation in vacuo has been considered equivalent to that in nonpolar solvent like hexane) and at 355 nm (3.50 eV) in MeCN (Table 3.1). Table 3.4 displays the comparison between theoretical and experimental values of vertical transition energies of 2-DMASP in vacuo and MeCN solvent for transition from S_0 state to S_1 state and one can see that theoretical and experimental results are in well agreement. The calculated emission energies of twisted donor and twisted acceptor ICT species in vacuo are 2.79 eV and 3.19 eV, respectively. Also, the calculated emission energies of twisted donor and twisted acceptor ICT species in MeCN solvent are 2.72 eV and 3.07 eV, respectively. There is a better agreement between the calculated and experimental emission energies for twisting at the donor site than twisting at the acceptor site. The calculated emission energy is lower in MeCN solvent than that in vacuo which is attributed to the experimentally observed red shift of fluorescence band in MeCN with respect to that in a nonpolar solvent.

For optimized structure of 2-DMASP, the HOMO-LUMO diagrams of planar and twisted geometries with donor and acceptor twisting are shown in Figure 3.15. The frontier molecular orbitals (FMO) of 2-DMASP for the global minimum structure given in Figure 3.15 reveal a more or less uniform distribution of π cloud density over the entire system for both HOMO (π) and LUMO (π). This indicates that the HOMO to LUMO transition is of allowed $\pi \rightarrow \pi^*$ type of transition and is supported by high oscillator strength value of 1.016 (Insets of Figure 3.13 and Figure 3.14). Due to mutual decoupling of orbitals as a result of twisted perpendicular ($\theta_1 = 90^\circ$) orientation of the donor part, $-\text{N}(\text{CH}_3)_2$ of 2-DMASP with respect to the benzene ring, the HOMO (π) to a major extent is the localized lone pair orbital of nitrogen atom of $-\text{N}(\text{CH}_3)_2$ group. This high degree of localization of electron density on the nitrogen atom at twisted conformation of donor group, $-\text{N}(\text{CH}_3)_2$ indicates the possibility of having TICT state.²⁴ However, the LUMO (π^*) is localized over the acceptor part of the molecule. For LUMO (π^*), the electron density on the nitrogen atom of donor group, $-\text{N}(\text{CH}_3)_2$ is reduced whereas the electron density at the acceptor part is increased as compared to that

for HOMO (π). Therefore, this HOMO-LUMO transition at twisted state ($\theta_1 = 90^\circ$) is of $n \rightarrow \pi^*$ nature and forbidden. The forbidden nature of transition is supported by the oscillator strength value.

The oscillator strength value is decreased from 1.016 at global minimum state to 0 at the twisted donor state in MeCN solvent (Figure 3.13(b)).

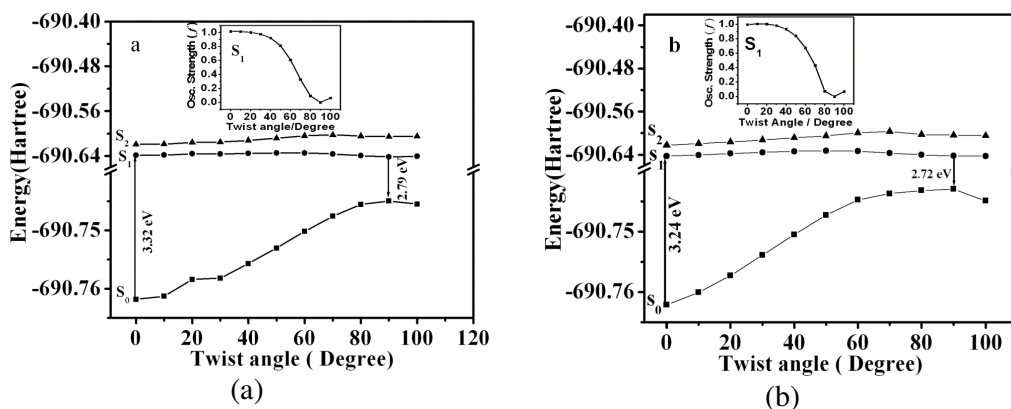


Figure 3.13: Potential energy surfaces for the ground and first two excited singlet states along the twisting coordinate of donor (θ_1) in (a) vacuo and in (b) MeCN solvent. Insets show the plots of variation of oscillator strength along twist angle

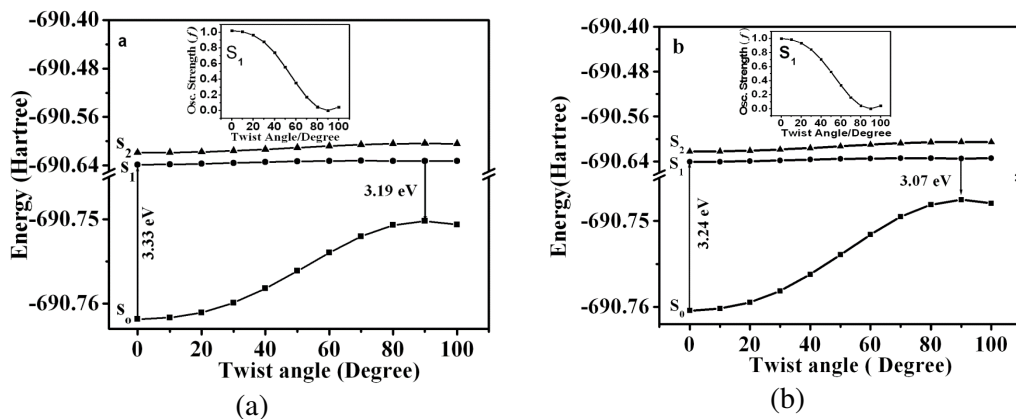


Figure 3.14: Potential energy surfaces for the ground and first two excited singlet states along the twisting coordinate of acceptor (θ_2) in (a) vacuo and in (b) MeCN. Insets show the plots of variation of oscillator strength along twist angle

However, in case of acceptor twisting conformation, the localization of HOMO (π) as the lone pair orbital of the nitrogen atom of $-\text{N}(\text{CH}_3)_2$ group is comparatively less than that in donor twisting conformation. To a significant extent HOMO (π) is also spreading throughout the benzene ring. The LUMO (π^*) is mostly localized at the

acceptor part of the molecule. This is a kind of $\pi_{\text{benzen}} \rightarrow \pi_{\text{acceptor}}$ type of transition and is forbidden supported by the very low oscillator strength value as 0.0002 in MeCN solvent (Inset of Figure 3.14).³ The electron density on the donor atom is reduced in both the cases of twisted donor and twisted acceptor structures, but twisting of donor is more favorable.

Table 3.4: Comparison between the experimental and computed energy values in vacuuo and MeCN solvent

Medium	state	Absorption		Emission		
		E_{ex} (eV) ^a	E_{th} (eV) ^b	E_{ex} (eV) ^a	E_{th} (eV) ^c	E_{th} (eV) ^d
Vacuuo	S ₁	3.52	3.32	2.98	3.19	2.79
	S ₂	-	3.85	-	3.96	3.77
MeCN	S ₁	3.50	3.24	2.62	3.07	2.72
	S ₂	-	3.77	-	3.85	3.76

^a E_{ex} is the experimental energy value. ^b E_{th} is the calculated energy value ($E_{\text{excited}} - E_{\text{ground}}$). ^cTheoretical emission energy value due to rotation of acceptor $-\text{CH}=\text{CH}-\text{C}_5\text{H}_4\text{N}$ group. ^dTheoretical emission energy value due to rotation of donor $-\text{N}(\text{CH}_3)_2$ group

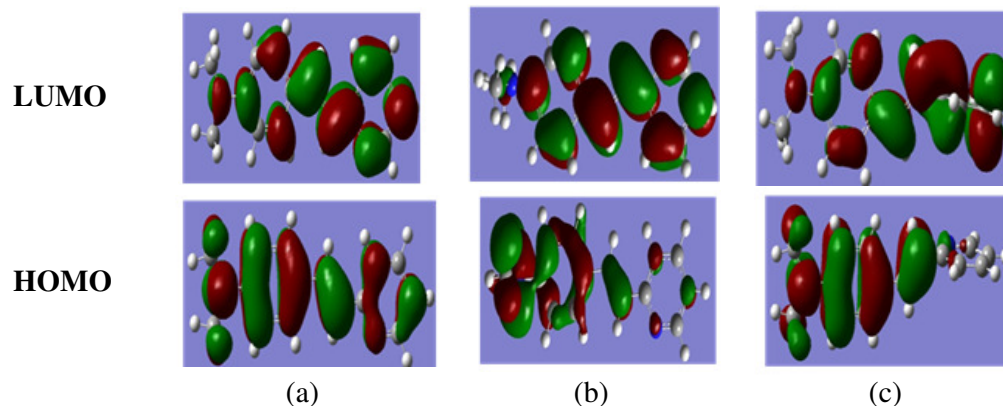


Figure 3.15: Frontier molecular orbitals (FMO) of 2-DMASP with (a) optimized planar structure in vacuuo, (b) donor twisted structure in acetonitrile, and (c) acceptor twisted structure in acetonitrile

3.1.1.6 Conclusions

Photophysical characterization of 2-DMASP has been undertaken in different pure solvents. Absorption and fluorescence studies show that excited states of 2-DMASP are more polar than the ground state. Both hydrogen bond donor ability of solvents and dipole-dipole interactions play significant role in the stabilization of ICT excited states.

The dipolar interactions have major contribution towards the stability of ICT excited state as compared to that by hydrogen bond donor ability of solvents. Fluorescence emission in a nonpolar solvent is originated from the LE state. However, LE state as well as a polar ICT state are responsible for the fluorescence in the polar solvent. The ICT excited state is not only created through rapid relaxation of singly excited LE species giving TICT species, but also by the excitation of ground state ICT species giving an excited ICT species. Monoexponential decay in a nonpolar solvent is due to the LE species, however in a highly polar solvent the monoexponential decay is because of the ICT species. The biexponential decay in solvents of intermediate polarity is due to the LE and ICT species where the decay of the ICT species is comparatively faster than that of the LE species. TDDFT and TDDFT-PCM have been used to explain the excited ICT state reaction of 2-DMASP in the light of TICT model. Results obtained from the theoretical calculations give a hint that the donor twisting coordinate is a possible path for the creation of ICT excited state. The ground state acidity constant, pK_a for dication-monocation and monocation-neutral equilibriums are calculated to be 3.1 and 5.6, respectively. However, the excited state acidity constant, pK_a^* for the same equilibriums are found to -12.5 and 11.2, respectively. Among neutral, monocation and dication species of 2-DMASP, the monocation one is the most stable at ground as well as excited states as a result of high extent of pulling of charge from the donor to the acceptor moiety.

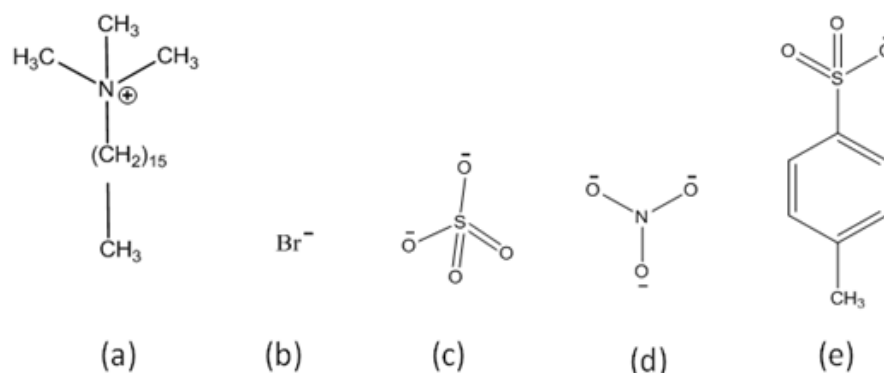
3.2 Study on microenvironmental properties of cetyltrimethylammonium surfactants with various counterions by using fluorescence properties of 2-DMASP

In this section, micellization behavior of cetyltrimethylammonium (CTA) surfactants with various counterions such as Br^- , SO_4^{2-} , NO_3^- , and PTSA (Scheme 3.4) have been studied using intramolecular charge transfer (ICT) fluorescence properties of 2-DMASP. Critical micelles concentrations (*cmc*) of cetyltrimethylammonium surfactants with various counterions have been estimated. Micropolarity and microviscosity of all the studied micelles also have been determined exploring the fluorescence properties of 2-DMASP.

3.2.1 Results and discussions

3.2.1.1 UV-Visible absorption and fluorescence spectra of 2-DMASP

Figure 3.16 shows the UV-Visible absorption spectra of 2-DMASP in presence of various concentration of CTAB. Absorption value increased with increasing the concentration of CTAB from 0 mM to 0.8 mM. Further increasing the concentration of CTAB the absorption value decreased. From 0.95 mM concentration of CTAB absorption value again increased with red shift in the absorption peak maxima as compared to that of 2-DMASP in pure water. These observations indicate that environment around 2-DMASP changes with varying the concentration of CTAB. Similar behavior of 2-DMASP was also observed with the concentration of CTA surfactant with different counterions.



Scheme 3.4: Representation of (a) CTA ion, (b) bromide ion, (c) sulphate ion, (d) nitrate ion, and (e) p-toluene sulphonate ion

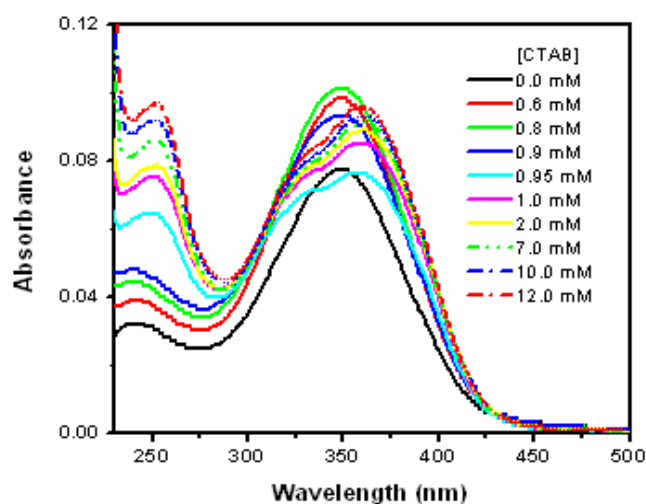


Figure 3.16: UV-Visible absorption spectra of 2-DMASP in presence of various concentration of CTAB

2-DMASP gives surfactant concentration dependent fluorescence spectra. Figure 3.17 shows the fluorescence spectra of 2-DMASP in presence of various concentration of CTAB. In presence of water 2-DMASP gives broad fluorescence band with fluorescence maxima at 512 nm (Table 3.1) with very low fluorescence intensity. In presence of low concentration of CTAB (0.0 mM-0.8 mM) fluorescence intensity of 2-DMASP shows very low enhancement with fluorescence maxima value at 512 nm. With further increasing the concentration (above 0.8 mM) of CTAB, large enhancement in the fluorescence intensity has been observed with concomitant blue shift in the fluorescence maxima of 2-DMASP with respect to the fluorescence maxima of 2-DMASP in water. This indicates that in presence of CTAB, environment around 2-DMASP has changed. The intensity of fluorescence is increased due to the decrease in the non-radiative processes for 2-DMASP in presence of CTAB. The blue shift in the fluorescence maximum of 2-DMASP in presence of CTAB is due to the destabilization of emitting state as a result of decrease in the polarity of the environment. In a polar medium like water the ICT state of 2-DMASP is highly stabilized which results in high rate of non-radiative processes because of close proximity of ICT state to the triplet state as well as ground ICT state.¹ With increasing concentration of surfactant, the probe molecule is transferred from the polar bulk phase to the non-polar micellar phase. Thus, the ICT state gets destabilized which results in increase in fluorescence intensity with blue shift in fluorescence peak maximum^{1,2}. Fluorescence band of 2-DMASP becomes narrower in presence of CTAB as compared to that in water. This also indicates that 2-DMASP interacts with CTAB.²⁵ Similar type of fluorescence behavior of 2-DMASP also has been observed in presence of other surfactants with different counter ions than bromide ions. Absorption and fluorescence peak maxima of 2-DMASP at 10 mM concentration of surfactants have been tabulated in Table 3.5.

Table 3.5: Critical micelle concentration (cmc), absorption peak maxima (λ_{max}^{ab}), fluorescence maxima (λ_{max}^{fl}), $E_T(30)$, steady-state anisotropy (r), and microviscosity values of cetyltrimethylammonium surfactants with different counterions (concentration of surfactant = 10 mM)

Counterions	cmc (mM) ^a	λ_{max}^{ab} (nm)	λ_{max}^{fl} (nm)	ϵ_{max}^{fl} (cm ⁻¹)	$E_T(30)$ (kcal mol ⁻¹)	r	Micro viscosity (cP)
SO ₄ ⁻²	0.52(0.54)	363	490	20408	52.7	0.204	0.34
Br ⁻	0.85(0.94)	361	485	20618	51.0	0.213	0.46
NO ₃ ⁻¹	0.72(0.89)	361	483	20703	50.4	0.225	0.66
PTSA	0.22	361	482	20746	50.1	0.246	1.23

^a Reported cmc values are given in paranthesis. (Ref. 29)

The change in fluorescence intensity of 2-DMASP in presence of varying concentration of surfactant has been used to determine the *cmc* value. Fluorescence intensity of 2-DMASP has been plotted with increasing concentration of surfactant and this is shown by Figure 3.18 as a representative one. The break point in the graph gives the *cmc* value (Table 3.5). The *cmc* values calculated by using this method for all the studied surfactants are in well agreement with the reported *cmc* values calculated by other methods.

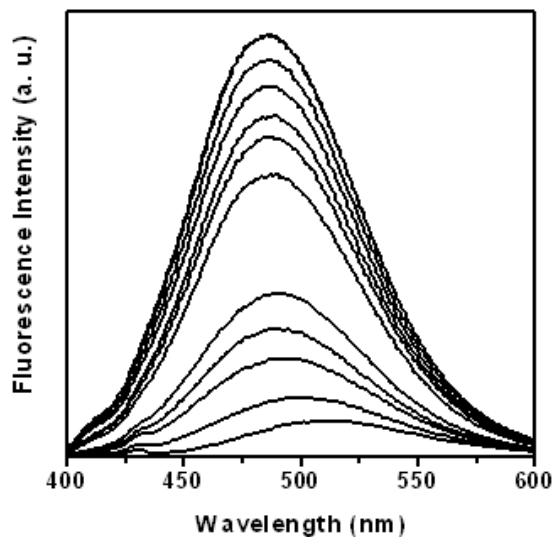


Figure 3.17: Fluorescence spectra of 2-DMASP with increasing concentration (from bottom to top) of CTAB

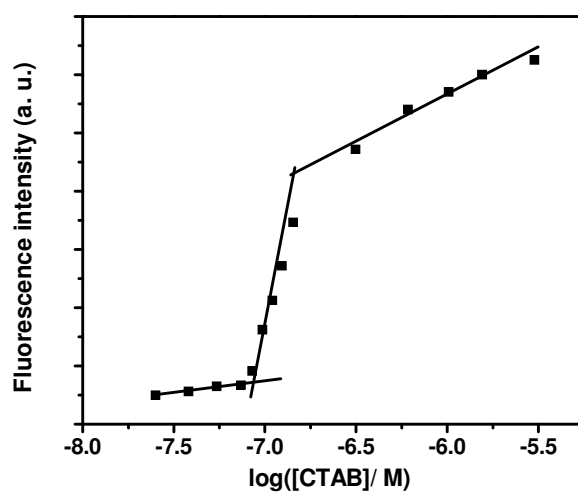


Figure 3.18: Variation of steady-state fluorescence intensity of 2-DMASP in presence of varying concentration of CTAB

3.2.1.2 Micropolarity and microviscosity

The environment around fluorophore molecule becomes complex when it is dissolved in micellar medium. Depending upon the characteristics (charge and polarity) of both fluorophores and micelles, fluorophores molecule can reside either in the core or interface region of micelles. Relative polarity of probe molecule in micellar medium can be determined through different photophysical parameters of the probe. Polarity around the probe molecule in biomimicking environment can be estimated by comparing the spectral properties of probe in the environment of known polarity. For the present study, $E_T(30)$ scale of polarity has been used which is an empirical solvent polarity parameter comparing the fluorescence behavior of a probe molecule in microheterogeneous systems to that in mixtures of homogeneous solvents of varying compositions.^{26,27} As referred by Kasha *et al.*²⁸ this is static polarity. Fluorescence spectra of 2-DMASP have been recorded in presence of different percentage of dioxane-water mixture and given in Figure 3.4. Calibration lines are obtained from the plot of fluorescence energy of 2-DMASP at peak maxima (ϵ_{max}^{fl}) in different percentage of dioxane-water mixtures versus $E_T(30)$ as shown by Figure 3.19. $E_T(30)$ values in micellar media have been calculated by comparing the ϵ_{max}^{fl} values in these media to that in dioxane-water mixture i.e. using the calibration lines in Figure 3.19 (Table 3.5). $E_T(30)$ values suggests that micropolarity sensed by 2-DMASP is lesser than that of water. This indicates that 2-DMASP is residing at micelle-water interface. $E_T(30)$ values are varying with counterions of surfactants. Micelles of surfactant molecules with sulphate counterions show higher micropolarity than that with other counter ions. Wang *et al.*²⁹ also reported the micropolarity of micelles of same surfactants using electron spin resonance method. The trend in the micropolarity values of micelles observed in the present study by using the ICT properties of 2-DMASP agrees well with that reported by Wang *et al.*²⁹ Higher micropolarity value for surfactant with sulphate counterions than surfactants with other counterions is due to the greater extent of penetration of water into the interfacial region of the micelles. More the penetration of water higher will be the micropolarity.

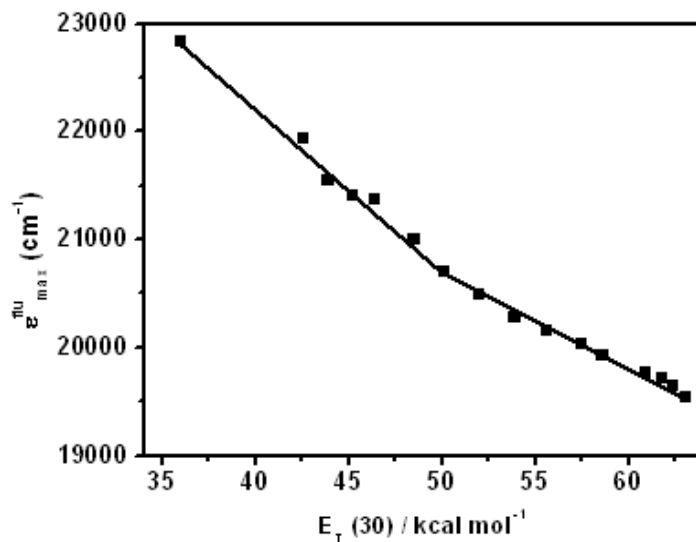


Figure 3.19: Plot of fluorescence energy at peak maxima ($\epsilon_{\max}^{\text{fl}}$) of 2-DMASP versus $E_T(30)$ of different percentage of dioxane-water mixture

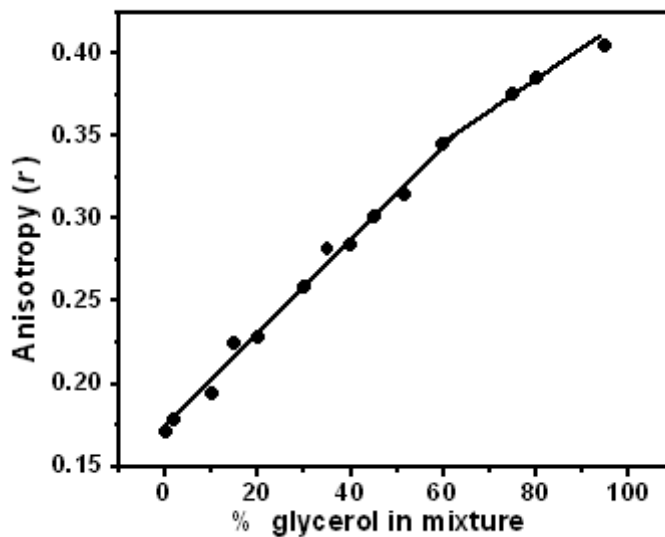


Figure 3.20: Variation of fluorescence anisotropy value of 2-DMASP in presence of different percentage of glycerol in methanol-glycerol mixture

Steady-state fluorescence anisotropy measurements give information about rigidity around the probe molecule. Steady-state fluorescence anisotropy of 2-DMASP have been measured in different percentage of glycerol in methanol-glycerol mixture. Figure 3.20 shows the plot of fluorescence anisotropy with different percentage of glycerol in methanol-glycerol mixture. Fluorescence anisotropy increases continuously with increasing the percentage of glycerol. This indicates that

restriction around the probe molecule increases with increasing the viscosity of the medium. The anisotropy values in different micellar media have been compared with that in different percentage of methanol-glycerol mixture. From this comparison, the microviscosity of micelles have been estimated using the plot of viscosity of different percentage of glycerol in methanol-glycerol mixture. Microviscosity values of micelles of surfactants with different counterions are given in Table 3.5. Surfactants with PTSA counterions give high anisotropy value. The high anisotropy value in this case may be due to highly compact environment around 2-DMASP in the micelles of this surfactant.

Observed trend in the microviscosity is due to difference in the hydrated radii of the counterion. A counterion of smallest size has largest hydrated radius. A counterion with larger hydrated radius interact less strongly with the oppositely charged headgroup of the surfactant than that with smaller hydrated radius.²⁹ Strong interactions of counterions with the headgroup of the micelles lead to tight packing of the micelles which give high microviscosity value of the micelles. In the present study, PTSA is the largest counterion of the surfactant. PTSA form smaller hydrated radius and interact strongly with the headgroup of the surfactant which make highly compact micelles. Moreover in case of PTSA as counterion due to the presence of phenyl ring, the counterion may also participate in the micelle formation which gives highly compact micelles and consequently high microviscosity value of micelles among the micelles of surfactants with studied counter ions.

3.2.1.3 Conclusions

ICT fluorescence properties of 2-DMASP have been used to determined the cmc values of cetyltrimethyl ammonium surfactants with various counterions. Cmc values obtained by using 2-DMASP are in well agreement with the reported values. Anisotropy values of 2-DMASP increases smoothly with increasing the percentage of glycerol in methanol-glycerol mixture. Micropolarity and microviscosity of environment around 2-DMASP in the micelles of surfactant with varying counter ions have been estimated. Micelles with sulphate counter ions have higher micropolarity and lesser microviscosity. Micelles with PTSA counterions have lesser micropolarity and higher microviscosity could be because of lesser extent of penetration of water molecules into the micelles.

References:

- (1) M. Sowmiya, A. K. Tiwari, Sonu, S. K. Saha, *J Photochem Photobiol A* **2011**, 218, 76.
- (2) S. Bruni, E. Cariati, F. Cariati, F.A. Porta, S. Quici, D. Roberto. *Spectrochim Acta Part A* **2001**, 57, 1417.
- (3) S. Jana, S. Dalapati, S. Ghosh, S. Kar, N. Guchhait. *J Mol Struct.* **2011**, 998, 136.
- (4) B. K. Paul, A. Samanta, S. Kar, N. Guchhait, *J Lumin* **2010**, 130, 1258.
- (5) C. C. Dubroca, S. A. Lyazidi, P. Cambou, A. Peirigua, P. Cazeau, M. Pesquer, *J Phys Chem.* **1989**, 93, 2347.
- (6) Y. Kim, M. Yoon, *Bull Korean Chem Soc.* **1998**, 19,980.
- (7) A. Chakraborty, S. Kar, N. Guchhait, *J Photochem Photobiol A* **2006**,181, 246.
- (8) T. A. Fayed, M. A. El-morsi, M. N. El-Nahass, *J Photochem Photobiol A* **2011**, 224.
- (9) M. J. Kamlet, J. L. M. Abboud, M. H. Abraham, R. W. Taft, *J Org Chem* **1983**, 48, 2877.
- (10) S. K. Saha, P. Purkayastha, A. B. Das, *J Photochem Photobiol A* **2008**,195, 368.
- (11) A. L. Sobolewski, W. Sudholt, W. Domcke, *J Phys Chem A* **1998**, 102, 2716.
- (12) A. Chakraborty, S. Kar, N. Guchhait, *Chem Phys* **2006**, 324,733.
- (13) A. Chakraborty, S. Kar, D. N. Nath, N. Guchhait, *J Phys Chem A* **2006**, 110, 12089.
- (14) A. B. J. Parusel, W. Rettig, W. Sudholt. *J Phys Chem A* **2002**, 106, 804.
- (15) B. Wandelt, P. Turkewitsch, B. R. Stranix, G. D. Darling, *J Chem Soc Faraday Trans* **1995**, 91, 4199.
- (16) N. Ghoneim, P. Suppan. *Pure Appl Chem* **1993**, 65, 1739.
- (17) C. Reichardt. *Weinheim*, **1979**.
- (18) H. Gusten, R. Maisner, *J Photochem* **1983**, 21, 53.
- (19) A. Ray. *Nature* **1971**, 231, 313.
- (20) R. Das, D. Guha, S. Mitra, S. Kar, S. Lahiri, S. Mukherjee, *J Phys Chem A* **1997**, 101, 4042.
- (21) F. D. Lewis, J. S. Yang, *J Am Chem Soc* **1997**, 11, 3834.
- (22) S. L. Wang, G. Y. Gao, T. Ho, L. Y. Yang, *Chem Phys Lett.* **2005**, 415, 217.
- (23) T. S. Singh, S. Mitra, *J Incl Phen Macrocycl Chem* **2009**, 63, 335.

- (24) Z. Grabowski, K. Rotkiewicz, W. Rettig, *Chem Rev* **2003**, *103*, 3899.
- (25) A. Mahata, D. Sarkar, D. Bose, D. Ghosh, P. Das, N. Chattopadhyay, *J. Colloids Interface Sci.* **2009**, *335*, 234.
- (26) D. Das, S. Guha, S. Mitra, S. Kar, S. Lahiri, S. Mukherjee, *J. Phys. Chem. A* **1997**, *101*, 4042.
- (27) A. Mallick, B. Haldar, S. Maiti, N. Chattopadhyay, *J. Colloids Interface Sci.* **2004**, *278*, 215.
- (28) A. Sytnik, M. Kasha, *Proc. Natl. Acad. Sci. U.S.A.* **1994**, *91*, 8627.
- (29) N. Jiang, P. Li, Y. Wang, J. Wang, H. Yan, R. K. Thomas, *J. Colloids Interface Sci.* **2005**, *286*, 755.

Chapter 4

Study on mixed micelles of cationic gemini surfactants having hydroxyl group in the spacers with conventional cationic surfactants: Effects of spacer group and hydrocarbon tail length*

In the present work, micellar properties of binary mixtures of monomeric cationic surfactants, hexadecyltrimethylammonium bromide (CTAB), tetradecyltrimethylammonium bromide (TTAB), and dodecyltrimethylammonium bromide (DTAB) (Scheme 2.2) with cationic gemini surfactants, Gemini-1 and Gemini-2 (Scheme 2.2) have been studied in aqueous solution at 303.15 K by means of conductivity, steady-state fluorescence, and fluorescence anisotropy techniques. Presence of a little amount of gemini surfactant improves the physicochemical properties of a conventional surfactant. The spacer group of a gemini surfactant and the hydrocarbon chain of a monomeric surfactant play a significant role in interactions between them in mixed micelles. The mixtures of CTAB/TTAB/DTAB and Gemini-1 show more negative deviation from ideality than the mixtures of CTAB/TTAB/DTAB and Gemini-2. These interactions are maximum when there are similarities in the structures of their hydrocarbon chains, however micellization process is favored by increasing hydrophobicity of the monomeric surfactant. The negative values of excess Gibbs free energy of micelles (G^E) indicates that, for the formation of mixed micelles, there are attractive interactions between the surfactant molecules. The magnitude of G^E increases with decreasing the chain length of the monomeric surfactants. The negative values of standard Gibbs free energy of mixed micelle formation (ΔG_m^0) indicate that mixed micelle formation is a spontaneous process for all of the mixtures. Microenvironments of mixed micelles have been studied using fluorescence techniques. The micropolarity of the environment around the probe molecule was found to be equivalent to that of ethanol. The binding constant of the fluorescent probe molecule increases with increasing content of gemini surfactant in the mixed micelle and also with increasing chain length of the monomeric surfactants.

* Sonu, Amit K. Tiwari, Subit K. Saha, *Ind. Eng. Chem. Res.* **2013**, 52, 5895.

4.1 Results and discussion

4.1.1 Determination of *cmc*

The *cmc* of mixed micellar systems of monomeric + Gemini-1 and monomeric + Gemini-2 in aqueous media with varying mole fractions of gemini surfactants (α_i) have been determined by conductometric measurements at 303.15 K. Carpena's method (discussed in Chapter 2, Section 2.2.12) has been applied in the present study to calculate the *cmc*.¹ This method is based on the fitting of the experimental raw data to a non-linear function obtained by direct integration of a Boltzmann type sigmoidal function. Plots of κ versus total surfactant concentration ($[\text{surfactants}]_T$) with fitted data obtained after applying Carpena's method for various mixed micellar systems are shown by Figures 4.1 to 4.6.

The values of *cmc* for pure and mixed surfactants systems obtained by using Carpena's method¹ are tabulated in Table 4.1 and these values have been used for calculations of mixed micellar properties. To avoid the criticism² for the determination of the *cmc* by conductivity measurement, we used the fluorescence method for the estimation of *cmc* and the values obtained were then compared with those determined by conductivity measurements. Pyrene is a well known probe for the determination of the *cmc* based on the ratio of intensities of first and third major vibrational peaks (I_1/I_3) in its fluorescence spectrum. However, an exact and direct determination of *cmc* is not possible with the pyrene's I_1/I_3 because of various ambiguities reported in the literature.³⁻⁶ To avoid all these ambiguities, we have measured the *cmc* of pure and mixed surfactants by monitoring the change in fluorescence intensity of a TICT fluorescence probe, DMACA with increasing concentration of surfactant. This probe is highly sensitive to the change in micropolarity and microviscosity of the environment.⁷ Figure 4.7 represents the fluorescence spectra of DMACA in presence of CTAB/TTAB/DTAB + Gemini-1 and CTAB/TTAB/DTAB + Gemini-2 mixed micellar systems. Before *cmc*, the fluorescence intensity is very low and a very less enhancement in the intensity with increase in the surfactant concentration in the solution is observed. However, just above *cmc* there is a sharp increase in the intensity with concomitant blue shift of the peak maximum. This result suggests the transfer of DMACA from the polar bulk aqueous medium to the hydrophobic environment of the micelles.⁸ Figure 4.8 represents the plots of fluorescence intensities of DMACA as a function of total surfactants concentration.

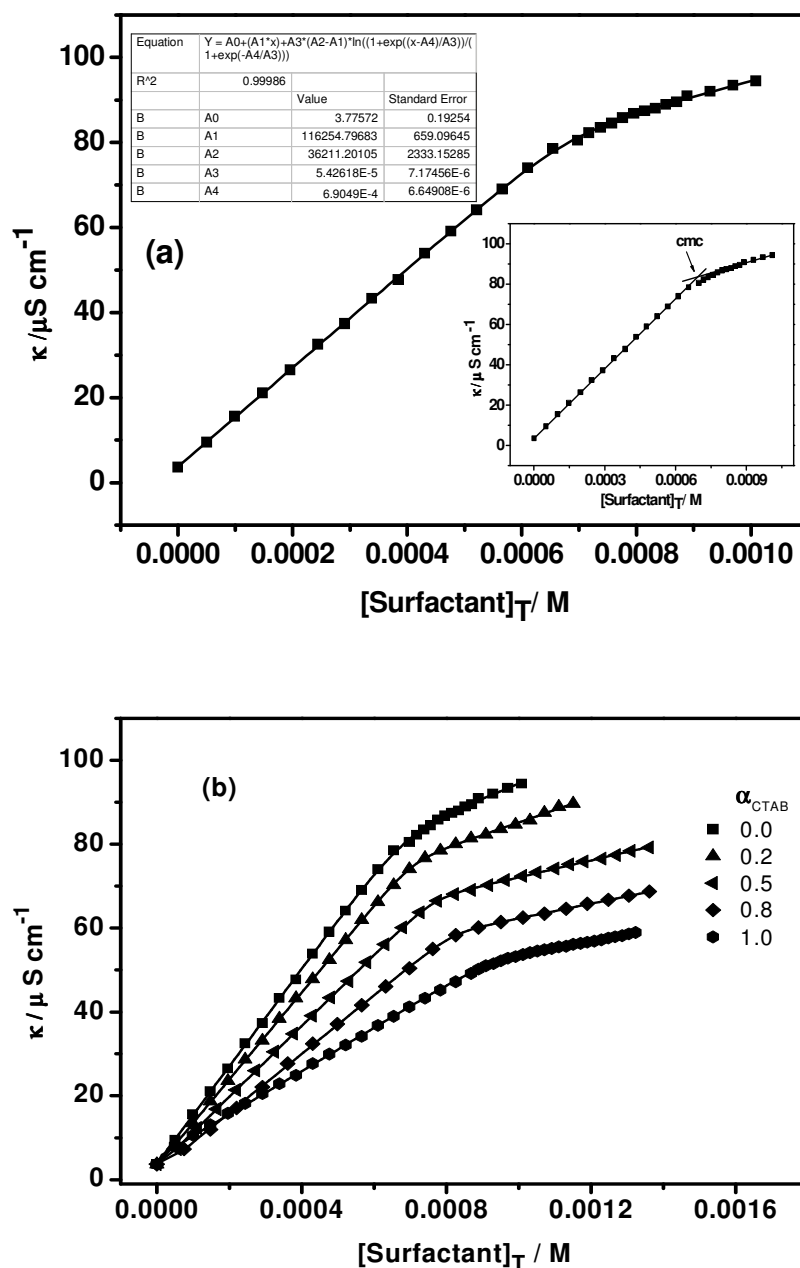


Figure 4.1: (a) Representative plot for the determination of *cmc* by Carpena's method by using experimental conductivity data for Gemini-1 + CTAB mixed systems at bulk mole fraction of CTAB, $\alpha_{\text{CTAB}} = 0.0$, (Inset shows the determination of *cmc* without Carpena's method), (b) Plot of experimental conductivity data for Gemini-1 + CTAB mixed system at different bulk mole fraction of CTAB (α_{CTAB}) using Carpena's method

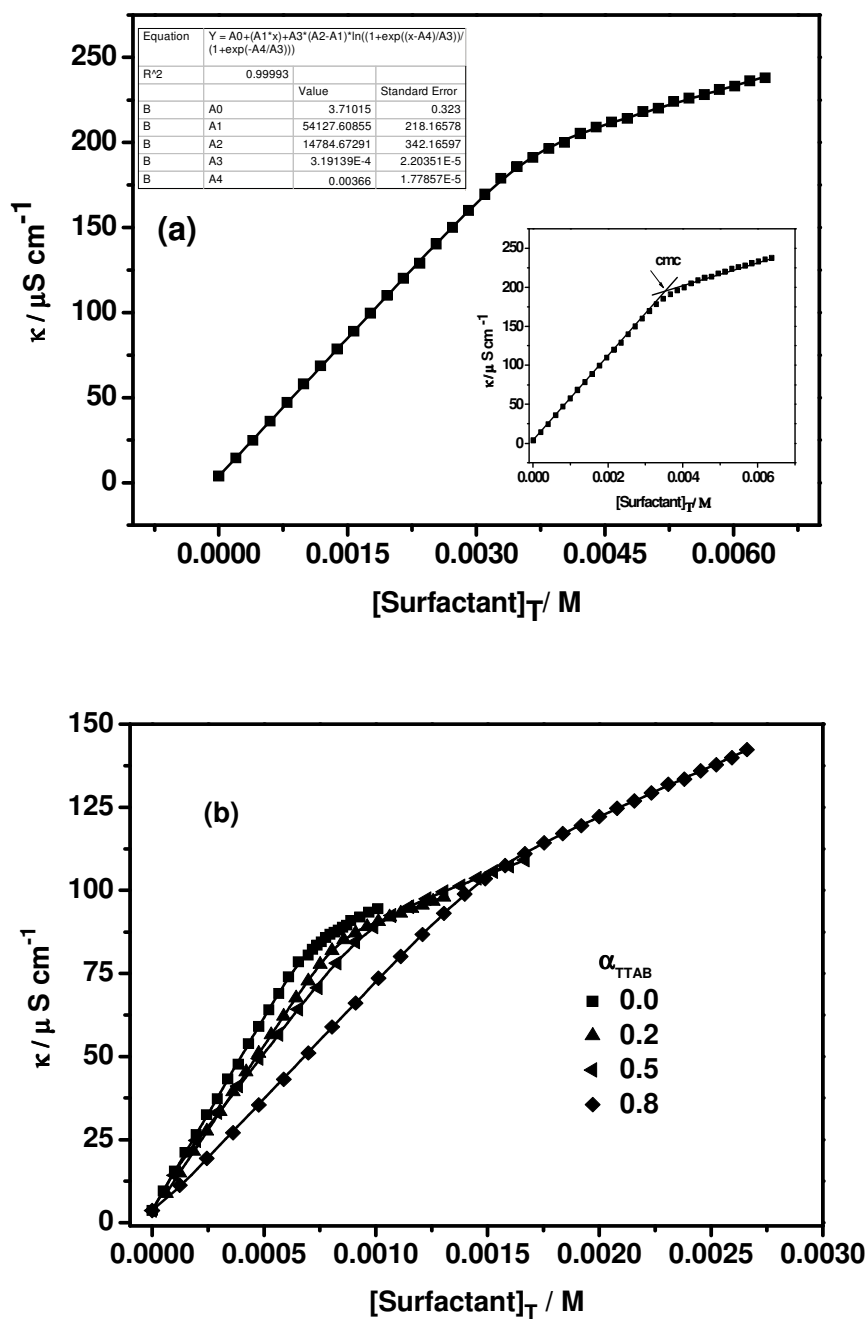


Figure 4.2: (a) Representative plot for the determination of cmc by Carpena's method by using experimental conductivity data for Gemini-1 + TTAB mixed systems at bulk mole fraction of TTAB, $\alpha_{TTAB} = 1.0$, (Inset shows the determination of cmc without Carpena's method), (b) Plot of experimental conductivity data for Gemini-1 + TTAB mixed system at different bulk mole fraction of TTAB (α_{TTAB}) using Carpena's method

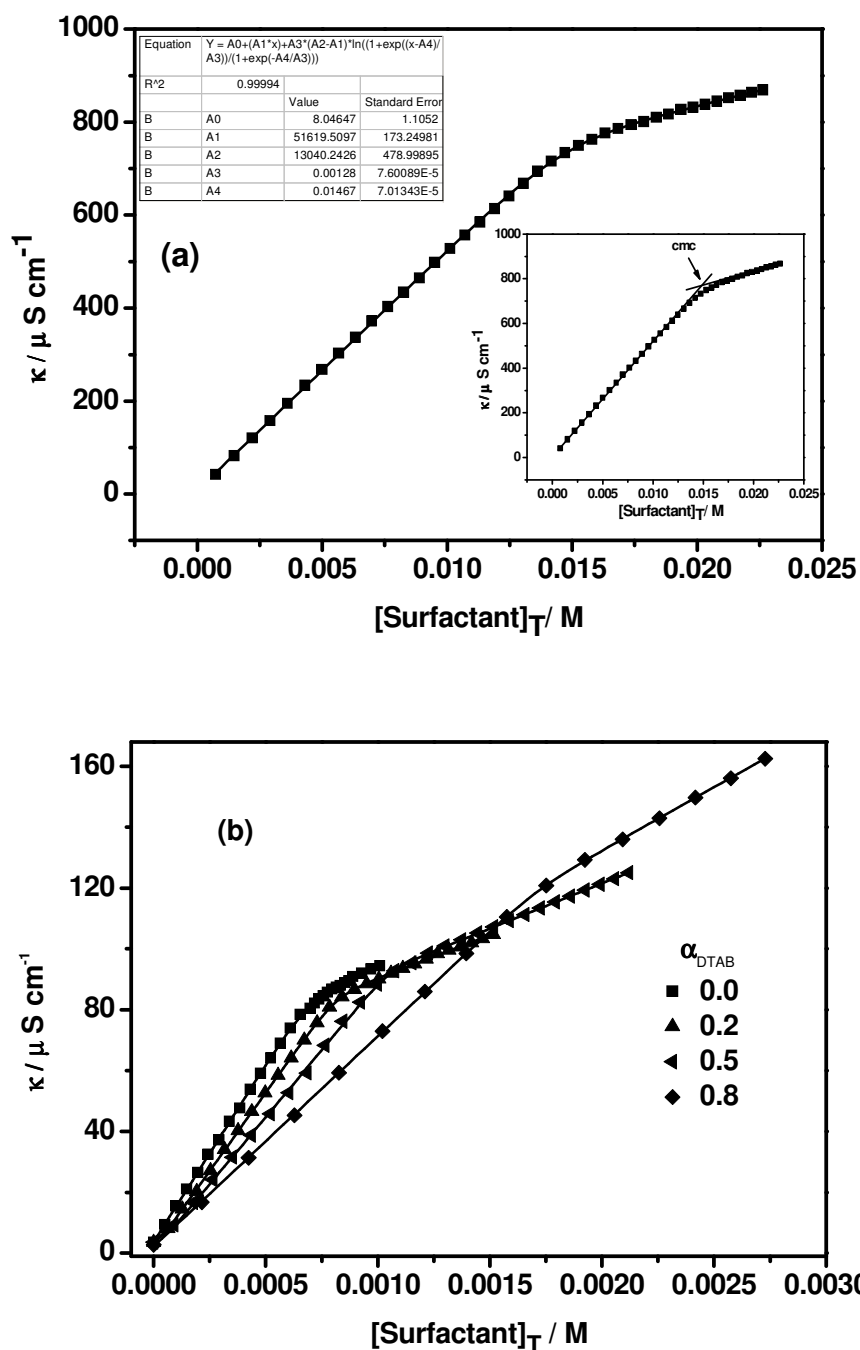


Figure 4.3: (a) Representative plot for the determination of *cmc* by Carpena's method by using experimental conductivity data for Gemini-1 + DTAB mixed systems at bulk mole fraction of DTAB, $\alpha_{\text{DTAB}} = 1.0$, (Inset shows the determination of *cmc* without Carpena's method), (b) Plot of experimental conductivity data for Gemini-1 + DTAB mixed system at different bulk mole fraction of DTAB (α_{DTAB}) using Carpena's method

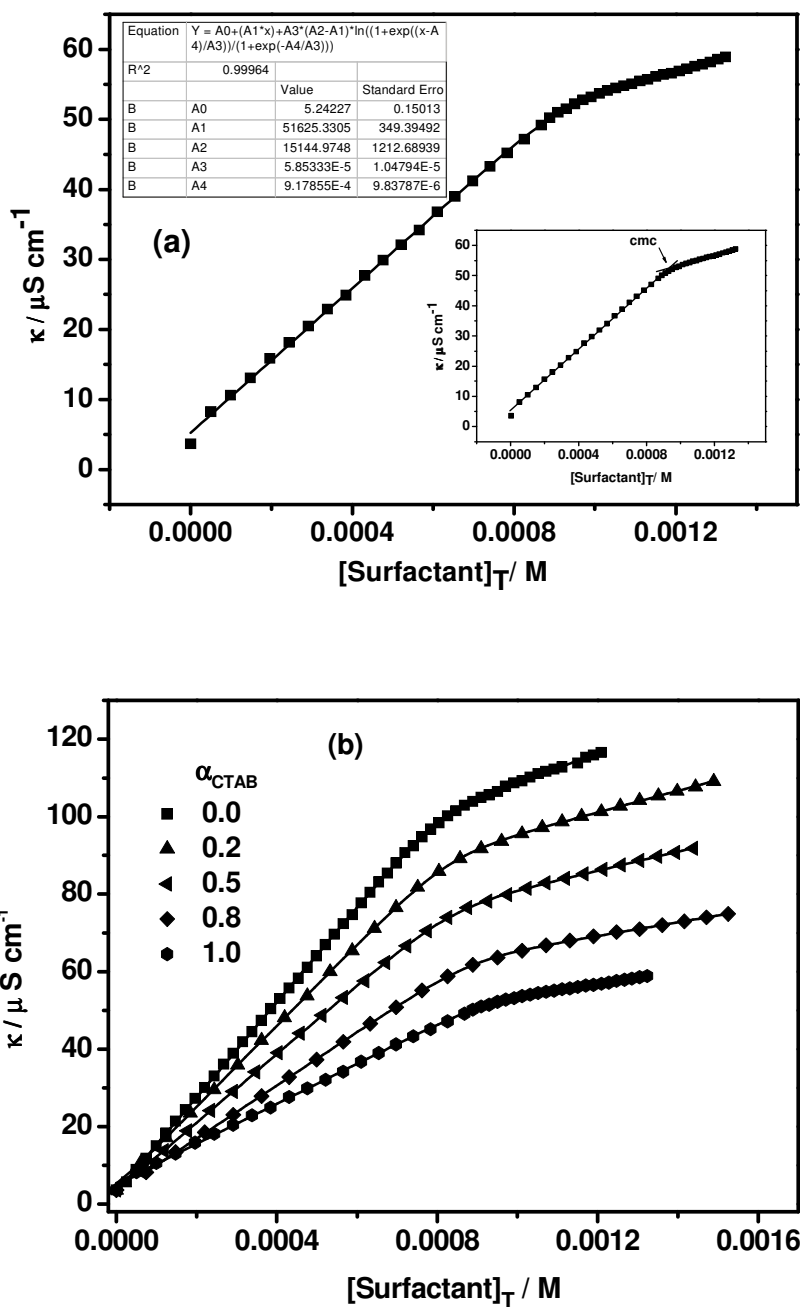


Figure 4.4: (a) Representative plot for the determination of *cmc* by Carpena's method by using experimental conductivity data for Gemini-2 + CTAB mixed systems at bulk mole fraction of CTAB, $\alpha_{CTAB} = 1.0$, (Inset shows the determination of *cmc* without Carpena's method), (b) Plot of experimental conductivity data for Gemini-2 + CTAB mixed system at different bulk mole fraction of CTAB (α_{CTAB}) using Carpena's method

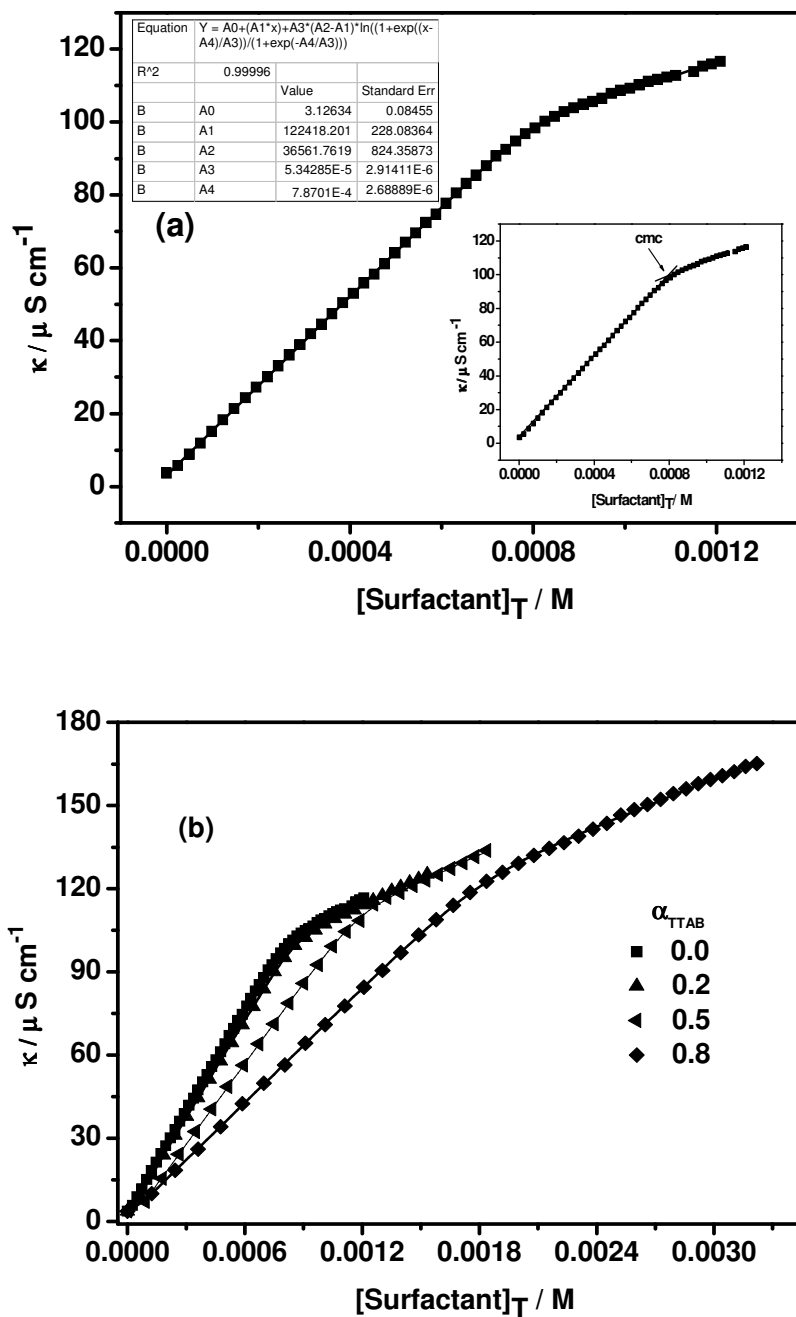


Figure 4.5: (a) Representative plot for the determination of *cmc* by Carpena's method by using experimental conductivity data for Gemini-2 + TTAB mixed systems at bulk mole fraction of TTAB, $\alpha_{\text{TTAB}} = 0.0$, (Inset shows the determination of *cmc* without Carpena's method), (b) Plot of experimental conductivity data for Gemini-2 + TTAB mixed system at different bulk mole fraction of TTAB (α_{TTAB}) using Carpena's method

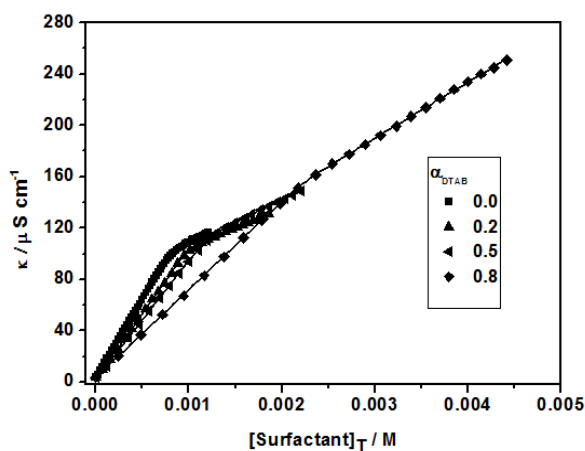


Figure 4.6: Plot of experimental conductivity data for Gemini-2 + DTAB mixed system at different bulk mole fraction of DTAB (α_{DTAB}) using Carpena's method

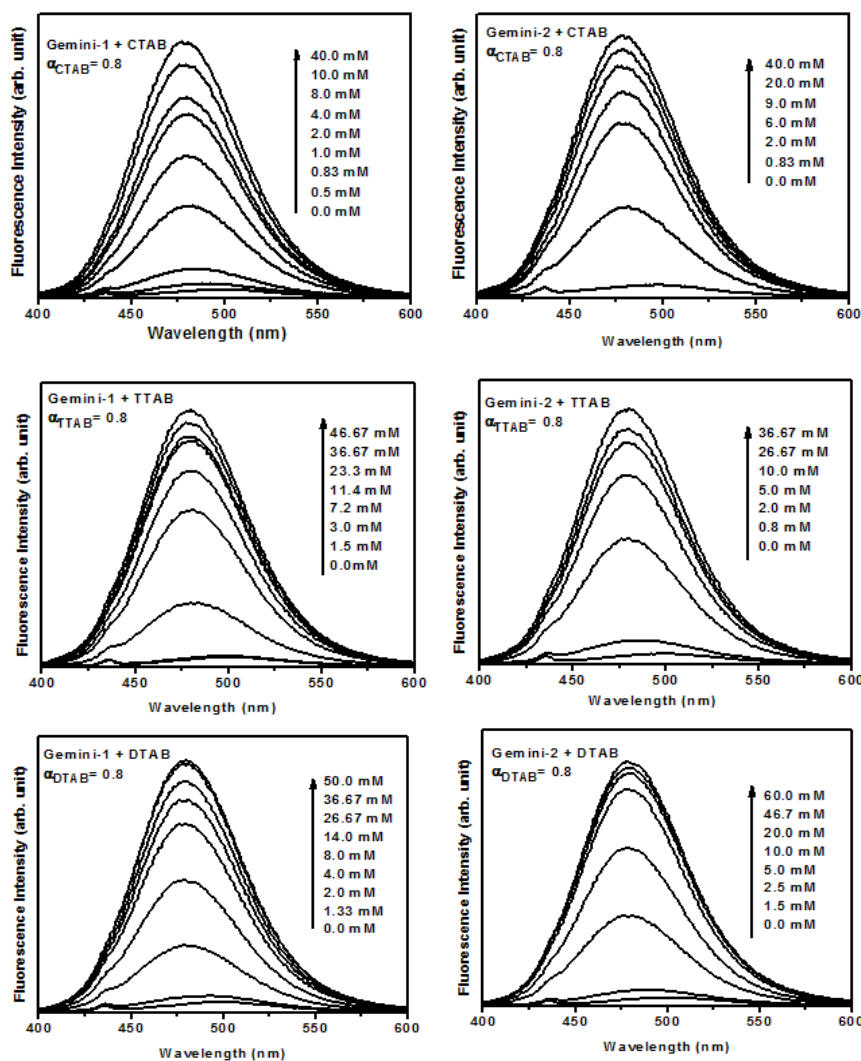


Figure 4.7: Fluorescence spectra of DMACA in presence of various mixed systems in aqueous solution. $\lambda_{\text{ex}} = 378 \text{ nm}$

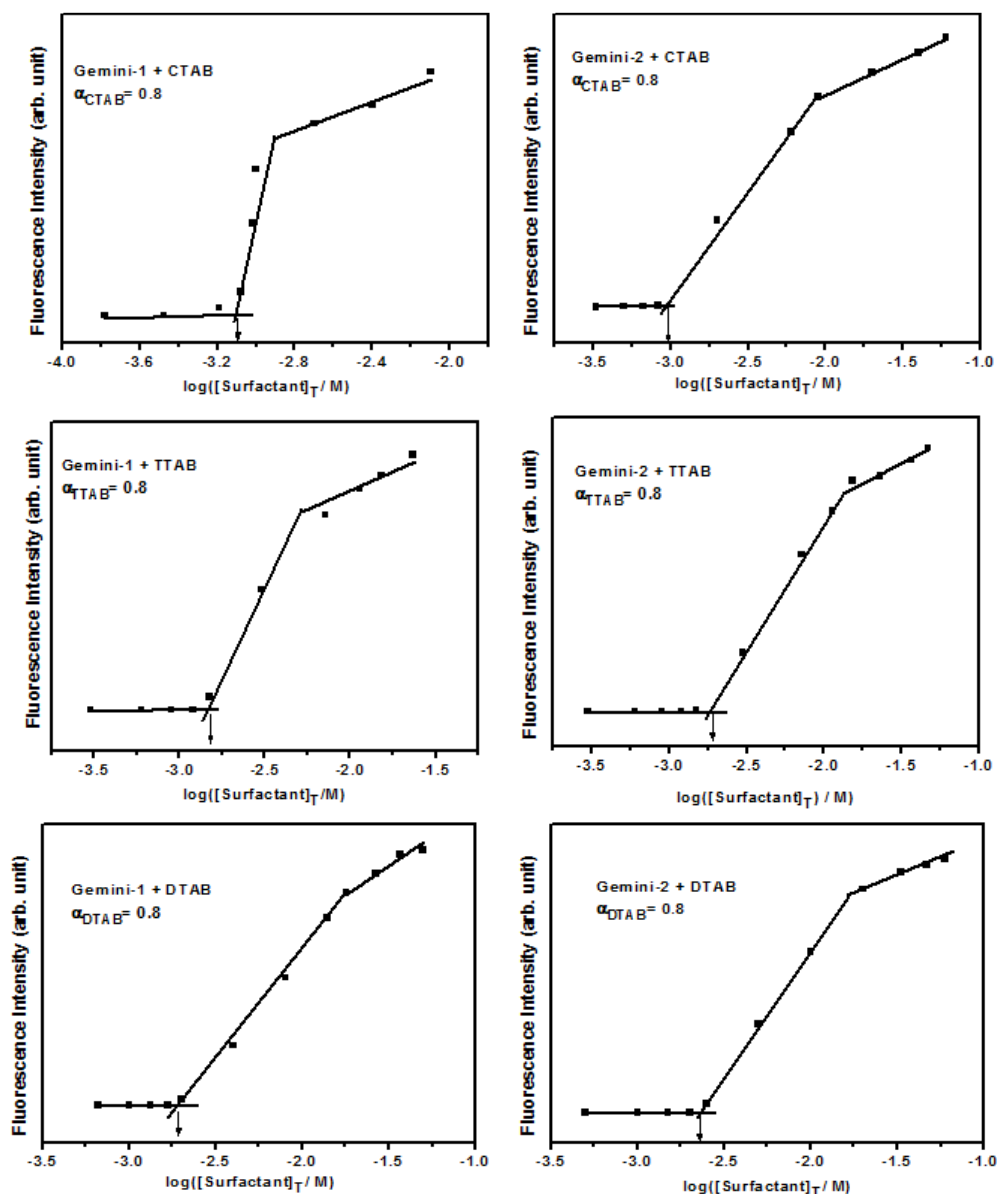


Figure 4.8: Plots of fluorescence intensities of DMACA as a function of total surfactants concentration of various mixed systems. $\lambda_{ex} = 378$ nm

The *cmc* values of pure surfactants estimated by fluorescence method are in good agreement with conductivity data and literature data (Table 4.1). For mixed systems, the *cmc* values have been determined using fluorescence technique only at 0.2, 0.4, 0.6 and 0.8 bulk mole fractions of monomeric surfactants to avoid recording a large number of emission spectra. These *cmc* values are consistent with those obtained using conductivity measurements and are also tabulated in Table 4.1.

Table 4.1: Values of *cmc* of monomeric + Gemini-1/Gemini-2 from conductivity and fluorescence measurements at 303.15 K

α_1	<i>cmc</i> ^{a,b} /10 ⁻⁴ M	<i>cmc</i> /10 ⁻⁴ M	<i>cmc</i> /10 ⁻⁴ M	<i>cmc</i> ^{a,b} /10 ⁻⁴ M	<i>cmc</i> /10 ⁻⁴ M	<i>cmc</i> /10 ⁻⁴ M
	CTAB + Gemini-1	TTAB + Gemini-1	DTAB + Gemini-1	CTAB + Gemini-2	TTAB + Gemini-2	DTAB + Gemini-2
0.0	6.90 (6.90) ^{c,d}			7.87 (8.10)		
0.2	7.10 (7.32)	7.99 (7.94)	8.22 (8.28)	8.03 (8.05)	9.02 (8.97)	9.35 (10.96)
0.3	7.20	8.80	8.96	8.20	9.85	10.10
0.4	7.43 (7.36)	9.30 (9.36)	9.96 (10.06)	8.25 (8.30)	10.40 (10.60)	11.00 (11.12)
0.5	7.66	9.94	10.60	8.33	11.20	12.10
0.6	7.78 (7.74)	11.70 (11.42)	12.00 (12.30)	8.50 (8.66)	13.10 (13.33)	13.50 (13.52)
0.7	7.99	12.80	14.40	8.74	15.10	15.80
0.8	8.24 (8.13)	15.20 (15.10)	18.00 (18.03)	8.82 (8.71)	18.40 (18.49)	20.40 (20.40)
0.9	8.40	19.40	23.60	9.10	20.10	32.60
1.0	9.20 (9.12)	36.60 (36.14)	146.00 (151.01)			

^a*cmc* measured by conductivity method, ^bSD = ± 0.02

^c*cmc* measured by fluorescence method given in parenthesis

^dSD = ± 0.04

4.2 Pure gemini surfactants: Aggregation behavior

In the aggregation properties of gemini surfactants, the spacer group plays a significant role. A gemini surfactant with hydrophilic, flexible spacer has higher affinity towards micelle formation which leads to lower *cmc*, smaller ionization degree, and larger aggregation number as compared to that of a gemini surfactant with rigid, hydrophobic spacer.^{9, 10} The hydroxyl groups in the spacers of Gemini-1 and Gemini-2 enhance their micellization processes. The *cmc* values of Gemini-1 and Gemini-2 are lesser than their corresponding gemini surfactants (12-3-12 and 12-4-12, respectively) without any hydroxyl group(s) in the spacer^{11, 12} and it is most likely due to hydrophilic nature⁹ of spacer group of Gemini-1 and Gemini-2. Although the spacer group of Gemini-2 is expected to be more hydrophilic than that of Gemini-1, the *cmc* of the former is found to be higher than that of the later (Table 4.1). Because of the presence of intramolecular hydrogen bonding between the hydroxyl groups of a spacer group of Gemini-2, the spacer group of Gemini-2 is comparatively rigid than that of Gemini-1. Moreover, there are four –CH₂– groups in the spacer of Gemini-2 as compared to three –CH₂– groups in the spacer of Gemini-1. Therefore, the increase in hydrophobicity of the spacer group of Gemini-2 with increasing one –CH₂– group might be predominating over the increase in the hydrophilicity with increasing one –OH group.

Thus the Gemini-2 surfactant molecule with a rigid and less hydrophilic spacer as compared to that of Gemini-1 faces difficulty in the formation of aggregate because of the difficulty in locating the spacer of less hydrophilicity at the micelle-water interface and the steric inhibition of the rigid spacer group. As a result of that the *cmc* value of Gemini-2 is found to be comparatively higher than that of Gemini-1. Moreover, in case of Gemini-1 due to greater extent of intermolecular hydrogen bonding the number of interfacial water molecules released will be more and hence increase in entropy will also be more during the formation of aggregates. The extent of intermolecular hydrogen bonding is less in case of Gemini-2 as two hydroxyl groups have already participated in intramolecular hydrogen bonding. As a result of this, the aggregates of Gemini-1 surfactant molecules will be formed at a concentration of surfactant which is lower than that of Gemini-2. So, Gemini-1 is more active towards the micelle formation than that of Gemini-2.

4.3 Mixed surfactant systems

4.3.1 Aggregation behavior

The data in Table 4.1 show that *cmc* values increase with increasing bulk mole fractions (α_j) of each monomeric surfactant with a given gemini surfactant (Gemini-1 or Gemini-2) in mixed surfactant systems. It is noteworthy that the process of micellization is progressively delayed with increasing α_j . Because of lower surface activity of a monomeric surfactant as compared to that of either Gemini-1 or Gemini-2, the former will have lesser tendency to form micelles than that of the latter which results in an increase in *cmc* with increasing α_j . The presence of two hydrocarbon chains in a gemini surfactant molecule results in excessive surface hydrophobicity in the mixed systems which leads to significant synergistic interactions in its binary mixtures with monomeric surfactants.^{13,14} A micelle is formed only when the hydrophobic interactions predominate over the coulombic repulsive interactions among the surfactant molecules.¹⁵ Gemini surfactant molecules may be contributing to the effective hydrophobicity of the mixed micelles leading to the decrease in *cmc*. One can see that the *cmc* of the mixed micelles are in between the individual *cmc* of a monomeric surfactant and a gemini and precisely more closer to the *cmc* of pure gemini surfactant than that of pure monomeric surfactant. It is pertinent to note from the data in Table 4.1 that the *cmc* of monomeric + Gemini-2 mixed surfactant systems are higher than that of monomeric + Gemini-1 mixed

surfactant systems. This could be because of lesser surface active properties of Gemini-2 as compared to that of Gemini-1 as discussed in Section 4.2.

The data in Table 4.1 also show that in the presence of a very small amount of gemini surfactants, the *cmc* values of conventional surfactants are reduced drastically. For example, *cmc* of pure DTAB is 146.0×10^{-4} M (Table 4.1), but at 0.9 mole fraction of DTAB i.e. at 0.1 mole fraction of Gemini-1, the *cmc* is reduced to 23.60×10^{-4} M (Table 4.1) which is one-sixth of its original value. It indicates that in the presence of a very small amount of Gemini-1, the surface active properties of DTAB increase significantly. However, in the presence of Gemini-2, the reduction in *cmc* value is low as compared to that of Gemini-1, since Gemini-2 is lesser surface active than Gemini-1. On the other hand, the *cmc* of pure Gemini-1 is 6.9×10^{-4} M (Table 4.1). However, in presence of a monomeric surfactant the *cmc* is increased. But one can see that this increase in *cmc* is not very high. For example, even at 0.5 bulk mole fraction of DTAB, the *cmc* of mixed system is 10.6×10^{-4} M (only 1.5 times the *cmc* of pure Gemini-1). These observations lead us to conclude that the use of gemini surfactants can be made cost-effective by mixing with conventional surfactants at the expense of very little surface activity of gemini surfactants. Although the *cmc* value of CTAB is close to that of gemini surfactants, but the reason for choosing CTAB as one of the monomeric surfactants is to show the effect of variation of hydrocarbon chain length.

4.3.2 Interactions and thermodynamic properties

Various methods described in Chapter 2 (section 2.2.14) are used to study the process of mixed micellization. Clint's equation²⁸ (Chapter 2 (section 2.2.14.1)) used to determine the ideality in the mixed micelles formation. This equation relates the theoretical *cmc* (cmc^*) of ideal binary mixture with experimental *cmc* (*cmc*) of the pure components. To identify the kind of interactions between the components as well as the deviation from the ideality, cmc^* and experimental *cmc* have been plotted as a function of mole fractions of monomeric surfactants in the solution at 303.15 K and the Figure 4.9 represents such plots as a representative figure for monomeric surfactants + Gemini-1 systems. It can be seen that for all the systems the experimental *cmc* values are lesser than the theoretically calculated cmc^* values at each mole fraction of the conventional surfactant.⁶ These results indicate the non-ideal behaviour. Since *cmc* lies

below the cmc^* value, it indicates the negative deviation from the ideality. These results are quite consistent with the findings of Rodriguez *et al.*¹¹ The negative deviation indicates that there are attractive interactions between the components of the investigated mixed surfactant systems.¹¹ The deviation from the ideality is varying with the chemical nature of the spacer group of the gemini surfactants and also with the chain length of the monomeric surfactants.¹¹ In case of binary mixture of a monomeric surfactant and Gemini-1, the deviation from the ideality increases with decreasing the chain length of the monomeric surfactants. As far as, Gemini-1 is concerned as one of the components, the deviation from the ideality for the mixed micellization of CTAB with Gemini-1 is very less. The maximum deviation is observed in case of DTAB + Gemini-1 system. Same trends are also observed for the binary mixtures, monomeric + Gemini-2 and are shown by Figure 4.10, however the deviations from the ideality are comparatively less in these cases as compared to that of monomeric + Gemini-1 systems. These results clearly show the effect of the spacer group of the gemini surfactants. An explanation for possible reasons for all these phenomena is given later.

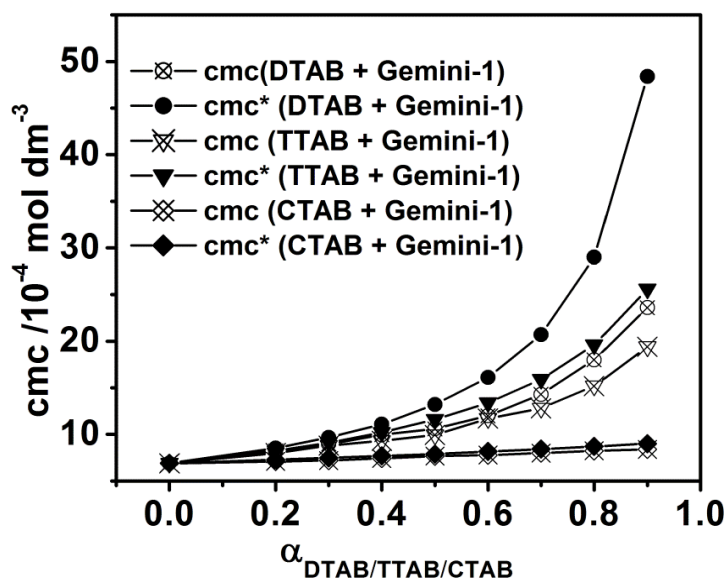


Figure 4.9: Critical micelle concentrations (cmc and cmc^*) versus bulk mole fraction, α_1 for monomeric + Gemini-1 systems

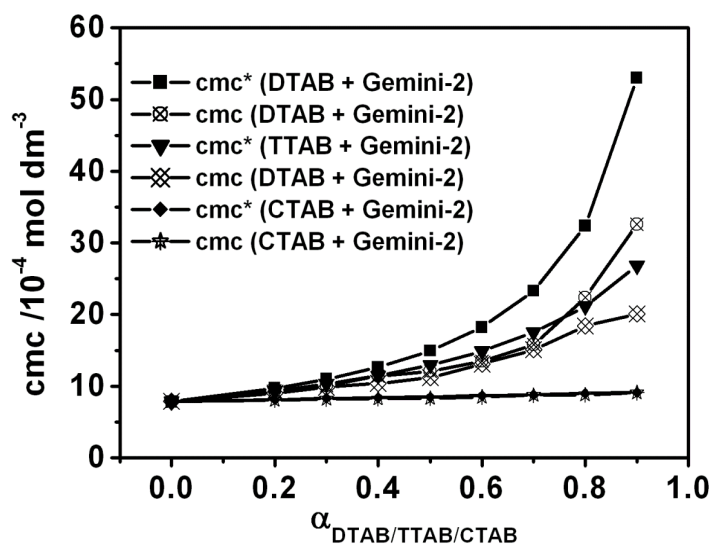


Figure 4.10: Critical micelle concentrations (cmc and cmc^*) and mole fraction, α_1 for monomeric +Gemini-2 systems

A quantitative interpretation of the experimental results has been done using Rubingh's model (Chapter 2, Section 2.2.14.2.). Using this theory it is possible to calculate the micelle mole fraction (X_I) as well as the interaction parameter (β). β indicates the magnitude of the interactions between the components in the mixed micelle and amount of deviation from ideality.^{11,17,18} The larger the negative value of β , stronger is the attractive interaction between two surfactant molecules. The interaction parameter, β has a negative value for all mixed surfactant systems (Table 4.2).

Table 4.2: Values of interaction parameter (β), for monomeric + Gemini-1/Gemini-2 mixed micellar systems

α_1	β	β	β	β	β	β
	CTAB + Gemini-1	TTAB + Gemini-1	DTAB + Gemini-1	CTAB + Gemini-2	TTAB + Gemini-2	DTAB + Gemini-2
0.2	-0.174	-0.563	-1.491	-0.070	-0.572	-1.750
0.3	-0.175	-0.442	-1.754	-0.031	-0.390	-1.754
0.4	-0.149	-0.768	-1.806	-0.070	-0.743	-1.961
0.5	-0.133	-0.976	-2.311	-0.092	-0.863	-2.144
0.6	-0.190	-0.739	-2.458	-0.079	-0.647	-2.344
0.7	-0.220	-0.991	-2.475	-0.041	-0.633	-2.453
0.8	-0.278	-1.058	-2.560	-0.100	-0.554	-2.398
0.9	-0.528	-1.165	-3.081	-0.028	-1.212	-2.076

These results show that the mixed micelles formations are due to the attractive interactions between the components. The negative values of β and the above mentioned negative deviation from the ideality are in support to the fact that hydrophobic interactions in the system predominate over the coulombic repulsive interactions. Although, the β values are negative but not constant for all binary combinations throughout the mole fractions range.¹¹ The β parameter should be independent of micellar composition, so an average value is commonly reported in the literature.^{11,19} The average values of interaction parameter (β_{av}) for the mixtures, CTAB/TTAB/DTAB + Gemini-1 are -0.231, -0.838, -2.242, respectively and that for the mixtures, CTAB/TTAB/DTAB + Gemini-2 are -0.064, -0.702, -2.070, respectively. These values indicate that the attractive interaction is increasing with decreasing the chain length of the monomeric surfactants. Similar trend has been reported by Rodriguez *et al.*¹¹ Maximum interaction is observed in case of DTAB + Gemini-1 mixed system. This can be explained on the basis of interactions between the hydrocarbon chains. As the chain lengths of monomeric and gemini surfactants become equal, the comfortable association of the components of the mixture is observed. Bakshi *et al.*²⁰ have reported that equal chain lengths of monomeric and gemini surfactants give compatibility at the level of headgroup region. Results also show that the magnitudes of β_{av} values decrease in case of Gemini-2 as compared to that of Gemini-1 with any monomeric surfactant. Based on our above mentioned discussion, it can be stated that Gemini-1 being more surface active than Gemini-2, the association of monomeric surfactant molecules with the former in mixed systems is expected to be friendlier than that with the latter.

The *cmc* data of mixed micelles summarized in Table 4.1 show some interesting trends. Although the interactions between the gemini and monomeric surfactants are maximum when they are having the equal hydrocarbon chain lengths, but the process of micellization becomes more favourable with increase in the hydrophobicity of the individual surfactant. This is attributed to the decrease in *cmc* values with increasing chain length of the monomeric surfactants (Table 4.1). The friendlier interactions depend on the similarity in the structures of components of mixed micelle, however, hydrophobicity of the surfactant molecules is the driving force for the formation of micelles. The micelle mole fraction (X_I) values for monomeric + Gemini-1/Gemini-2 mixed systems calculated using Rubingh's model are tabulated in Tables 4.3 and Table 4.4. For the calculation of X_I values, Rodenas's and Motomura's models also have been used (Chapter 2, Sections 2.2.14.3). The micelle mole fraction values at various bulk mole fractions calculated

using these models are coming close to those calculated by Rubbing's method (Tables 4.3 and Table 4.4). The micelle mole fraction in the ideal state (X_I^{ideal}) has been evaluated by applying the equation proposed by Clint²⁰ (Chapter 2, Section 2.2.14.1) and given by Tables 4.3 and 4.4.

Table 4.3: Various mixed micellar parameters for monomeric + Gemini-1 mixed systems based on conductivity measurement

α_1	X_1^{ideal}	X_1^{Rubingh}	X_1^{Motomura}	X_1^{Rodenas}	f_1	f_2
CTAB + Gemini-1						
0.2	0.156	0.172	0.151	0.171	0.887	0.997
0.3	0.241	0.256	0.233	0.261	0.908	0.988
0.4	0.331	0.341	0.317	0.340	0.937	0.987
0.5	0.426	0.430	0.415	0.441	0.958	0.976
0.6	0.527	0.524	0.521	0.533	0.958	0.949
0.7	0.634	0.621	0.620	0.616	0.969	0.920
0.8	0.748	0.724	0.742	0.733	0.980	0.864
0.9	0.870	0.826	0.886	0.815	0.984	0.698
TTAB + Gemini-1						
0.2	0.045	0.071	0.072	0.075	0.615	0.997
0.3	0.075	0.103	0.107	0.098	0.701	0.995
0.4	0.112	0.172	0.178	0.167	0.591	0.978
0.5	0.159	0.239	0.239	0.230	0.568	0.946
0.6	0.220	0.281	0.299	0.286	0.683	0.943
0.7	0.306	0.365	0.368	0.349	0.671	0.876
0.8	0.429	0.454	0.464	0.447	0.729	0.804
0.9	0.629	0.583	0.596	0.604	0.817	0.673
DTAB + Gemini-1						
0.2	0.012	0.044	0.042	0.053	0.256	0.997
0.3	0.019	0.081	0.079	0.082	0.227	0.989
0.4	0.031	0.113	0.136	0.116	0.241	0.977
0.5	0.045	0.175	0.127	0.187	0.207	0.932
0.6	0.066	0.220	0.199	0.223	0.224	0.888
0.7	0.099	0.263	0.280	0.255	0.261	0.843
0.8	0.159	0.321	0.355	0.302	0.307	0.768
0.9	0.298	0.416	0.434	0.459	0.350	0.587

Table 4.4: Various mixed micelles parameters for monomeric + Gemini-2 surfactants based on conductivity measurement at 303.15K

α_1	X_1^{ideal}	X_1^{Rubingh}	X_1^{Motomura}	X_1^{Rodenas}	f_1	f_2
CTAB + Gemini-2						
0.2	0.175	0.181	0.177	0.175	0.954	0.997
0.3	0.266	0.269	0.279	0.272	0.983	0.997
0.4	0.361	0.365	0.372	0.364	0.972	0.990
0.5	0.458	0.460	0.447	0.460	0.973	0.980
0.6	0.559	0.557	0.534	0.548	0.984	0.975
0.7	0.664	0.661	0.679	0.654	0.995	0.982
0.8	0.772	0.763	0.751	0.771	0.998	0.980
0.9	0.885	0.881	0.873	0.873	0.999	0.978
TTAB + Gemini-2						
0.2	0.051	0.080	0.078	0.079	0.616	0.996
0.3	0.084	0.119	0.116	0.125	0.739	0.994
0.4	0.125	0.186	0.189	0.194	0.611	0.974
0.5	0.177	0.249	0.248	0.252	0.614	0.948
0.6	0.244	0.296	0.316	0.280	0.726	0.945
0.7	0.334	0.371	0.383	0.387	0.778	0.917
0.8	0.462	0.470	0.483	0.474	0.856	0.885
0.9	0.659	0.600	0.591	0.593	0.824	0.646
DTAB + Gemini-2						
0.2	0.013	0.047	0.046	0.040	0.272	0.996
0.3	0.023	0.089	0.093	0.093	0.233	0.986
0.4	0.035	0.132	0.130	0.124	0.228	0.966
0.5	0.051	0.177	0.119	0.186	0.234	0.935
0.6	0.070	0.226	0.229	0.221	0.246	0.887
0.7	0.112	0.275	0.257	0.290	0.275	0.831
0.8	0.177	0.329	0.359	0.317	0.340	0.771
0.9	0.327	0.598	0.624	0.599	0.715	0.476

For the mixture, CTAB + Gemini-1, X_I values calculated using various methods are very close to X_I^{ideal} . This result is shown by Figure 4.11, where X_I values calculated using Rubingh's model are plotted. It depicts that this system is comparatively less deviated from the ideality. More the difference between X_I and X_I^{ideal} , greater will be the

deviation from the ideality.²¹ The X_I value is higher than X_I^{ideal} upto bulk mole fraction of 0.5 after that X_I is lowered as compared to X_I^{ideal} . In case of TTAB + Gemini-1, the difference between X_I and X_I^{ideal} is increased as compared to that in CTAB + Gemini-1 system showing larger deviation from the ideality. For the formation of mixed aggregates, Gemini-1 is participating more even at higher composition of TTAB. Mixed micelle composition of TTAB is higher than that of Gemini-1 only at $\alpha_{\text{TTAB}} = 0.9$.

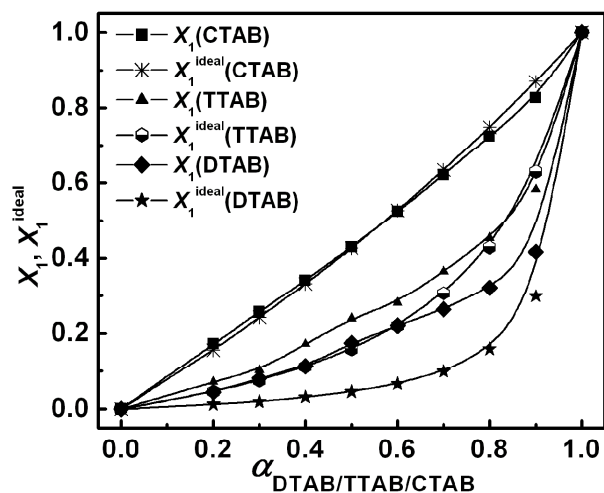


Figure 4.11: Micellar mole fractions, X_1 calculated using Rubbing's method and X_1^{ideal} versus bulk mole fraction, α_1 for monomeric + Gemini-1 systems

Further, for the system, DTAB + Gemini-1, there is a large difference between X_I and X_I^{ideal} . All these results further support the fact that the deviation from the ideality increases with decrease in the difference between the hydrocarbon chain lengths of monomeric and gemini surfactants.

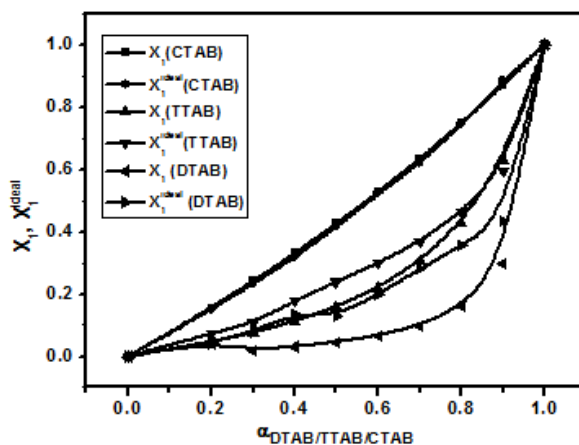


Figure 4.12: Micellar mole fractions, X_1 calculated using Motomura's method and X_1^{ideal} versus bulk mole fraction, α_1 for monomeric + Gemini-1 systems

Figures 4.12 and Table 4.13 show micellar mole fractions, X_I calculated using Motomura and Rodenas methods, respectively and also X_I^{ideal} versus bulk mole fraction, α_1 for monomeric + Gemini-1 systems. Results are similar to that obtained using Rubingh method.

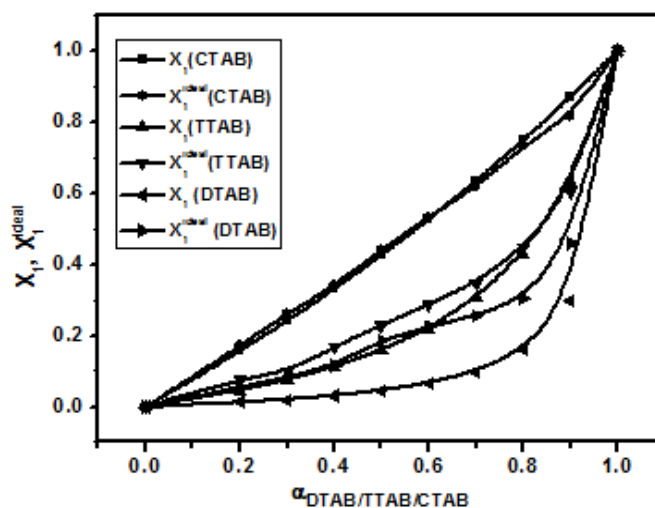


Figure 4.13: Micellar mole fractions, X_I calculated using Rodena's method and X_I^{ideal} versus bulk mole fraction, α_1 for monomeric + Gemini-1 systems

If the hydrocarbon chain of a monomeric surfactant is longer than that of a gemini surfactant, then the former would not give a proper room to the latter to adjust its hydrocarbon chains in the core of the micelle.²⁰ As the chain lengths of monomeric and gemini surfactants become equal, there will be more interactions between them because their chains are adjusted well in the core of the micelle. That is why maximum interaction has been observed in the case of DTAB + Gemini-1 system. Interestingly, in the case of DTAB + Gemini-1 system, the micellar composition of Gemini-1 is higher than that of DTAB even at a high bulk composition of DTAB because of their well adjustment in the micelle core. The longer hydrocarbon tail of a monomeric surfactant than that of a gemini surfactant may also induce incompatibility in the headgroup region²⁰. For the mixed systems of monomeric and Gemini-2 surfactants, similar types of interactions have been observed and are shown by Figures 4.14 to 4.16, where micellar mole fractions are calculated using Rubingh, Motomura, and Rodenas methods, respectively. However, the magnitudes of deviations from the ideality are less as compared to that of the mixed systems, monomeric + Gemini-1. This is due to the fact that the participations

of Gemini-2 molecules in mixed micelle are less than that of Gemini-1 as the former is less surface active than that of the latter. This result is supported by higher micelle mole fraction (X_2) of Gemini-1 than that of Gemini-2 at any bulk composition and tabulated in Table 4.3 and Table 4.4, respectively. Singh *et al.*²² observed the effect of the spacer group of gemini surfactant on zwitterionic-gemini surfactants mixed system. They reported that synergism in the mixed micellar system decreases with an increase in the length of the spacer. However, they worked with gemini surfactant with unsubstituted spacer. As discussed above, the spacer of Gemini-2 is rigid, however the spacer of Gemini-1 is comparatively flexible. As a result of this rigidity, the hydrocarbon chains of Gemini-2 would not get proper room in the core of the micelle. Thus the hydrophobic interactions between Gemini-2 and monomeric surfactants are lesser than that between Gemini-1 and monomeric surfactants. Moreover, as discussed above, the spacer group of Gemini-2 is expected to be less hydrophilic than that of Gemini-1.

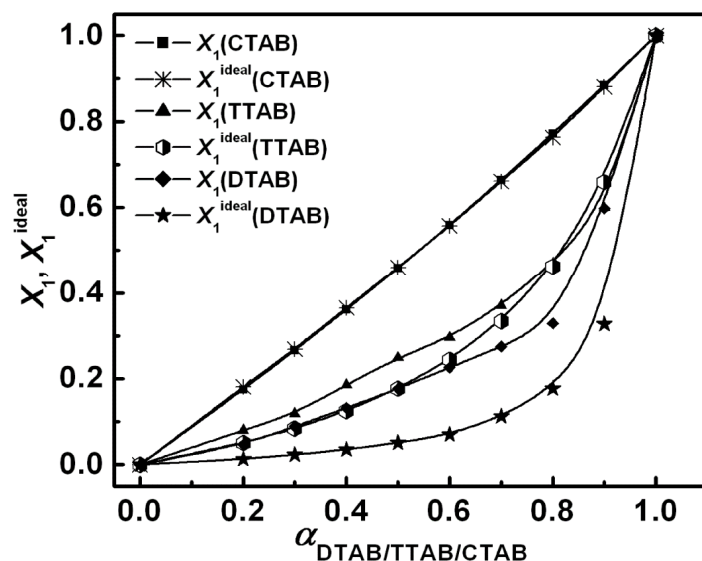


Figure 4.14: Micellar mole fractions, X_1 calculated using Rubbing's method and X_1^{ideal} , vs, solution mole fraction α_1 of monomeric + Gemini-2

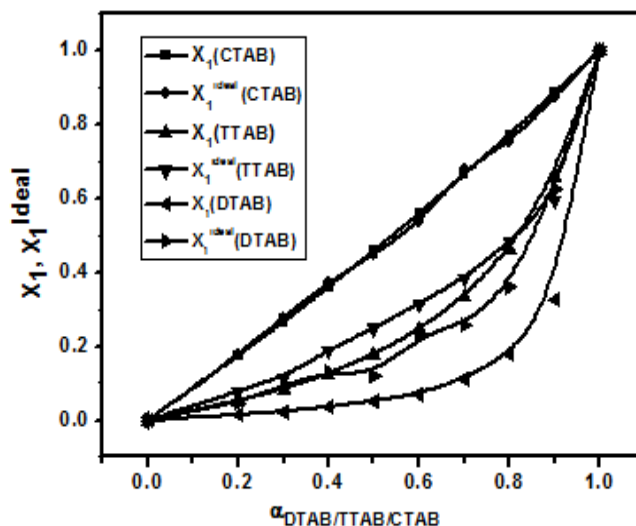


Figure 4.15: Micellar mole fractions, X_1 calculated using Motomura's method and X_1^{ideal} , vs, solution mole fraction α_1 of monomeric + Gemini-2

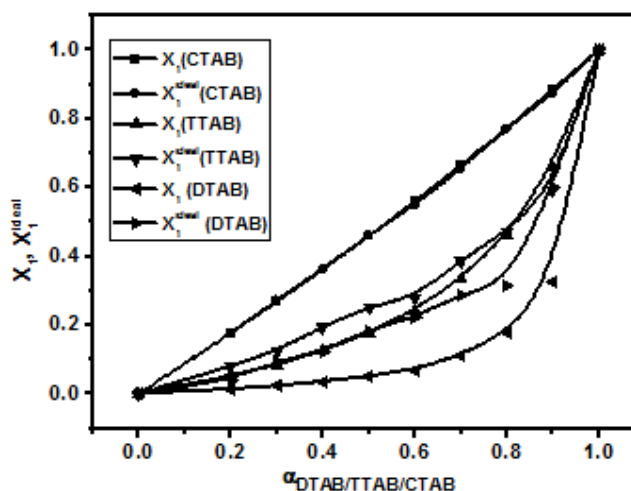


Figure 4.16: Micellar mole fractions, X_1 calculated using Rodena's method and X_1^{ideal} , vs, solution mole fraction α_1 of monomeric + Gemini-2

The above discussed results are also supported by the calculation of activity coefficients (Table 4.3 and Table 4.4). If β is zero, the activity coefficients will be unity and mixture of surfactants will be ideal.²³ The activity coefficients for monomeric (f_1) and gemini surfactants (f_2) are calculated by equations 2.49 and 2.50 (Chapter 2, Section 2.2.14.2). It can be seen that the activity coefficient values in all mixed systems are less than unity showing the non-ideal behavior with attractive interactions.¹⁸ However, in case of CTAB + Gemini-1/Gemini-2 systems, the deviations from the

ideality are very less and are supported by the activity coefficient values close to unity. The maximum differences between the f_1 and f_2 values are found in DTAB + Gemini-1/Gemini-2 systems. For both TTAB + Gemini-1 and DTAB + Gemini-1 systems, the activity coefficients of gemini are higher than that of monomeric surfactants. It is also noteworthy that the activity coefficient values of gemini are higher than that of CTAB below $\alpha_1 = 0.5$, whereas this trend is reversed above $\alpha_1 = 0.5$. All these results are in accordance with the cmc and X_1 values discussed above.

Quantitatively, deviation from the ideality can be demonstrated by the excess Gibbs energy of micelle (G^E). A positive value of G^E indicates that the interactions in the mixed micelles are less attractive or more repulsive than those in the one-component micelles and vice-versa for a negative G^E value.⁶⁹ G^E is calculated by the Equation 2.55 (Chapter 2, Section 2.2.14.4). The calculated G^E values for all the mixtures are negative at all the bulk mole fractions. For consideration of Motomura's and Rodenas's approaches, activity coefficients, f_1 and f_2 are calculated by equations 2.49 and 2.50 (Chapter 2, Section 2.2.14.4).^{11,22} In all the cases the values of G^E are negative. It indicates that for the formation of mixed micelles there are attractive interactions between the surfactant molecules.³⁰ The G^E values for monomeric + Gemini-1 and for monomeric + Gemini-2 systems at some selective mole fractions are tabulated in Tables 4.5 and 4.6, respectively. The magnitude of G^E increases with decreasing the chain length of the monomeric surfactants. This result is also in accordance with the fact that the non-ideality increases with decreasing the chain length of the monomeric surfactants.

The stability of the micelles can be studied by the calculation of the standard Gibbs free energy of mixed micelle formation (ΔG_m^o). In all the cases, ΔG_m^o values are coming out to be negative (Tables 4.5 and 4.6). The values of ΔG_m^o indicate that the mixed micelle formation is a spontaneous process for all the mixtures. The spontaneity of micellization process increases with increasing bulk mole fraction of gemini surfactants and this phenomenon is significantly prominent in case of TTAB/DTAB + Gemini-1 surfactant systems. It is worth mentioning that the average values of ΔG_m^o for DTAB, TTAB and CTAB with Gemini-1 are -60.45, -64.22, and -69.87 kJ mol⁻¹, respectively and the average values of counterions dissociation, g for DTAB, TTAB and CTAB with Gemini-1 are 0.386, 0.328, and 0.262, respectively (Tables 4.5).

Table 4.5: Excess Gibbs free energy of micelle, G^E , counter ions dissociation, g and standard Gibbs free energy of micellization, ΔG_m^o for monomeric + Gemini-1 systems at 303.15 K

α_1	$G^{E(\text{Rubingh})}/$ kJ mol^{-1}	$G^{E(\text{Rodenas})}/$ kJ mol^{-1}	$G^{E(\text{Motomura})}/$ kJ mol^{-1}	g	$\Delta G_m^o/$ kJ mol^{-1}
CTAB + Gemini-1					
0.2	-0.062	-0.064	-0.062	0.292	-68.61
0.3	-0.085	-0.098	-0.096	0.243	-71.31
0.4	-0.084	-0.089	-0.089	0.244	-71.05
0.5	-0.081	-0.086	-0.085	0.226	-71.87
0.6	-0.119	-0.122	-0.121	0.264	-69.63
0.7	-0.129	-0.134	-0.134	0.234	-71.15
0.8	-0.139	-0.137	-0.136	0.248	-70.17
0.9	-0.191	-0.200	-0.173	0.221	-69.32
TTAB + Gemini-1					
0.2	-0.094	-0.099	-0.095	0.239	-70.72
0.3	-0.103	-0.099	-0.107	0.251	-69.46
0.4	-0.276	-0.273	-0.287	0.287	-67.25
0.5	-0.447	-0.435	-0.446	0.303	-65.96
0.6	-0.376	-0.380	-0.393	0.362	-61.78
0.7	-0.578	-0.569	-0.581	0.387	-59.91
0.8	-0.661	-0.659	-0.663	0.422	-57.11
0.9	-0.714	-0.706	-0.709	0.286	-51.07
DTAB + Gemini-1					
0.2	-0.158	-0.192	-0.152	0.245	-70.02
0.3	-0.328	-0.332	-0.320	0.260	-68.98
0.4	-0.456	-0.469	-0.545	0.312	-65.45
0.5	-0.841	-0.889	-0.682	0.343	-63.38
0.6	-1.061	-1.065	-0.984	0.405	-59.30
0.7	-1.208	-1.184	-1.259	0.491	53.33
0.8	-1.406	-1.364	-1.491	0.583	-47.01
0.9	-1.885	-1.954	-1.914	0.737	-38.72

One can see that both ΔG_m^o and g decrease with increasing the hydrocarbon chain length of monomeric surfactants. This result is consistent with the fact that the micellization process becomes favorable with increasing hydrophobicity of one of the components of mixed micelle that has lead to the decrease in *cmc* values (Table 4.1). As far as Gemini-2 is concerned as one of the components of mixed micelle, the trend is little different. The average values of ΔG_m^o for DTAB, TTAB and CTAB with Gemini-2 are -58.44, -49.90, and -68.79 kJ mol^{-1} , respectively and the average values of counter ions dissociation, g

for DTAB, TTAB and CTAB with Gemini-2 are 0.416, 0.472, and 0.271, respectively (Table 4.6).

Table 4.6: Excess Gibbs energy of micelle formation, G^E , counter ions dissociation, g and standard Gibbs energy of micellization, ΔG_m^o for monomeric + Gemini-2 at 303.15K

α_1	$G^E(\text{Rubingh})/$ kJ mol^{-1}	$G^E(\text{Rodenas})/$ kJ mol^{-1}	$G^E(\text{Motomura})/$ kJ mol^{-1}	g	$\Delta G_m^o /$ kJ mol^{-1}
CTAB + Gemini-2					
0.2	-0.028	-0.028	-0.028	0.263	-69.49
0.3	-0.017	-0.016	-0.017	0.311	-66.67
0.4	-0.042	-0.041	-0.042	0.271	-68.87
0.5	-0.059	-0.058	-0.059	0.276	-68.53
0.6	-0.051	-0.051	-0.053	0.283	-68.02
0.7	-0.024	-0.023	-0.024	0.295	-68.17
0.8	-0.016	-0.044	-0.047	0.265	-68.79
0.9	-0.009	-0.011	-0.011	0.273	-69.16
TTAB + Gemini-2					
0.2	-0.106	-0.104	-0.103	0.286	-53.89
0.3	-0.103	-0.135	-0.126	0.269	-54.29
0.4	-0.284	-0.295	-0.288	0.328	-50.76
0.5	-0.407	-0.411	-0.407	0.350	-49.34
0.6	-0.340	-0.329	-0.354	0.332	-49.23
0.7	-0.372	-0.383	-0.381	0.367	-46.94
0.8	-0.348	-0.352	-0.354	0.369	-45.73
0.9	-0.733	-0.751	-0.752	0.424	-43.03
DTAB + Gemini-2					
0.2	-0.163	-0.104	-0.122	0.296	-66.64
0.3	-0.359	-0.429	-0.429	0.291	-66.53
0.4	-0.567	-0.538	-0.559	0.342	-63.22
0.5	-0.787	-0.821	-0.619	0.366	-61.37
0.6	-1.032	-1.019	-1.045	0.420	-57.85
0.7	-1.233	-1.276	-1.184	0.559	-49.66
0.8	-1.334	-1.307	-1.399	0.606	-46.03
0.9	-1.258	-1.616	-1.690	0.755	-36.59

The different trend in case of Gemini-2 may be because of one or more free energy terms contribute differently to ΔG_m^o .¹⁴ The most probable factor responsible for difference in ΔG_m^o could be different extent of influence on the conformation of linked tails inside the core due to the difference in the chemical structure of spacers.¹⁴ The longer spacer of Gemini-2 as compared to that of Gemini-1 may help in better accommodation of hydrocarbon chains of DTAB in the core of a micelle. The

corresponding Gibbs free energy term contributed to the ΔG_m^o could be more negative in case of DTAB than that of TTAB as one of the components of mixed micelle. However, greater ΔG_m^o in case of DTAB+Gemini-2 as compared to that of DTAB+Gemini-1 is because of lesser surface activity of Gemini-2 than that of Gemini-1. But similar trends in *cmc* values in both the cases of mixed systems of Gemini-1 and Gemini-2 with monomeric surfactants could be as a result of predominant effect of hydrophobicity of surfactant tails over other possible effects. It is also pertinent to note that the micellization processes are comparatively more spontaneous with Gemini-1 surfactant as compared to that with Gemini-2 surfactant.

4.4 Microenvironmental properties

Micropolarity around the probe molecule reveals important information regarding the probable location of the probe molecule in the micelle.²⁵⁻²⁷ With the introduction of a suitable environmental polarity and viscosity sensitive fluorescent probe, it could be possible to predict the micellization process. Since the TICT fluorescence is very much sensitive to the polarity and viscosity of environment, in the present study DMACA molecule showing TICT fluorescence⁵⁷ has been explored to characterize the microenvironment of mixed micelles. The fluorescence spectra of DMACA have been recorded at 0.2, 0.4, 0.6, and 0.8 bulk mole fractions of monomeric surfactants for all the mixed systems at $\lambda_{ex} = 378$ nm. For the evaluation of microenvironmental properties, we have focused on the TICT fluorescence band. It has been reported in the literature that a TICT band is more sensitive to the environment than a locally excited (LE) band.²⁸⁻³⁰ The emission spectra of DMACA in dioxane-water mixture have been recorded and then the emission maxima (in terms of wavenumber) have been plotted against $E_T(30)$, a solvent polarity parameter³¹ (Figure 4.17). For the measurement of micropolarity of mixed micelles, the emission spectra of DMACA in mixed surfactant solutions at a concentration well above the *cmc* (10 times) have been recorded. Micropolarity sensed by DMACA has been estimated by correlating the fluorescence peak maxima in mixed micellar systems with that in different percentages of dioxane-water mixtures. Micropolarity values expressed in equivalent scale of $E_T(30)$ have been tabulated in Table 4.7 and Table 4.8 for monomeric + Gemini-1 and monomeric + Gemini-2 mixed systems, respectively. The average $E_T(30)$ value for all the systems is found to be 51.6 and we can say that the micropolarity of DMACA binding sites in the mixed micelle is close to that of ethanol ($E_T(30) = 51.9$). These results show that the probe molecules reside in the micelle-water interface. Panja *et al.*⁸ reported the orientations of

DMACA in different types of micelles. In cationic micelle, the acceptor part (C=O) of DMACA oriented toward the positively charged Stern layer and donor part (-NMe₂) oriented towards the Gouy-Chapman layer. Micropolarities of mixed systems also have been determined by using the pyrene as a probe molecule. The I_1/I_3 for pyrene in ethanol is found to be 1.05 (intensities measured at 375 nm and 386 nm for I_1 and I_3 , respectively at $\lambda_{ex} = 339$ nm). The average value of I_1/I_3 of all mixed systems is calculated to be 1.05 (Tables 4.7 and 4.8). It indicates that pyrene molecule also residing at the micelle-water interface.

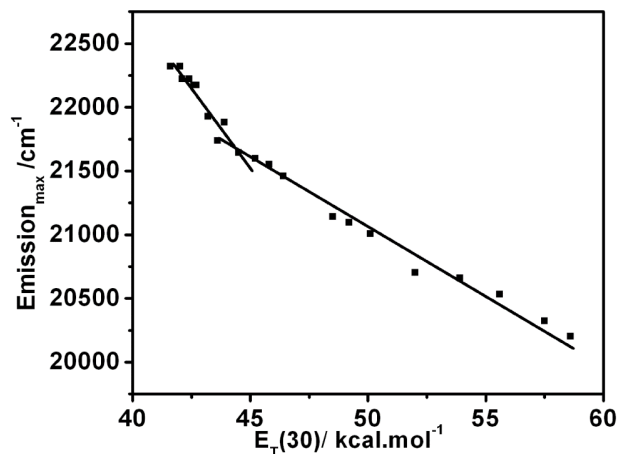


Figure 4.17: Emission peak maxima (cm⁻¹) of DMACA in different % of dioxane-water mixture versus solvent polarity parameter ($E_T(30)$)

Table 4.7: Microenvironmental properties of monomeric + Gemini-1 mixed systems

α	$E_T(30)^a$ / kcal mol ⁻¹	Anisotropy (r) ^b	Microviscosity ^c /cP	I_1/I_3 ^d	K_S ^e /M ⁻¹
CTAB + Gemini -1					
0.2	51.8	0.241	1.41	1.06	590
0.4	51.8	0.239	1.38	1.07	544
0.6	51.3	0.239	1.38	1.06	470
0.8	51.8	0.241	1.41	1.06	450
TTAB + Gemini -1					
0.2	51.8	0.248	1.62	1.06	372
0.4	51.8	0.245	1.43	1.06	290
0.6	51.8	0.242	1.42	1.06	250
0.8	51.8	0.245	1.43	1.06	246
DTAB + Gemini -1					
0.2	50.9	0.238	1.26	1.02	353
0.4	51.8	0.216	1.03	1.02	264
0.6	51.3	0.246	1.50	1.03	244
0.8	51.8	0.241	1.41	1.06	164

^aSD = ± 0.2 , ^bSD = ± 0.004 , ^cSD = ± 0.04 , ^dSD = ± 0.02 , ^eSD = ± 15

Table 4.8: Microenvironmental properties of monomeric + Gemini-2 mixed systems

α	$E_T(30)^a/$ kcal mol ⁻¹	Anisotropy (r) ^b	Microviscosity ^c /cp	I_1/I_3 ^d	K_S ^e /M ⁻¹
CTAB + Gemini -2					
0.2	51.3	0.216	1.03	1.03	469
0.4	51.3	0.235	1.31	1.03	415
0.6	51.3	0.240	1.41	1.03	413
0.8	51.3	0.223	1.07	1.04	417
TTAB + Gemini -2					
0.2	51.3	0.220	1.03	1.02	353
0.4	51.3	0.220	1.03	1.03	292
0.6	51.3	0.239	1.38	1.05	242
0.8	51.8	0.241	1.41	1.04	238
DTAB + Gemini -2					
0.2	51.3	0.220	1.03	1.06	232
0.4	51.3	0.220	1.03	1.05	211
0.6	51.3	0.238	1.36	1.05	190
0.8	51.8	0.216	1.03	1.07	171

^aSD = ± 0.2 , ^bSD = ± 0.004 , ^cSD = ± 0.04 , ^dSD = ± 0.02 , ^eSD = ± 15

To get further information regarding the microenvironment around the probe molecule, the steady-state fluorescence anisotropy of DMACA have been estimated in various mixed micellar systems measuring fluorescence intensities at 490 nm.³² Fluorescence anisotropy experiments are often carried out to estimate the microviscosity of environment.^{10,33} For the determination of microviscosity of each system, we first determined the fluorescence anisotropy of DMACA in glycerol-water mixtures of various compositions (Chapter 2, Section 2.2.7) and represented by Figure 4.18.^{10,33}

By correlating the anisotropy of DMACA in surfactant mixtures with that in glycerol-water mixtures, we first determined the microenvironment in equivalent scale of composition of glycerol-water mixtures. We then determined the microviscosity from the correlation diagram drawn between the viscosity of glycerol-water mixtures and compositions of same mixtures (Figure 4.19). Fluorescence anisotropy values of DMACA in various mixed micellar systems of monomeric+Gemini-1/Gemini-2 surfactants and corresponding microviscosity values are tabulated in Tables 4.7 and 4.8, respectively. Microviscosity determined in this way is more or less same for each mixed system. The average value of microviscosity is found to be 1.39 cP. It is pertinent to note

that similar to micropolarity, the microviscosity of environment around probe is also same for each mixed system.

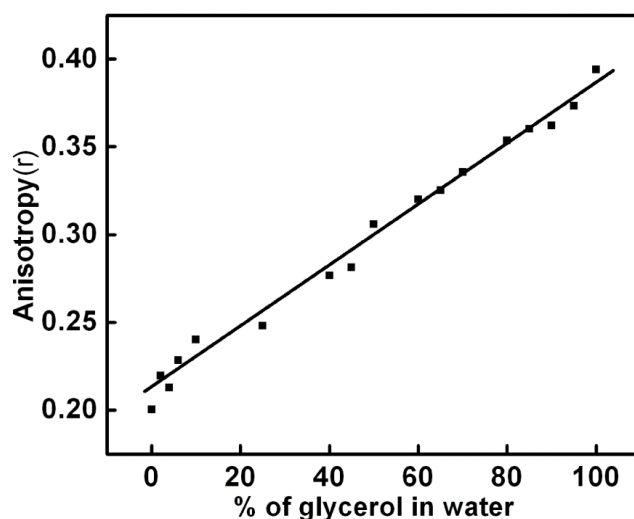


Figure 4.18: Plot of anisotropy (r) of DMACA in different % of glycerol-water mixtures

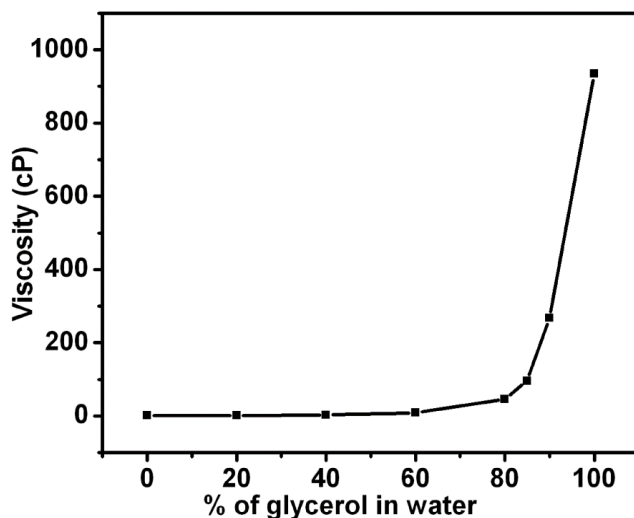


Figure 4.19: Plot of viscosity (cP) of different % of glycerol-water mixtures

4.5 Binding of DMACA with mixed surfactant systems

To know how strongly the probe molecule (DMACA) is binding with the mixed micelle, binding constant (K_s) has been calculated. The emission intensity of DMACA increased with increasing the concentration of surfactants (Figure 4.7). The binding constant has been calculated using equation 2.18 (Chapter 2, Section 2.2.9). Figure 4.20 shows a typical plot of $(F - F_o) / ([S]_{TOTAL} - cmc)$ vs fluorescence

intensity, F of DMACA in DTAB + Gemini-1/Gemini-2 mixed system at $\alpha_{\text{DTAB}} = 0.2$ as a representative one. From the slope of a fitted straight line K_S has been calculated. The K_S values for monomeric + Gemini-1/Gemini-2 mixed systems are tabulated in Tables 4.7 and 4.8, respectively. The binding constant increases with increasing the composition of gemini surfactant in mixed micelles. It could be due to more hydrophobic nature of the gemini surfactants as compared to that of monomeric surfactants. The average values of K_S of DMACA with mixed micelles of DTAB, TTAB and CTAB with Gemini-1 are 256, 290 and 513 M^{-1} , respectively. The same values with Gemini-2 surfactant are 201, 281, and 429 M^{-1} , respectively. These results also support our aforementioned discussion that the hydrophobicity of the micelles increases with increasing hydrocarbon chain length of monomeric surfactants in the mixed micelles with gemini surfactants. With the increase in the hydrophobicity of the mixed micelle, DMACA binds strongly with it. The data are also consistent with the fact that the mixed micelles of monomeric surfactants with Gemini-1 are more hydrophobic than that with Gemini-2.

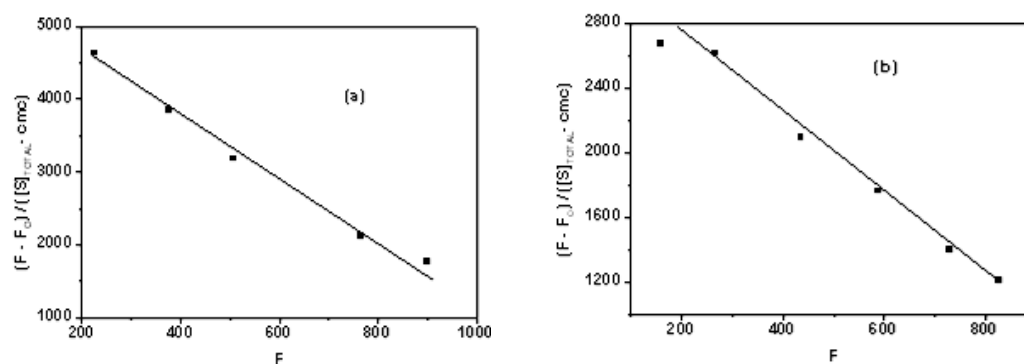


Figure 4.20: Plot of $(F - F_o) / ([S]_{\text{TOTAL}} - \text{cmc})$ vs F in (a) DTAB + Gemini-1 and (b) DTAB + Gemini-2 mixed system at $\alpha_{\text{DTAB}} = 0.2$

4.6 Conclusions

The cationic gemini surfactant, Gemini-1 with flexible and hydrophilic spacer group is more active in aggregating than that of Gemini-2 with comparatively rigid and less hydrophilic spacer group. Mixed micellar properties of these gemini surfactants with cationic conventional surfactants with varying chain length have been studied. The cmc of all the mixed systems have been determined conductometrically as well as using a TICT fluorescence probe molecule. The use of gemini surfactants can be made cost-effective by mixing with conventional surfactants at the expense of very little surface

activity of gemini surfactants. The surface activity of monomeric surfactants can be enhanced significantly by mixing with gemini surfactants. The *cmc* values of all the mixed systems are in between the *cmc* values of gemini surfactants and that of monomeric surfactants. Different theoretical models have been used to analyze the mixed surfactant systems. The interactions between the gemini and monomeric surfactant molecules in the mixed micelle are found to be attractive. Interestingly, it has been found that although the extent of interactions are maximum when there are similarities in the structures of their hydrocarbon chains, but the process of micellization is favored with increasing hydrophobicity of the monomeric surfactant. The longer spacer of a gemini surfactant may help in better accommodation of hydrocarbon tail of same length of a monomeric surfactant in the core of a micelle. The corresponding Gibbs free energy term may contribute to the negative ΔG_m^o . The participations of gemini surfactant molecules in mixed micelle formation are found to be increased with decreasing the spacer chain length and number of substituted hydroxyl groups in it. The *cmc* value of each mixed micellar system decreases with increasing bulk mole fraction of gemini surfactant. All these results depict that the mixed micellar properties can be tuned by changing the chemical structures of spacer group and hydrocarbon chain, and also by changing the solution composition. The mixed micelle formations are thermodynamically spontaneous for all the mixed systems. Keeping in mind the fact that the micelles are used as drug molecules solubilizers and as bio-mimicking systems, the microviscosity and micropolarity of all the mixed systems have been determined using a viscosity and polarity sensitive TICT fluorescence probe, DMACA. The micropolarity of environment around the probe molecule is equivalent to ethanol. The average value of microviscosity of mixed systems is 1.39 cP. The binding constant of the fluorescent probe molecule increases with increasing composition of gemini surfactant in the mixed micelle and also with increasing chain length of the monomeric surfactants. This is because of increase in the hydrophobicity of the mixed micelle for either of the two factors. DMACA can be potentially used to estimate *cmc* to avoid ambiguities in the use of pyrene.

References:

- (1) P. Carpena, J. Aguiar, P. Bernaola-Galván, C. C. Ruiz, *Langmuir* **2002**, *18*, 6054.
- (2) A. Rodríguez, M. M. Graciani, A. J. Moreno-Vargas, M. L. Moyá, *J. Phys. Chem. B* **2008**, *112*, 11942.
- (3) M. Vasilescu, D. Angelescu, M. Almgren, A. Valstar, *Langmuir* **1999**, *15*, 2635.
- (4) R. G. Alargova, I. I. Kochijashky, M. L. Sierra, K. Kwetkat, R. Zana, *J. Colloid Interface Sci.* **2001**, *235*, 119.
- (5) M. S. Bakshi, P. Sharma, G. Kaur, S. Sachar, T. S. Banipal, *Colloids Surf. A* **2006**, *278*, 218.
- (6) C. C. Ruiz, J. A. Molina-Bolívar, *J. Colloid Interface Sci.* **2011**, *361*, 178.
- (7) P. R. Bangal, S. Panja, S. Chakravorti, *J. Photochem. Photobio. A* **2001**, *139*, 5.
- (8) S. Panja, P. Chowdhury, S. Chakravorti, *Chem. Phys. Lett.* **2003**, *368*, 654.
- (9) M. J. Rosen, L. D. Song, *J. Colloid Interface Sci.* **1996**, *179*, 261.
- (10) X. Wang, J. Wang, Y. Wang, H. Yan, P. Li, R. K. Thomas, *Langmuir* **2004**, *20*, 53.
- (11) A. Rodríguez, M. M. Graciani, A. J. Moreno-Vargas, M. L. Moyá, *J. Phys. Chem. B* **2008**, *112*, 11942.
- (12) X. Pei, Y. You, J. Zhao, Y. Deng, E. Li, Z. Li, *J. Colloid Interface Sci.* **2010**, *351*, 457.
- (13) M. J. Rosen, Z. H. Zhu, T. Gao, *J. Colloid Interface Sci.* **1993** *157*, 254.
- (14) T. A. Camesano, R. Nagarajan, *Colloids Surf. A* **2000**, *167*, 165.
- (15) M. A. Muherei, R. Junin, *Asian J. Appl. Sci.* **2009**, *2*, 115.
- (16) K. S. Sharma, S. R. Patil, A. K. Rakshit, K. Glenn, M. Doiron, R. M. Palepu, P. A. Hassan, *J. Phys. Chem. B* **2004**, *108*, 12804.
- (17) M. S. Bakshi, J. Singh, K. Singh, G. Kaur, *J. Photochem. Photobio. A* **2005**, *169*, 63.
- (18) Kabir-ud-Din; M. S. Sheikh, A. A. Dar, *J. Phys. Chem. B* **2010**, *114*, 6023.
- (19) A. Rodríguez-Pulido, A. Casado, M. Muñoz-Úbeda, E. Junquera, E. Aicart, *Langmuir* **2010**, *26*, 9378.
- (20) M. S. Bakshi, J. Singh, K. Singh, G. Kaur, *Colloids Surf. A* **2004**, *234*, 77.
- (21) N. Azum, A. Z. Naqvi, M. Akram, Kabir-ud-Din, *J. Colloid Interface Sci.* **2008**, *328*, 429.
- (22) K. Singh, D. G. Marangoni, *J. Colloid Interface Sci.* **2007**, *315*, 620.

-
- (23) K. Holmberg, B. Jonson, B. Kornberg, B. Lindman, *Surfactants and Polymers in Aqueous Solution*; Wiley: Chichester, **2007**.
- (24) P. Wydro, M. Paluch, *Colloids Surf. A* **2009**, *348*, 70.
- (25) P. Banerjee, S. Pramanik, A. Sarkar, S. C. Bhattacharya, *J. Phys. Chem. B* **2008**, *112*, 7211.
- (26) P. Quagliotto, N. Barbero, C. Barolo, K. Costabello, L. Marchese, S. Coluccia, K. Kalyanasundaram, G. Viscard, *Dyes Pigm.* **2009**, *82*, 124.
- (27) A. Chakrabarty, P. Das, A. Mallick, N. Chattopadhyay, *J. Phys. Chem. B* **2008**, *112*, 3684.
- (28) A. Samanta, B. K. Paul, N. Guchhait, *Spectrochim. Acta, Part A* **2011**, *78*, 1525.
- (29) N. Dash, G. Krishnamoorthy, *J. Fluoresc.* **2010**, *20*, 135.
- (30) S. K. Saha, P. Purkayastha, A. B. Das, *J. Photochem. Photobiol. A* **2008**, *195*, 368.
- (31) C. Reichardt, *Chem. Rev.* **1994**, *94*, 2319.
- (32) K. Kalyanasundaram, *Photochemistry in Microheterogeneous Systems*; Academic Press: New York, **1987**.
- (33) A. Mallick, N. Chattopadhyay, *Photochem. Photobiol.* **2005**, *81*, 419.

Chapter 5

Effect of polymethylene spacer of cationic gemini surfactants on solvation dynamics and rotational relaxation of Coumarin 153 in aqueous micelles*

The present work demonstrates the solvation dynamics and rotational relaxation of Coumarin 153 (C-153) in the micelles of a series of cationic gemini surfactants, 12-*s*-12, 2Br⁻ containing a hydrophobic polymethylene spacer with *s* = 3, 4, 6, 8, 12. Steady-state and time-correlated single photon counting (TCSPC) fluorescence spectroscopic techniques have been used to carry out this study. Steady-state and TCSPC fluorescence data suggest that C-153 molecules are located at the Stern layer of micelles. While probe molecules feel more or less same micropolarity in micellar phase, the microviscosity of micelles decreases with spacer chain length. Solvation dynamics in the Stern layer is bimodal in nature with fast solvation as a major component. Counterions and water molecules bonded with the polar headgroups of surfactant molecules are responsible for slow component. Average solvation time increases with spacer chain length because of increased degree of counter ion dissociation. Some water molecules are involved in the solvation of counter ions itself. It results in decrease in 'free' water molecules to be available for solvation of C-153. Hydrophobic spacer chain also has an effect on increasing solvation time with increasing chain length. Average rotational relaxation time for C-153 decreases with spacer chain length with rapid decrease at *s* > 4. Anisotropy decay of C-153 in micelles is bi-exponential in nature. The slow rotational relaxation is due to the lateral diffusion of C-153 in micelles. Lateral diffusion is much faster than rotational motion of micelle as a whole. Rotational motion of micelle as a whole becomes faster with decreasing size of micelles.

* Sonu, Sunita Kumari, Subit K. Saha, *J. Phys. Chem. B.* **2015**, *119*, 9751.

5.1 Results and discussion

5.1.1 UV-Visible absorption and steady-state fluorescence spectra

The absorption and fluorescence spectra of C-153 in the micellar environment of five different gemini surfactants with varying spacer chain length at 10 mM concentration have been represented by Figure 5.1. The chosen concentration (10 mM) of surfactants is well above their respective *cmc* values which have been estimated by conductometric method¹ at 298.15 K (Figure 5.2)

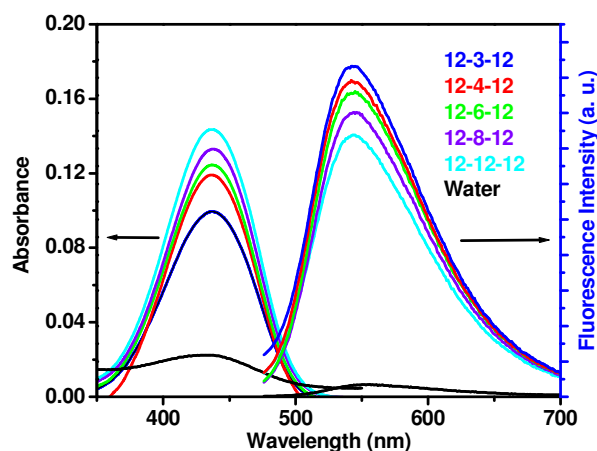


Figure 5.1: Absorption and fluorescence spectra of C-153 in pure water and in aqueous solutions of 12-s-12, 2Br⁻. $\lambda_{\text{ex}} = 375 \text{ nm}$

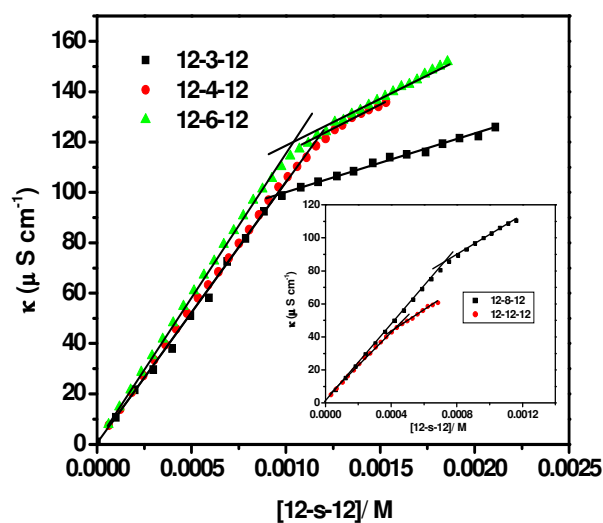


Figure 5.2: Plots of specific conductivity (κ) versus concentration of aqueous solutions of gemini surfactants at 298.15 K

The absorption and fluorescence spectra of C-153 have also been recorded in three pure solvents (cyclohexane, methanol and water, spectra in water is only shown by Figure 5.1 for clarity). The peak maxima of these spectra along with the same in micellar solutions of each of five gemini surfactants at 10 mM concentration are also tabulated in Table 5.1.

Table 5.1: Absorption ($\lambda_{\max}^{\text{abs}}$) and steady-state fluorescence peak maxima ($\lambda_{\max}^{\text{fl}}$) of C-153 in pure solvents and the micelles of gemini surfactants, *cmc* of surfactants and aggregation number of micelles (*N*)

Systems	$\lambda_{\max}^{\text{abs}}$ (nm)	$\lambda_{\max}^{\text{fl}}$ (nm) ^a	<i>cmc</i> ^b (mM)	<i>N</i>
Water	433	552	-	-
Methanol	424	538	-	-
Cyclohexane	394	460	-	-
12-3-12	438	542	0.93 (0.96 ^c)	74 ^f
12-4-12	438	542	1.17 (1.17 ^d)	65
12-6-12	438	542	1.03 (1.09 ^e)	52 ^f
12-8-12	438	542	0.72 (0.83 ^e)	48
12-12-12	438	542	0.41 (0.46 ^c)	40 ^f

^a $\lambda_{\text{ex}} = 375$ nm, ^b*cmc* values are calculated by conductivity method, values in brackets are reported in literature, ^cRef. 2, ^dRef. 3, ^eRef. 4, ^fAggregation numbers are taken from Ref. 2.

The absorption peak maximum of C-153 in pure water is found at 433 nm which is in well corroborated with the literature value⁵, but in the presence of 10 mM of each of five gemini surfactants it is red shifted by 5 nm (438 nm). The red shift of absorption maximum of C-153 in presence of gemini surfactants indicates the destabilization of ground state of C-153.⁶ Results also indicate that C-153 feels different environments in water and in presence of gemini surfactants. Same absorption peak maximum value of C-153 in all micellar media was also observed in case of structurally similar compound, Coumarin-480 (C-480).^{3,7} The possible reason could be structurally constrained nature of C-153.⁸ Like absorption spectra, fluorescence peak maximum of C-153 in 10 mM solution of each of five different gemini surfactants also appears at same wavelength (542 nm). C-153 has a fluorescence peak maximum at 552 nm in pure water which is in good agreement with the literature value.⁵

5.1.2 Micropolarity

The peak maximum of C-153 in pure water is red shifted by 10 nm as compared to micelles of gemini surfactants. This result depicts that C-153 is facing less polar environment in micelles as compared to pure water. Because fluorescence peak maxima of C-153 appear at 460 nm and 538 nm in cyclohexane and methanol, respectively. Comparing fluorescence peak maxima of C-153 in micellar media to that in pure solvents it can be concluded that the polarity of environment around probe in micellar media is close to that of methanol.

Therefore, C-153 molecules reside neither in the core of the micelles ($\lambda_{\max}^{\text{fl}}$ in cyclohexane is 460 nm) nor in the bulk aqueous phase ($\lambda_{\max}^{\text{fl}}$ in water is 552 nm), but at the Stern layer of micelles.^{3,9} Same values of absorption and fluorescence peak maxima in all five gemini micellar media indicate that C-153 molecules are mainly solubilized in the Stern layer and feel more or less same polarity in the micellar phase.¹⁰ This result is in contrast to Zana et al.¹¹ findings on the micropolarity of 12-*s*-12, 2Br⁻ micelles as measured by the pyrene polarity ratio I_1/I_3 which shows that the micropolarity goes through a maximum at *s* around 5. It infers that the location of C-153 is different from that of pyrene. The results of the microenvironment around C-153 in the micelles have been supported by calculating the micropolarity expressed in equivalent scale of $E_T(30)$, an empirical polarity parameter.^{12,13} The fluorescence energies of C-153 at peak maximum, $\epsilon_{\max}^{\text{fl}}$ in different compositions of dioxane-water mixture have been calculated by correcting $\epsilon_{\max}^{\text{fl}}$ for the λ^2 factor. These $\epsilon_{\max}^{\text{fl}}$ values are plotted against $E_T(30)$ (Figure 5.3).

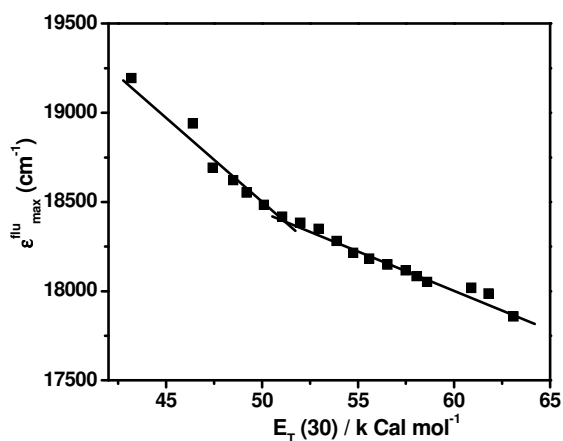


Figure 5.3: Variation of the fluorescence energy at peak maximum of C-153 in dioxane-water mixture with $E_T(30)$ of dioxane-water mixture at 298.15 K

The ϵ_{max}^{fl} value of C-153 in 10 mM solution of each of studied gemini surfactants is found to be same (18248 cm^{-1}) and the value of $E_T(30)$ obtained from Figure 5.3 is $55.1 \text{ kcal mol}^{-1}$. This $E_T(30)$ value is close to that of methanol ($55.4 \text{ kcal mol}^{-1}$). This result further supports that C-153 molecules reside at the Stern layer of micelles of all five different gemini surfactants.^{3,7,9} To further establish the fact that the probe molecules are located at the Stern layer the excited singlet state lifetimes of C-153 have been estimated in micelles of 10 mM concentration of each of five gemini surfactants and in three pure solvents. Decays are mono-exponential in pure solvents and bi-exponential in all micellar media. The fluorescence decay of C-153 at 445 nm in the micelles of 12-3-12, 2Br⁻ along with the best fit and residuals are shown by representative Figure 5.4. All lifetime data along with pre-exponential factors and χ^2 values are tabulated in Table 5.2.

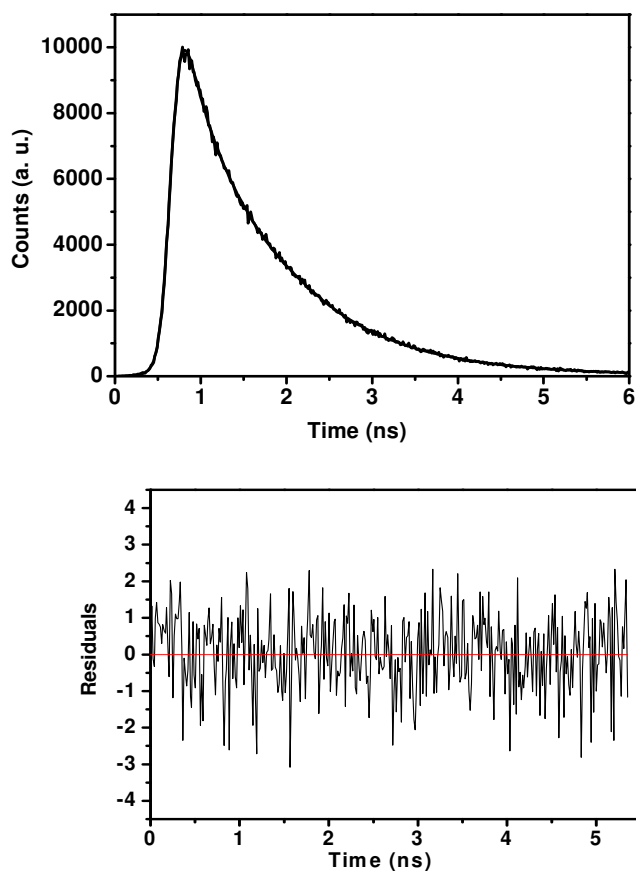


Figure 5.4: Time resolved fluorescence decay of C-153 at 445 nm in 12-3-12 micelles along with the best fit and residuals. [12-3-12] = 10 mM. $\lambda_{ex} = 375 \text{ nm}$

The slow component is the major component in all micellar media. On comparison of lifetime values in micelles to that in pure solvents, it can be seen that the lifetimes of the major components in all micellar media are close to that in methanol. These results are also in accordance with the fact that C-153 molecules are residing at the Stern layer of micelles.

Table 5.2: Excited singlet state lifetime (τ)^a, pre-exponential factors (a), fluorescence quantum yield (ϕ_f), radiative (k_r) and non-radiative (k_{nr}) rate constants of C-153 in various homogeneous and micellar media

System	ϕ_f	a_1^b	τ_1 (ns)	a_2^b	τ_2 (ns)	$\langle\tau\rangle$ (ns)	χ^2	$k_r \times 10^{-8}$ (s ⁻¹)	$k_{nr} \times 10^{-8}$ (s ⁻¹)
Water	0.02	1.00	1.73	-	-	-	1.11	0.12	5.66
Methanol	0.57	1.00	4.03	-	-		1.10	1.41	1.07
cyclohexane	0.81	1.00	4.68	-	-		1.05	1.73	0.41
12-3-12	0.72	0.30	0.32	0.70	3.63	2.64	1.01	2.73	1.06
12-4-12	0.68	0.29	0.39	0.71	3.55	2.63	1.01	2.59	1.21
12-6-12	0.55	0.34	0.38	0.66	3.50	2.44	1.11	2.25	1.85
12-8-12	0.46	0.34	0.43	0.66	3.44	2.42	1.10	1.90	2.23
12-12-12	0.37	0.32	0.39	0.68	3.43	2.46	1.01	1.50	2.57

^a $\lambda_{ex} = 375$ nm, $\lambda_{em} = 475$ nm, ^bAll pre-exponential factors are normalized.

5.1.3 Microviscosity

Above mentioned fluorescence lifetime data have been used to calculate the radiative (k_r) and non-radiative (k_{nr}) rate constants (Equation 1.23, Chapter 1). Rate constants values in pure solvents and in micellar media are tabulated in Table 5.2. It can be seen from the data that k_r decreases whereas k_{nr} increases with increase in spacer chain length of gemini surfactants. This result shows that the free rotational motions of C-153 in the micelles become progressively less restricted with increasing spacer chain length. It indicates that the microviscosity of environment around C-153 decreases with increase in spacer chain length. This result is in agreement with that observed by Zana *et al.*^{11,14} for their study on microviscosity of 12-s-12,2Br⁻ micelles, as determined using fluorescence probe dipyranylpropane. They have observed that microviscosity decreases rather rapidly at $s > 4$.

To further support the fact of change in microviscosity of micelles with increasing spacer chain length, 1,6-diphenyl-1,3,5-hexatriene (DPH) has been used as a viscosity probe molecule. It is to be noted here that we do not get any proper trend while

using C-153 as a probe molecule to determine microviscosity using our earlier method.³ To calculate the absolute values of microviscosities of micelles, η_m using DPH, the Debye-Stokes-Einstein relation has been used (Equation 2.11, Chapter 2). The rotational correlation time, τ_r is obtained from Perrin's equation (Equation 2.12, Chapter 2). The values of r_f , r , τ_r and η_m are presented in Table 5.3. It is evident from the data in Table 5.3 that the microviscosity decreases with increase in spacer chain length. If at all this result does not give the exact values of microviscosities of environment around C-153, but it still fulfils our purpose as we could show the change in microviscosities of 12-s-12, 2Br⁻ micelles with changing the length of spacer chain.

Table 5.3: Fluorescence anisotropy (r)^a, excited singlet state lifetime (τ_f)^b, rotational correlation time (τ_r) of DPH^c, microviscosities (η_m) of micelles, binding constant (K) and standard gibbs free energy of binding (ΔG°) of C-153 at 298.15 K

System	r	τ_f (ns)	χ^2	τ_r (ns)	η_m (mPa s)	$K \times 10^{-5}$ (M ⁻¹)	ΔG° (kJ mol ⁻¹)
12-3-12	0.094	5.38	1.01	1.88	24.7	3.44	-31.59
12-4-12	0.088	5.41	1.10	1.74	22.9	3.22	-31.43
12-6-12	0.075	5.21	1.10	1.36	17.9	2.10	-30.37
12-8-12	0.068	5.50	1.01	1.27	16.7	1.32	-29.22
12-12-12	0.056	5.82	1.02	1.07	14.1	1.06	-28.63

^a Fluorescence anisotropy measured at 430 nm. $\lambda_{ex} = 375$ nm. ^b $\lambda_{ex} = 375$ nm, $\lambda_{em} = 430$ nm. ^c[DPH] = 5 μ M. Solutions of DPH was prepared in tetrahydrofuran

5.1.4 Binding of C-153 with micelles

To get the information about the effect of spacer chain length on the binding interaction of the probe molecule, C-153 with the micelles, the binding constant (K) and the standard Gibbs free energy of binding (ΔG°) have been estimated at 298.15 K. The method given by Almgren *et al.* has been used for the calculation of K (Chapter 2, Equation 2.19). The values of N of 12-3-12, 12-6-12 and 12-12-12 are taken from the literature⁴⁰ while the N values of 12-4-12 and 12-8-12 have been calculated (Chapter 2, Equation 2.25). Figure 5.5 shows the plot of $(I_i - I_o)/(I_c - I_o)$ against $[M]^{-1}$ for C-153 in the presence of 12-3-12, 2Br⁻ as a representative one. Similar plots have also been obtained for other gemini surfactants as well. The K values have been calculated from the slope and are given in Table 5.3. The binding constant value is decreasing with increasing the spacer chain length of gemini surfactants. This result reveals that the binding interaction

of C-153 is decreasing with increasing the spacer chain length of the investigated gemini surfactants. A gemini surfactant with a short spacer chain (12-3-12, 2Br⁻) makes a highly compact environment around the probe molecule than a gemini surfactant with comparatively longer spacer (12-12-12, 2Br⁻) due to higher aggregation number of the former than the latter. There are reports on the decrease in binding constant for the conventional surfactants with decreasing aggregation numbers.^{6,15}

The standard Gibbs free energy of binding (ΔG^o) of the C-153 with gemini surfactants has been calculated using the relation, $\Delta G^o = -RT \ln K$ and values obtained are also compiled in Table 5.3. The values of ΔG^o are negative for all the studied systems. The negative values indicate that the binding of C-153 with the micelles of a gemini surfactant is thermodynamically feasible. The increase in ΔG^o values with increasing the spacer chain length further infers that binding interaction becomes progressively less feasible with increasing spacer chain length.

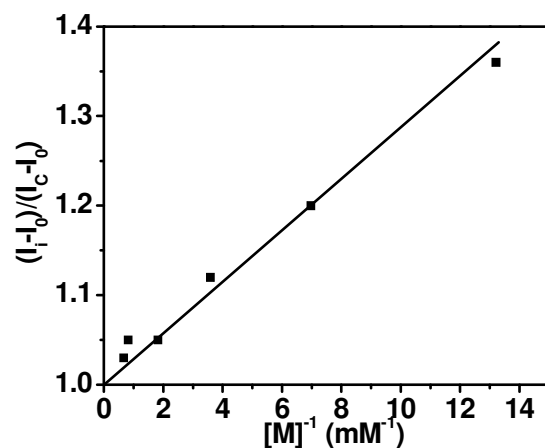


Figure 5.5: Plot of $(I_i - I_o) / (I_C - I_o)$ against $[M]^{-1}$ for 12-3-12 micelles

5.2 Solvation dynamics

To study the solvation dynamics, the fluorescence decays of C-153 in 10 mM solution of each of five gemini surfactants have been monitored at different emission wavelengths. The fluorescence decays of C-153 in presence of gemini surfactants are found to be emission wavelengths-dependent. Figure 5.5 shows the fluorescence decays of C-153 in presence of 12-3-12, 2Br⁻ surfactant at different wavelengths as a representative one. The decay is very fast toward the blue edge of fluorescence spectrum of C-153 (Figure 5.6, 460 nm). At a short wavelength, the decay corresponds to the fluorescence

from the unsolvated dipoles of C-153 created at the excited state without undergoing any relaxation process. Of course, in the present case, the initial fast decay is not completely from the unsolvated dipoles and there are some contributions from the solvated dipoles as well, because there are some limitations of our TCSPC setup. On the other hand, decay becomes slower toward the red edge of fluorescence spectrum of C-153 (Fig. 5.6, 655 nm). At a long wavelength, there is a clear growth in the decay followed by a slow decay with a negative pre-exponential factor. It indicates that the dipoles created at the excited state undergoes a solvent relaxation process followed by fluorescence emission and is therefore delayed by relaxation time.^{16,17} In case of 12-3-12, 2Br⁻ the decay is bi-exponential at 460 nm with two components of 887 ps and 1.765 ns. While at 655 nm, C-153 shows a distinct rise of 960 ps followed by a time constant of 3.779 ns. Similar behaviors of fluorescence decays of C-153 have been observed in presence of other gemini surfactants as well. If probe molecules are mostly present in hydrocarbon core of the micelles, then they should not show any wavelength dependent decay. Dynamics exclusively in the bulk water is too fast to be detected by our instrumental set up (time resolution ~ 165 ps). So, the observed time dependent Stokes shift is mostly due to the probe molecules which are present in the Stern layer of the micelles.¹⁸

The dynamics of solvent is studied by calculating solvent correlation function (SCF), $C(t)$ explained by Fleming and Maroncelli.¹⁹ The peak frequencies $\nu(0)$, $\nu(t)$ and $\nu(\infty)$ at time zero, t , and infinity, respectively have been calculated by constructing time resolved emission spectra (TRES).

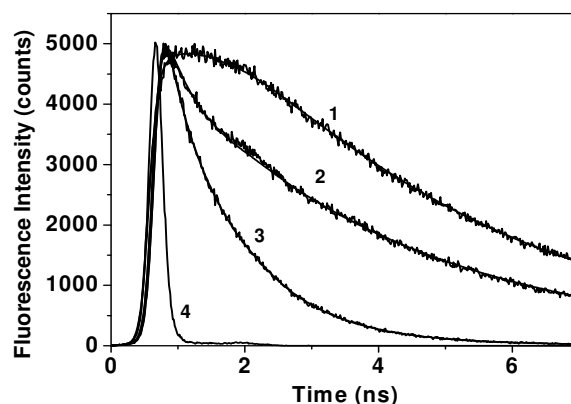


Figure 5.6: Time-resolved fluorescence decays of C-153 in 12-3-12, 2Br⁻ micelles at (1) 655 nm, (2) 520 nm, (3) 460 nm, and (4) for instrument response function

Figure 5.7 represents TRES of C-153 in the micelles of 12-s-12, 2Br⁻ surfactants with $s = 3, 4, 6, 8, 12$. The decays of $C(t)$ versus time for micelles of each of five gemini surfactants are shown in Figure 5.7. The decay parameters of C-153 in various micellar systems are tabulated in Table 5.4.

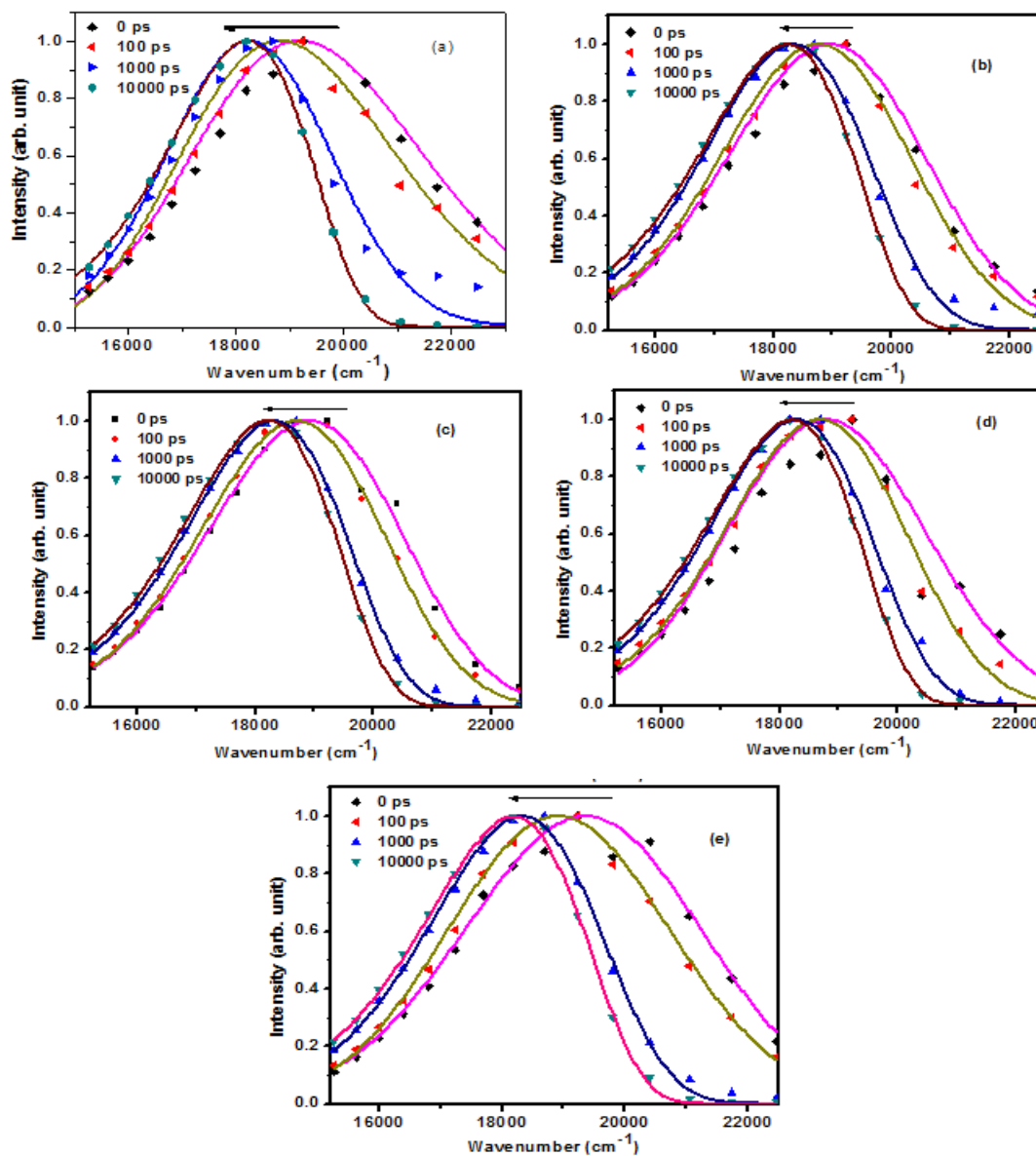


Figure 5.7: Time-resolved emission spectra (TRES) of C-153 in the micelles of (a) 12-3-12, 2Br⁻ (b) 12-4-12, 2Br⁻ (c) 12-6-12, 2Br⁻ (d) 12-8-12, 2Br⁻ (e) 12-12-12, 2Br⁻ surfactants of concentration 10mM

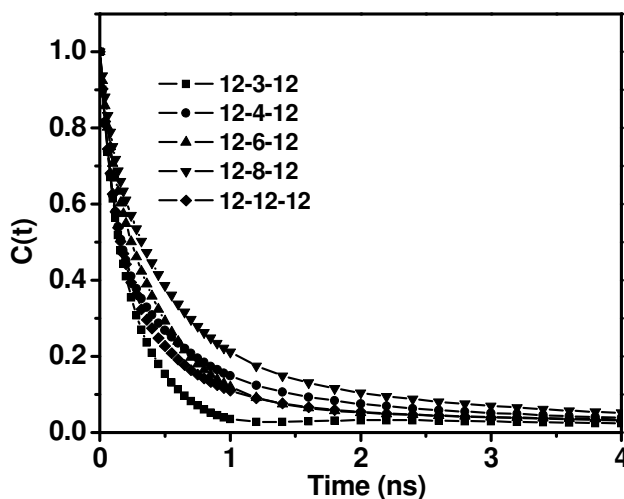


Figure 5.8: Decays of solvent correlation function, $C(t)$ of C-153 in the micelles of gemini surfactants, 12-s-12, 2Br^- of concentration of 10mM

Table 5.4: Decay characteristics of $C(t)$ of C-153 in different micellar systems

System	$\Delta\nu^a$ (cm^{-1})	a_{1s}	τ_{1s} (ps)	a_{2s}	τ_{2s} (ns)	$\langle\tau_s\rangle$ (ps)
12-3-12	976	0.95	217	0.05	4.494	431
12-4-12	842	0.67	146	0.33	1.445	574
12-6-12	846	0.83	319	0.17	2.825	745
12-8-12	720	0.69	305	0.31	1.980	824
12-12-12	1186	0.74	175	0.26	1.507	522

$$^a\Delta\nu = \nu(0) - \nu(\infty)$$

The data in Table 5.4 shows that the solvation dynamics of C-153 has two solvation components, fast and slow i.e the dynamics is bimodal in nature. It has been reported in the literature that these fast and slow solvation components are because of “free” and “bound” water molecules, respectively those are at dynamic equilibrium with each other.²⁰ As far as present micellar systems are concerned, many factors such as water molecules, headgroups, spacer groups and counterions could be responsible for solvation of dipoles created at the excited state. However, polar headgroups attached to long hydrocarbon chain as well as spacer group of surfactant contributes to a very slow solvation process of nanosecond time scale (~ 100 ns).^{1,21} Hydrophobic spacer group of surfactant is expected not to be taken part in solvation. Therefore, water molecules and counterions are mostly responsible for solvation dynamics. Since the hydrogen bond

strength between two water molecules is much weaker than the bond strength between water molecules and polar headgroups of surfactant molecules^{9,22,23}, two kinds of water molecules take part in solvation process. While water molecules bonded with polar headgroups of surfactant molecules are responsible for slow component, the other type of water molecules contributes to fast solvation dynamics. In the present case, the fast component is the major component and the time scale is 146-319 ps which is slightly at lower side as compared to micelles of conventional surfactants.⁹ The present time scale is almost 3 orders of magnitude slower than that in bulk water (310 fs) reported by Vajda et al.²⁴ with C-480 as a probe molecule.

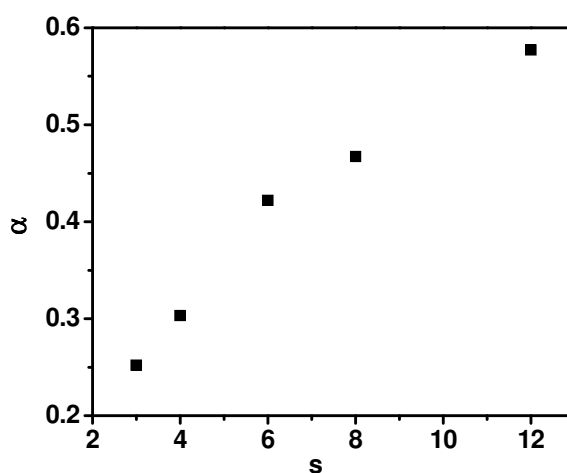


Figure 5.9: Degree of counter ion dissociation (α) versus spacer chain, s of 12- s -12, 2Br^-

While there is no clear trend in solvation time for fast and slow components, an increase in average solvation time, $\langle\tau_s\rangle$ with increasing spacer chain length of surfactant molecules from $s = 3$ to $s = 8$ in 12- s -12, 2Br^- surfactants has been observed. Like Zana *et al.*⁴, we have also noticed that degree of counterion dissociation, α increases with increasing spacer chain length (Figure 5.9). Counterions affect the solvation process by interacting with water molecules through hydrogen bonding. Possibly with increasing degree of dissociation of counterions, more and more water molecules get involved in solvation of counterions itself. It results in decrease in ‘free’ water molecules to be available for solvation of C-153 in the Stern layer of micelles. That is why solvation dynamics becomes slower with increasing degree of counterion dissociation. Of course the effect of hydrophobic spacer chain cannot be ruled out. Increase in hydrophobicity of spacer with increasing its chain length reduces the availability of water molecules for

solvation. As a result of that solvation time increases. The decrease in availability of water molecules for solvation process is also supported by the results of hydration of micelles of 12-*s*-12, 2Br⁻ surfactants reported by Borse *et al.*²⁵ They have found that the volume of water molecules per gram of surfactant molecules in micellar phase decreases with increasing spacer chain length.²⁵ It is the reason that in case of 12-3-12, 2Br⁻ surfactant, the fast component is the only component contributes to solvation dynamics. For other geminis from *s* = 4 to *s* = 8, there is an increasing tendency of solvation time of fast component with decreasing tendency of relative amplitudes. Consequently there is an increasing tendency of relative amplitudes of slow component. It is noteworthy that microviscosity of environment around probe is not responsible to slow down the solvation dynamics for gemini surfactants, 12-*s*-12, 2Br⁻ with *s* = 3 to *s* = 8. This conclusion is based on our observation that microviscosity decreases with increasing spacer chain length (Table 5.3). Had the change in microviscosity been a reason for changing solvation time, there would have been decrease in solvation time with increasing spacer chain length. It could be that only in case of 12-12-12, the viscosity effect predominates over the effect of counterions. It is to be noted that microviscosity is lowest in case of 12-12-12, 2Br⁻ surfactant amongst five studied gemini surfactants (Table 5.3). Low values of solvation times for both fast and slow components have been obtained. As a result of that a low average solvation time, $\langle \tau_s \rangle$ has been obtained for 12-12-12, 2Br⁻ as compared to 12-8-12, 2Br⁻.

It has been reported for the present series of gemini surfactants, 12-*s*-12, 2Br⁻ that in aqueous solution two covalently linked positively charged headgroups try to maintain a critical distance between the headgroups to reduce the Coulombic force of repulsion.²⁵ The equilibrium distance between the charged headgroups of gemini surfactants increases with spacer chain length.²⁵ It is expected that with increasing the average equilibrium distance between the charged headgroups within micelles the hydration of headgroups would be lowered. Consequently the amount of water molecules responsible for slow solvation component should be reduced. It could be the reason that there is a tendency of lowering of slow solvation time with increasing spacer chain length (Table 5.4).

It is noteworthy that at spacer *s* ≤ 5-6 methylene units, there is a conformational change in the surfactant molecule of type *m-s-m* and spacer remains mainly in extended

conformation.²⁶ As a result of that *cmc* increases with *s* for $s \leq 5-6$ (Table 5.1).² However, for $s > 5-6$, the spacer chain tries to form a loop extended towards the hydrophobic core of micelles. Because of it a decrease in *cmc* is observed for $s > 5-6$ (Table 5.1).²⁶ All these factors could be the reasons for not having any proper trend for solvation times for fast and slow components. Because of conformational change at $s \leq 5-6$, there could be some difference in morphology of micelles of 12-4-12, 2Br⁻ surfactant as compared to other surfactants. This could be the reason that there are some deviations in solvation parameters from the trend observed in case of 12-3-12, 12-6-12 and 12-8-12.

5.3 Rotational relaxation or time-resolved fluorescence anisotropy

The time resolved fluorescence anisotropy decays of C-153 in different gemini surfactants are shown by Figure 5.10. All the decays are found to be bi-exponential in nature in micellar media and single exponential in water. The rotational relaxation time (Table 5.5) for C-153 in pure water is found to be 148 ps which is higher than the reported value (100 ps) due to high resolution time of our instrument.¹⁸ The τ_r values of C-153 in studied micelles of gemini surfactants are many fold longer than that in the pure water. It indicates that the random motion of the probe molecule is restricted in the micellar environment. Data in Table 5.5 show that the average rotational relaxation time decreases with increasing the spacer chain length of the gemini surfactants. The aggregation number of micelles at 10 mM concentration of each of gemini surfactant is found to be decreased (Table 5.1) with spacer chain length.

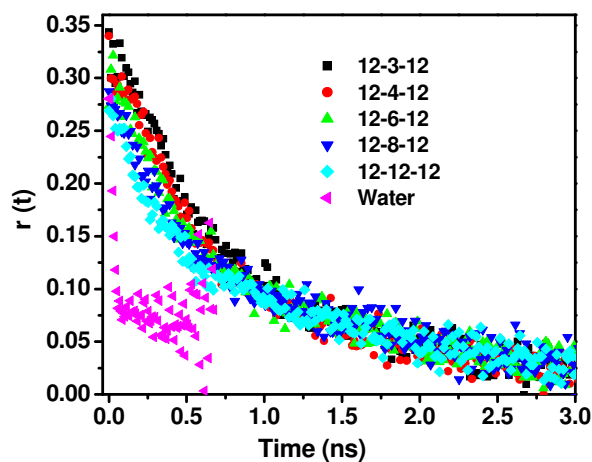


Figure 5.10: Fluorescence anisotropy decays of C-153 in pure water and in micelles of 12-s-12, 2Br⁻ surfactants

The hydrodynamic diameters of 12-*s*-12, 2Br⁻ gemini surfactants with *s* = 3, 4, 6, 8, 12 are found to be 1.24 ± 0.03 , 1.23 ± 0.03 , 1.01 ± 0.03 , 1.00 ± 0.03 and 0.86 ± 0.03 nm, respectively (Figure 5.11 represents hydrodynamic distributions). To the best of our knowledge there is no report on hydrodynamic diameter of micelles of this series of gemini surfactants. However, there is a report on hydrodynamic distributions of gemini surfactant, 14-4-14, 2Br⁻ of 10 mM concentration studied by Wang *et al.*²⁷ They have noticed two hydrodynamic distributions for this gemini surfactant; one centered at 0.82 nm and the other centered at 70 nm. According to them, the former one is for micelles and the latter one is for vesicles. It is to be noted that we did not find any distribution which corresponds to vesicle for the present gemini surfactants. The fact that the values of hydrodynamic diameters of present gemini micelles corroborating well with the reported hydrodynamic diameter of similar cationic gemini surfactant, 14-4-14,2Br⁻ except their tail length supports the authenticity of hydrodynamic diameter values estimated by us. The DLS results depict that with increasing spacer chain length micelles become progressive less compact. As a result of that microviscosity of environment around probe molecules decreases which is supported by the above mentioned microviscosity values given in Table 5.3. The data in Table 5.3 also show that the binding constant of C-153 decreases with increasing spacer chain length. All these results are in support of the fact that C-153 molecules feel less compact and less viscous environment with spacer chain length and as a result of that average rotational relaxation time, $\langle \tau_r \rangle$ decreases.

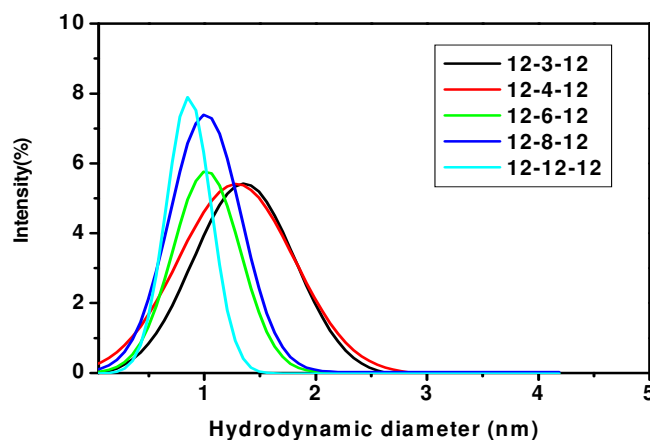


Figure 5.11: The size distribution graph for the micelles of gemini surfactants obtained from DLS measurement

The trend in microviscosity (Table 5.3) and $\langle\tau_r\rangle$ has very close correlation. There are significant decreases in microviscosity and $\langle\tau_r\rangle$ for $s > 4$. Zana *et al.*²⁶ have also reported the rapid decrease in microviscosity of 12-*s*-12, 2Br⁻ at $s > 4$. Maroncelli and co-worker²⁸ have noticed that the rotational relaxation times correlate well with viscosity. The decrease in the rotational relaxation time of the probe molecule with decreasing the aggregation number of micelles has been reported in the literature.^{6,15}

Table 5.5: Rotational relaxation parameters for C-153 in micelles of 12-*s*-12, 2Br⁻ gemini surfactants

System	r_0	a_{1r}	τ_{1r} (ps)	a_{2r}	τ_{2r} (ps)	$\langle\tau_r\rangle$ (ps)	χ^2
Water	0.26	1.00 ± 0.02	148 ± 47	-	-	148	1.05
12-3-12	0.35	0.81 ± 0.02	659 ± 72	0.19 ± 0.01	5735 ± 455	1623	1.05
12-4-12	0.34	0.78 ± 0.02	582 ± 63	0.22 ± 0.02	5218 ± 426	1601	1.07
12-6-12	0.32	0.54 ± 0.02	409 ± 60	0.46 ± 0.01	2307 ± 165	1282	1.08
12-8-12	0.29	0.50 ± 0.02	349 ± 68	0.50 ± 0.01	2189 ± 146	1269	1.07
12-12-12	0.28	0.49 ± 0.02	283 ± 44	0.51 ± 0.02	2137 ± 140	1228	0.99

Table 5.6: Hydrodynamic radius, wobbling motion time (τ_w), lateral diffusion time (τ_D), time for overall rotational motion of the micelle (τ_m), lateral diffusion coefficient (D_L), wobbling diffusion coefficient (D_w), cone angle (θ_o) and order parameter ($|S|$) obtained from the anisotropy decays of C-153 in different 12-*s*-12, 2Br⁻ micelles

System	Hydrodynamic radius (nm)	τ_w (ps)	τ_m (ns)	τ_D (ps)	$D_L \times 10^7$ (cm ² s ⁻¹)	$D_w \times 10^{-8}$ (s ⁻¹)	θ_o (deg)	$ S $
12-3-12	0.620	745 ± 72	216 ± 0.455	5890 ± 455	1.63	3.70	55.7	0.44
12-4-12	0.615	655 ± 63	218 ± 0.426	5350 ± 426	1.77	3.93	53.8	0.47
12-6-12	0.505	497 ± 60	116 ± 0.165	2350 ± 165	2.71	2.82	39.7	0.68
12-8-12	0.500	415 ± 68	114 ± 0.146	2230 ± 146	2.80	3.03	37.6	0.71
12-12-12	0.430	326 ± 44	073 ± 0.140	2200 ± 140	2.10	3.85	37.6	0.71

The fluorescence anisotropy decays of C-153 in all micellar media are bi-exponential in nature. A bi-exponential anisotropy decay is because of various kinds of rotational motions, but not due to different locations of the probe.²⁹ The model often used to describe the bi-exponential behavior of an anisotropy decay as a result of various kinds of rotational motions is the two-step and wobbling-in-a-cone model (Section 2.2.12.1 and 2.2.12.2, Chapter 2). According to two-step model, the slow rotational relaxation time (τ_{2r}) is related to the relaxation time corresponding to the lateral diffusion of the fluorophore (τ_D) and relaxation time corresponding to the rotational motion of the

micelle as a whole (τ_m) (Equation 2.35, Chapter 2). The values of τ_m at 298.15 K calculated using estimated hydrodynamic radii mentioned above ((Equation 2.36, Chapter 2) are presented in Table 5.6. It can be seen from the data given in Tables 5.5 and 5.6 that the τ_{2r} value in a given micellar system is very close to the τ_D value and very different from τ_m value in the same micelles. It infers that the slow rotational relaxation in a micellar medium is mainly due to the lateral diffusion of the fluorophore. The main motion which causes the anisotropy to decay to zero in these micellar systems is lateral diffusion. Lateral diffusion of the fluorophore in micelles is a much faster process than rotational motion of the micelle as a whole. τ_m values are found to be 30 to 50 times longer than τ_D . Data also show that lateral diffusion time decreases rather rapidly at $s > 4$. Lateral diffusion process becomes progressively faster with spacer chain length i.e. with decreasing microviscosity of environment around fluorophore. It is supported by increasing tendency of the values of lateral diffusion coefficient (D_L) with spacer chain length (Table 5.6) calculated using equation 2.42 (Chapter 2).³⁰ It is pertinent to note that like $\langle\tau_r\rangle$ values, τ_D values also have very good correlation with microviscosities. As expected, rotational motion of the micelles as a whole is found to be faster with progressive decrease in the size of micelles. The fast component of rotational relaxation is modeled as restricted rotational diffusion. Effective relaxation time (τ_w) corresponding to the restricted rotational diffusion is related to the fast relaxation time, τ_{fr} and slow relaxation time, (Equation 2.40, Chapter 2). The relaxation of the local structure of the micelles decreases with spacer chain length. We have discussed that the microviscosity of micelles decreases with spacer chain length. Thus, the relaxation of local structure becomes faster with decreasing microviscosity of micelles. Using wobbling-in-a-cone model the values of order parameter ($|S|$), cone angle (θ_0), and wobbling diffusion coefficient (D_w), have been calculated (Equations 2.37, 2.39 and 2.41 respectively, Chapter 2) and listed in Table 5.6. The order parameter, $|S|$ is a measure of spatial restriction. In the present study the value of $|S|$ ranges from 0.44 to 0.71. The high values of $|S|$ support that the probe molecules are located at the Stern layer and experiencing restricted motions. However, the values of $|S|$ and θ_0 are not correlating well with the microviscosity of micelles. It has been observed that for 12-3-12, and 12-4-12 micelles, θ_0 values are higher and $|S|$ values are lower as compared to micelles of other three surfactants. To overcome this discrepancy, another model i.e. spinning-in-equatorial band model^{30, 31} (Equation 2.39, Chapter 2) has been used for which $|S|$

should not exceed 0.5 which is the case for 12-3-12 and 12-4-12 micelles (Table 5.6). According to this model the alignment of rod-like probe molecule is different from that in wobbling-in-a-cone model. The probe molecule should be aligned in such a way so that emission moment is perpendicular to the long axis and $|S|$ is related to θ_0 (Equation 2.39, Chapter 2). The θ_0 values are found to be 69.7° and 75.8° for 12-3-12 and 12-4-12 micelles, respectively those are different from that calculated using wobbling-in-a-cone model. While the values of wobbling diffusion coefficient, D_w are in reasonably good correlation with the microviscosities of micelles of 12-6-12, 12-8-12 and 12-12-12, it is not the case for 12-3-12 and 12-4-12 micelles. This could also be because of the fact that probe molecules are oriented differently in the micelles of 12-3-12 and 12-4-12 as compared to other three micelles. More compact micelles of 12-3-12 and 12-4-12 could be the reason that probe molecules are oriented differently in these micelles as compared to micelles of other three surfactants.

5.4 Conclusions

C-153 molecules reside at the Stern layer of 12-*s*-12, 2Br⁻ micelles and feel more or less same polarity. The micropolarity of environment around C-153 in micelles expressed in equivalent scale of $E_T(30)$ is 55.1 kcal mol⁻¹ which is close to that of methanol. The microviscosity of micelles decreases with increase in spacer chain length of gemini surfactants, 12-*s*-12, 2Br⁻. Binding interactions of C-153 decrease with increasing spacer chain length of surfactants. The negative values of ΔG^o indicate that the binding of C-153 with the micelles of gemini surfactants is thermodynamically feasible. Solvation dynamics in the Stern layer of gemini micelles is bimodal in nature. Water molecules and counter ions are mostly responsible for solvation dynamics. Water molecules bonded with the polar headgroups of surfactant molecules are responsible for slow component. Other water molecules contribute to fast component. Fast component is the major component and the time scale of solvation is ~ 3 orders of magnitude slower than that in bulk water. Counter ions are indirectly responsible for slow component. Average solvation time increases because of increased degree of counter ion dissociation for gemini, 12-*s*-12, 2Br⁻ with *s* = 3 to 8. A portion of water molecules get involved in solvation of counter ions itself. As a result of it there is a decrease in 'free' water molecules to be available for solvation of C-153. Hydrophobic spacer chain also has an effect on increasing solvation time with increasing chain length. The availability of water

molecules for solvation is reduced with increasing hydrophobicity of spacer as a result of increase in its chain length. In case of micelles of 12-12-12, 2Br⁻ surfactant, however, low solvation time is because of the fact that viscosity effect predominates over the effect of counterions. The change in conformation of surfactant at $s \leq 5-6$ and the formation of loop of spacer extended towards the hydrophobic core of micelles have some effect on solvation dynamics. The random motion of C-153 is restricted in the micellar environment. Average rotational relaxation time for C-153 decreases with increasing spacer chain length as the micelles become progressively less compact and less viscous. There is a very good correlation between average rotational relaxation time and microviscosity of micelles with rapid decrease in these two parameters at $s > 4$. Anisotropy decays of C-153 are bi-exponential in nature because of various kinds of rotational motions. The slow relaxation in micellar media is due to the lateral diffusion of the fluorophores. Lateral diffusion of the fluorophore in the micelles is much faster than the rotational motion of the micelle as a whole. The lateral diffusion process also correlates well with the microviscosity of micelles. Rotational motion of micelle as a whole becomes faster with decreasing size of micelles. Effective relaxation time decreases with spacer chain length. The relaxation of local structure becomes faster with decreasing microviscosity of micelles. The probe molecules seem to be oriented differently in the micelles of 12-3-12 and 12-4-12 as compared to micelles of other three surfactants. This could be because of very compact nature of micelles of former two surfactants.

References:

- (1) A. K. Tiwari, Sonu, M. Sowmiya, S. K. Saha. *J. Mol. Liq.* **2012**, 167, 18.
- (2) X. Wang, J. Wang, Y. Wang, J. Ye, H. Yan, R. K. Thomas. *J. Colloid Interface Sci.* **2005**, 286, 739.
- (3) A. K. Tiwari, Sonu, S. K. Saha. *J. Phys. Chem. B.* **2014**, 118, 3582.
- (4) R. Zana, M. Benraou, R. Rueff. *Langmuir*, **1991**, 7, 1072.
- (5) R. Pramanik, S. Sarkar, C. Ghatak, V. G. Rao, S. Mandal, N. Sarkar. *J. Phys. Chem. B.* **2011**, 115, 6957.
- (6) A. Mahata, D. Sarkar, D. Bose, D. Ghosh, P. Das, N. Chattopadhyay. *J. Colloid Interface Sci.* **2009**, 335, 234.

- (7) D. Chakrabarty, A. Chakraborty, D. Seth, P. Hazra, N. Sarkar. *J. Chem. Phys.* **2005**, *122*, 184516.
- (8) R. W. Yip, Y. X. Wen, A. G. Szabo. *J. Phys. Chem.* **1993**, *97*, 10458.
- (9) N. Sarkar, A. Datta, S. Das, K. Bhattacharyya. *J. Phys. Chem.* **1996**, *100*, 15483.
- (10) M. Kumbhakar, T. Goel, T. Mukherjee, H. Pal. *J. Phys. Chem. B.* **2005**, *109*, 18528.
- (11) R. Zana, M. In, H. L. Duportail. *Langmuir* **1997**, *13*, 5552.
- (12) C. Reichardt, H. Ratajazak, W. J. O. Thomas. *Molecular Interaction*; Wiley: New York, **1982**.
- (13) E. M. Kosower, H. Dodiuk, K. Tanizawa, M. Ottolenghi, N. Orbach. *J. Am. Chem. Soc.* **1975**, *97*, 2167.
- (14) M. In, V. Bec, O. Aguerre-Chariol, R. Zana. *Langmuir* **2000**, *16*, 141.
- (15) B. K. Paul, D. Ray, N. Guchhait. *J. Phys. Chem. B.* **2012**, *116*, 9704.
- (16) K. Bhattacharyya. *Chem. Commun.* **2008**, 2848.
- (17) S. Muthusubramanian, A. K. Tiwari, Sonu, S. K. Saha. *Soft Matter* **2012**, *8*, 11072.
- (18) V. G. Rao, C. Banerjee, S. Mandal, S. Ghosh, N. Sarkar. *Spectrochimica Acta Part A.* **2012**, *120*, 371.
- (19) M. Maroncelli, G. R. Fleming. *J. Chem. Phys.* **1987**, *86*, 6221.
- (20) N. Nandi, B. Bagchi. *J. Phys. Chem. B* **1997**, *101*, 10954.
- (21) R. Dutta, M. Chowdhary, M. A. Winnik. *Polymer* **1995**, *36*, 4445.
- (22) S. Balasubramanian, B. Bagchi. *J. Phys. Chem B* **2001**, *105*, 12529.
- (23) S. Balasubramanian, S. Pal, B. Bagchi. *Phys. Rev. Lett.* **2002**, *89*, 115505.
- (24) S. Vajda, R. Jimenez, S. Rosenthal, V. Fidler, G. R. Fleming, E. W. J. Castner. *J. Chem. Soc. Faraday Trans.* **1995**, *91*, 867.
- (25) M. Borse, V. Sharma, V. K. Aswal, P. S. Goyal, S. Devi. *J. Colloid Interface Sci.* **2005**, *284*, 282.
- (26) R. Zana. *J. Colloid Interface Sci.* **2002**, *248*, 203.
- (27) C. Hu, R. Li, H. Yang, J. Wang. *J. Colloid Interface Sci.* **2011**, *356*, 605.
- (28) M. Kumbhakar, T. Goel, T. Mukherjee, H. Pal. *J. Phys. Chem. B* **2004**, *108*, 19246.
- (29) J. Kinoshita, S. Kawato, A. Ikegami. *J. Biophys.* **1977**, *20*, 289.
- (30) E. L. Quitevis, A. H. Marcus, M. D. Fayer. *J. Phys. Chem.* **1993**, *97*, 5762.
- (31) L. B. A. Johansson, A. Niemi. *J. Phys. Chem.* **1987**, *91*, 3020.

Chapter 6

Solvation dynamics and rotational relaxation of Coumarin 153 in mixed micelles of Triton X-100 and cationic gemini surfactants: Effect of composition and spacer chain length of gemini surfactant*

The present work demonstrates the solvation dynamics and rotational relaxation of Coumarin 153 (C-153), (Scheme 2.1) in mixed micelles of non-ionic surfactant, Triton X-100 and a series of cationic gemini surfactants, 12-*s*-12, 2Br⁻ with varying polymethylene spacer chain length (*s* = 3, 6, 8, 12), (Scheme 2.2) at different bulk mole fractions of a surfactant. Studies have been carried out by means of UV-Vis absorption, steady-state fluorescence and fluorescence anisotropy, time-resolved fluorescence and fluorescence anisotropy, and dynamic light scattering measurements. While micropolarity of environment around C-153 in mixed micelles increases, microviscosity decreases with increasing amount of a gemini surfactant. It is because the thickness of the Stern layer of micelles increases as a result of greater extent of penetration of water molecules. Solvation dynamics and rotational relaxation of C-153 become faster with increasing mole fraction of a gemini surfactant in the mixed micelles. Increasing thickness of Stern layer leads to increase in the number of water molecules hydrogen bonded among themselves resulting in increase in polarity and microfluidity of environment. At a given bulk mole fraction of a surfactant, microviscosity of micelles decreases with increasing spacer chain length of gemini surfactant resulting in an increase in the rate of rotational relaxation process. However, at a given bulk mole fraction of a surfactant, solvation dynamics becomes slower with increasing spacer chain length from *s* = 3 to 8 because of increasing degree of counter ion dissociation. Slow rotational relaxation process is mainly due to the lateral diffusion of C-153 along the surface of micelles. Rotational motion of micelle as a whole is much slower than lateral diffusion of C-153.

* Sonu, Sunita Kumari, Subit K. Saha, *Phys. Chem. Chem. Phys.* **2016**, *18*, 1551.

6.1 Results and discussion

6.1.1 UV-visible absorption and steady-state fluorescence spectra

The UV-visible absorption and steady-state fluorescence spectra of C-153 have been recorded in mixed systems of TX-100 and a gemini surfactant with bulk mole fraction of a surfactant, $X = 0.2$ to 0.8 at a total concentration of surfactant of 10 mM. Figure 6.1 and Figure 6.2 show such absorption and fluorescence spectra, respectively for TX-100+12-6-12 mixed system as representative spectra.

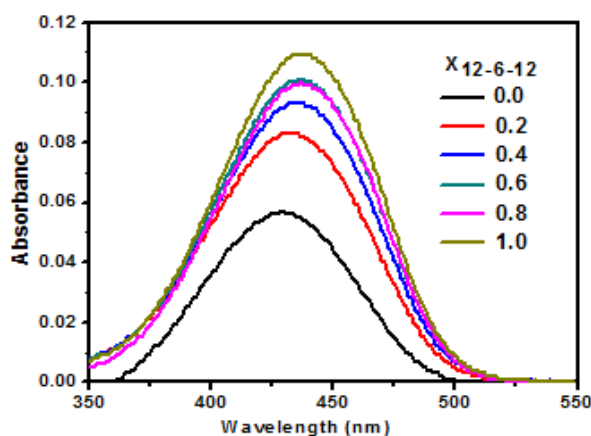


Figure 6.1: Absorption spectra of C-153 in presence of pure and mixed surfactant systems of TX-100 and 12-6-12

The absorption and fluorescence peak maxima of C-153 in solutions of varying mole fractions of a surfactant are given in Table 6.1a and 6.1b for each of mixed system of TX-100 plus gemini surfactant, 12- s -12 with $s = 3, 6, 8, 12$. The absorption peak maximum and especially fluorescence peak maximum of C-153 are progressively red-shifted with increasing bulk mole fraction of a gemini surfactant. It indicates that the microenvironment of C-153 in mixed micelles changes with increasing mole fraction of a gemini surfactant. The progressive red-shift in absorption and fluorescence peak maximum with increasing bulk mole fraction of a gemini surfactant infers that the probe molecules are getting located at more and more polar environment. With increasing composition of gemini surfactant, the observed increase in absorbance could be because of greater extent of interaction of C-153 with the micelles of gemini than that of TX-100 surfactant. The decrease in fluorescence intensity is due to the progressive increase in the rate of non-radiative processes as a result of greater extent of stabilization of emitting states.¹⁻⁴ All these studies have been carried out at a total concentration of 10 mM of surfactants. This concentration which is much above their cmc is chosen to ensure the

complete solubilization of the probe molecule, C-153 in the micelles. The excitation wavelength-independent fluorescence peak maxima is in support to this fact.

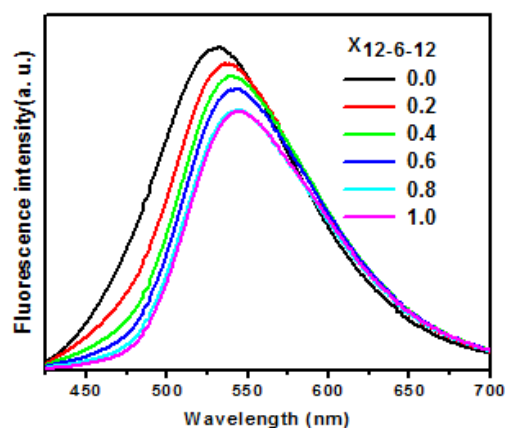


Figure 6.2: Fluorescence spectra of C-153 in presence of pure and mixed surfactant systems of TX-100 and 12-6-12. $\lambda_{ex} = 375$ nm

Cmc values of pure and mixed surfactant systems at various bulk mole fractions of a surfactant have been calculated from the plot of variation of fluorescence intensity of C-153 with increasing concentration of surfactant (Figure 6.3). Inset of Figure 6.3 represents such a plot. Calculated cmc values are tabulated in Table 6.1(a) and Table 6.2(b) along with the reported values wherever available in the literature.⁵ Cmc value increases with increasing bulk mole fraction of a gemini surfactant in the mixed micelles. Similar results were also observed by Wang *et al.*⁵ Difference in cmc values noted could be because of two different methods used for cmc measurements.

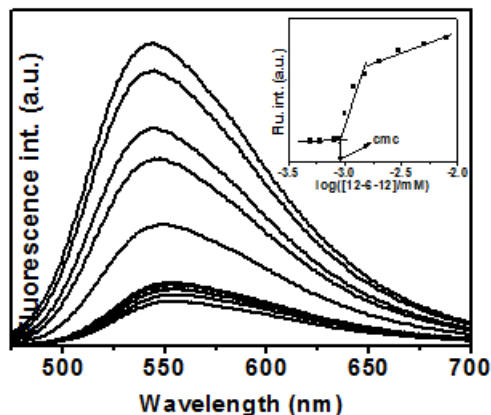


Figure 6.3: Fluorescence spectra of C-153 with increasing concentration (from bottom to top) of 12-6-12. Inset shows the plot of fluorescence intensity with concentration of 12-6-12, ($\lambda_{exc} = 375$ nm)

Table 6.1(a): UV-visible absorption peak maxima (λ_{\max}^{ab}) and fluorescence peak maxima^a (λ_{\max}^{fl}) of C-153 in mixed systems, TX-100+12-s-12 (s = 3 and 6), cmc and $E_T(30)$ values of pure and mixed systems, TX-100+12-s-12 (s = 3 and 6)

$X_{12-3-12}$	cmc (mM)	λ_{\max}^{ab} (nm)	λ_{\max}^{fl} (nm)	$E_T(30)$ (kcal mol ⁻¹)	$X_{12-6-12}$	cmc (mM)	λ_{\max}^{ab} (nm)	λ_{\max}^{fl} (nm)	$E_T(30)$ (kcal mol ⁻¹)
0.0	0.41(0.33)	429	530	47.9	0.0	0.41(0.33)	429	530	47.9
0.2	0.43(0.35)	432	535	50.9	0.2	0.42(0.35)	432	538	51.9
0.4	0.44(0.36)	434	538	51.9	0.4	0.45(0.37)	434	540	53.1
0.6	0.49(0.38)	437	539	52.9	0.6	0.47(0.38)	437	541	53.9
0.8	0.51(0.42)	437	541	53.9	0.8	0.55(0.45)	437	542	55.1
1.0	1.12(0.96)	437	542	55.1	1.0	1.48(1.09)	437	542	55.1
Water	-	433	552	63.1	Water	-	433	552	63.1

^a $\lambda_{ex} = 375$ nm. Cmc values in parenthesis are taken from the ref 5

Table 6.1(b): UV-visible absorption peak maxima (λ_{\max}^{ab}) and fluorescence peak maxima^a (λ_{\max}^{fl}) of C-153 in mixed systems, TX-100+12-s-12 (s = 8 and 12), cmc and $E_T(30)$ values of mixed systems, TX-100+12-s-12 (s = 8 and 12)

$X_{12-8-12}$	cmc (mM)	λ_{\max}^{ab} (nm)	λ_{\max}^{fl} (nm)	$E_T(30)$ (kcal mol ⁻¹)	$X_{12-12-12}$	cmc (mM)	λ_{\max}^{ab} (nm)	λ_{\max}^{fl} (nm)	$E_T(30)$ (kcal mol ⁻¹)
0.0	0.41	429	530	47.9	0.0	0.41(0.33)	429	530	47.9
0.2	0.42	432	538	51.9	0.2	0.41(0.34)	432	538	51.9
0.4	0.42	435	540	53.1	0.4	0.43(0.36)	435	540	53.1
0.6	0.43	438	541	53.9	0.6	0.45(0.38)	438	541	53.9
0.8	0.45	438	542	55.1	0.8	0.50(0.40)	438	542	55.1
1.0	0.81	438	542	55.1	1.0	0.63(0.46)	438	542	55.1
Water	-	433	552	63.1	Water	-	433	552	63.1

^a $\lambda_{ex} = 375$ nm. Cmc values in parenthesis are taken from the ref 5

6.1.2 Micropolarity

Figure 6.4 shows the plot of fluorescence energy of C-153 at peak maxima ($\epsilon_{\max}^{\text{flu}}$) versus $E_T(30)$ values of different percentage of dioxane-water mixture. It is to be noted that $\epsilon_{\max}^{\text{flu}}$ have been corrected for the λ^2 factor. The values of $\epsilon_{\max}^{\text{flu}}$ of C-153 in 10 mM of total concentration of surfactant at various mole fractions have been calculated and $E_T(30)$ values have been estimated from Figure 6.4. All $E_T(30)$ values are also tabulated in Table 6.1a and Table 6.1b. Data in these tables show that the micropolarity around the probe molecules inside the micelles is less than that in pure water.⁶ The $E_T(30)$ values of the present micellar systems are higher than that of *n*-hexane (32.2 kcal mol⁻¹) and lesser than that of pure water (63.1 kcal mol⁻¹). It indicates that the probe molecule, C-153 neither resides at the core of the micelles nor in the bulk water, but at the Stern layer of micelles.^{5,7,8} It is also noteworthy that the micropolarity increases with increasing bulk mole fraction of a gemini surfactant which is well corroborated with the results reported by Wang *et al.*⁵ using electron spin resonance (ESR) technique. This observation shows that C-153 feels more polar environment in the mixed micelles of TX-100 and gemini surfactants as compared to the micelles of pure TX-100.

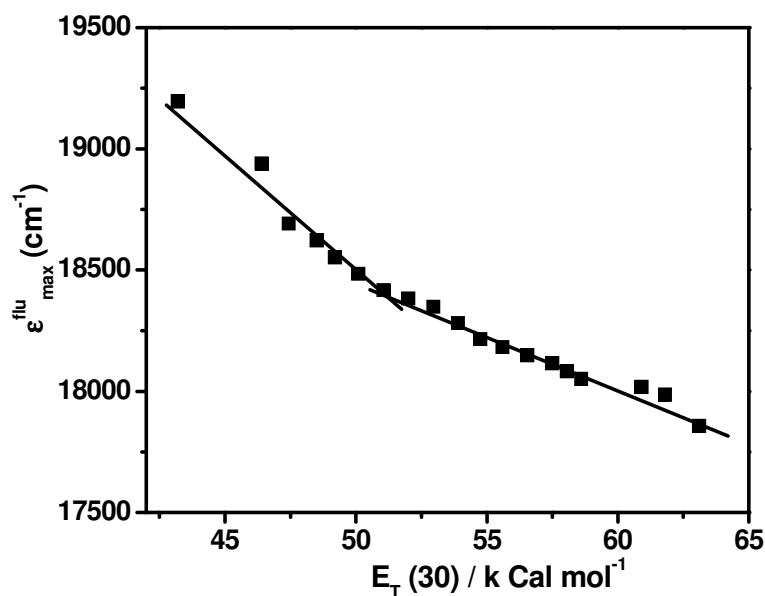


Figure 6.4: Plot of fluorescence energy at peak maxima ($\epsilon_{\max}^{\text{flu}}$) of C-153 versus $E_T(30)$ of different percentage of dioxane-water mixture $\lambda_{\text{ex}} = 375 \text{ nm}$

6.1.3 Microviscosity

Fluorescence anisotropy value reflects the microviscosity of the microenvironment around the probe molecule. Higher the microviscosity around the probe molecule greater will be the fluorescence anisotropy.^{6,8-10} 1,6-diphenyl-1,3,5-hexatriene (DPH) has been used as a probe molecule to estimate the microviscosity (η_m) for pure and mixed surfactant systems at 298.15 K using Equations 2.11 and 2.12 (Section 2.2.6, Chapter 2).

It is noteworthy that the proper trend was not observed when we used C-153 as a probe molecule to determine the microviscosity using our earlier method.⁷ The values of η_m for pure and mixed surfactant systems are presented in Table 6.2(a) and Table 6.2(b). Figure 6.5 represents the variation of η_m with bulk mole fraction of all four gemini surfactants in mixed systems. The data in Table 6.2(a) and Table 6.2(b) and Figure 6.5 show that fluorescence anisotropy and microviscosity values are decreasing with increasing the bulk mole fraction of a gemini surfactant. It indicates that micellar environment is becoming less viscous in presence of a gemini surfactant as compared to pure TX-100 micelles. Headgroup-headgroup repulsions in a micelle of ionic surfactants make the micelle less compact and less viscous as compared to micelle of nonionic surfactants with no such interactions.^{5,11}

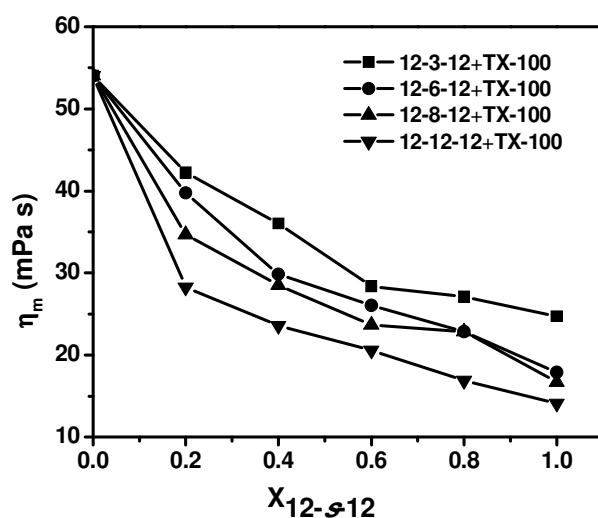


Figure 6.5: Plot of microviscosity (η_m) versus bulk mole fraction of gemini surfactants, $12-s-12.[TX-100+12-s-12] = 10$ mM

Table 6.2(a): Fluorescence anisotropy (r)^a, excited singlet state lifetime (τ_f)^b, rotational correlation time (τ_R) of DPH, microviscosities (η_m) of micelles of pure and mixed surfactant systems of TX-100 + 12-3-12 and TX-100 + 12-6-12. Total concentration of surfactants = 10 mM

$X_{12-3-12}$	r	τ_f (ns)	χ^2	τ_r (ns)	η_m (mPa s)	$X_{12-6-12}$	r	τ_f (ns)	χ^2	τ_r (ns)	η_m (mPa s)
0.0	0.128	7.52	1.0	4.11	54.05	0.0	0.128	7.52	1.0	4.11	54.05
0.2	0.115	6.90	1.0	3.21	42.25	0.2	0.112	6.75	1.1	3.02	39.76
0.4	0.110	6.28	1.1	2.74	36.02	0.4	0.098	6.11	1.0	2.27	29.84
0.6	0.098	5.82	1.0	2.16	28.38	0.6	0.095	5.57	1.0	1.98	26.04
0.8	0.097	5.63	1.1	2.06	27.09	0.8	0.089	5.34	1.0	1.74	22.87
1.0	0.094	5.38	1.0	1.88	24.70	1.0	0.075	5.21	1.1	1.36	17.90

^aFluorescence anisotropy at 430 nm. $\lambda_{ex} = 375$ nm

^b[DPH] = 5 μ M. A solution of DPH was prepared in tetrahydrofuran ^b $\lambda_{ex} = 375$ nm, $\lambda_{em} = 430$ nm

Table 6.2(b): Fluorescence anisotropy (r)^a, excited singlet state lifetime (τ_f)^b, rotational correlation time (τ_R) of DPH, microviscosities (η_m) of micelles of pure and mixed surfactant systems of TX-100+12-8-12 and TX-100+12-12-12. Total concentration of surfactants = 10 mM

$X_{12-8-12}$	r	τ_f (ns)	χ^2	τ_r (ns)	η_m (mPa s)	$X_{12-12-12}$	r	τ_f (ns)	χ^2	τ_r (ns)	η_m (mPa s)
0.0	0.128	7.52	1.0	4.11	54.05	0.0	0.128	7.52	1.0	4.11	54.05
0.2	0.102	6.72	1.1	2.64	34.68	0.2	0.091	6.40	1.0	2.15	28.27
0.4	0.094	6.18	1.0	2.17	28.51	0.4	0.083	6.03	1.0	1.79	23.59
0.6	0.091	5.37	1.0	1.80	23.68	0.6	0.076	5.89	1.0	1.56	20.57
0.8	0.087	5.50	1.1	1.74	22.85	0.8	0.065	5.88	1.1	1.29	16.91
1.0	0.068	5.50	1.0	1.27	16.70	1.0	0.056	5.82	1.0	1.07	14.10

^aFluorescence anisotropy at 430 nm. $\lambda_{ex} = 375$ nm

^b[DPH] = 5 μ M. A solution of DPH was prepared in tetrahydrofuran ^b $\lambda_{ex} = 375$ nm, $\lambda_{em} = 430$ nm

With increasing composition of TX-100 in a mixed micelle, the incorporation of TX-100 molecules between the two gemini surfactant molecules increases. As a result of that the headgroup-headgroup electrostatic repulsions between the gemini surfactant molecules decrease and more viscous micelles are formed. That is why the hydrodynamic radius (Figure 6.6 for size distribution) of TX-100 micelle is 5.57 ± 0.02 nm and the hydrodynamic radii of 12-*s*-12 micelles with *s* = 3, 6, 8, 12 are 0.62 ± 0.02 , 0.51 ± 0.02 , 0.50 ± 0.02 , and 0.43 ± 0.02 nm, respectively.¹² Pandey *et al.*¹³ have reported the increase in thickness of palisade layer of mixed micelles of TX-100 and a surface active ionic liquid with increasing concentration of ionic liquid because of greater extent of penetration of water molecules. That is the reason for the increase in microfluidity with increasing composition of a gemini surfactant in the mixed micelles.

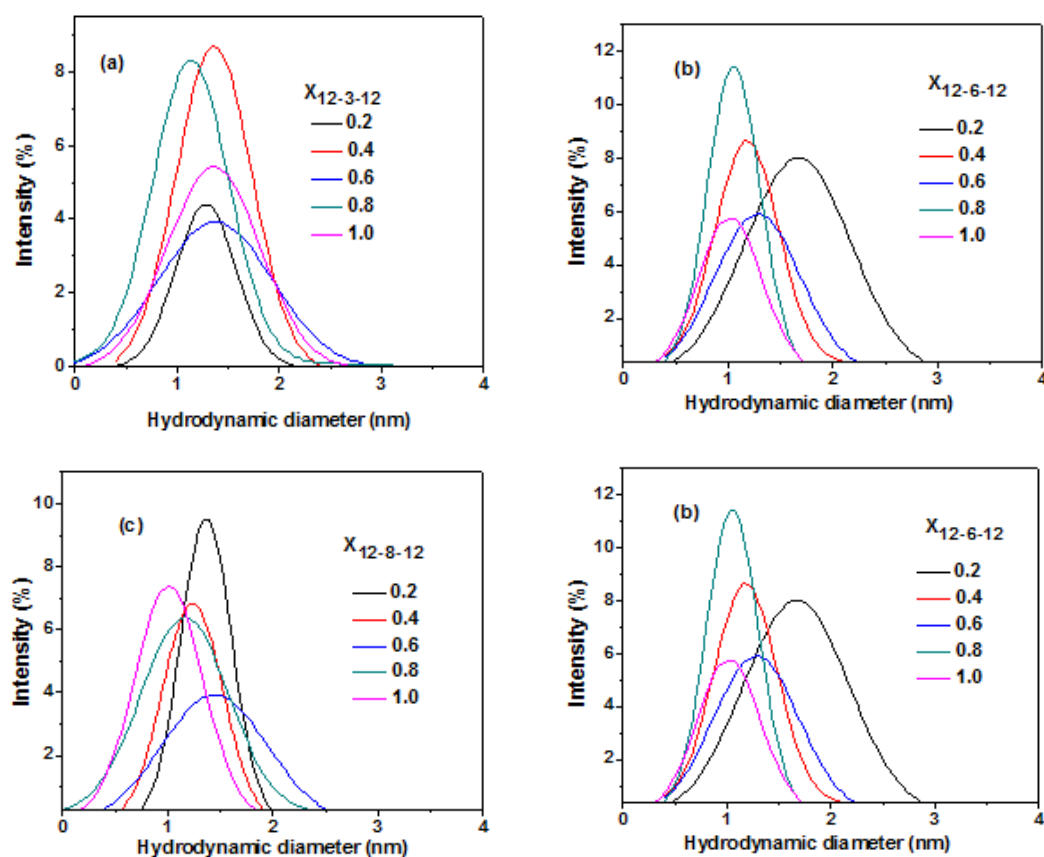


Figure 6.6: The size distribution graph for the micelles of TX-100 + 12-*s*-12 obtained from DLS measurement (a) *s* = 3, (b) *s* = 6, (c) *s* = 8, and (d) *s* = 12

We have supported the fact of progressive increase in penetration of water molecules by the $E_T(30)$ values given in Tables 6.1(a) and 6.1(b) which show that there is an increasing tendency of $E_T(30)$ value with increasing amount of gemini surfactant in the mixed micelle. Wang *et al.*⁵ also have noticed the decrease in microviscosity with increasing mole fraction of a gemini surfactant. It can also be noted in Figure 6.5 that the microviscosity of micelles decreases with increasing spacer chain length at a given bulk mole fraction. This observation is consistent with the literature report.^{1,14} Although this result does not give the exact values of microviscosities of environment around C-153, but it still fulfils our purpose to show the change in microviscosities of mixed micelles with changing composition of micelles.

6.2 Solvation dynamics

In presence of surfactant molecules, C-153 shows emission wavelength dependent decays. Wavelengths are chosen from the entire range of steady-state fluorescence spectra of C-153 (e.g. Figure 6.2 for TX-100+12-6-12) in presence of surfactants. For a representative one Figure 6.7 shows the time-resolved fluorescence decays of C-153 in presence of TX-100+12-6-12 micelles at a bulk mole fraction of 12-6-12 of 0.8 with total concentration of surfactant of 10 mM at different emission wavelengths. At a shorter wavelength (445 nm) of emission spectrum, a fast decay is observed and at a longer wavelength (565 nm), there is a clear growth in the decay followed by a slow decay with a negative pre-exponential factor. The growth in the decay indicates that the dipoles created at the excited state undergoes a solvent relaxation process followed by fluorescence emission and is therefore delayed by relaxation time.¹⁵ ¹⁶ At 445 nm, the decay is fitted bi-exponentially with two components of excited state lifetimes of 448 ps and 2.339 ns. However, at 565 nm, C-153 shows a distinct rise of 1.922 ns followed by a time constant of 3.526 ns. Similar behaviors have been observed at other bulk mole fraction of a surfactant and also in other mixed surfactant systems. It is worthy to be mentioned here that the observed wavelength dependent decays is mostly due to the probe molecules which are present in the Stern layer of the micelles.¹⁷ This is because wavelength dependent decays in bulk water are not observed due to the high time resolution (~165 ps) of our instrument. Also probe molecules present in the hydrocarbon core of the micelles should not show wavelength dependent decays.⁷

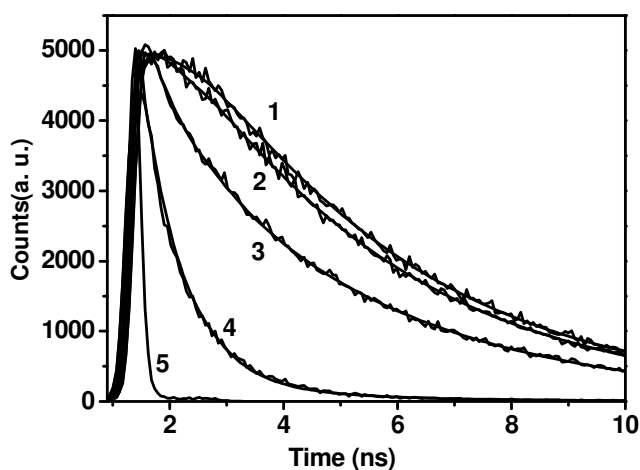


Figure 6.7: Time-resolved fluorescence decays of C-153 in TX-100+12-6-12 micelles at 0.8 bulk mole fraction of 12-6-12. 1 to 4 at 620 nm, 565 nm, 520 nm, 445 nm, respectively and 5 for instrument response function

The time resolved emission spectra (TRES) have been constructed by following the procedure of Fleming and Maroncelli.¹⁸ The dynamic Stokes shifts in the emission spectra of C-153 have been observed in all the investigated surfactant systems. Figure 6.8 represents the time-resolved emission spectra of C-153 in presence of 10 mM of TX-100+12-s-12 at a bulk mole fraction of 0.8 of 12-s-12. Similar spectra have been obtained for samples with other mole fraction as well. The dynamics of solvent is monitored by solvent response function (SRF), $C(t)$ calculated using Equation 2.26 (Section 2.2.11, Chapter 2). Figure 6.9 represents plots of $C(t)$ against time in mixed surfactant systems of TX-100+12-s-12 at various bulk mole fractions of gemini surfactant. All decays of solvent correlation function, $C(t)$ are found to be bi-exponential (Equation 2.31, Chapter 2) in nature. The average solvation times, $\langle \tau_s \rangle$ have been calculated using Equation 2.32 (Chapter 2). The decay parameters of C-153 in all the investigated surfactant systems are given in Table 6.3(a) and Table 6.3(b).

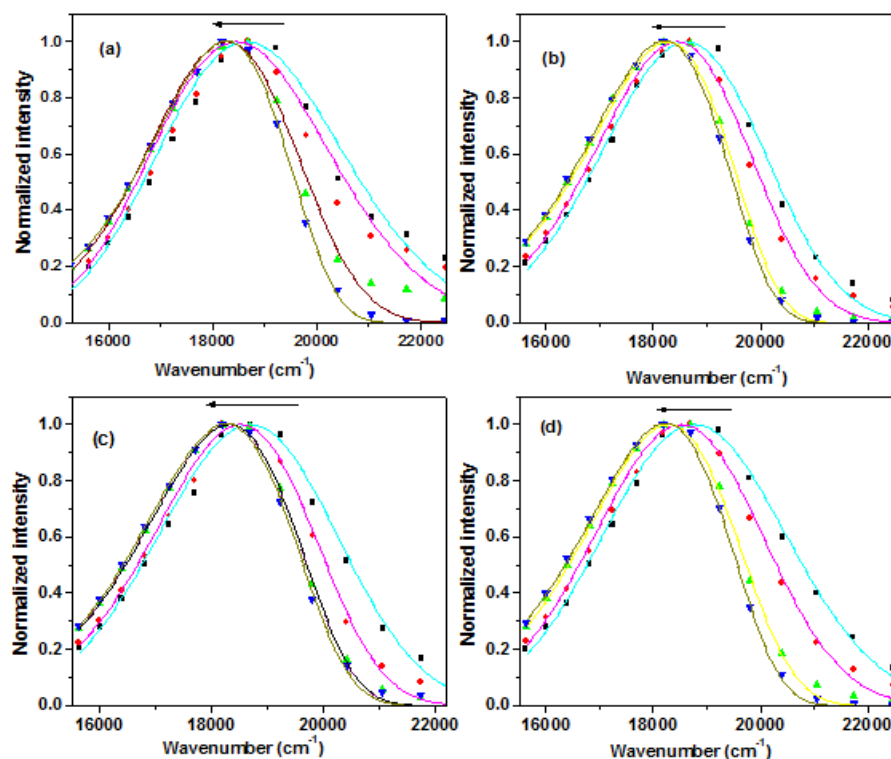


Figure 6.8: Time resolved emission spectra of C-153 in TX-100 + 12-s-12 at 0.8 bulk mole fraction (a) TX-100 + 12-3-12, (b) TX-100 + 12-6-12, (c) TX-100 + 12-8-12, and (d) TX-100 + 12-12-12, (from right to left) 200ps, 500ps, 2000ps, and 10000 ps

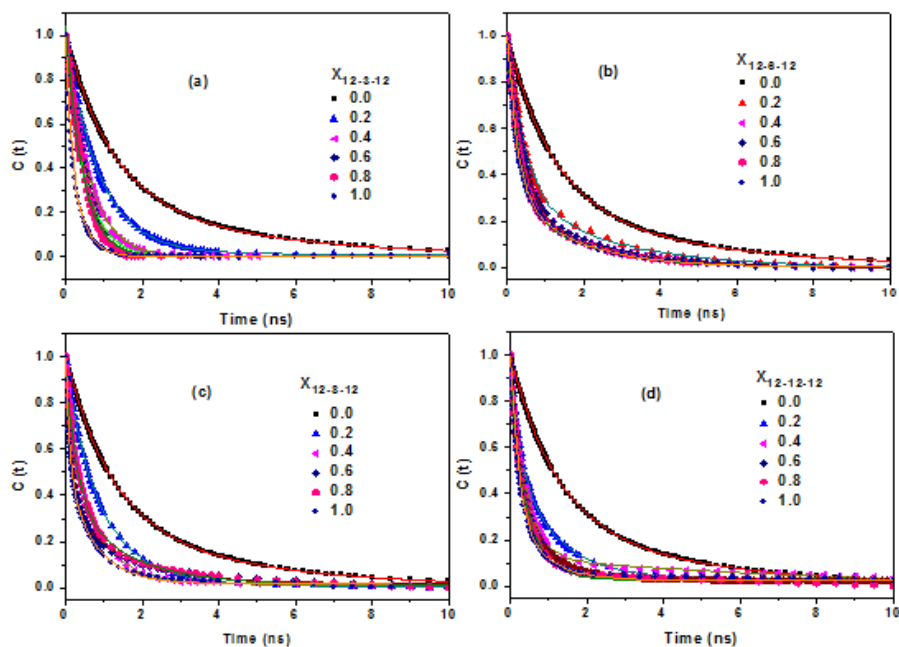


Figure 6.9: Decay of solvent correlation function, $C(t)$ of C-153 in pure and mixed surfactant systems of TX100+12-s-12 with (a) $s = 3$, (b) $s = 6$, (c) $s = 8$ and (d) $s = 12$ at different bulk mole fractions of gemini surfactants. $[TX-100+12-s-12] = 10 \text{ mM}$

Table 6.3(a): Decay characteristic of solvent correlation function, $C(t)$ of C-153 in presence of pure and mixed surfactants systems. [TX-100+ 12- s -12, $s = 3,6$] =10 mM

$X_{12-3-12}$	a_{1s}	τ_{1s} (ns)	a_{2s}	τ_{2s} (ns)	$\langle \tau_s \rangle$ (ns)	$X_{12-6-12}$	a_{1s}	τ_{1s} (ns)	a_{2s}	τ_{2s} (ns)	$\langle \tau_s \rangle$ (ns)
0.0	0.73	1.16	0.27	4.11	1.96	0.0	0.73	1.16	0.27	4.11	1.96
0.2	0.98	0.86	0.02	10.07	1.04	0.2	0.70	0.96	0.30	3.49	1.72
0.4	0.63	0.57	0.38	0.82	0.67	0.4	0.70	0.46	0.30	2.50	1.07
0.6	0.89	0.48	0.11	0.51	0.48	0.6	0.73	0.40	0.27	2.12	0.86
0.8	0.79	0.44	0.21	0.44	0.44	0.8	0.71	0.32	0.29	2.08	0.83
1.0	0.95	0.22	0.05	4.49	0.43	1.0	0.83	0.32	0.17	2.83	0.75

Table 6.3(b): Decay characteristic of solvent correlation function, $C(t)$ of C-153 in presence of pure and mixed surfactants systems. [TX-100+ 12- s -12, $s = 8,12$] =10 mM

$X_{12-8-12}$	a_{1s}	τ_{1s} (ns)	a_{2s}	τ_{2s} (ns)	$\langle \tau_s \rangle$ (ns)	$X_{12-12-12}$	a_{1s}	τ_{1s} (ns)	a_{2s}	τ_{2s} (ns)	$\langle \tau_s \rangle$ (ns)
0.0	0.73	1.16	0.27	4.11	1.96	0.0	0.73	1.16	0.27	4.11	1.96
0.2	0.69	1.02	0.31	3.84	1.89	0.2	0.75	0.42	0.21	3.75	1.11
0.4	0.71	0.74	0.29	4.56	1.85	0.4	0.87	0.32	0.13	4.42	0.85
0.6	0.76	0.55	0.24	4.43	1.48	0.6	0.87	0.28	0.13	4.67	0.85
0.8	0.80	0.47	0.20	4.35	1.25	0.8	0.86	0.26	0.14	4.22	0.82
1.0	0.69	0.32	0.31	1.98	0.82	1.0	0.74	0.18	0.26	1.51	0.52

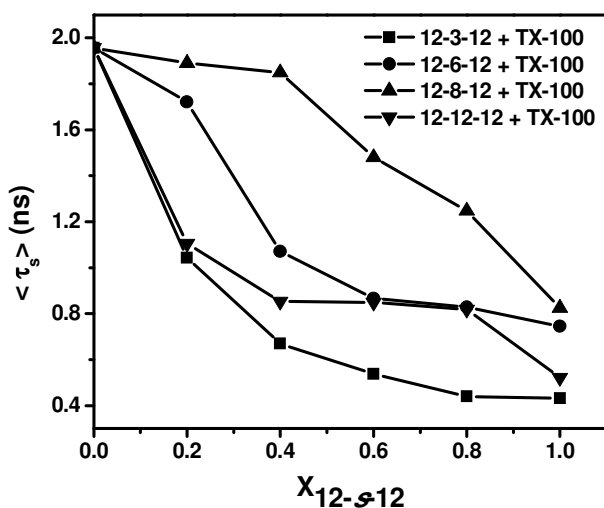


Figure 6.10: Plot of average solvation time, $\langle \tau_s \rangle$ versus bulk mole fraction of gemini surfactant in the mixture, TX-100+12-*s*-12 with *s* = 3, 6, 8, 12

The data in Table 6.3(a) and Table 6.3(b) show that solvation dynamics for C-153 is bimodal in nature (slow and fast components) in all the studied micellar systems. The bound and free water molecules are responsible for the slow and fast components of solvation, respectively.¹⁹ Apart from water molecules other factors responsible for solvation are counter ions, spacer group of gemini surfactant and polar headgroups of surfactant. However, the polar headgroups of a surfactant molecule are connected to the hydrocarbon tails and the spacer group is connected to the tails through headgroups. Their mobility is restricted to a very large extent as they are connected to the long hydrocarbon tails and it is reported that the dynamics of polymer chain occur on very slow time scale (~ 100 ns).^{7,20,21} Therefore, water molecules and counter ions are mostly responsible for solvation dynamics. Figure 6.10 represents the plots of variation of average solvation times with increasing bulk mole fraction of all four gemini surfactants in the mixed systems. The average solvation time decreases with increasing amount of a gemini surfactant in the mixed micelles. Data in Table 6.3(a) and Table 6.4(b) show that apparently there are tendencies for increasing weightage of fast component and decreasing weightage of slow component with increasing amount of a gemini surfactant in the mixed micelles. Water molecules hydrogen bonded with polar headgroups are more restricted (bound water) as compared to water molecules hydrogen bonded among themselves (free water).^{15,19} Free and bound water molecules are in equilibrium with each other.^{15,22,23} The structure of water molecules around the probe molecules in the

Stern layer of micelles controls the solvation dynamics. Hydrogen bonded water molecules in the bulk water undergo mutual polarization which results in an increase in the dipole moment and dielectric constant.^{15,24} However, because of lack of such kind of polarization in case of water molecules hydrogen bonded to a biological system like proteins, these water molecules are comparatively less polar than bulk water. Similarly in our case the water molecules interacting with the polar headgroups of gemini surfactants and hydrogen bonded with the polyoxyethylene group of TX-100 are expected to behave differently from that of the bulk water molecules. As discussed above with increasing percentage of a gemini surfactant in the mixed micelles, the thickness of the Stern layer increases with increasing penetration of water molecules resulting in decreasing microviscosity of micelles (Figure 6.5). With increasing thickness of the Stern layer, while the number of water molecules interacting with the polar headgroups of surfactants and also hydrogen bonded with the polyoxyethylene group of TX-100 decreases, the number of water molecules hydrogen bonded among themselves increases. As a result of it polarity of water molecules increases^{15,24} which is supported by the increase in $E_T(30)$ value [Tables 6.1(a) and 6.1(b)]. In addition, the process of solvation dynamics becomes faster. TX-100 molecule has a long polyoxyethylene group in it which interacts with water molecules along oxyethylene chain through hydrogen bonds. Response to the solvation process from a few water molecules very near to the probe molecules, C-153 is most likely to be slower than the collective response from the large number of water molecules away from the probe molecules.²⁵⁻²⁷ Thus it is likely that while a few water molecules closer to the probe molecules in the Stern layer of micelles contribute to the slow solvation dynamics, the comparatively large number of free water molecules away from the probe molecules are responsible for fast component. In addition, the water molecules interacting with the headgroups of gemini surfactant molecules also contribute to the slow solvation dynamics. Counter ions contribute to the slow solvation process as described in the next paragraph.¹² In addition, looking into the fact that the full width at half the maximum of TRES decreases at longer time scale (Figure 6.8) for all kinds of mixed systems, one can guess that possibly the self-diffusion of the probe, C-153 also contributing towards the slower component of solvation.²⁸ Sarkar et al.²⁵ have studied the effect of ionic liquid concentration on solvation dynamics in aqueous mixed micelles with TX-100. They have also observed that solvation dynamics become faster with increasing the concentration of ionic liquid. Like their results, we have noticed that the faster and the slower components become faster on addition of gemini surfactant in the

mixed micelles. They have reported that the weightage of both the fast and the slow components decrease on addition of ionic liquid. However, unlike that report, in our case we have found that there is an increasing tendency of the weightage of the fast component, and decreasing tendency in the weightage of the slow component. As a result of that average solvation time decreases with the addition of gemini surfactant. Solvation times reported in the study by Sarkar et al.²⁵ are little longer than the solvation times observed in the present investigation.

It can be noted from the Figure 6.10 that at a given bulk mole fraction of a gemini surfactant, the average solvation time increases with increasing spacer chain length from $s = 3$ to $s = 8$, then falls for gemini surfactant with $s = 12$ and lies in between $s = 3$ and $s = 6$. We have found in our earlier study that the degree of counter ion dissociation increases with spacer chain length of the same series of gemini surfactants, 12- s -12.¹² We have also found that the solvation time increases in the similar manner as that is observed in the present work. Kumbhakar *et al.*²⁹ have reported the impact of added electrolytes (NaCl, KCl, and CsCl) of various concentrations on the nature of water molecules present in the palisade layer of Triton X-100 micelles using solvation dynamics studies of coumarin 153 (C-153) dye. They have observed that in the presence of added salts the solvation dynamics becomes slower for the all cases of salts. Added salt enhances the mechanically trapped water content in the palisade layer of micelles which results in the increase in micellar hydration. Authors have rationalized their results assuming that the ions present in the palisade layer induce the formation of clustering of water molecules causing slow solvation process. Levinger *et al.*³⁰ have reported that when the Na^+ ion as counterion of the Aerosol-OT (AOT) surfactant is exchanged for an NH_4^+ cation, solvation dynamics becomes faster. Here, Na^+ ion in normal AOT reverse micelles is responsible for reducing a large fraction of the water motion thereby increasing solvation time. Based on these literature reports, we state that in the present case the anionic counter ions, Br^- of gemini surfactants, 12- s -12 are mainly responsible for the increase in solvation time. Counter ions indirectly reduce the rate of solvation process. It is known that anions can form strong hydrogen bonds with water molecules.³¹ With increasing spacer chain length the number of dissociated counter ions increases.¹² As a result of that more and more water molecules get involved in solvation of counter ions themselves through hydrogen bonding. The solvation time

increases because of clustering of water molecules in the Stern layer as the percentage of water molecules contribute to the fast solvation process decreases. Of course we are not ruling out the effect of increasing hydrophobic spacer chain length on decreasing rate of solvation process. Availability of water molecules for solvation process is reduced with increasing hydrophobicity of spacer as a result of increase in spacer chain length. Borse *et al.*³² have studied on the hydration of micelles of 12-*s*-12, 2Br⁻ surfactants. They have found that the volume of water molecules per gram of surfactant molecules in the micellar phase decreases with increasing spacer chain length. In case of mixed micelles with 12-12-12 gemini surfactant the effect of low microviscosity (Figure 6.5) dominates over the effect of counter ions resulting in decrease in solvation time. It is pertinent to note that the fall of the value of average solvation time with increasing bulk mole fraction of 12-3-12 surfactant in mixed micelles is much faster as compared to 12-*s*-12 surfactants with *s* = 6, 8 and 12 (Figure 6.10).

6.3 Rotational relaxation or time-resolved fluorescence anisotropy

Figure 6.11 shows the anisotropy decays of C-153 in micelles and mixed micelles with various bulk mole fractions of gemini surfactants. While anisotropy decay is mono-exponential in pure water, it is bi-exponential in presence of surfactants. Rotational relaxation parameters are tabulated in Tables 6.4(a) and 6.4(b). The rotational relaxation time of C-153 in presence of pure water is reported to be 100 ps.¹⁷ In presence of surfactant molecules it becomes many folds longer than that in pure water which infers that C-153 experiences motionally restricted environment in the micelles. Figure 6.12 shows that the average relaxation time decreases with increasing amount of a gemini surfactant in the mixed micelles. With increasing percentage of a gemini surfactant in the mixed micelles the thickness of the Stern layer increases resulting in decreasing microviscosity of micelles (Figure 6.5). Due to this reason average rotational relaxation time decreases. It is noteworthy that the decrease in relaxation time with increasing amount of a gemini surfactant is faster in case of gemini surfactants with longer spacer chain i.e. *s* = 8 and 12. In fact it is so effective in presence of 12-12-12 gemini surfactant that saturation is reached at its ~0.6 bulk mole fraction only.

Table 6.4(a): Rotational relaxation parameters for C-153 in the mixed micelles of TX-100+12-*s*-12, 2Br⁻ with *s* = 3 and 6

$X_{12-3-12}$	a_{1r}	τ_{1r} (ns)	a_{2r}	τ_{2r} (ns)	$\langle\tau_r\rangle$ (ns)	$X_{12-6-12}$	a_{1r}	τ_{1r} (ns)	a_{2r}	τ_{2r} (ns)	$\langle\tau_r\rangle$ (ns)
0.0	0.27	0.67	0.73	6.23	4.73	0.0	0.27	0.67	0.73	6.23	4.73
0.2	0.46	0.48	0.54	8.21	4.65	0.2	0.39	0.50	0.61	5.92	3.81
0.4	0.50	0.49	0.50	8.23	4.36	0.4	0.40	0.57	0.60	5.75	3.68
0.6	0.50	0.46	0.50	7.69	4.01	0.6	0.40	0.37	0.60	5.18	3.26
0.8	0.52	0.43	0.48	5.85	3.03	0.8	0.43	0.48	0.57	3.87	2.41
1.0	0.81	0.65	0.19	5.74	1.63	1.0	0.54	0.41	0.46	2.31	1.28

Table 6.4(b): Rotational relaxation parameters for C-153 in the mixed micelles of TX-100+12-*s*-12, 2Br⁻ with *s* = 8 and 12

$X_{12-8-12}$	a_{1r}	τ_{1r} (ns)	a_{2r}	τ_{2r} (ns)	$\langle\tau_r\rangle$ (ns)	$X_{12-12-12}$	a_{1r}	τ_{1r} (ns)	a_{2r}	τ_{2r} (ns)	$\langle\tau_r\rangle$ (ns)
0.0	0.27	0.67	0.73	6.23	4.73	0.0	0.27	0.67	0.73	6.23	4.73
0.2	0.81	0.85	0.19	8.35	2.28	0.2	0.76	0.66	0.24	4.79	1.65
0.4	0.78	0.64	0.22	5.40	1.69	0.4	0.65	0.57	0.35	3.29	1.52
0.6	0.55	0.55	0.45	2.65	1.50	0.6	0.73	0.56	0.27	3.15	1.26
0.8	0.44	0.36	0.56	2.05	1.31	0.8	0.75	0.54	0.25	3.39	1.25
1.0	0.50	0.35	0.50	2.19	1.27	1.0	0.49	0.28	0.51	2.14	1.23

One can also see from Figure 6.12 that at a given bulk mole fraction, the rotational relaxation time decreases with increasing spacer chain length. It is due to the fact that microviscosity of micelles decreases with increasing polymethylene spacer chain length of the gemini surfactant, 12-*s*-12 (Figure 6.5).

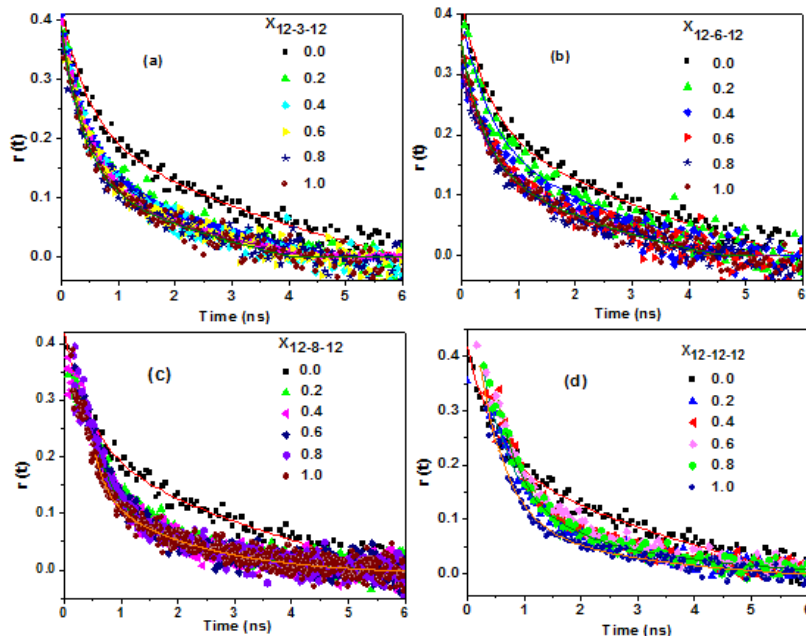


Figure 6.11: Anisotropy decays of C-153 in pure surfactants and in mixed surfactant systems of TX-100 and 12-*s*-12 with (a) $s = 3$, (b) $s = 6$, (c) $s = 8$ and (d) $s = 12$ at various bulk mole fractions of 12-*s*-12

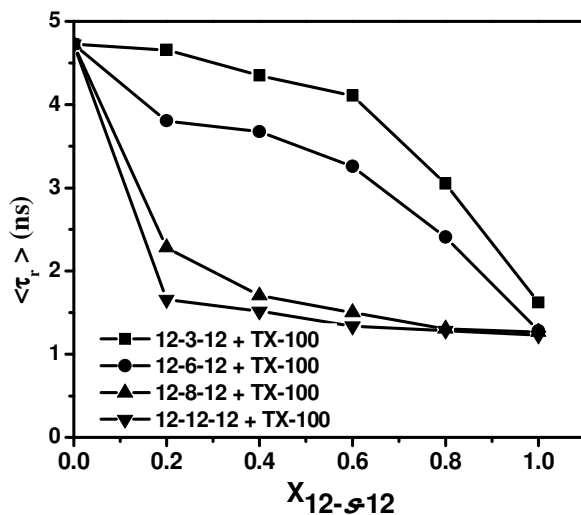


Figure 6.12: Variation of average rotational relaxation time, $\langle \tau_r \rangle$ with bulk mole fraction of a gemini surfactant in the mixed micelles of TX-100 and 12-*s*-12 with $s = 3$, 6, 8 and 12

The decrease in microviscosity with increasing polymethylene spacer chain for a series of gemini surfactants, 12-*s*-12 has been reported before by Zana *et al.*¹⁴ and also has been observed by us in our previous work.¹² Results in present study indicate that the same trend is in place even in mixed micelles of each of these gemini surfactants with TX-100. The anisotropy decays of C-153 in all micellar systems are bimodal in nature. While the time scale for fast rotational relaxation lies in the range of ~280 ps to ~850 ps, the same for slow rotational relaxation is ~2 ns to ~8 ns. The longer time for fast relaxation process as compared to that in water (100 ps) and complete solubilization of probe molecules in micelles infer that rotational relaxation of probe molecules takes place only in micellar environment. The bimodal behavior of anisotropy decay is reported to be for different kind of rotational motions.^{7,33,34} To explore these rotational motions, the two-step and wobbling-in-the cone models have been used (Sections 2.2.12.1 and 2.2.12.2, Chapter 2).

According to the two step model the slow rotational relaxation time (τ_{2r}) is related to the time for lateral diffusion of the probe molecule (τ_D) and the time for rotational motion of the micelle as a whole (τ_m) (Equation 2.35, Chapter 2). Hydrodynamic radii of micelles of various mixed surfactant systems have been estimated and tabulated in Table 6.5(a) and Table 6.5(b) (Figure. 6.6 for the plots of size distribution). Knowing the values of τ_m , the values of τ_D have been calculated using experimental value of τ_{2r} following Equation 2.35 (Chapter 2). Values of τ_m and τ_D are also tabulated in Table 6.5(a) and Table 6.5(b). One can see from Tables 6.4(a), 6.4(b), 6.5(a) and 6.5(b) that the slow rotational relaxations in all micellar systems are due to the lateral diffusion of the probe molecule along the surface of micelle. The rotational motion of micelle as a whole containing probe molecule is a much slower process than lateral diffusion of the probe molecule.

Table 6.5(a): Hydrodynamic radius (r_h)^a, lateral diffusion time (τ_D), time for overall rotational motion of the micelle (τ_m), wobbling motion time (τ_w), wobbling diffusion coefficient (D_w), cone angle (θ_o) and order parameter ($|S|$) obtained from the anisotropy decays of C-153 in different micelles of TX-100+12-*s*-12, 2Br⁻ with *s* = 3 and 6

$X_{12-3-12}$	r_h (nm)	τ_m (μ s)	τ_w (ns)	τ_D (ns)	θ_o (deg)	S	$D_w \times 10^{-8}$ (s^{-1})	$X_{12-6-12}$	r_h (nm)	τ_m (μ s)	τ_{wob} (ns)	τ_D (ns)	θ_o (deg)	S	$D_w \times 10^{-8}$ (s^{-1})
0.0	5.57	157.00	0.75	6.23	25.89	0.85	0.80	0.0	5.57	157.00	0.75	6.23	25.89	0.85	0.80
0.2	0.65	0.24	0.51	8.50	35.76	0.73	2.22	0.2	0.79	0.45	0.66	6.00	32.21	0.78	1.39
0.4	0.66	0.30	0.52	8.50	37.81	0.71	2.44	0.4	0.63	0.23	0.63	5.89	32.72	0.77	1.52
0.6	0.63	0.23	0.49	7.95	37.81	0.71	2.61	0.6	0.62	0.22	0.58	5.31	32.72	0.77	1.64
0.8	0.55	0.15	0.47	6.08	38.83	0.69	2.87	0.8	0.54	0.14	0.54	3.98	34.24	0.75	1.91
1.0	0.62	0.22	0.75	5.89	56.00	0.43	3.74	1.0	0.51	0.12	0.50	2.35	39.87	0.67	2.84

^aStandard deviation: ± 0.02

Table 6.5(b): Hydrodynamic radius (r_h)^a, lateral diffusion time (τ_D), time for overall rotational motion of the micelle (τ_m), wobbling motion time (τ_w), wobbling diffusion coefficient (D_w), cone angle (θ_o) and order parameter ($|S|$) obtained from the anisotropy decays of C-153 in different micelles of TX-100+12-*s*-12, 2Br⁻ with *s* = 8 and 12

$X_{12-8-12}$	r_h (nm)	τ_m (μ s)	τ_w (ns)	τ_D (ns)	θ_o (deg)	S	$D_w \times 10^{-8}$ (s^{-1})	$X_{12-12-12}$	r_h (nm)	τ_m (μ s)	τ_{wob} (ns)	τ_D (ns)	θ_o (deg)	S	$D_w \times 10^{-8}$ (s^{-1})
0.0	5.57	157.00	0.75	6.23	25.89	0.85	0.80	0.0	5.57	157.00	0.75	6.23	25.89	0.85	0.80
0.2	0.67	0.27	0.95	8.61	56.00	0.43	2.95	0.2	0.65	0.24	0.76	4.89	52.48	0.48	3.20
0.4	0.61	0.20	0.73	5.55	53.84	0.46	3.52	0.4	0.58	0.17	0.69	3.35	45.79	0.59	2.68
0.6	0.67	0.27	0.70	2.68	40.39	0.67	2.08	0.6	0.57	0.17	0.69	3.21	50.54	0.51	2.69
0.8	0.59	0.18	0.44	2.08	34.75	0.74	2.45	0.8	0.49	0.11	0.64	3.50	51.82	0.50	3.42
1.0	0.50	0.11	0.42	2.23	37.81	0.71	3.05	1.0	0.43	0.72	0.33	2.20	37.29	0.71	3.89

^aStandard deviation: ± 0.02

It is noteworthy that the time constant for lateral diffusion of the probe molecule (τ_D) in the micelles mostly decreases with increasing bulk mole fraction of a gemini surfactant as result of decrease in microviscosity of micelles. It is pertinent to note that the time constant for rotational motion of the micelle as a whole (τ_m) is a function of size of the micelle. τ_m decreases with decreasing size of a micelle. It is very long for a micelle of pure TX-100 because the size of this micelle is much bigger as compared to mixed micelles or a micelle of pure gemini surfactants. The time constant for the wobbling motion (τ_w) of the probe molecule has been calculated by Equation 2.40 (Chapter 2). Calculated τ_w values are given in Tables 6.5(a) and 6.5(b). τ_w values mostly decrease with increasing bulk mole fraction of a gemini surfactant in the mixed micelle which is in accordance with the fact that τ_w is a measure of the relaxation of the local structure of the micelle.³⁵ To obtain further information about the motional restriction of the probe within the micelles, the generalized order parameter, $|S|$, the wobbling cone angle (θ_o) (Equation 2.38, Chapter 2) and wobbling diffusion coefficient (D_w) (Equation 2.41, Chapter 2) have been calculated and values obtained are also given in Table 6.5(a) and 6.5(b). The values of $|S|$ are higher than 0 which indicate restricted motion of the probe molecule in presence of micelles. There is a decreasing tendency of S values with increasing the mole fraction of a gemini surfactant which supports reduced motional restriction of the probe molecule with increasing proportion of gemini surfactant in the mixed micelles as a result of increase in microfluidity. Data in Tables 6.5(a) and 6.5(b) show that there is increasing tendency of the values of θ_o and D_w with increasing mole fraction of a gemini surfactant which is also in accordance with the decrease in motional restriction of C-153 with increasing mole fraction of a gemini surfactant in the mixed micelles.

6.4 Conclusions

The solvation dynamics and rotational relaxation of C-153 in the mixed micelles of TX-100 and a series of cationic gemini surfactants, 12-*s*-12 with *s* = 3, 6, 8 and 12 have been studied. With increasing mole fraction of a gemini surfactant in the mixed micelles, the thickness of the Stern layer of micelles increases due to the greater extent of penetration of water molecules. As a result of it while the micropolarity of environment around the fluorophore increases, the microviscosity of the same decreases. The time constants for the solvation process as well as the rotational relaxation process decrease

with increasing amount of a gemini surfactant in the mixed micelles. It is due to the increase in the thickness of Stern layer of micelles with increasing amount of a gemini surfactant in the micelles. With the increase in the thickness of the Stern layer, while there is a decrease in the number of water molecules interacting with the polar headgroups of surfactants and also hydrogen bonded with the polyoxyethylene group of TX-100, there is a concomitant increase in the number of water molecules hydrogen bonded among themselves. Due to this reason the polarity of water molecules increases which is supported by the increase in $E_T(30)$ value. Increase in the number of hydrogen bonded water molecules makes the solvation process faster. Increase in microfluidity with increasing composition of a gemini surfactant in the mixed micelles enhances the rate of rotational relaxation process. At a given bulk mole fraction of a surfactant, the microviscosity of micelles decreases with increasing spacer chain length resulting in faster rotational relaxation process. However, at a given bulk mole fraction of a surfactant, solvation dynamics becomes slower with increasing spacer chain length from $s = 3$ to 8, because of increasing degree of dissociation of counter ions which indirectly contribute to the slow solvation process. For micelles of 12-12-12, the fast solvation process is due to the dominating effect of low microviscosity of micelles. The slow rotational relaxation process in all micellar systems is dominated by the lateral diffusion of the probe molecule along the surface of micelles. Decreasing tendency in the time constant values for lateral diffusion process and increasing tendencies in the values of wobbling diffusion coefficient, and cone angle are in accordance with the increase in microfluidity of micelles with increasing amount of gemini surfactant present in the mixed micelles.

References:

- (1) Sonu, A. K. Tiwari, S. Kumari, S. K. Saha, *RSC Adv.* **2014**, *4*, 25210.
- (2) C. C. Ruiz, *Photochem. Photobiol. Sci.* **2012**, *11*, 1331.
- (3) G. Jones, W. R. Jackson, C. Y. Choi, W. R. Bergmark, *J. Phys. Chem.* **1985**, *89*, 294.
- (4) K. Rechthaler, G. Kohlar, *Chem. Phys.* **1994**, *189*, 99.
- (5) X. Wang, J. Wang, Y. Wang, J. Ye, H. Yan, R. K. Thomas, *J. Colloid Interface Sci.* **2005**, *286*, 739.
- (6) A. Mallick, B. Haldar, S. Maiti, N. Chattopadhyay, *J. Colloid Interface Sci.* **2004**, *278*, 215.

- (7) A. K. Tiwari, Sonu, S. K. Saha, *J. Phys. Chem. B* **2014**, *118*, 3582.
- (8) A. Mallick, B. Haldar, S. Maiti, S. C. Bera, N. Chattopadhyay, *J. Phys. Chem. B* **2005**, *109*, 14675.
- (9) A. A. Hassanali, T. P. Li, D. P. Zhong, S. J. Singer, *J. Phys. Chem. B* **2006**, *110*, 10497.
- (10) Sonu, A. K. Tiwari, S. K. Saha, *Ind. Eng. Chem. Res.* **2013**, *52*, 5895.
- (11) M. Shinitzky, Y. Baranholz, *J. Biol. Chem.* **1974**, *249*, 2652.
- (12) Sonu, S. Kumari, S. K. Saha, *J. Phys. Chem. B* **2015**, *119*, 9751.
- (13) K. Behera, M. D. Pandey, M. Porel, S. Pandey, *J. Chem. Phys.* **2007**, *127*, 184501.
- (14) R. Zana, *J. Colloid Interface Sci.* **2002**, *248*, 203.
- (15) K. Bhattacharyya, *Chem. Commun* **2008**, 2848.
- (16) J. R. Lakowicz, *Principles of Fluorescence Spectroscopy*; Kluwer Academic: New York, 1999.
- (17) V. G. Rao, C. Banerjee, S. Mandal, S. Ghosh, N. Sarkar, *Spectrochimica Acta Part A* **2012**, *120*, 371.
- (18) M. Maroncelli, G. R. Fleming, *J. Chem. Phys.* **1987**, *86*, 6221.
- (19) N. Nandi, B. Bagchi, *J. Phys. Chem. B* **1997**, *101*, 10954.
- (20) N. Sarkar, A. Datta, S. Das, K. Bhattacharyya, *J. Phys. Chem.* **1996**, *100*, 15483.
- (21) R. Dutta, M. Chowdhury, M. A. Winnik, *Polymer* **1995**, *36*, 4445.
- (22) R. Jimenez, G. R. Fleming, P. V. Kumar, M. Maroncelli, *Nature* **1994**, *369*, 471.
- (23) D. Zhong, S. K. Pal, A. Zewail, *Chem. Phys. Lett.* **2011**, *503*, 1.
- (24) S. W. Rick, S. J. Stuart, B. J. Berne, *J. Chem. Phys.* **1994**, *101*, 6141.
- (25) R. Pramanik, S. Sarkar, C. Ghatak, V. G. Rao, S. Mandal, N. Sarkar, *J. Phys. Chem. B*, **2011**, *115*, 6957.
- (26) R. S. Fee, M. Maroncelli, *Chem. Phys.* **1994**, *183*, 235.
- (27) M. Maroncelli, J. Macinnis, G. R. Fleming, *Science* **1989**, *243*, 1674.
- (28) B. Roy, S. Satpathi, K. Gavvala, R. K. Koninti, and P. Hazra, *J Phys. Chem. B* **2015**, *119*, 11721.
- (29) M. Kumbhakar, T. Goel, T. Mukherjee, H. Pal, *J. Phys. Chem. B* **2005**, *109*, 14168.
- (30) R. E. Riter, E. P. Undiks, N. E. Levinger, *J. Am. Chem. Soc.* **1998**, *120*, 6062.

- (31) T.W.G. Solomons and C.B. Fryhle, *Organic Chemistry*, eighth ed., John Wiley & Sons (Asia), Singapore, **2004**.
- (32) Borse, M.; Sharma, V.; Aswal, V. K.; Goyal, P. S.; Devi, S, *J. Colloid Interface Sci.* **2005**, *284*, 282.
- (33) D. Chakrabarty, D. Seth, A. Chakraborty, N. Sarkar, *J. Phys. Chem. B* **2005**, *109*, 5753.
- (34) D. Chakrabarty, A. Chakraborty, D. Seth, P. Hazra, N. Sarkar, *J. Chem. Phy.* **2005**, *122*, 184516.
- (35) E. L. Quitevis, A. H. Marcus, M. D. Fayer, *J. Phys. Chem.* **1993**, *97*, 5762.

Chapter 7

Effect of added urea on solvation dynamics and rotational relaxation of Coumarin 480 in aqueous micelles of cationic gemini surfactant

This chapter deals with the effect of added urea on solvation dynamics and rotational relaxation of Coumarin 480 (C-480), (Scheme 2.1) in aqueous micelles of cationic gemini surfactant, 12-4-12 (Scheme 2.2). UV-Vis absorption, steady-state fluorescence and fluorescence anisotropy, time-resolved fluorescence and fluorescence anisotropy, and dynamic light scattering measurements have been used to carry out these studies. With the addition of urea micropolarity of the micelles remains unaltered. Microviscosity, mole fraction partition coefficient and Gibbs free energy of micellization are found to be decreased with the addition of urea in aqueous micelles of 12-4-12. Steady-state and time resolved fluorescence studies show that C-480 resides at the Stern layer of the micelles. Rotational relaxation is bimodal in nature. Solvation dynamics in aqueous micelles depends upon the concentration of urea. While at low concentration of urea the process of solvation dynamics is fast due to the disruption of tetrahedral structure of water, at high concentration of urea solvation dynamics becomes slower which is due to hydrogen bonding interaction between water and urea. This study shows that urea molecules interact directly as well as indirectly with the micelles.

7.1 Results and discussions

7.1.1 Effect of urea on cmc value of 12-4-12: Study with DMACA

Cmc values of aqueous solutions of pure 12-4-12 and 12-4-12 in presence of various concentration of urea have been calculated by using fluorescence properties of DMACA.¹ Fluorescence spectra of DMACA have been recorded in presence of pure 12-4-12 and 12-4-12 in presence of various concentration of urea. Figure 7.1 represents fluorescence spectra of DMACA with increasing concentration of 12-4-12 as a representative one. In pure water, the charge transfer (CT) state of DMACA gets stabilized and comes closer to the low-lying triplet or ground state which results in increase in the rate for non-radiative processes. That is why fluorescence intensity is very low in pure water. In the micellar phase due to low polarity of environment around

DMACA molecules as compared to that of water, the CT state gets destabilized resulting in decrease in the rate of non-radiative processes.¹ That is why an enhancement of fluorescence intensity with blue-shift of fluorescence band has been noticed with increasing concentration of the surfactant. Figure 7.2 shows the plot of fluorescence intensity of DMACA with increasing concentration of 12-4-12. Cmc value has been calculated from the break point of first two intersecting lines. Similar plots have been obtained at different concentration of urea as well. Calculated *cmc* values are tabulated in Table 7.1. It is observed that *cmc* value of 12-4-12 increases with increasing the concentration of urea. Urea molecules disrupt the water structures which enhance the solubility of surfactant molecules in water.² Increased solubility of surfactant molecule in the solution delays the aggregation process of surfactant molecules and consequently the concentration at which surfactant molecules form aggregates increases as compared to that in absence of urea. Increasing concentration of urea in the solution results in the decrease in hydrophobic interactions between the surfactant molecules.²

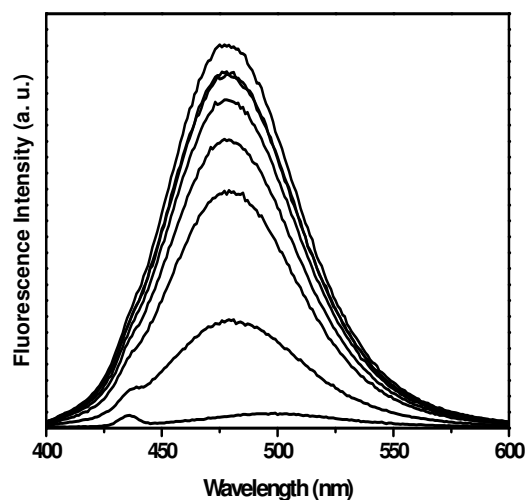


Figure 7.1: Fluorescence spectra of DMACA in presence of increasing concentration (bottom to top) of pure 12-4-12. $\lambda_{\text{ex}} = 378 \text{ nm}$, $[\text{DMACA}] = 5 \mu\text{M}$

The mole fraction partition coefficient of surfactant molecules from the aqueous phase to the micellar phase (K^{mic}) has been calculated by using the following equation³:

$$K^{\text{mic}} = \frac{55.5M}{\text{CMC}} \quad (7.1)$$

K^{mic} values are given in Table 7.1. The value of standard molar Gibbs free energy upon micellization has been calculated by the given equation:

$$\Delta G^{o, mic} = -RT \ln K^{mic} \quad (7.2)$$

The values of $\Delta G^{o, mic}$ at various concentrations of urea are also given in Table 7.1. $\Delta G^{o, mic}$ values are increased and K^{mic} values are decreased with increasing the concentration of urea. It indicates that micellization process becomes less favourable with increasing the concentration of urea.

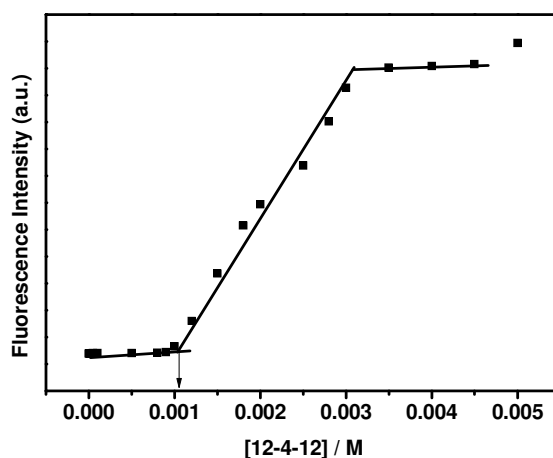


Figure 7.2: Plot of fluorescence intensity of DMACA with increasing concentration of pure 12-4-12

Table 7.1: Critical micelles concentration (*cmc*), mole fraction partition coefficient (K^{mic}), standard molar Gibbs free energy ($\Delta G^{o, mic}$), absorption peak maxima (λ_{max}^{ab})^a, fluorescence peak maxima (λ_{max}^{fl})^b of C-480, in aqueous solution of pure 12-4-12 and 12-4-12 with various concentrations of urea

Systems	<i>Cmc</i> (mM)	K^{mic} (10^4)	$\Delta G^{o, mic}$ (kJ mol^{-1})	λ_{max}^{ab} (nm)	λ_{max}^{fl} (nm)
12-4-12	1.05	5.29	-26.96	395	475
12-4-12 + 0.5 M Urea	1.16	4.91	-26.72	395	475
12-4-12 + 1 M Urea	1.19	4.78	-26.65	395	475
12-4-12 + 2 M Urea	1.26	4.66	-26.51	395	475
12-4-12 + 3 M Urea	1.50	4.40	-26.08	396	475
12-4-12 + 4 M Urea	2.03	3.70	-25.33	396	475
12-4-12 + 5 M Urea	2.87	2.73	-24.47	396	475
Water	-	-	-	389	489
Methanol	-	-	-	390	475

^a[C-480] = 5 μM , ^b λ_{ex} (C-480) = 375 nm

7.1.2 UV-Visible absorption and steady-state fluorescence study of C-480

UV-Visible absorption and steady-state fluorescence spectra of C-480 have been recorded in presence of aqueous solutions of 10 mM of pure 12-4-12 and 10 mM of 12-4-12 in presence of various concentrations of urea. Figure 7.3 shows the absorption spectra of C-480 in pure 12-4-12 and 12-4-12 + urea at different concentrations. Figure 7.4 shows the fluorescence spectra of C-480 in presence of pure water, aqueous solution of 10 mM of pure 12-4-12 and 10 mM of 12-4-12 + 5M urea as representative spectra. Absorption and fluorescence peak maxima values of C-480 are given in Table 7.1. Absorption and fluorescence peak maxima of C-480 in pure water are observed at 389 nm and 489 nm, respectively. In presence of 12-4-12 and 12-4-12 + urea, the absorption and fluorescence peak maxima of C-480 are different from that in presence of pure water. These observations indicate that microenvironment around C-480 in presence of 12-4-12 and 12-4-12 + urea are different from that in presence of pure water. Fluorescence peak maxima of C-480 in presence of 12-4-12 and 12-4-12 with various concentrations of urea are observed at 475 nm. There is a 14 nm of blue shift (475 nm) as compared to that in pure water (489 nm). The blue shifts in fluorescence peak maxima in micellar media as compared to that in pure water suggest that C-480 feels less polar environment in micellar media than that in pure water.

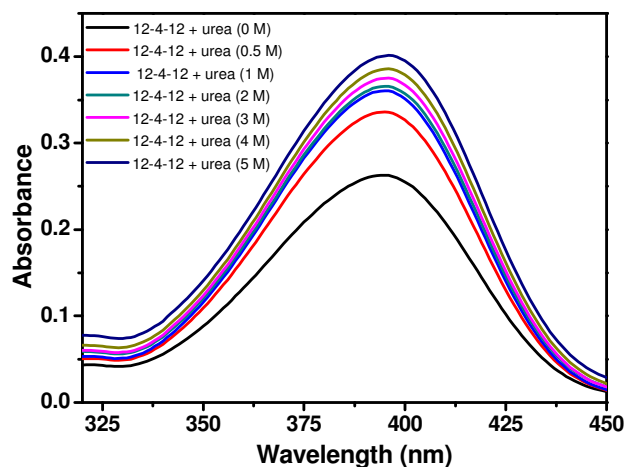


Figure 7.3: Absorption spectra of C-480 in presence of 10 mM of pure 12-4-12 and 10 mM of 12-4-12 + urea at different concentrations. [C-480] = 5 μ M

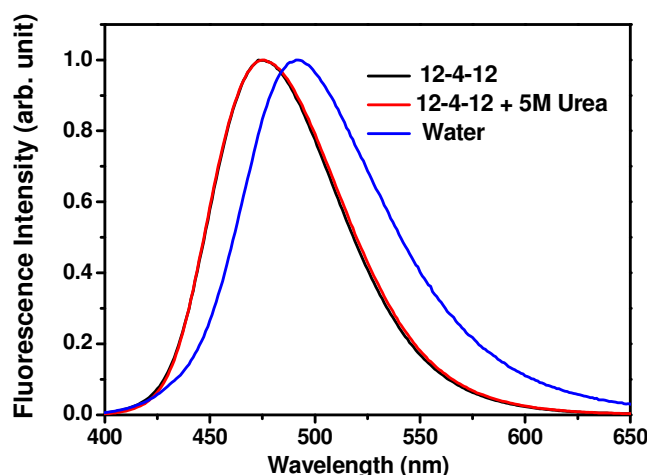


Figure 7.4: Fluorescence spectra of C-480 in presence of water, pure 10 mM of pure 12-4-12 and 10 mM of 12-4-12 + 5 M urea concentration. $[C-480] = 5\mu\text{M}$. $\lambda_{ex} = 375\text{ nm}$

7.1.3 Micropolarity

As explained earlier the micropolarity values expressed in equivalent scale of $E_T(30)$ have been used to get the information about microenvironment around the probe molecule inside the micelles.⁴ To determine the micropolarity around C-480 in various studied systems, the fluorescence behavior of C-480 in presence of pure 12-4-12 and 12-4-12 in presence of various concentration of urea has been compared with that in various compositions of dioxane-water mixtures. Fluorescence energy of C-480 at peak maxima ($\epsilon_{\text{max}}^{\text{fl}}$) after correction of λ^2 factor in different percentage of dioxane-water mixture have been plotted with $E_T(30)$ values of dioxane-water mixture (Figure 7.5). The values of $\epsilon_{\text{max}}^{\text{fl}}$ of C-480 in presence of pure 10 mM of 12-4-12 and also in presence of 10 mM of 12-4-12 with various concentration of urea have been calculated and $E_T(30)$ values have been estimated from Figure 7.5. $E_T(30)$ values for all the systems are found to be $55.6\text{ kcal mol}^{-1}$ since $\lambda_{\text{max}}^{\text{fl}}$ is same for all systems. The calculated $E_T(30)$ values for the investigated systems indicating that micropolarity around C-480 in these systems is lesser than that of water. Fluorescence peak maxima of C-480 and $E_T(30)$ values in 12-4-12 and 12-4-12 + urea are matching with fluorescence peak maximum of C-480 and $E_T(30)$ value in methanol. This again confirms that in presence of gemini surfactant micelles, C-480 neither resides at the core of the micelles nor in the bulk water, but at

the Stern layer of micelles as the polarity of the Stern layer is similar to that of methanol.⁵⁻⁸

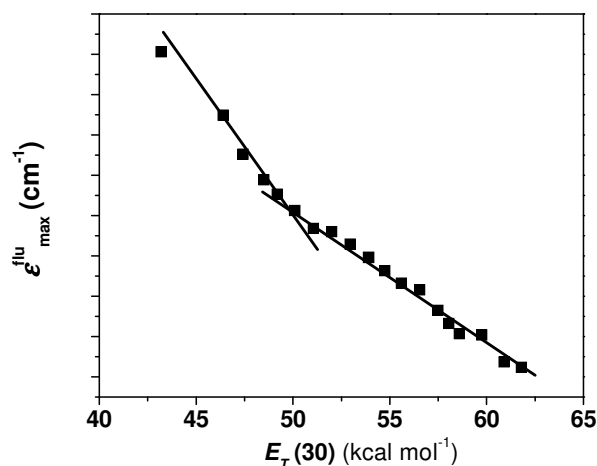


Figure 7.5: Variation of the fluorescence energy at peak maximum ($\epsilon_{\max}^{\text{flu}}$) of C-480 in dioxane-water mixture with $E_T(30)$ of dioxane-water mixture. $[\text{C-480}] = 5\mu\text{M}$. $\lambda_{\text{ex}} = 375\text{ nm}$

7.1.4 Microviscosity

Well known probe molecule, 1,6-diphenyl-1,3,5-hexatriene (DPH) has been used to measure the microviscosity (η_m) of the 10 mM of pure 12-4-12 and 10 mM of 12-4-12 + urea systems by following Debye-Stokes-Einstein relation (Equation 2.11, Chapter 2). The rotational correlation time, τ_r is obtained from Perrin's equation (Equation 2.12, Chapter 2). The method of estimating microviscosity value using DPH has been discussed in Chapter 2. The values of τ_f , r , τ_r and η_m for pure 12-4-12 and in presence of urea are given by Table 7.2. The microviscosity values are decreasing with increasing the amount of urea.⁹ It shows that urea molecule interacts directly with the surfactant headgroups.¹⁰ To further confirm the microenvironmental properties, the probe molecule, DMACA also has been explored. The ultra fast molecular rotators are very sensitive toward the microenvironmental properties.¹² It has been reported that DMACA molecule also resides at the micelle water interface in micellar environment.¹ As mentioned above the steady-state emission spectra of DMACA have been recorded in micellar media in absence and presence of urea and presented by Figure 7.6. With increasing the concentration of urea fluorescence spectra of DMACA shows continuous decrease in intensity without any shift in the fluorescence peak maxima value. Fluorescence intensity of DMACA is decreased due to the decrease in microviscosity around DMACA.¹ No

change in fluorescence peak maxima of DMACA suggests that the micropolarity around the DMACA molecule in micelles is not changing with increasing the concentration of urea. It is also mentioned above that micropolarity sensed by C-480 is not changing with the concentration of urea. Thus, the site where both the probe molecules are located in micellar media, the micropolarity remains unchanged with increasing the concentration of urea. This result also depicts that the microenvironment around both the probe molecules in the micelles is more or less similar.

Table 7.2: Fluorescence anisotropy (r)^a, excited singlet state lifetime (τ_f)^b, rotational correlation time (τ_r) of DPH, microviscosities (η_m) of micelles of 10 mM of pure 12-4-12 and 10 mM of 12-4-12 + urea at various concentrations

Systems	r	τ_f (ns)	χ^2	τ_r (ns)	η_m (mPa s)
12-4-12	0.088	5.41	1.0	1.735	22.9
12-4-12 + 0.5 M Urea	0.079	4.64	1.1	1.286	16.9
12-4-12 + 1 M Urea	0.068	4.56	1.1	1.049	13.8
12-4-12 + 2 M Urea	0.063	4.46	1.0	0.945	12.4
12-4-12 + 3 M Urea	0.060	4.29	1.0	0.845	11.1
12-4-12 + 4 M Urea	0.056	4.20	1.0	0.769	10.1
12-4-12 + 5 M Urea	0.053	4.08	1.0	0.698	9.2

^aFluorescence anisotropy measured at 430 nm. $\lambda_{ex} = 375$ nm. ^b[DPH] = 5 μ M. A solution of DPH was prepared in tetrahydrofuran. ^b $\lambda_{ex} = 375$ nm, $\lambda_{em} = 430$ nm.

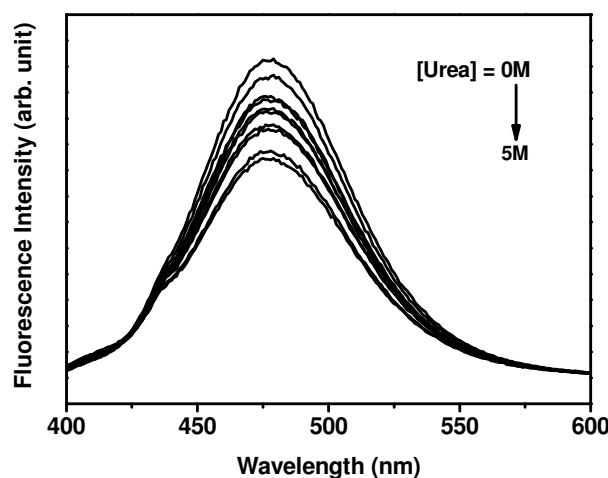


Figure 7.6: Fluorescence spectra of DMACA in presence of 10 mM of 12-4-12 and 10 mM of 12-4-12 in presence of various concentrations of urea. $\lambda_{ex} = 378$ nm, [DMACA] = 5 μ M

The interfacial concentration of urea in micellar medium is increased with increasing the concentration of urea in the bulk.¹² Urea molecules replace the water molecules from the interface of micelles. At a high concentration, urea molecules penetrate to the hydrocarbon core of the micelles. As a result of it with increasing concentration of urea, the micelle structure becomes less compact and rotational restriction around the probe molecule is decreased. Penetration of urea molecules to the hydrocarbon core of the micelles should increase the size of the micelles. To check it the hydrodynamics diameters of micelles in absence and presence of urea have been measured (Figure 7.7 and Table 7.5). Hydrodynamic diameter of the micelle is decreased at 0.5M concentration of urea as compared to that of the micelle in absence of urea. However, above 0.5M concentration of urea, a continuous increase in the hydrodynamics diameter of micelles has been observed. Mahajan *et al.*² also have reported the decrease in hydrodynamics diameter of micelles of gemini surfactant at low concentration range of urea. Raghuraman *et al.*¹³ have studied the effect of urea on TX-100 micelles. Fluorescence anisotropy of DPH in TX-100 aqueous micelles increases with increasing the concentration of urea. However, in the present case of micelles of cationic gemini surfactant, we have seen that the fluorescence anisotropy of DPH progressively decreases with increasing concentration of urea. This may be due to the difference in the nature of surfactant used. The decrease in fluorescence anisotropy and microviscosity with increasing concentration of urea are consistent with the formation of progressively less compact micelles. In case of cationic conventional surfactant also the microviscosity of micelles is decreased with increasing concentration of urea.¹²

Excited singlet state lifetimes of C-480 have been determined in pure solvents water, methanol, cyclohexane and in presence of 10 mM of pure 12-4-12 and 10 mM of 12-4-12 with various concentrations of urea (Table 7.3). The observed lifetime of C-480 in pure water is close to the reported value.¹⁴ The average lifetime of C-480 decreases slowly with increasing the concentration of urea. $E_T(30)$ results show that the micropolarity around C-480 is not changing with the variation of urea concentration. Thus, the variation in the excited state life time of C-480 is only due to the change in microviscosity around C-480 in presence of urea. Although the nature of microenvironment obtained by DPH and DMACA may not be same around C-480, but it clearly reflects the change in microviscosities of 12-4-12 with the addition of urea.

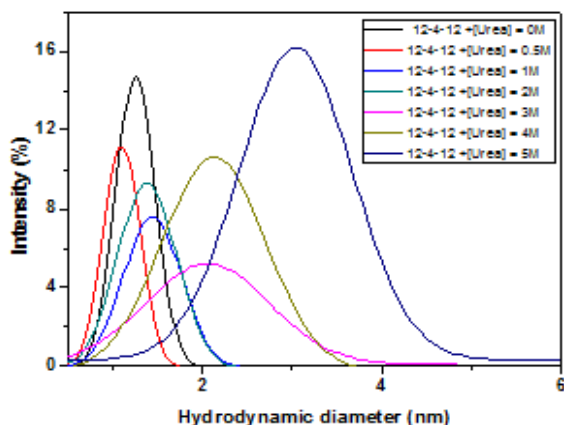


Figure 7.7: Size distribution graph for the micelles of 10 mM of pure 12-4-12 and 10 mM 12-4-12 in presence of various concentration of urea

Table 7.3: Excited singlet state life times (τ_i)^a of C-480 in aqueous solutions of pure 12-4-12 and 12-4-12+ urea

System	a_1	τ_1 (ns)	a_2	τ_2 (ns)	$\langle\tau\rangle$ (ns)
12-4-12	0.10	2.869	0.90	5.884	5.575
12-4-12 + 0.5 M Urea	0.12	2.922	0.88	5.801	5.456
12-4-12 + 1 M Urea	0.09	2.676	0.91	5.711	5.441
12-4-12 + 2 M Urea	0.11	3.074	0.89	5.674	5.383
12-4-12 + 3 M Urea	0.10	2.922	0.90	5.606	5.327
12-4-12 + 4 M Urea	0.13	3.603	0.87	5.526	5.284
12-4-12 + 5 M Urea	0.11	3.199	0.89	5.471	5.232
Water	1.0	5.891			
Methanol	1.0	4.904			
Cyclohexane	1.0	3.130			

^a $\lambda_{ex} = 375$ nm, λ_{em} is fluorescence peak maxima in respective systems, [C-480] = 5 μ M

7.2 Rotational relaxation study

Dynamical behavior of C-480 in micelles of gemini surfactant, 12-4-12 and in presence of various concentration of urea have been characterized. The time dependent fluorescence anisotropies of C-480 have been determined in pure water and in presence of studied micellar systems. In pure water, C-480 shows monoexponential anisotropy decay, whereas in presence of 12-4-12 and with various concentration of urea, the bi-exponential decays have been observed. Figure 7.8 shows the time dependent

fluorescence anisotropy decays of C-480 and Table 7.4 gives rotational relaxation times in various micellar systems.

Rotational relaxation time of C-480 in presence of pure water is found to be 132 ps which is in well agreement with the reported value of 125 ps.¹⁵ Rotational relaxation time of C-480 is many folds slower in micelles than that in pure water. This suggests that random motions of the probe molecule are restricted in micellar medium. The average rotational relaxation time, $\langle\tau_r\rangle$ decreases with increasing the concentration of urea in the micelles which is consistent with the microviscosity values of the micellar systems. The time resolved fluorescence anisotropy of fluorophore molecule gives information about the distribution and/or location of the fluorophore in molecular assemblies. Bi-exponential decays of C-480 in micellar systems might mean that two different distributions of the probe molecules. Fast (τ_{1r}) and slow (τ_{2r}) rotational relaxation times of the probe may be due to free and micelles bound probes, respectively. However, the rotational relaxation times of C-480 in micelles are quite different from that in presence of pure water which rejects this proposition. Another possible reason for the bi-exponential decays of C-480 in micellar systems is due to two different binding sites (headgroup region and core group region) of C-480. The above mentioned steady-state fluorescence and micropolarity results rule out this possibility as well. Higher rotational time of C-480 in micelles than that in pure water indicates that C-480 is bound at Stern layer of the micelles. Actually the bi-exponential anisotropy decays in presence of micelles are due to the different kind of rotational motions of the probe molecule.^{5,6,15,16} These rotational motions can be explained by following the two-step and wobbling in a cone models. According to the two-step model, the slow rotational relaxation time (τ_{2r}) is related to the relaxation time corresponding to the rotational motion of the micelles as a whole (τ_m) and that corresponding to the lateral diffusion (τ_D) of the probe (Section 2.2.12.1 and 2.2.12.2, Chapter 2). Calculated values of τ_m and τ_D are given in Table 7.5. From the data in Table 7.4 and Table 7.5 it can be concluded that the slow rotational motion of C-480 in micelles is due to lateral diffusion of C-480 along the surface of the micelle. τ_D and τ_{2r} values are very close. The rotational motion of the micelle as a whole is significantly higher than the slow rotational motion of the probe. The wobbling motion time (τ_w) has been calculated by using fast (τ_{1r}) and slow (τ_{2r}) components of anisotropy decay of C-480 (Equation 2.40, Chapter 2). Values of τ_w are also given in Table 7.5. The decrease in τ_w with increasing the concentration of urea represents that the local structure

of the environment around the probe molecule becomes less compact with increasing the concentration of urea. The values of wobbling diffusion coefficient (D_w) have been calculated using the equation 2.41 (Chapter 2). Wobbling diffusion occurs due to the wobbling motion of the probe at cone angle θ_0 (Equation 2.38, Chapter 2). Values of D_w , θ_0 , and $|S|$ are summarized in Table 7.5. $|S|$ is measure of spatial restriction. In the present case, the high values of $|S|$ suggest that the restriction is imposed around the probe molecules in the micelles and the surface of micelles is more ordered than core of the micelles.¹⁷ High values of $|S|$ also support the location of the probe molecules at the Stern layer of the micelles.^{5,6}

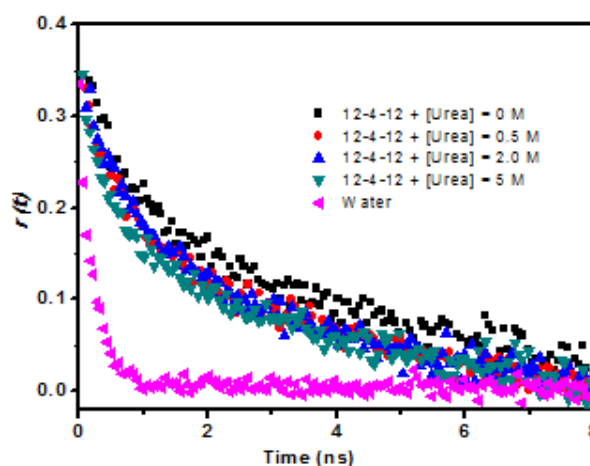


Figure 7.8: Decays of fluorescence anisotropy of C-480 in the pure water, 10 mM of pure 12-4-12 and 10 mM of 12-4-12 in presence of various concentration of urea. $\lambda_{ex} = 375$ nm, $\lambda_{em} = 475$ nm

Table 7.4: Rotational relaxation times of C-480 in aqueous solution of 10 mM 12-4-12 and 10 mM 12-4-12 + urea at various concentrations

Systems	a_1	τ_{1r} (ns)	a_2	τ_{2r} (ns)	$\langle\tau_r\rangle$ (ns)
12-4-12	0.66	0.339	0.34	3.423	1.387
12-4-12 + 0.5 M Urea	0.63	0.301	0.37	2.522	1.122
12-4-12 + 1 M Urea	0.62	0.292	0.38	2.359	1.077
12-4-12 + 2 M Urea	0.58	0.287	0.42	1.939	0.981
12-4-12 + 3 M Urea	0.61	0.267	0.39	1.831	0.876
12-4-12 + 4 M Urea	0.62	0.247	0.38	1.766	0.824
12-4-12 + 5 M Urea	0.57	0.231	0.43	1.523	0.786

Table 7.5: Hydrodynamic radius (r_h), lateral diffusion time (τ_D), time for rotational motion of the micelle as a whole (τ_m), wobbling motion time (τ_w), wobbling diffusion coefficient (D_w), cone angle (θ_0) and order parameter ($|S|$) obtained from the anisotropy decays of C-480 in different systems

Systems	r_h (nm)	τ_m (μ s)	τ_w (ns)	τ_D (ns)	θ_0 (deg)	S	$D_w \times 10^{-8}$ (s^{-1})
12-4-12	0.625	0.221	0.376	3.477	46.36	0.58	5.076
12-4-12 + 0.5 M Urea	0.550	0.151	0.342	2.565	44.68	0.61	5.189
12-4-12 + 1 M Urea	0.690	0.298	0.333	2.376	44.13	0.62	5.192
12-4-12 + 2 M Urea	0.720	0.338	0.337	1.950	41.97	0.65	4.646
12-4-12 + 3 M Urea	1.038	1.017	0.313	1.834	43.58	0.62	5.399
12-4-12 + 4 M Urea	1.066	1.101	0.287	1.769	44.13	0.62	6.025
12-4-12 + 5 M Urea	1.521	3.197	0.272	1.524	41.44	0.65	5.604

7.3 Solvation dynamics

Solvation dynamics of C-480 in the micelle of 10 mM of pure 12-4-12 and in 10 mM of 12-4-12 in presence of various concentration of urea have been studied. The time resolved fluorescence decays of C-480 in presence of different concentration of urea in micelles of 12-4-12 have been recorded. In these systems, C-480 shows emission wavelength dependent decays. Wavelengths are chosen from the entire steady-state spectra of C-480 (Figure 7.4). Figure 7.9 shows the emission wavelength dependent decays of C-480 in 12-4-12 (10mM) + 5M urea as representative one. A fast decay is observed at short wavelength (455nm). At higher wavelength (565nm), fluorescence decay shows a clear growth in the spectra. Growth in the decay indicates the solvation of the probe molecule in the excited state. At short wavelength, the decay is fitted bi-exponentially with two components of excited state lifetimes. Similar behaviors have also been observed in 12-4-12 + urea at various concentrations. The observed wavelength dependent decays are for the probe molecules located at the Stern layer of the micelles.^{5,6,18} Reason is that in the bulk water, the wavelength dependent decays are too fast to be measured by our instrument (FWHM = \sim 165 ps). Probe molecules present in the hydrocarbon core of the micelles should not show wavelength dependent decays.^{5,6} Hence, the observed time dependent Stokes shift is only due to the probe molecules present in the Stern layer of the micelles.

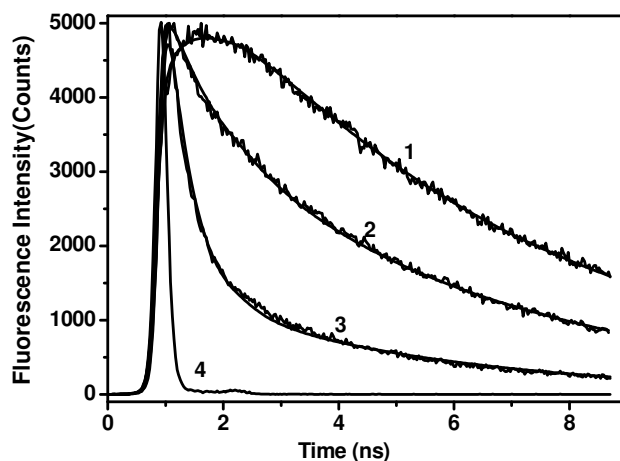


Figure 7.9: Time-resolved fluorescence decays of C-480 in 12-4-12 ([12-4-12] = 10 mM) + 5 M urea concentration. 1 to 3 at 565 nm, 515 nm, 455 nm, respectively and 4 for instrument response function

Time resolved emission spectra (TRES) have been constructed by following the method of Fleming and Maroncelli.¹⁹ The dynamic Stokes shifts in the emission spectra of C-480 have been observed in all the studied systems. Figure 7.10 shows the time resolved emission spectra of C-480 in presence of 10 mM 12-4-12 and 5 M urea as representative spectra. Solvent response function (SRF), $C(t)$ have been used to monitor the dynamics of solvent. Figure 7.11 shows the plot of $C(t)$ with time in various systems. The decays of $C(t)$ are found to be bi-exponential in nature. Solvation time constant are given in Table 7.6. In presence of pure 12-4-12 and 12-4-12 with various concentrations of urea, the solvation response time constants are bimodal (slow and fast components) in nature. The bimodal behaviors of solvation in the microheterogeneous systems arise due to the presence of free and bound water molecules.²⁰ While the free water molecules are responsible for the fast solvation, the bound water molecules are responsible for slow solvation. Polar headgroups, counterions and spacer group of 12-4-12 can be responsible for the slow solvation. However in gemini surfactant, the polar headgroups are connected to the long hydrocarbon tails and the spacer group. That is why the mobility of the polar headgroups are restricted to a large extent and it has been reported that the dynamics of polymer chain occur on very slow time scale (~ 100 ns) because of the same reason.^{5-7,}

21,22

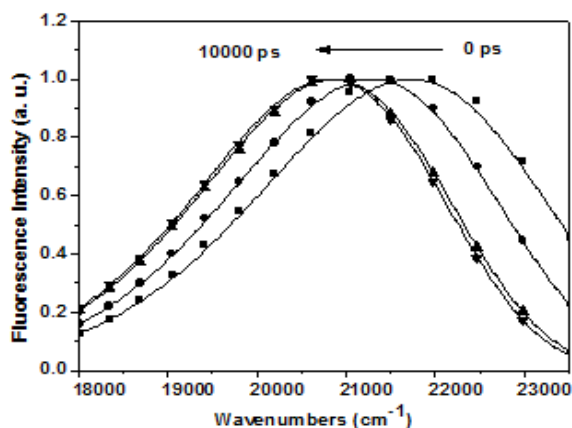


Figure 7.10: Time resolved emission spectra of C-480 in 12-4-12 + urea ([12-4-12] = 10 mM, [Urea] = 5 M) (from right to left) 0 ps, 500 ps, 5000 ps, and 10000 ps

It is evident from the data in Table 7.6 that the solvation dynamics depends on the concentration of urea. Increasing the concentration of urea upto 1 M, the solvation time for the slower component decreases, but solvation time for the fast component do not show any order. The observed decrease in solvation time for the slow component at low concentration range of urea indicating that the urea molecules replace the water molecules from the headgroup region of the gemini surfactant in the micelles instead of making hydrogen bonds with water.² This increase in the number of bulk type water molecules in the solution and the collective response from the water molecules away from probe molecule contributes to the fast solvation component. Sarkar *et al.*¹⁶ have studied the solvation dynamics in the mixture of conventional surfactant and ionic liquid. The rate of solvation dynamics decreases with increasing the concentration of ionic liquid. They have reported that decrease in solvation time is due to the decrease in microviscosity value with increasing the concentration of ionic liquid. It is noteworthy that the microviscosity decreases in our case as well with increasing the concentration of urea.

Table 7.6: Decay characteristic of solvent correlation function, $C(t)$ of C-480 in presence of various systems

Systems	a_{1s}	τ_{1s} (ns)	a_{2s}	τ_{2s} (ns)	$\langle\tau_s\rangle$ (ns)
12-4-12	0.74	0.523	0.26	3.765	1.366
12-4-12 + 0.5 M Urea	0.77	0.461	0.23	3.622	1.188
12-4-12 + 1 M Urea	0.75	0.575	0.25	3.049	1.193
12-4-12 + 2 M Urea	0.75	0.567	0.25	4.888	1.647
12-4-12 + 3 M Urea	0.74	0.581	0.26	4.897	1.654
12-4-12 + 4 M Urea	0.72	0.685	0.28	5.338	1.988
12-4-12 + 5 M Urea	0.74	0.578	0.26	5.405	1.833

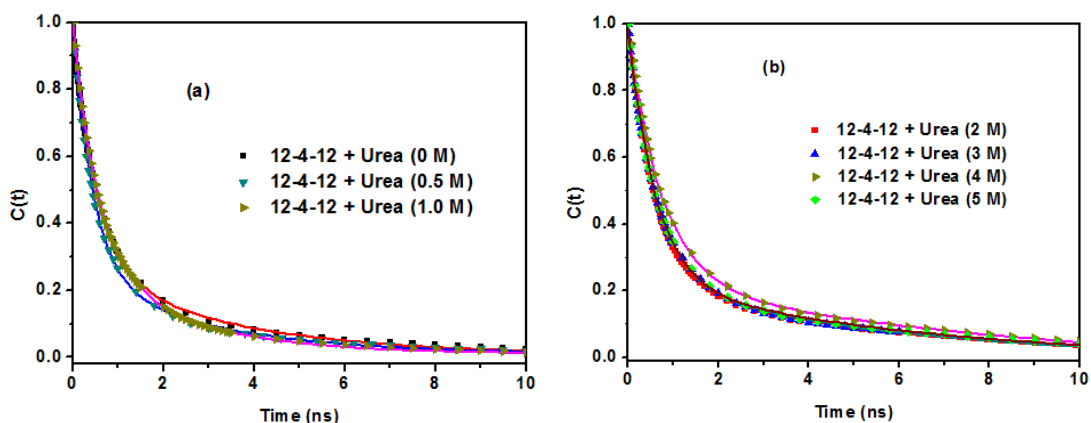


Figure 7.11: Decays of solvent correlation function, $C(t)$ of C-480 in the micelles of 12-4-12 in presence of various concentration of urea

Another possible mechanism of reduction of solvation time of water in the investigated system is the tetrahedral water structure breaker nature of urea. In case of pure 12-4-12 micelles solvation time for slow component is 3.765 ps. However, at 1M urea concentration the solvation time is decreased to 3.049 ps. This decreased in solvation time indicates that the urea molecule break the tetrahedral structure of water. Urea molecules occupy the tetrahedral vertices in the tetrahedral structure of water by replacing the water molecules. The breaking of the tetrahedral structure of water results in the increase in the number of free water molecules because of that the solvation time of C-480 is reduced. Choudhury *et al.*²³ in their molecular dynamics simulation study have shown that urea molecules do not break the tetrahedral structure of water. Contrary to their study our study shows the possibility of displacement of water molecule from tetrahedral structure. Ultrasonic attenuation measurements study have shown the reduction in relaxation time between 2M to 4M urea concentration due to the breakdown of the water structure around the polymer.²⁴ Raman band analysis and NMR analysis have also indicated the urea to be a water structure breaker.^{25,26}

From 2M to 5M urea concentration region, the solvation time for the slow component increases. However, the solvation time for the fast component remains almost same. The weightage of the slow component is lesser than that of faster component. The enhancement in the solvation time at this concentration range of urea indicates that the urea molecules are making hydrogen bonds with the water

molecules. Kumbhakar *et al.*²⁷ have studied the effect of concentration of Li⁺ ion on solvation dynamics. At low concentration of Li⁺ ions, the solvation time for the slow component decreases and at high concentration of Li⁺ ions the solvation time increases for both slow and fast components. They have reported that at a higher concentration, Li⁺ ions occupy effectively at the available binding sites and remaining Li⁺ are strongly hydrated. Similarly in our case at a concentration higher than 1M, urea molecules replace the water molecules from the headgroups of gemini surfactant and after saturation of headgroups of gemini surfactant, urea molecules form hydrogen bonds with water molecules.²⁸ Rezus *et al.*²⁸ reported that two types of water molecules exist in urea-water mixture. These are bulk-like water molecules and strongly immobilized water molecules. Immobilized water molecules are due to formation of hydrogen bond with urea. Enhancement in the solvation time for the slow component is due to hydrogen bonded water molecules with urea. At a high urea concentration, the water molecules become the part of urea solvation shell. Molecular, dynamics simulation study shows that at a high concentration of urea five to seven water molecules are hydrogen bonded with urea.²⁹ Quantum chemical study shows that due to the right size of water molecule it form simultaneously two hydrogen bonds with urea. One hydrogen bond is with the carbonyl oxygen of urea and, other hydrogen bond accepted from cis hydrogen.³⁰ This study also supports the observed slow solvation dynamics in the present case. At 4M and 5M urea concentration the increase in solvation time for slower component is little higher than the solvation times at 2M and 3M urea concentration. This increase in solvation time is due to the contribution of dynamics of urea molecules themselves.³¹ Solvation dynamics study shows that urea molecules interact directly as well as indirectly with the water molecule. This study would be useful to understand the urea induced denaturation of protein because same basic intermolecular and ionic forces control both surfactant aggregates and protein stabilities.^{32,33}

7.4 Conclusions

Cmc value of gemini surfactant, 12-4-12 in aqueous medium increases with increasing concentration of urea. Increasing the concentration of urea enhances the solubility of gemini surfactant in aqueous solution. The value of mole fraction partition coefficient of detergent from aqueous phase to micellar phase (K^{mic}) decreases with

increasing the concentration of urea. The standard molar Gibbs free energy upon micellization ($\Delta G^{\circ, \text{mic}}$) increases with increasing the concentration of urea which shows that micellization process becomes less feasible with increasing the concentration of urea. C-480 probe molecules reside at the Stern layer of micelles of 12-4-12. The micropolarity of environment around C-480 in micelles in absence and in presence of urea expressed in equivalent scale of $E_T(30)$ is $55.6 \text{ kcal mol}^{-1}$ which is close to that of methanol. Microviscosity around C-480 decreases with increasing the concentration of urea. Anisotropy decays of C-480 are bi-exponential in nature because of various kinds of rotational motions. The slow relaxation in micellar media is due to the lateral diffusion of the fluorophores. Lateral diffusion of the fluorophore in the micelles is much faster than the rotational motion of the micelle as a whole. The lateral diffusion process also correlates well with the microviscosity of micelles. Effective relaxation time decreases with increasing the concentration of urea. Solvation time is bimodal in nature in absence and presence of urea. Water molecules bonded to counterions are responsible for the slow solvation time. At low concentration of urea the solvation time is decreased as compared to that in the absence of urea. The solvation time decreases due to the breaking of the hydrogen bonded tetrahedral structure of water by urea. Solvation time increases at higher concentration of urea. The enhancement in the solvation time is due to hydrogen bonding of water molecule with urea and solvation by urea molecule themselves.

References:

- (1) Sonu, A. K. Tiwari, S. K. Saha. *Ind. Eng. Chem. Res.* **2013**, *52*, 5895.
- (2) R. K. Mahajana, R. Kaur, V. K. Aswal. *Colloids and Surfaces A: Physicochem. Eng. Aspects* **2013**, *419*, 61.
- (3) J. Broecker, S. Keller, *Langmuir* **2013**, *29*, 8502.
- (4) C. Reichardt, *Chem. Rev.* **1994**, *94*, 2329.
- (5) A. K. Tiwari, Sonu, S. K. Saha. *J. Phys. Chem. B.* **2014**, *118*, 3582.
- (6) Sonu, S. Kumari, S. K. Saha. *J. Phys. Chem. B.* **2015**, *119*, 9751.
- (7) Sonu, S. Kumari, S. K. Saha, *Phys.Chem.Chem.Phys.* **2016**, *18*, 1551.
- (8) A. Mallick, B. Haldar, S. Maiti, S. C. Bera, N. Chattopadhyay. *J. Phys. Chem. B.* **2005**, *109*, 14675.

-
- (9) P. Alexandridis, V. Athanassiou, T. A. Hatton. *Langmuir* **1995**, *11*, 2442.
- (10) C. C. Ruiz, F. G. Sanchez, *J. Colloid Interface Sci.* **1994**, *165*, 110.
- (11) T. Asakawa, M. Hashikawa, K. Amada, S. Miyagishi. *Langmuir* **1995**, *11*, 2376.
- (12) L. S. Romsted, J. Zhang. *Langmuir* **2003**, *19*, 9179.
- (13) H. Raghuraman, S. K. Pradhan, A. Chattopadhyay. *J. Phys. Chem. B.* **2004**, *108*, 2489.
- (14) G. Jones, W. R. Jackson, C. Y. Choi, W. R. Bergmark. *J. Phys. Chem.* **1985**, *89*, 294.
- (15) D. Chakrabarty, A. Chakraborty, D. Seth, P. Hazra, N. Sarkar. *J. Chem. Phys.* **2005**, *122*, 184516.
- (16) R. Pramanik, S. Sarkar, C. Ghatak, V. G. Rao, S. Mandal, N. Sarkar. *J. Phys. Chem. B.* **2011**, *115*, 6957.
- (17) G. B. Dutt, *J. Phys. Chem. B.* **2002**, *106*, 7398.
- (18) V. G. Rao, C. Banerjee, S. Mandal, S. Ghosh and N. Sarkar. *Spectrochim. Acta, Part A.* **2012**, *120*, 371.
- (19) M. Maroncelli, G. R. Fleming. *J. Chem. Phys.* **1987**, *86*, 6221.
- (20) N. Nandi, B. Bagchi. *J. Phys. Chem. B.* **1997**, *101*, 10954.
- (21) N. Sarkar, A. Datta, S. Das, K. Bhattacharyya. *J. Phys. Chem.* **1996**, *100*, 15483.
- (22) R. Dutta, M. Chowdhury, M. A. Winnik. *Polymer*, **1995**, *36*, 4445.
- (23) D. Bandyopadhyay, S. Mohan, S. K. Ghosh, N. Choudhury. *J. Phys. Chem. B.* **2014**, *118*, 11757.
- (24) G. G. Hammes, P. R. Schimme. *J. Am. Chem. Soc.* **1967**, *89*, 442.
- (25) G. E. Walrafen. *J. Chem. Phys.* **1966**, *44*, 3726.
- (26) A. Sacco, M. Holz. *J. Chem. Soc., Faraday Trans.* **1997**, *93*, 1101.
- (27) M. Kumbhakar, T. Goel, T. Mukherjee, H. Pal. *J. Phys. Chem. B.* **2005**, *109*, 18528.
- (28) Y. L. Rezus, H. Bakker. *J. Proc. Natl. Acad. Sci.* **2006**, *103*, 18417.
- (29) B. Kallies. *Phys Chem Chem Phys.* **2002**, *4*, 86.
- (30) C. Lee, E. A. Stahlberg, G. Fitzgerald. *J Phys Chem.* **1995**, *99*, 17737.
- (31) A. Sengupta, R. V. Khade, Partha Hazra. *J. Phys. Chem. A.* **2011**, *115*, 10398.
- (32) A. Wallqvist, D. G. Covell, D. Thirumalai. *J. Am. Chem. Soc.* **1998**, *120*, 427.
- (33) P. Baglioni, E. Ferroni, L. Kevan, *J. Phys. Chem.* **1990**, *94*, 4296.

Chapter 8

Study on intramolecular charge transfer processes, solvation dynamics and rotational relaxation of Coumarin 490 in reverse micelles of cationic gemini surfactant*

In this chapter intramolecular charge transfer processes, solvation dynamics and rotational relaxation of Coumarin 490 (C-490), (Scheme 2.1) have been studied in presence of cationic gemini surfactant, 12-4-12/ cyclohexane/*n*-pentanol/water reverse micelles (RMs). C-490 resides in the water pool of RMs. A lesser extent of hydrogen bonding interactions between –OH group of alcohol and C-490 molecule takes place at the interface of present RMs as compared to RMs of reported conventional cationic surfactants. C-490 migrates to the water pool with increasing content of water molecules. As a result of this, the steady-state fluorescence properties, rotational relaxation and solvation dynamics results depend on the water loading of RMs unlike RMs of conventional cationic surfactants. Because of the same reason, the solvation dynamics in gemini surfactant RMs is one order of magnitude faster as compared to RMs of conventional cationic surfactants. The faster solvation dynamics in gemini surfactant RMs as compared to reported AOT RMs is due to the absence of hydrogen bonding interaction between water molecules and quaternary ammonium headgroups of gemini surfactant. The polarity of the surrounding microenvironment is found to have very little effect on the rates of non-radiative processes in the water pool of gemini surfactant RMs. The rates of non-radiative processes in the present RMs are found to be higher than that in reported AOT RMs.

8.1 Results and discussions

8.1.1 UV-Visible absorption spectra

UV-Visible absorption spectra of C-490 have been measured in pure solvents, CHX (Cyclohexane) + *n*-pentanol (2.4%) mixed solvent (mentioned as bulk solvent hereafter) and in RMs systems. The absorption peak maxima values are tabulated in Table 8.1. The representative absorption spectra of C-490 in bulk solvent, pure water and RMs are shown by Figure 8.1.

* Sonu, Amit K. Tiwari, Sunita Kumari, Subit K. Saha. *RSC Adv.*, **2014**, *4*, 25210.

In bulk solvent, a broad peak observed at 356 nm. In pure water, the peak maximum appears at 366 nm which is 10 nm red-shifted with respect to that in bulk solvent and 16 nm blue-shifted with respect to that in pure *n*-pentanol. This blue shift in the absorption spectra of C-490 in water is due to intermolecular hydrogen bonding interactions between water molecules and at several positions of C-490. This behavior is common in the ICT molecule.¹⁻⁴ On addition of 20 mM of 12-4-12 gemini surfactant to the bulk solvent, RMs are formed.⁵ There is a remarkable red-shift of absorption band of C-490 to 387 nm as peak maximum with increase in absorbance in RMs with respect to that in bulk solvent (peak maximum at 356 nm). With the addition of water in RMs, there is a blue shift in peak maximum by 2 nm with the decrease in absorbance at 356 nm. This observation indicates that C-490 molecules are getting localised in the pool of RMs. At $w_o = 0$ and 30, the absorption peak maxima for C-490 are 387 nm and 385 nm, respectively those are significantly different from that in pure water (peak maximum 366 nm). It implies that the microenvironment around C-490 in RMs is different from that in bulk water.

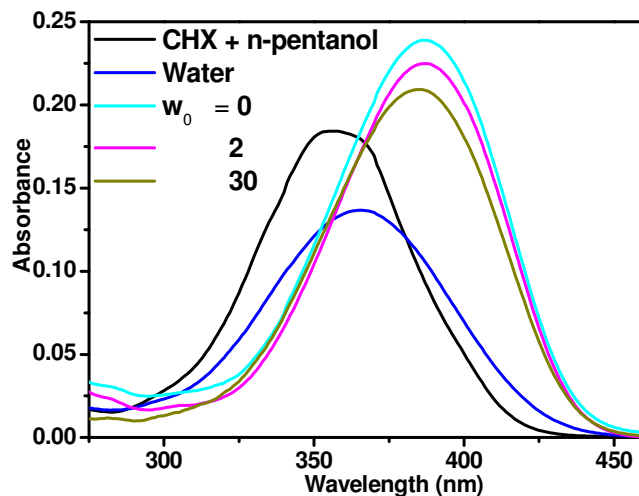


Figure 8.1: UV-Visible absorption spectra of C-490 in water, CHX + *n*-pentanol (2.4%) mixed solvent (bulk solvent) and in RMs systems

Table 8.1: Absorption and fluorescence peak maxima of C-490 in pure solvents, mixed solvent and in RMs systems, and $E_T(30)$

Systems	λ_{max}^{abs} (nm)	λ_{max}^{fl} (nm) ^a	λ_{max}^{fl} (nm) ^b	$E_T(30)$ (kcal mol ⁻¹)
CHX + n-pentanol (2.4%)	356	457	460	39.8
n-pentanol	382	477	478	49.1
Water	366	496	498	63.1
$w_o = 0$	387	474	477	47.3
$w_o = 2$	387	477	480	48.7
$w_o = 20$	385	482	485	51.3
$w_o = 25$	385	482	485	51.3
$w_o = 30$	385	482	485	51.3

^a $\lambda_{exc} = 375$ nm, ^b $\lambda_{exc} = 412$ nm

8.1.2 Steady-state fluorescence spectra

Steady-state fluorescence spectra of C-490 in the above mentioned systems have been recorded and fluorescence peak maxima data are given in Table 8.1. Figures 8.2a and 8.2b are the representative fluorescence spectra of C-490 in bulk solvent, pure water and in RMs at $\lambda_{exc} = 375$ nm and 412 nm, respectively. When C-490 is excited at 375 nm, the peak maximum for fluorescence band in the bulk solvent appears at 457 nm. On addition of 20 mM ($w_o = 0$) of 12-4-12 gemini surfactant to the bulk solvent, the fluorescence band is red-shifted remarkably with peak maximum at 474 nm as compared to bulk solvent. Fluorescence intensity is lower than that in the bulk solvent. On addition of water to the RMs there are red-shifts in fluorescence band maxima with decrease in fluorescence intensity at 457 nm. The fluorescence peak maxima in RMs at $w_o = 0$ and 30 are at 474 nm and 482 nm, respectively and in pure water it is at 496 nm. Thus, fluorescence results also imply that with increasing the water content from $w_o = 0$ to 30, the probe molecules start residing in the pool of RMs and the microenvironment around the probe molecules is different from that in bulk water.

To see the effect of excitation wavelength on the fluorescence properties, the fluorescence spectra have also been recorded at $\lambda_{exc} = 412$ nm (Figure 8.2b). At this excitation wavelength, molecules residing in the pool of RMs are mostly excited. Therefore, emission characteristics reflect the properties of probe molecules entrapped in

the pool of the RMs only⁶. It can be seen from Figure 8.2b that the fluorescence intensities of C-490 in all the RMs are much higher than that in the bulk solvent. The fluorescence peak maxima in all systems are approximately red-shifted by 2-3 nm as compared to excitation at 375 nm. These results indicate that the probe molecules are partitioned to the interior of the RMs. Figure 8.3 displays the excitation spectra of C-490 in RMs at $w_o = 30$ monitored at two different emission wavelengths, 435 nm and 550 nm. The excitation spectrum monitored at 435 nm emission wavelength resembles with the absorption spectrum of C-490 in bulk solvent while the spectrum at 550 nm resembles with the absorption spectrum of C-490 at $w_o = 30$. These observations further depict that C-490 molecules are located at two different environments in the RMs.⁶⁻⁸

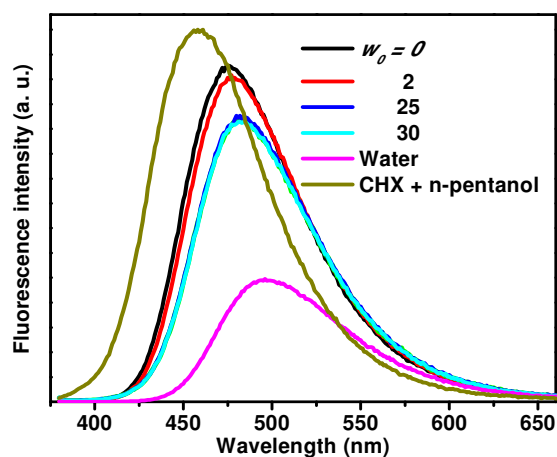


Figure 8.2(a): Steady-state fluorescence spectra of C-490 in water, bulk solvent and in RMs systems. $\lambda_{exc} = 375$ nm

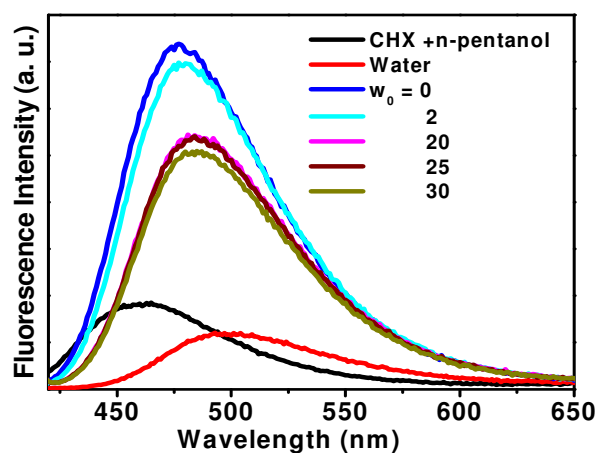


Figure 8.2(b): Steady-state fluorescence spectra of C-490 in water, bulk solvent and in RMs systems. $\lambda_{exc} = 412$ nm

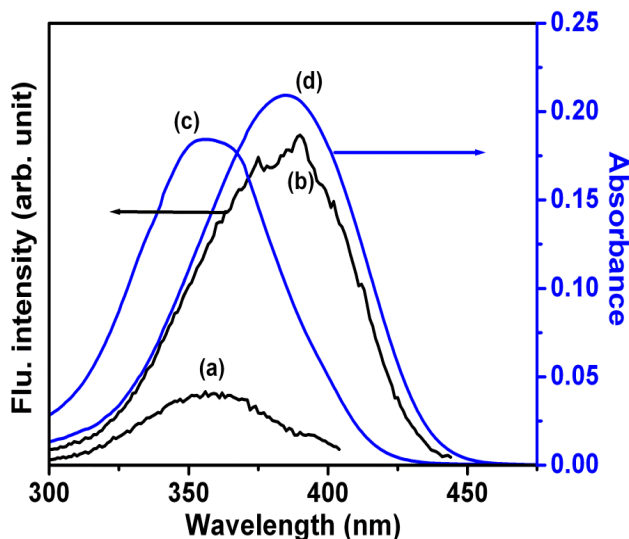


Figure 8.3: Excitation spectra of C-490 recorded in $w_o = 30$ and monitored at (a) $\lambda_{\text{ems}} = 435$ nm, (b) 550 nm and absorption spectra of C-490 in (c) bulk solvent and (d) $w_o = 30$

A red-shift in fluorescence peak maximum and a gradual decrease in fluorescence intensity have been observed with increase in w_o from 0 to 30. Of course it does not change significantly with changing water content in the RMs pool. Hazra *et al.*⁷ studied the RMs of conventional surfactants using Coumarin 480 (C-480) as a probe. They noticed the location of probe molecules at the interface of RMs of cationic surfactant, CTAB. Different location of C-490 as compared to C-480 is because of the fact that the latter is a much more hydrophobic probe with a tertiary amine substituent that is not a hydrogen bond donor. However, C-490 is having a primary amine substituent which is a hydrogen bond donor. The red shift of fluorescence band is due to the stabilization of the emitting state as a result of increase in the static polarity of the pool of RMs with increasing water content and decrease in intensity is due to increase in the rate of non-radiative processes in more polar environment of the pool. Nature of water molecules becoming more of bulk water with increasing number of water molecules in the RMs pool.⁹ The decrease in intensity can be explained by introducing the model, suggested by Jones II *et al.*^{10,11} In 7-aminocoumarin derivatives, a planer highly fluorescent ICT excited state deactivates to a non-fluorescent twisted intramolecular charge transfer (TICT) state.^{12,13} The conversion of ICT to a TICT state depends on the static polarity of the environment and conversion becomes feasible with increase in the polarity of the medium.^{8,14,15} Fluorescence intensity decreases with increasing polarity of the

environment as a result of increasing population of TICT state. In C-490 also the main non-radiative path for ICT is the generation of TICT state.⁸ Hazra *et al.*⁸ also observed red shifted fluorescence spectra with decrease in intensity in AOT RMs for C-490.

8.1.3 Micropolarity and microviscosity

To have the idea about the microenvironment of C-490 mostly entrapped in the pool of RMs, the micropolarity expressed in equivalent scale of $E_T(30)$ ^{17,18} have been determined. The fluorescence spectra of C-490 in different percentage of dioxane-water mixture have been recorded at $\lambda_{exc} = 412$ nm. The fluorescence peak maxima of C-490 in dioxane-water mixture of various compositions are plotted against $E_T(30)$ ^{10,16} (Figure 8.4). Using this plot and fluorescence peak maxima value of C-490 in different RMs, the micropolarities in terms of $E_T(30)$ have been calculated and given in Table 8.1. For the calculation of $E_T(30)$, the λ_{max}^{fl} values obtained after excitation at 412 nm have been considered to make sure that the probe molecules residing in the pool of RMs are only emitting. One can see that the $E_T(30)$ values for the RMs systems are lesser than the $E_T(30)$ of water. This indicates that the average microenvironment of the probe molecules is less polar than that of bulk water. At $w_0 = 30$, the $E_T(30)$ value is close to that of ethanol [$E_T(30) = 51.9$ kcal mol⁻¹].¹⁷ This result implies that the probe molecules are mostly located in the water pool of the RMs. Little lower polarity found as compared to AOT RMs^{2,7} is due to the presence of some probe molecules in the bulk solvent.

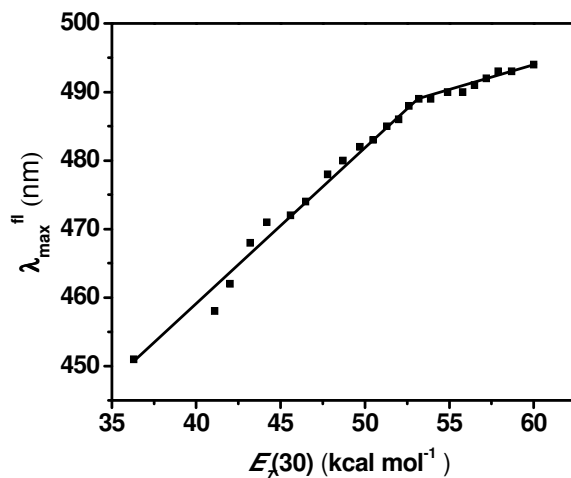


Figure 8.4: Plot of fluorescence peak maxima of C-490 in different percentage of dioxane-water mixture

The steady-state fluorescence anisotropies of C-490 in all the RMs systems have been determined. The steady-state anisotropy values of C-490 in all the RMs systems are shown by Figure 8.5. With increase in w_0 , the steady-state anisotropy gradually decreases. It indicates that the microenvironment around the C-490 becomes less rigid with increasing water content in RMs. In the RMs of cationic gemini surfactant, Zhao *et al.*⁹ observed that with increasing w_0 the number of bulk like water per surfactant rapidly increases. As a result of that RMs swell. At higher w_0 , there is a decrease in the microviscosity of the environment around C-490 which is reflected by lowering of steady-state anisotropy values. An increase in the polarity and a decrease in the microviscosity of environment around C-490 for changing w_0 from 0 to 30 indicate that the probe molecules are getting entrapped in the water pool of the RMs.

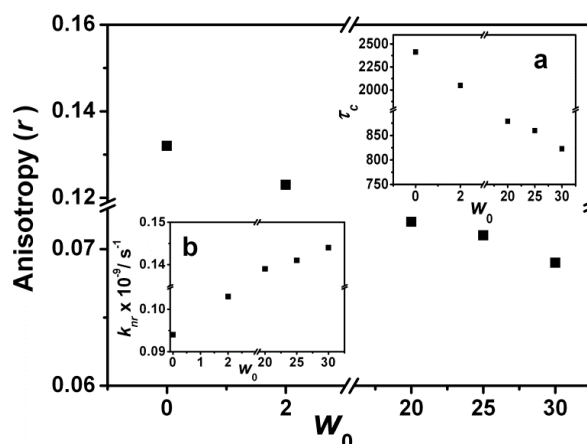


Figure 8.5: Steady-state fluorescence anisotropy (r) of C-490 vs w_0 . Inset (a) plot for average rotational correlation times (τ_c) vs w_0 and (b) non-radiative rate constant (k_{nr}) vs w_0 . $\lambda_{exc} = 375 \text{ nm}$

The average rotational correlation times for C-490 in RMs with increasing w_0 have been calculated by using Perrin's equation (Equation 2.12, Section 2.2.6, Chapter 2). It ensures that the observed change in the steady-state anisotropy of C-490 with increasing w_0 is not due to any change in lifetime. We can approximately use the Perrin's equation by using mean fluorescence lifetime since this equation is not strictly valid in heterogeneous media.^{19,20} Using the above mentioned equation the rotational correlation times have been determined at different w_0 values. It can be seen from the inset of Figure 8.5 that the rotational correlation time decreases with increasing w_0 . This result clearly indicates that the observed change in steady-state anisotropy is not due to any lifetime-induced artifacts. The decrease in rotational correlation time with increasing w_0 supports our above mentioned conjecture that the

rotational restriction experienced by C-490 molecule is reduced with increasing w_0 . Mallick *et al.*¹⁹ also observed the decrease in rotational correlation times with increase in hydration in AOT RMs using 3-acetyl-4-oxo-6,7-dihydro-12*H*-indolo-[2,3-*a*] quinolizine (AODIQ) probe molecule.

8.2 Excited singlet state lifetime

8.2.1 Radiative and non-radiative rate constants in RMs

In case of ICT type of molecular rotors due to the existence of TICT state, the rates of non-radiative (k_{nr}) processes increase with increase in the polarity of the medium as a result of greater extent of stabilization of the TICT state.⁷ The rates of radiative (k_r) and non-radiative (k_{nr}) processes for C-490 in RMs have been calculated using Equations 2.16 and 2.17, respectively (Section 2.2.8, Chapter 2). The rates for non-radiative decay processes increase for RMs with $w_0 = 0$ to $w_0 = 20$ and beyond that rates remain unchanged. It has been stated above that the steady-state emission spectra of C-490 show bathochromic shift with increase in the water content of RMs. Quantum yield (ϕ_f) decreases with increasing water content of the RMs (Table 8.2). With increasing water content, the probe molecule, C-490 experiences more polar environment in the water pool of RMs and the excited singlet state gets stabilized. As a result of this the rates for non-radiative processes increase.¹⁴ However, the change in the rates for non-radiative processes is not much sensitive to the polarity of the environment as reported by Hazra *et al.*⁸ as well. The rates for non-radiative processes in this gemini surfactant RMs are found to be almost doubled as compared to AOT RMs.⁸

Table 8.2: Fluorescence quantum yield (ϕ_f), excited singlet state lifetimes (τ_i), radiative (k_r) and non-radiative (k_{nr}) rate constants of C-490 in different systems

Systems	ϕ_f	τ_1 (ns)	a_1	τ_2 (ns)	a_2	$\langle \phi \rangle$ (ns)	$k_r \times 10^9$ (s ⁻¹)	$k_{nr} \times 10^9$ (s ⁻¹)	χ^2
CHX+ <i>n</i> -pentanol	0.604	2.670	0.20	4.990	0.80	4.520	0.133	0.088	1.05
$w_0 = 0$	0.610	3.690	0.27	4.347	0.73	4.169	0.146	0.094	1.08
$w_0 = 2$	0.594	2.950	0.15	4.127	0.85	3.950	0.150	0.103	1.05
$w_0 = 20$	0.511	2.680	0.21	3.738	0.79	3.516	0.145	0.139	1.03
$w_0 = 25$	0.504	2.675	0.24	3.761	0.76	3.500	0.144	0.141	1.06
$w_0 = 30$	0.499	2.188	0.13	3.662	0.87	3.470	0.143	0.144	1.07
Water	0.266	4.560	1.00	-	-	4.560	0.058	0.161	1.02

λ_{exc} for both steady-state and time resolved = 375 nm. Lifetime measured at λ_{max} [†]

8.3 Time-resolved fluorescence anisotropy

To have further and more accurate information about the microenvironment surrounding the probe molecule in RMs, the time-resolved fluorescence anisotropy measurements have been done. The rotational relaxation time of C-490 in RMs has been calculated using Equation 2.33 (Section 2.2.11, Chapter 2) by monitoring fluorescence intensity at 477 nm (Table 8.3). The time resolved fluorescence anisotropy decays are shown by Figure 8.6. The anisotropy decay in the pure solvents is fitted by single exponential decay function and in all the RMs systems it is bi-exponential. The relaxation process is much slower in RMs than that in the bulk solvent and bulk water.¹⁹ The average rotational relaxation time of C-490 decreases with increasing amount of water in the pool of RMs. It indicates that with increasing the water content in the RMs from $w_o = 0$ to $w_o = 30$, the restrictive environment around C-490 becomes flexible. With increasing the water content in RMs, the size of RMs pool increases and also the number of bulk like water increases.⁹ These results further infer that the probe molecules are mostly located in the pool of RMs. However, these results are in contrast to a study on the RMs formed by CTAB carried out by Hazra *et al.*⁷ They have reported that the probe molecule, C-480 resides at the interface of the RMs. One reason for dependency of relaxation time of C-490 on w_o in the present study is because of a possibility of forming larger droplets in case of RMs of gemini surfactant as compared to the RMs of conventional surfactants.²⁰ Of course the other reason could be as mentioned above the less hydrophobic nature of C-490 as compared to C-480.

Table 8.3: Rotational relaxation time of C-490 in pure solvents and RMs of gemini surfactant (12-4-12)

System	r_o	a_{1r}	τ_{1r} (ns)	a_{2r}	τ_{2r} (ns)	$\langle\tau_r\rangle^a$ (ns)
CHX + n-pentanol (2.4%)	0.20	1	0.194	-	-	0.194
n-pentanol	0.30	1	0.613	-	-	0.613
$w_o = 0$	0.36	0.45	0.691	0.55	4.692	2.892
$w_o = 2$	0.36	0.39	0.518	0.61	4.026	2.658
$w_o = 25$	0.36	0.58	0.473	0.42	3.335	1.675
$w_o = 30$	0.36	0.62	0.457	0.38	3.295	1.535

$$^a \langle\tau_r\rangle = a_{1r} \tau_{1r} + a_{2r} \tau_{2r}$$

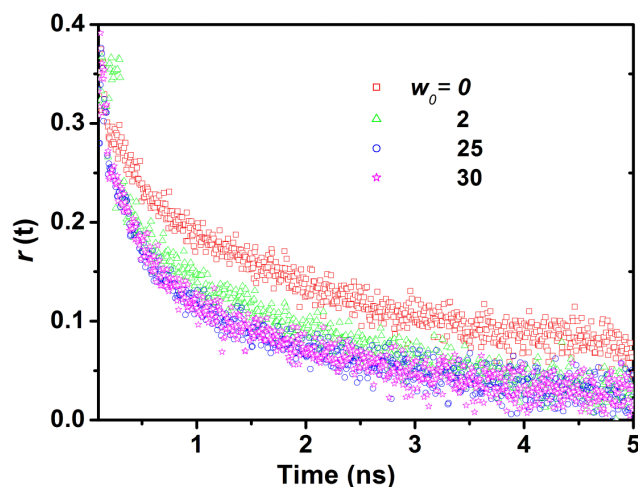


Figure 8.6: Time-resolved fluorescence anisotropy decay of C-490 in RMs of 12-4-12

The rotational relaxation time of C-490 in pure water is reported to be 95 ps.²¹ At $w_o = 2$, the relaxation process of C-490 in present RMs is ~ 14 times slower as compared to bulk solvent and ~ 28 times slower as compared to bulk water. These results suggest that C-490 molecules are experiencing more rigid environment in the pool of RMs than that in bulk solvent and bulk water. Therefore, the environment around the probe in the RMs pool is different from that in bulk solvent and bulk water. The decrease in rotational relaxation time with increase in the amount of polar solvent in the AOT RMs has also been observed in other studies.^{22, 23}

8.4 Solvation dynamics

The fluorescence decays of C-490 in all the RMs systems, *n*-pentanol and bulk solvent have been recorded. In all these systems, the wavelength dependent decays have been observed. In pure CHX and water, C-490 does not show any wavelength dependent fluorescence decay. Figure 8.7 represents the fluorescence decays of C-490 in RMs at $w_o = 0$ and $w_o = 2$. Similar wavelength dependent decays are also observed for $w_o = 25$ and 30. The decay at a short wavelength (425 nm) is very fast. However, at a longer wavelength (560 nm) it becomes slower and initially there is a clear growth in the decay followed by a slow decay with a negative pre-exponential factor. The fast decay at a short wavelength corresponds to the fluorescence from the unsolvated dipoles of C-490 created at the excited state without undergoing any relaxation process. However, decay occurs at longer wavelength corresponds to the relaxation of the solvated dipoles followed by the fluorescence emission, and is thus delayed by relaxation time.^{24,25}

The time resolved emission spectrum (TRES) have been constructed by applying the procedure of Fleming and Maroncelli²⁶ (Chapter 2, Section 2.2.11, Equation 2.27) The dynamic Stokes shifts have been observed for the emission spectra of C-490 in *n*-pentanol, bulk solvent and RMs. TRES are shown by the Figure 8.8. The dynamics of solvent is monitored by solvent correlation function (SCF), $C(t)$. Figure 8.9 represents a plot for $C(t)$ with respect to time (t) at different w_o . The decay characteristics of $C(t)$ for RMs at different w_o , *n*-pentanol, and for bulk solvent are tabulated in Table 8.4. The solvation time for *n*-pentanol is found to be 128 ps with single exponential. Corbeil *et al.*²⁷ reported this value as 97 ps with a probe molecule, C-343. Some difference observed in solvation time could be due to the use of different probe molecule and technique.

The average solvation time of C-490 in the bulk solvent is found to be 1.78 ns. This solvation time is greater as compared to pure *n*-pentanol. The slower solvation process in the mixed solvent system as compare to pure solvent has also been observed by Hazra *et al.*⁷ The data in Table 8.4 reveal that $C(t)$ consists of two components for the RMs, one with longer lifetime and other one with shorter lifetime. The bimodal decay arises due to the presence of bound and free water molecules and there is a dynamic exchange between them.²⁸

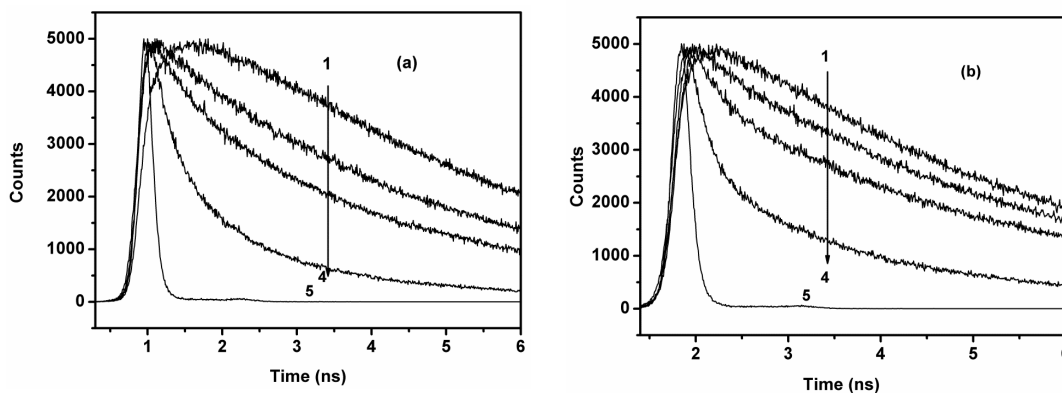


Figure 8.7: Time-resolved fluorescence decay of C-490 in 12-4-12 RMs for (a) $w_o = 0$ and (b) $w_o = 2$. 1 to 4 at 560 nm, 470 nm, 455 nm, 425 nm, respectively and 5 for instrument response function

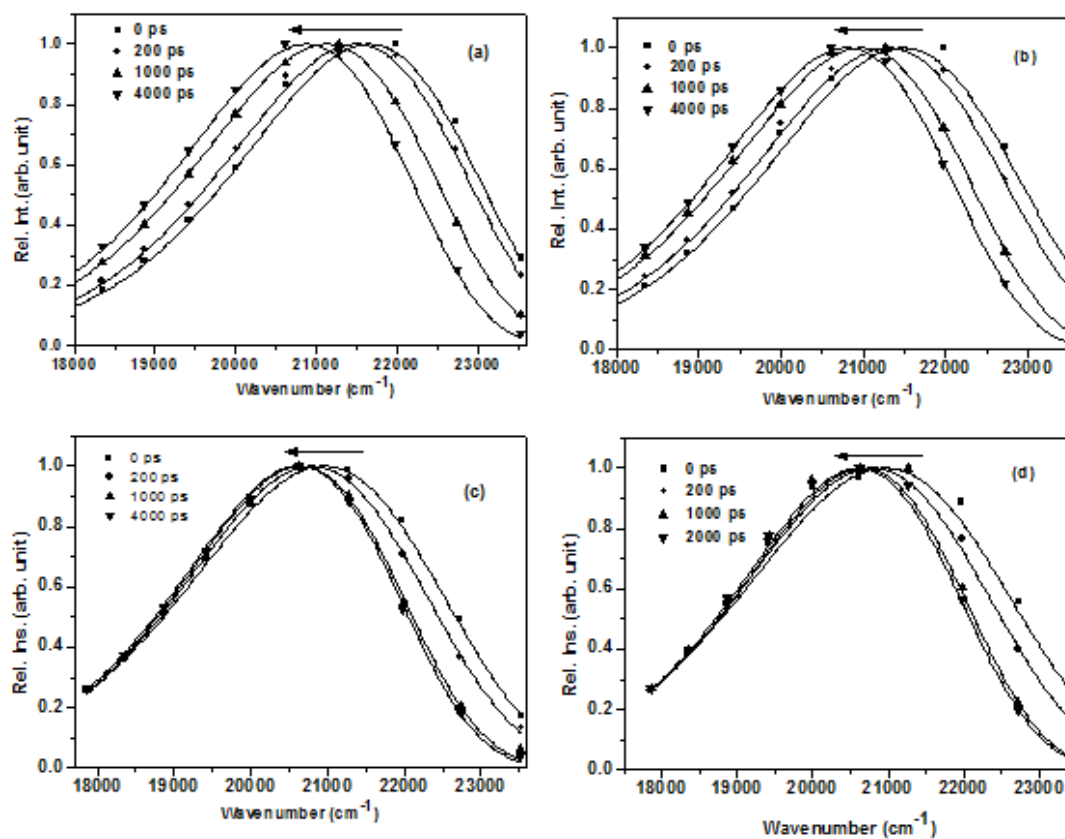


Figure 8.8: TRES of C-490 in RMs for (a) $w_o = 0$, (b) $w_o = 2$, (c) $w_o = 25$, and (d) $w_o = 30$

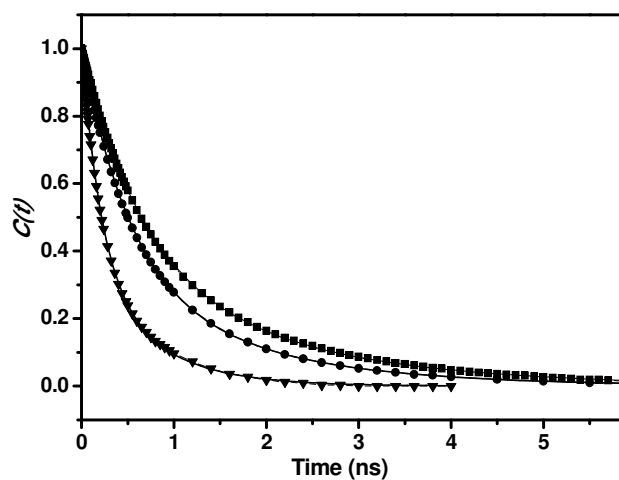


Figure 8.9: Decays of solvent correlation function, $C(t)$ of C-490 in RMs at (■) $w_o = 0$, (●) $w_o = 2$, (▼) $w_o = 30$

Table 8.4: Decay characteristic of $C(t)$ of C-490 in RMs of gemini surfactant

Systems	$\Delta\nu$ (cm ⁻¹)	a_{1s}	τ_{1s} (ns)	a_{2s}	τ_{2s} (ns)	$\langle\tau_s\rangle$ (ns)	Missing Component
CHX + n-pentanol (2.4%)	852	0.68	1.797	0.32	1.756	1.784	-
n-pentanol	918	1	0.128	-	-	0.128	-
$w_o = 0$	816	0.60	0.612	0.40	1.828	1.098	0.053
$w_o = 2$	691	0.65	0.514	0.35	1.561	0.880	0.172
$w_o = 25$	386	0.71	0.356	0.29	1.624	0.724	0.703
$w_o = 30$	331	0.76	0.203	0.24	0.682	0.318	0.710

In the present work, the bulk solvent in RMs consists of 2.4% of *n*-pentanol. The presence of *n*-pentanol affects the solvent reorganization in RMs. Corbeil *et al.*²⁷ also observed the effect of *n*-pentanol in case of RMs of conventional surfactants. It is evident from the data in Table 8.4 that the solvation time corresponding to the slow component in RMs at $w_o = 0$ is close to that in the bulk solvent. However, the solvation time corresponding to the fast component in RMs with major weightage is very different from that in bulk solvent. The solvation time in RMs is also much different from that in pure *n*-pentanol. It is much faster in pure *n*-pentanol than that in RMs. Hence, the observed solvation dynamics in RMs is not exclusively the dynamics of *n*-pentanol in bulk solvent. The increase in solvation time of *n*-pentanol in the vicinity of cationic headgroups of gemini surfactant is obvious as there is an electrostatic interaction between lone pair of electrons of oxygen atom of hydroxyl group of *n*-pentanol and positively charged nitrogen atom of gemini surfactant.⁷

The solvation time for the slow component at $w_o = 30$ is reduced to more than half as compared to $w_o = 0$. On comparison to the steady-state fluorescence spectra of C-490 in bulk solvent and in RMs at $w_o = 30$, we have found that the band in RMs is 25 nm red-shifted as compared to bulk solvent. These results indicate that C-490 molecules are moving towards the polar core of the RMs with increasing water loading. The number of free water molecules becomes more at $w_o = 30$ than that at lower w_o and the solvation dynamics becomes faster.^{23,29} It has been found that the relative contribution of the fast component is gradually increasing with a subsequent decrease in that of the slow component of solvation with increasing water content in RMs (Table 8.4). Moreover, the solvation time for the fast components along with the average solvation time are gradually decreasing. Hazra *et al.*²⁹ in their study on non-aqueous AOT RMs have

noticed that the average solvation time decreases with increasing content of polar solvents and concluded that the probe molecules, C-490 are approaching the core of the RMs. However, in their different study on microemulsion of conventional cationic surfactant, CTAB with C-480 as a probe, they have noticed that the solvation dynamics at the interface is independent of water loading.⁷ In contrast to that in the present study with RMs of cationic gemini surfactant, the solvation dynamics is mostly occurring in the water pool of RMs and that is why the dynamics is dependent on water loading. Although the location of the probe molecules could be a reason for this difference in solvation dynamics, but Corbeil *et al.*²⁷ have noticed water loading independent dynamics even with a more polar dye, C-343 as compared to C-480 and C-490. Of course in case of C-343, there are electrostatic interactions between the quaternary ammonium headgroup of CTAB and the $-\text{COO}^-$ functional group of C-343.²⁷ However, the difference between the structure of RMs of gemini surfactant and that of conventional cationic surfactants is also responsible for dependence of solvation dynamics on water loading as discussed in the following paragraph.

In the present work dependency of solvent relaxation time of C-490 on w_o is due to the fact that larger droplets are formed in the case of RMs of 12-4-12 gemini surfactant⁴² as compared to the RMs of conventional surfactants. Larger droplets are suitable to solubilize more water.²⁰ Zhao *et al.*²⁰ have reported that the variation in the size of water pool with increasing w_o is more sensitive in case of RMs of gemini surfactants as compared to conventional surfactants.²⁰ It is noteworthy that the solvation dynamics does not depend on the chain length of alcohol used to form RMs as reported by Corbeil *et al.*²⁷ for CTAB/*n*-heptanol/cyclohexane/water and CTAB/*n*-pentanol/cyclohexane/water RMs. The -OH group of alcohol molecules interact with the headgroups of gemini surfactant. With increasing size of water pool, the interfacial curvature is reduced which allows more water molecules to associate with the ionic heads of gemini surfactant. As a result of this a part of alcohol molecules are expelled from the interface.⁹ Based on the results obtained by Zhao *et al.*²⁰ on gemini surfactant RMs, we can suggest in the present case that the surfaces of larger droplets formed by 12-4-12 gemini surfactant need lesser amount of an alcohol to be present in the gaps among the headgroups of the surfactant as compared to conventional surfactants. A lesser extent of hydrogen bonding interaction between -OH group of alcohol and C-490 molecule is expected at the interface of present RMs of gemini surfactant than that of

conventional surfactants. Consequently, the solvation time in gemini surfactant RMs is faster as compared to conventional surfactants. Since the location of the probe molecules in the present gemini surfactant RMs is different from that in the reported RMs of conventional surfactants, the time scale of solvation dynamics is also different in these two cases. The solvation dynamics in the pool of present gemini surfactant RMs is faster than that in the bulk solvent which is different from that in RMs of conventional surfactants.²⁷ The solvation time for pure water is 0.5 ps.⁸ Thus, the water dynamics is retarded by many fold in the pool of RMs as compared to bulk water. It is noteworthy that the contribution from the Br⁻ ions to the measured solvation dynamics in the pool of RMs is known to be negligible.⁷ Of course there would be some contribution to the solvation dynamics from some of *n*-pentanol molecules present at the interface as well.

It is reported that solvation time depends upon the nature of molecular assemblies.³⁰ The solvation time observed in the present study with cationic gemini surfactant RMs is different from that observed by other groups in AOT RMs using the same probe, C-490⁸ and also by using the different probe molecules.²³ The solvation time of solvent molecules in organised assemblies depends on the interactions between the solvent molecules and the organised assemblies.³⁰ Hydrogen bonding, electrostatic interaction, counter-ion interaction etc. make the relaxation process of a solvent many fold slower in organised assemblies as compared to bulk solvent. We have observed faster solvation as compared to the reported solvation (at $w_o = 4$ and $w_o = 32$ the average solvation time respectively, are 2.97 and 1.17 ns) in AOT RMs using the same probe, C-490 by Hazra *et al.*⁸ They reported the average solvation time in nanosecond time scale, but we are getting the average solvation time in subnanosecond time scale at different water content in the RMs except at $w_o = 0$ where, there is no water molecule added externally. Obviously, the solvation time will be different because the headgroups of AOT and gemini surfactant are different. In AOT RMs, there is a strong hydrogen bonding between the water molecules and the oxygen atoms of AOT surfactant. The hydrogen bonding between water molecule and quaternary ammonium headgroup of gemini surfactant is absent in the RMs of gemini surfactant. Although, there are *n*-pentanol molecules present at the interface of RMs of studied gemini surfactant, but the hydrogen bonding of water molecule with *n*-pentanol may not be as much strong as with oxygen atom of AOT surfactant.⁹ Zhao *et al.*⁹ on the basis of their FT-IR study concluded the weak interaction between *n*-hexanol and water molecules at the interface of RMs.

The method proposed by Fee and Maroncelli^{26,31} has been used for the calculation of time zero frequency (Equation 8.1) for C-490 in RMs since the excitation wavelength 375 nm and absorption maxima ~385 nm in RMs are very close:

$$\nu_{p,md}(t = 0) \approx \nu_{p,md}(abs) - [\nu_{np,md}(abs) - \nu_{np,md}(ems)] \quad (8.1)$$

In this equation the subscript ‘*p*’ and ‘*np*’ refer to the polar and nonpolar solvent, respectively. The frequencies here are not the frequencies at the maxima, but correspond to the midpoint frequencies, ν_{md} , in the solvent. CHX is used as the non-polar solvent. It can be seen from Table 8.4 that the missing component increases with increasing w_o values. The increase in missing component with w_o is reasonable, since with increase in w_o , the water inside the RMs behaves like bulk water. Shirota *et al.*³⁰ also observed the increasing tendency of missing component with increasing the methanol content in AOT RMs using C-343 as a fluorescent probe molecule.

8.5 Conclusions

The steady-state fluorescence, steady-state fluorescence anisotropy, rotational relaxation and solvation dynamics data suggest that the probe molecule, C-490 resides in the water pool of gemini surfactant, 12-4-12/cyclohexane/*n*-pentanol/water RMs. This result is unlike C-480 and C-343 those are reported to be present at the interface of RMs of conventional cationic surfactants. C-490 is less hydrophobic than C-480. C-343 feels electrostatic interactions with the quaternary ammonium headgroup of a cationic surfactant. However, the structure of RMs is also responsible for the different locations of the probe molecules. The droplet size of present RMs is larger than the RMs of conventional cationic surfactant. Thus a lesser extent of hydrogen bonding interaction between –OH group of alcohol and the probe molecule takes place at the interface of present RMs as compared to conventional cationic surfactants. In the present case more and more probe molecules move towards the water pool with increasing content of water molecules and that is why the rotational relaxation, solvation dynamics and other steady-state fluorescence properties depend on w_o . Because of the same reason, the solvation dynamics in gemini surfactant RMs is one order of magnitude faster as compared to the reported RMs of conventional cationic surfactant. As compared to AOT RMs, the comparatively faster solvation dynamics found in gemini RMs is due to the absence of hydrogen bonding interaction between water molecules and quaternary ammonium

headgroup of surfactant in the latter case. The polarity of the medium has very little effect on the rates of non-radiative processes in the water pool of RMs. These rates are found to be doubled than that in AOT RMs.

References:

- (1) A. Maciejewski, J. Kubicki, and K. Dobek, *J. Phys. Chem. B*, **2003**, *107*, 13986.
- (2) B. K. Paul, A. Samanta, S. Kar, and N. Guchhait, *J. Lumin.* **2010**, *130*, 1258.
- (3) Z. Grabowski, K. Rotkiewicz, and W. Rettig, *Chem. Rev.* **2003**, *103*, 3899.
- (4) A. Mallick, P. Purkayastha, and N. Chattopadhyaya, *J. Photochem. Photobiol. C* **2007**, *8*, 109.
- (5) D. Shukla, and V. K. Tyagi, *J. Oleo Sci.* **2006**, *55*, 381.
- (6) P. Hazra, D. Chakrabarty, and N. Sarkar, *Langmuir* **2002**, *18*, 7872.
- (7) P. Hazra, D. Chakrabarty, A. Chakraborty, and N. Sarkar, *Chem. Phys. Lett.* **2003**, *382*, 71.
- (8) P. Hazra, and N. Sarkar, *Chem. Phys. Lett.* **2001**, *342*, 303.
- (9) J. Zhao, S. Deng, J. Liu, C. Lin, and O. Zheng, *J. Colloid Interface Sci.*, **2007**, *311*, 237.
- (10) G. Jones, W. R. Jackson, C. Y. Choi, and W. R. Bergmark, *J. Phys. Chem.* **1985**, *89*, 294.
- (11) K. Rechthaler, and G. Kohlar, *Chem. Phys.* **1994**, *189*, 99.
- (12) O. Zheng, J. X. Zhao, and X. M. Fu, *J. Colloid Interface Sci.* **2006**, *300*, 310.
- (13) X. Li, M. Liang, A. Chakraborty, M. Kondo, and M. Maroncelli, *J. Phys. Chem. B*, **2011**, *115*, 6592.
- (14) J. M. Hicks, M. Vandersall, Z. Babarogic, and K. B. Eisenthal, *Chem. Phys. Lett.* **1985**, *116*, 18.
- (15) A. Dutta, D. Mandal, S. K. Pal, and K. Bhattacharyya, *J. Phys. Chem. B* **1997**, *101*, 10221.
- (16) A. K. Tiwari, Sonu, and S. K. Saha, *J. Phys. Chem. B* **2014**, *118*, 3582.
- (17) C. Reichardt, *Chem. Rev.* **1994**, *94*, 2329.
- (18) E. M. Kosower, H. Dodiuk, K. Tanizawa, M. Ottolenghi, and N. Orbach, *J. Am. Chem. Soc.* **1975**, *97*, 2167.
- (19) D. Chakrabarty, P. Hazra, A. Chakraborty, and N. Sarkar, *Chem. Phys. Lett.* **2004**, *392*, 340.

-
- (20) O. Zheng, J. Zhao, and X. Fu, *Langmuir* **2006**, *22*, 3528.
- (21) H. Raghuraman, S. K. Pradhan, and A. Chattopadhyay, *J. Phys. Chem. B* **2004**, *108*, 2489.
- (22) R. E. Riter, D. M. Willard, and N. E. Levinger, *J. Phys. Chem. B* **1998**, *102*, 2705.
- (23) H. Shirota, and K. Horie, *J. Phys. Chem. B* **1999**, *103*, 1437.
- (24) J. R. Lakowicz, *Principles of fluorescence spectroscopy*, Kluwer Academic, New York, **1999**.
- (25) K. Bhattacharyya, *Chem. Comm.* **2008**, 2848.
- (26) M. Maroncelli, and G. R. Fleming, *J. Chem. Phys.* **1987**, *86*, 6221.
- (27) E. M. Corbeil, and N. E. Levinger, *Langmuir* **2003**, *19*, 7264.
- (28) N. Nandi, and B. Bagchi, *J. Phys. Chem. B* **1997**, *101*, 10954.
- (29) P. Hazra, and N. Sarkar, *Phys. Chem. Chem. Phys.* **2002**, *4*, 1040.
- (30) Y. Tamoto, H. Segawa, and H. Shirota, *Langmuir* **2005**, *21*, 3757.
- (31) R. S. Fee, and M. Maroncelli, *Chem. Phys.* **1994**, *183*, 235.

Chapter 9

Study on interaction of bovine serum albumin with cationic gemini surfactants: The spacer group effect

This chapter deals with the interaction of two cationic gemini surfactants, 12-4(OH)_n-12 (n = 0,1), (Scheme 2.2) with bovine serum albumin (BSA). Study has been carried out by using UV-Visible absorption, steady-state fluorescence, and time-resolved fluorescence spectroscopic techniques. Gemini surfactant with hydroxyl group in the spacer unfolds the BSA more efficiently than the gemini surfactant without hydroxyl group in the spacer. The binding isotherm displays characteristic regions with increasing gemini surfactants concentration. The excited singlet state lifetime of tryptophan residue of BSA varies with the concentration of the gemini surfactants. Interaction of unfolded BSA with gemini surfactants also has been studied. The gemini surfactant without hydroxyl group in the spacer interacted with the unfolded BSA to greater extent than the gemini surfactant with hydroxyl group in the spacer. Excited state lifetime values of unfolded BSA for interaction process in the presence of gemini surfactants show that interaction of gemini surfactants with unfolded BSA also occurs in a stepwise manner.

9.1 Results and discussions

9.1.1 UV-Visible absorption study

Surfactants bind strongly to proteins and bring a substantial change in the protein conformation. Figure 9.1 shows the UV-Visible absorption spectra of BSA in presence and absence of gemini surfactant, 12-4-12. Absorption spectra of pure BSA show two absorption peak maxima one at 210 nm and other at 279 nm. The absorption maximum at 210 nm is due to $\pi \rightarrow \pi^*$ transition of characteristic C=O group in polypeptide backbone structure,¹ and absorption maximum at 279 nm is due to $n \rightarrow \pi^*$ transition of aromatic amino acids, i.e., Phenylalanine (Phe), Tryptophan (Trp), and Tyrosine (Tyr). In presence of gemini surfactant, absorption spectra of BSA show ample changes in absorption peak maxima and absorbance values. The absorption peak maximum for pure BSA located at 210 nm shifts towards longer wavelength with increasing the concentration of gemini surfactant (Figure 9.2). Absorbance at 210 nm decreases continuously with increasing the concentration of gemini surfactant (Figure 9.2).

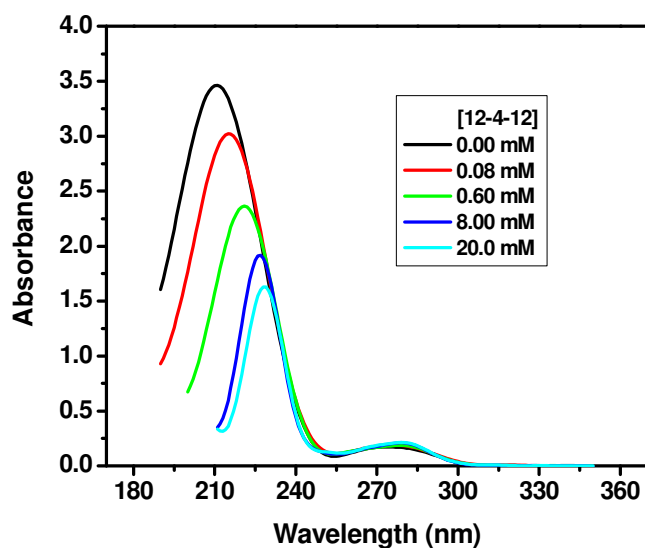


Figure 9.1: Absorption spectra of BSA at different concentrations of 12-4-12. [BSA] = 5 μ M

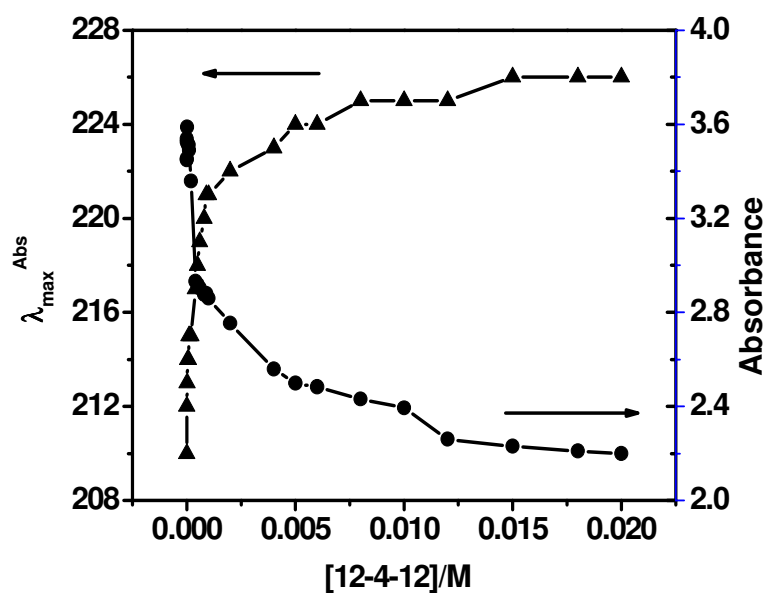


Figure 9.2: Variation of absorption peak maximum and absorbance of BSA with the concentration of gemini surfactant, 12-4-12

The observed changes in the spectroscopic properties of BSA are due to the interaction of gemini surfactant with BSA. In presence of gemini surfactant the microenvironment around amide group of BSA is different as compared to that of native protein. When amide groups of BSA are exposed to water environment the energy of $\pi \rightarrow \pi^*$ transition is decreased. The chromophore, C=O has higher polarity in the excited state than that in the ground state. Polar water molecules stabilize the energy of excited state

more than that of ground state and that is why absorption spectrum of BSA shows bathochromic shift with increasing the concentration of gemini surfactant. Absorption maximum at 279 nm shows very little change in absorbance with increasing the concentration of gemini surfactant. Similar behaviors in the absorption spectra are also observed in presence of 12-4(OH)-12 gemini surfactant as well.

9.1.2 Steady-state fluorescence study

BSA has three types of aromatic amino acids residues, Phe, Trp, and Tyr. These amino acids give intrinsic fluorescence of BSA. The intrinsic fluorescence of BSA is mainly contributed by Trp and Tyr residues. Phe has very low quantum yield and therefore fluorescence from Phe can be ignored. BSA has two Trp amino acid residues at 134 and 212 (Trp 134 and Trp 212) position of amino acid sequence in domain I and II, respectively. Trp 134 is located at the protein surface in domain I (subdomain IC), and Trp 212 is located in the hydrophobic binding pocket of protein in domain II (subdomain IIA). The intrinsic fluorescence of BSA is sensitive towards the change in microenvironment. Thus, fluorescence analysis is used as an effective method for the study of interaction of BSA with surfactant molecules.¹⁻⁶ Figure 9.3 (a) shows the emission spectra of BSA in absence and presence of gemini surfactants. Spectrum of pure BSA shows fluorescence maximum at 347 nm. At very low concentration (0.0 mM-0.005 mM) of gemini surfactant (12-4-12) fluorescence intensity of BSA is increased without any change in the fluorescence peak maximum. The rise in fluorescence intensity is due to the interaction of gemini surfactant at very high energy binding sites of BSA which give rise to compactness to the BSA native structure.^{5,7} It indicates that at a low concentration of surfactant (1:1 molar ratio of BSA and 12-4-12) the secondary structure of BSA remains unaltered and the tertiary structure gets affected.⁵ With increasing the concentration of gemini surfactant (12-4-12) upto 0.2 mM, the fluorescence intensity of BSA is decreased with a shift in the fluorescence peak maximum towards shorter wavelength at 334 nm. Further increase in the concentration of 12-4-12 upto 0.8 mM, a rise in fluorescence intensity has been observed without any change in fluorescence peak maximum. Beyond 0.8mM, fluorescence intensity remains almost constant. Similar type of variation in the fluorescence intensity of BSA has been observed for the other gemini surfactant, 12-4(OH)-12 as well.

These observations indicate that gemini surfactants, 12-4-12 and 12-4(OH)-12 interact with BSA and alter the native structure of BSA. Variation in the fluorescence intensity of fluorophores indicates that microenvironment around fluorophores change with the concentration of gemini surfactant. Surfactant molecules unfold the native structure of protein.⁸ Ionic surfactants interact strongly with protein by hydrophobic interaction between surfactant tail and nonpolar amino acids, and by electrostatic attraction of headgroups of surfactant and oppositely charged amino acids. The secondary structure of BSA is altered at high concentration of surfactant.² It has been observed that the percentage of α -helix decreases with increasing the amount of surfactant.² As mentioned above for 12-4-12 surfactant fluorescence intensity is decreased upto 0.2 mM which is due to the unfolding of BSA. In the unfolded state of BSA, Trp and Tyr residues are exposed to the polar environment and that is why fluorescence intensities of Trp and Tyr residues are reduced.⁹ Enhancement in the fluorescence intensities at higher concentration of gemini surfactant indicates that Trp and Tyr residues get located in the nonpolar environment.⁴ Figure 9.3 (b) shows variation of fluorescence peak maximum of BSA with increasing the concentration of 12-4-12 surfactant.

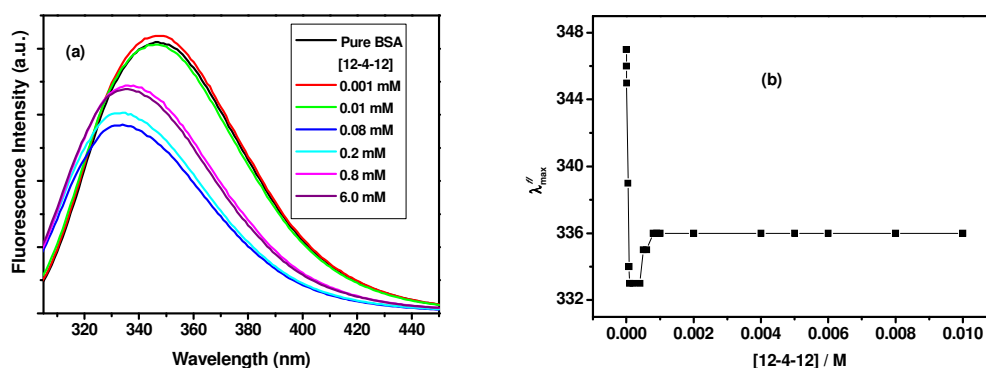


Figure 9.3: (a) Steady-state fluorescence spectra and (b) $\lambda_{\text{max}}^{\text{fl}}$ of BSA in presence of various concentration of 12-4-12. $\lambda_{\text{exc}} = 295 \text{ nm}$. $[\text{BSA}] = 5 \mu\text{M}$

Figure 9.4 shows the variation of fluorescence intensity with concentration of gemini surfactants, 12-4-12 and 12-4(OH)-12. It is clear from the figure that the change in fluorescence intensity is low for 12-4-12 as compared to change in fluorescence intensity in presence of 12-4(OH)-12. It indicates that gemini surfactant, 12-4(OH)-12 interacts

more strongly with BSA than 12-4-12 does. This may be due to the presence of one hydroxyl group in the spacer part of 12-4(OH)-12. Gemini surfactant, 12-4(OH)-12 may interact with BSA through hydrogen bonding and through lone pair of oxygen atom.¹⁰ This observation is also supported by the difference in the peak positions of the fluorescence band of BSA in presence of 12-4-12 and 12-4-(OH)-12. While in presence of 12-4-12, the fluorescence peak position is observed at 334 nm, the peak position is observed at 332 nm in presence of 12-4(OH)-12.

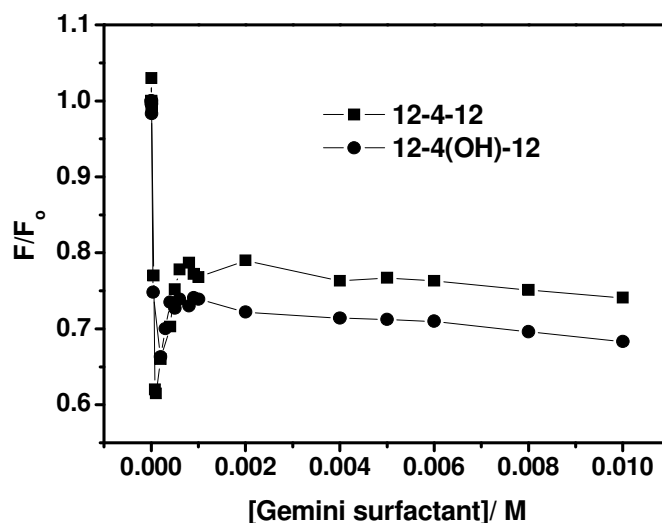


Figure 9.4: Plot of fluorescence intensity of BSA with concentration of gemini surfactant

9.1.3 Synchronous fluorescence spectroscopy study

Synchronous fluorescence spectroscopy is an effective technique to explore the microenvironment of amino acid residues.^{2,11} Synchronous fluorescence technique involves simultaneous scanning of excitation and emission monochromators while maintaining a constant wavelength interval between them. When the wavelength interval ($\Delta\lambda$, difference between excitation and emission wavelength) is kept at 15 nm and 60 nm, synchronous fluorescence spectra give information about Tyr and Trp residues, respectively.^{2,11} Figure 9.5 shows the synchronous fluorescence spectra of BSA for $\Delta\lambda = 60$ nm in presence of 12-4-12 and 12-4(OH)-12. With increasing the concentration of 12-4-12 and 12-4(OH)-12, fluorescence intensity is decreased with blue shift of fluorescence peak maxima. It indicates that the conformation of BSA is changed in the presence of gemini surfactant. Figure 9.6 shows the synchronous fluorescence spectra of

BSA for $\Delta\lambda = 15$ nm in presence of 12-4-12 and 12-4(OH)-12. At $\Delta\lambda = 15$ nm, fluorescence intensity increases with increasing the concentration of gemini surfactants.² It indicates that gemini surfactants create hydrophobic environment around Tyr residues of BSA. The variation in the fluorescence intensity is higher when $\Delta\lambda = 60$ nm as compare to $\Delta\lambda = 15$ nm. Moreover, when $\Delta\lambda = 60$ nm, the synchronous fluorescence peak maximum (337 nm) is close to that as observed in figure 9.3 (347 nm). From these observations it is clear that the microenvironment around Trp residues of BSA is perturbed to a greater extent in presence of gemini surfactants.

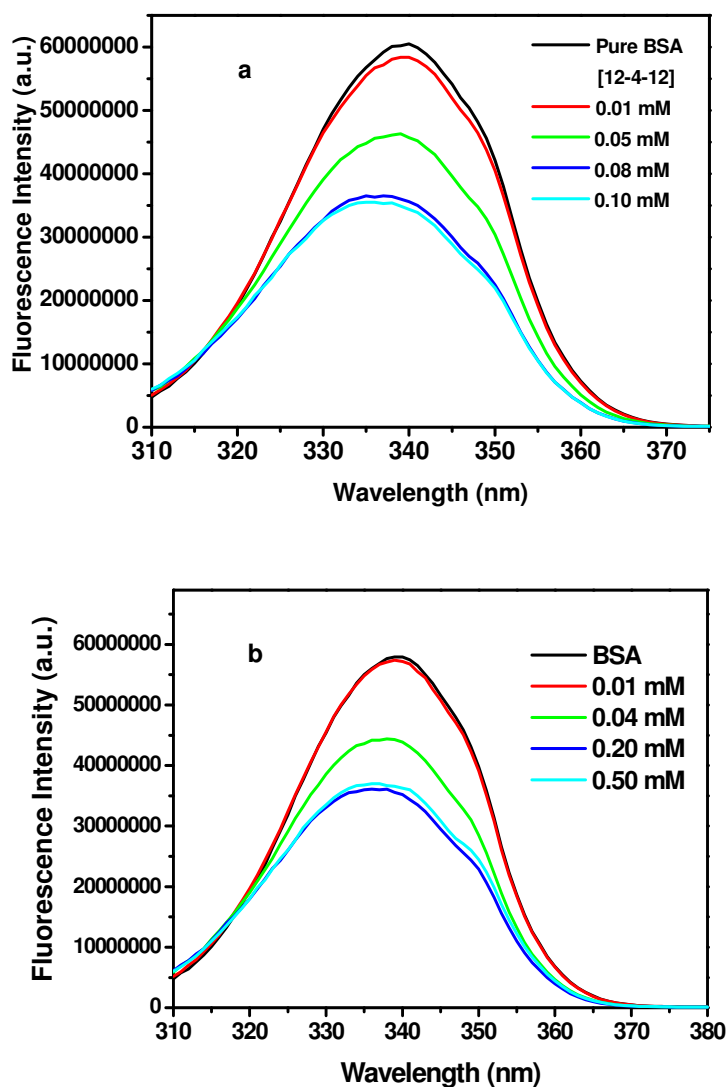


Figure 9.5: Synchronous fluorescence spectra of BSA at $\Delta\lambda = 60$ nm in presence of (a) 12-4-12 and (b) 12-4(OH)-12. [BSA] = $5\mu\text{M}$

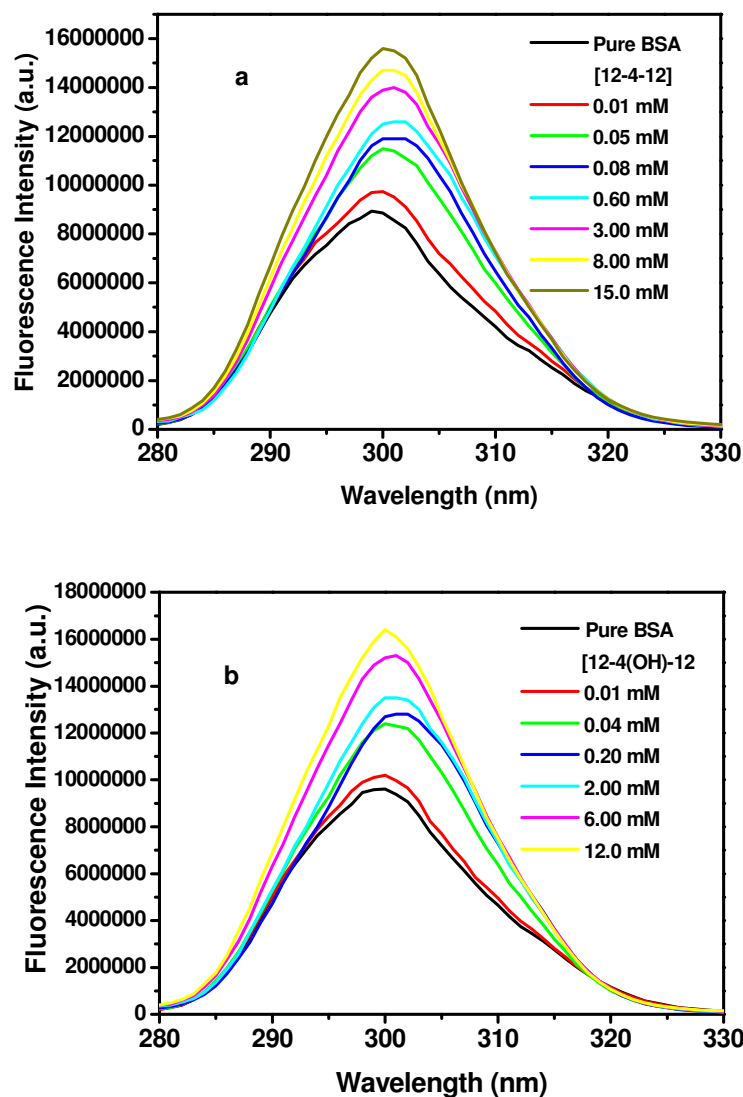


Figure 9.6: Synchronous fluorescence spectra of BSA at $\Delta\lambda = 15$ nm in presence of (a) 12-4-12 and (b) 12-4(OH)-12. [BSA] = 5 μ M

9.1.4 Binding of gemini surfactant with BSA: Study of binding isotherm

The nature of protein-surfactant interaction can be understood by using the binding isotherm of protein and surfactant. The binding isotherm can be calculated by plotting the average number of surfactant molecules (ν) bound per protein molecule as a function of surfactant concentration. ν was calculated by the following equation^{3,4,9}:

$$\nu = \alpha \times \frac{C_s}{C_p} \quad (9.1)$$

where α is the fraction of BSA bound to surfactant, C_s and C_p are the total surfactant and protein concentrations, respectively. α can be calculated from the Trp fluorescence intensity by using the following equation:

$$\alpha = \left(\frac{I - I_o}{I_{\min} - I_o} \right) \quad (9.2)$$

where I is the fluorescence intensity at any surfactant concentration, I_o is the fluorescence intensity in the absence of surfactants and I_{\min} is the fluorescence intensity at saturation level. Figure 9.7 displays the variation of ν with concentration of gemini surfactants, 12-4-12 and 12-4(OH)-12. With increasing the concentration of surfactant, generally the protein-surfactant isotherm shows three regions prior to the saturation region³ viz.(1) specific binding, (2) non-cooperative binding, and (3) cooperative binding. In figure 9.7, region 1 includes the total surfactant concentration from 0 mM to 0.04 mM. In this concentration region the binding isotherm rises very slowly due to ionic binding of surfactant molecules with protein at specifically high energy binding sites⁶ (Scheme 9.1). Region 2 shows the non-cooperative binding region. In this region, the binding isotherm rises gradually with surfactant concentration from 0.04 mM to 0.4 mM. As mentioned above in this concentration range the fluorescence intensity is dropped drastically and BSA conformation is altered (Scheme 9.1). Above 0.4 mM the binding isotherm rises sharply. This represents the massive cooperative binding between BSA and surfactant molecules.⁴ In this region surfactant molecules form micelles like structure along the protein chain (Scheme 9.1). Hence, binding of surfactants with BSA passes through three different stages.

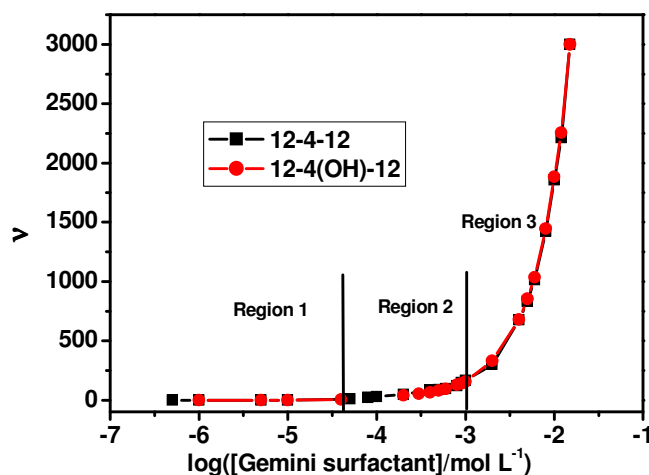
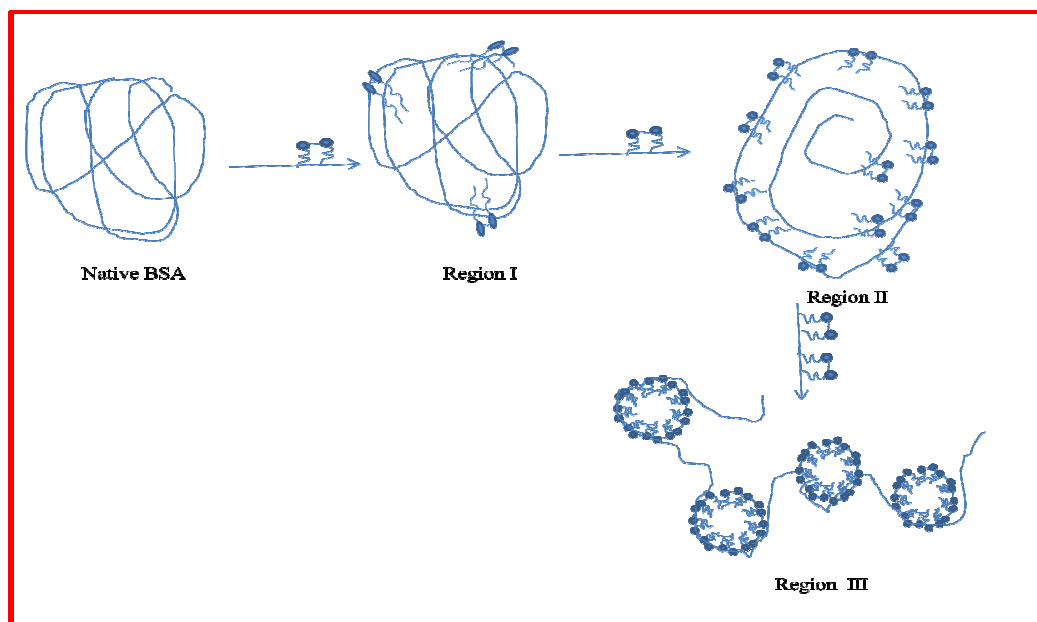


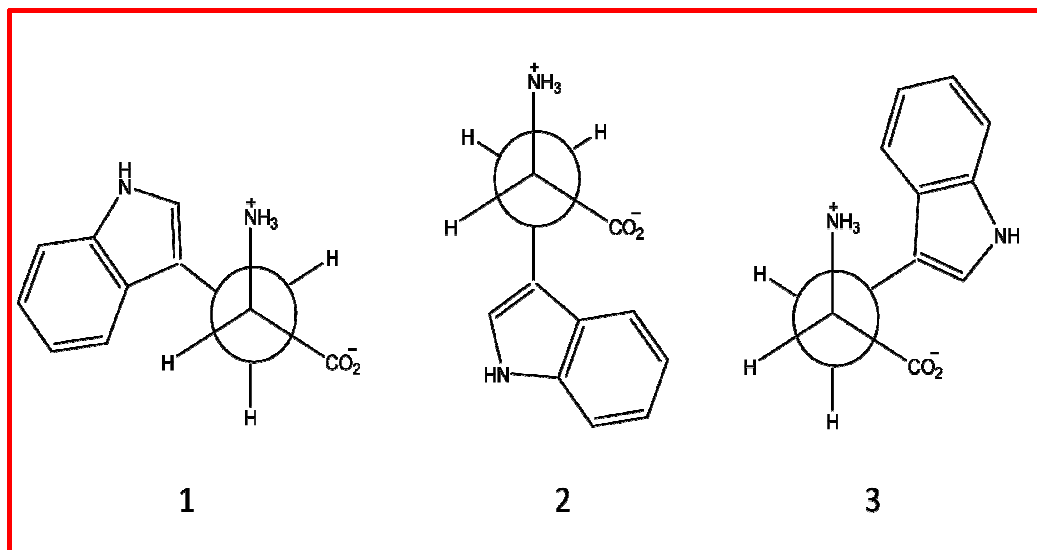
Figure 9.7: Binding isotherm of 12-4-12 and 12-4(OH)-12 with BSA



Scheme 9.1: Representation of binding of gemini surfactant with BSA in different concentration range of the former

9.2 Time-resolved fluorescence spectroscopic study

Time resolved fluorescence measurement is an effective method to study protein conformational dynamics. Trp exists in various rotational conformers and due to this Trp exhibits multiple exponential decays.^{12,13} The three rotational conformers of Trp are shown by scheme 9.2.



Scheme 9.2: Rotational conformers of Tryptophan (Trp)

It is believed that conformer 3 is quite stable and conversion from 3 to either 1 or 2 is difficult in nanosecond time scale. The short excited state lifetime of Trp is due to the existence of conformer 3 and the long excited state lifetime arises due to the rapid inter-conversion of conformers 1 and 2. It is also believed that in the ground state the indole ring is slightly puckered, but it becomes planer in the excited state, which leads to the delocalization of lone pair of electron from nitrogen atom to the aromatic ring. Upon unfolding process of protein the interacting ligand approaches to the Trp residues of protein and distorts the planarity of indole ring. Trp residue also exposed to the bulk solvent and that is why the excited state lifetime of Trp is decreased.^{5,7} We have measured the excited state lifetime of Trp moiety of BSA by exciting the sample using a 300 nm light emitting diode (LED). Bi-exponential decays of BSA were observed in presence and absence of studied gemini surfactants.

Table 9.1: Excited state lifetimes^{a,b} of BSA in presence of 12-4-12

[12-4-12] (mM)	a_1	τ_1 (ns)	a_2	τ_2 (ns)	$\langle \tau \rangle$ (ns)	χ^2
0.0	0.29	3.048	0.71	6.802	5.713	1.01
0.001	0.28	3.027	0.72	6.850	5.780	1.06
0.005	0.31	3.054	0.69	6.905	5.711	1.07
0.01	0.31	2.992	0.69	6.858	5.660	1.16
0.05	0.49	2.836	0.51	6.687	4.800	1.15
0.1	0.66	2.393	0.34	6.116	3.659	1.06
0.2	0.67	2.679	0.33	6.464	3.928	1.04
0.6	0.55	2.492	0.45	6.462	4.279	1.12
1.0	0.54	2.572	0.46	6.387	4.327	1.10
2.0	0.58	2.812	0.42	6.485	4.355	1.07
4.0	0.60	2.859	0.40	6.352	4.256	1.10
5.0	0.61	2.813	0.39	6.334	4.186	1.06
8.0	0.58	2.476	0.42	5.897	3.913	1.15
15.0	0.59	2.400	0.41	5.809	3.798	1.10

^a $\lambda_{ex} = 300$ nm, ^b λ_{em} is the fluorescence peak maximum in respective system

Table 9.1 and 9.2 show the excited state lifetime values of BSA in presence of various concentration of 12-4-12 and 12-4(OH)-12. Average excited state life time, $\langle \tau \rangle$ has been calculated by using Equation 1.22 (Section 1.4.9, Chapter 1). Figure 9.8 represents the variation of average excited state lifetime of BSA in presence of both the gemini surfactants. Excited state lifetime of pure BSA is close to the reported lifetime value.^{5,7} Excited state lifetime of BSA in presence of 12-4-12 and 12-4(OH)-12 vary with the concentration of gemini surfactants. Lifetime increases upto 0.005 mM

concentration of 12-4-12 and 12-4(OH)-12. This increment in the lifetime of BSA in presence of low concentration of gemini surfactants is due to the interaction of gemini surfactant at high energy binding sites of BSA. Lifetime decreases from 0.01mM to 0.1mM concentration of 12-4-12 and from 0.01 to 0.2 mM concentration of 12-4(OH)-12. It is mentioned that steady-state fluorescence intensity of Trp is decreased in these concentration range due to the conformational change in the native structure of BSA. Lowering of excited state lifetime of BSA also supports the conformational change of BSA in presence of gemini surfactants.

As mentioned above the short lifetime for the conformer 3 and long lifetime is due to the rapid interconversion between conformers 1 and 2. The contribution of fast component is increased from concentration 0.01 mM to 0.1 mM for 12-4-12 gemini surfactant and simultaneously the contribution of slow component is decreased. It means that in this concentration range due to unfolding of BSA the interconversion between conformers 1 and 2 becomes easy. Similar behavior also has been observed in presence of 12-4(OH)-12 as well. Enhancement in the excited state lifetime has been observed with further increasing the concentration of gemini surfactants from 0.4 mM to 1.0 mM for 12-4-12 and 0.3 mM to 0.9 mM for 12-4(OH)-12. After these concentrations excited state lifetime values become almost steady.

Table 9.2: Excited state lifetimes^{a,b} of BSA in presence of 12-4(OH)-12

[12-4(OH)-12] (mM)	a_1	τ_1 (ns)	a_2	τ_2 (ns)	$\langle\tau\rangle$ (ns)	χ^2
0	0.29	3.048	0.71	6.802	5.713	1.01
0.001	0.41	3.994	0.59	7.071	5.809	1.10
0.005	0.43	4.001	0.57	7.096	5.765	1.08
0.01	0.33	3.116	0.67	6.769	5.564	1.04
0.04	0.53	2.532	0.47	6.398	4.349	1.11
0.2	0.67	2.538	0.33	6.229	3.756	1.04
0.4	0.61	2.516	0.39	6.246	3.971	1.09
0.6	0.39	2.490	0.61	6.169	4.734	1.09
1.0	0.60	2.547	0.40	6.167	3.995	1.11
2.0	0.60	2.549	0.40	6.049	3.949	1.10
4.0	0.59	2.454	0.41	5.792	3.823	1.12
5.0	0.62	2.590	0.38	5.878	3.839	1.10
8.0	0.60	2.397	0.40	5.602	3.679	1.15
15.0	0.61	2.470	0.39	5.732	3.742	1.11

^a $\lambda_{ex} = 300$ nm, ^b λ_{em} is the fluorescence peak maximum in respective system

From Figure 9.8 it is clear that at higher concentration of 12-4(OH)-12 the average excited state lifetime values of BSA are lower than that in presence of 12-4-12 gemini surfactant. Excited state lifetime values are also showing the effect of hydroxyl group of gemini surfactant, 12-4(OH)-12 on interaction with BSA. It is noteworthy that the effect of concentration of gemini surfactants on steady-state fluorescence intensities of BSA (Figure 9.4) is in consistent with that on the excited state life time of BSA (Figure 9.8).

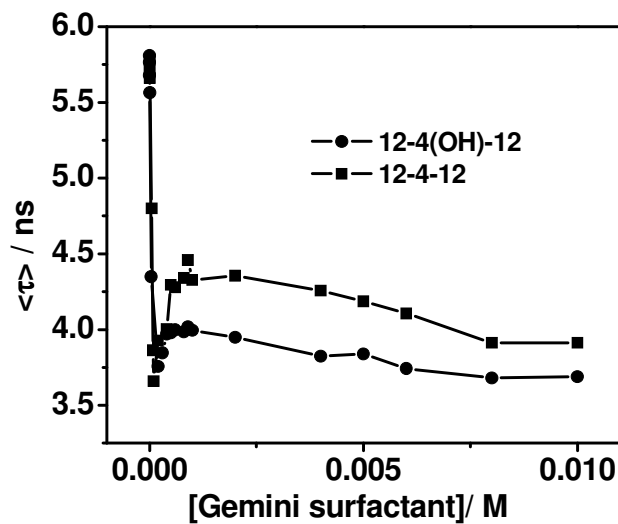


Figure 9.8: Variation of excited state average lifetime of BSA with the concentration of gemini surfactants. $\lambda_{ex} = 300$ nm, λ_{em} is the fluorescence peak maximum in respective system, [BSA] = 5 μ M

9.3 Fluorescence quenching of BSA by acrylamide

Fluorescence spectra of BSA have been recorded at various concentration of acrylamide in presence and absence of gemini surfactants. Fluorescence intensity of BSA continuously decreases with increasing the concentration of acrylamide. The quenching data were analysed by using Stern-Volmer equation (Equation 1.24, Section 1.4.10.1, Chapter 1). The Stern-Volmer plot in case of pure BSA is deviated from the linearity at high concentration of acrylamide (Figure 9.9). The upward curvature implies that quenching of pure BSA is dynamics as well as static in nature.¹² However, the Stern-Volmer plots are linear in presence of surfactants and fluorescence lifetimes of BSA decrease with increasing concentration of quencher. These results infer that the quenching mechanism is only dynamic in nature in presence of surfactants (Figure 9.9).

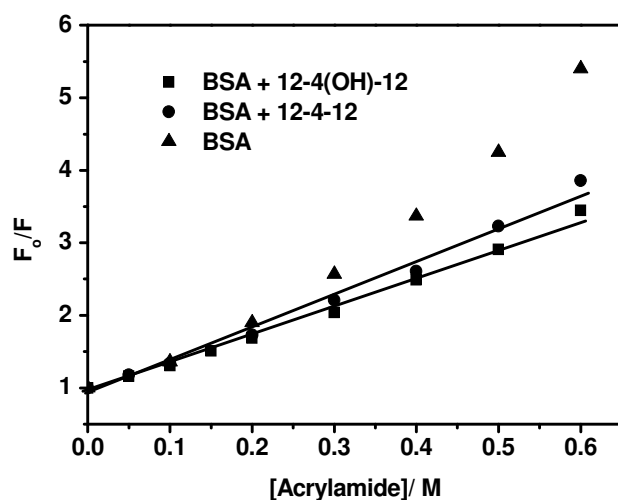


Figure 9.9: Stern -Volmer plot of BSA and BSA -12-4-12/12-4(OH)-12 systems. [BSA] = 5 μ M . [12-4-12] = [12-4(OH)-12] = 5 mM

The Stern-Volmer quenching constant (K_{SV}) values in all the studied systems have been calculated using Equation 1.24 (Chapter 1). For the calculation of K_{SV} linear part of the quenching data have been used. While the K_{SV} value for pure BSA was found to be $6.55M^{-1}$, the K_{SV} values for BSA in presence of 12-4-12 and 12-4(OH)-12 were found to be $4.68M^{-1}$ and $4.02M^{-1}$, respectively. The values of bimolecular quenching rate constant (k_q) for pure BSA and in presence of both the gemini surfactants have been calculated using Equation 1.24 (Chapter 1) and found to be $1.15 \times 10^9 M^{-1}S^{-1}$, $8.16 \times 10^8 M^{-1}S^{-1}$, and $7.03 \times 10^8 M^{-1}S^{-1}$, respectively. K_{SV} and k_q for pure BSA are higher than that in presence of gemini surfactants. In absence of gemini surfactant Trp residues of pure BSA are accessible to the acrylamide and fluorescence quenching takes place. In presence of gemini surfactants, there is a change in the conformation of BSA. It is expected that buried Trp residues would be more exposed to the quencher in presence of gemini surfactants. However, the values of K_{SV} and k_q show that it is not the case. The surfactant molecules form micelles along the BSA chain. As a result of that a lesser extent of quenching of BSA by acrylamide takes place. That is why K_{sv} and k_q values are lower in presence of gemini surfactants. K_{sv} and k_q values are less in presence of 12-4(OH)-12 than that in presence of 12-4-12. This could be because of the fact that -OH group of 12-4(OH)-12 interacts with acrylamide through H-bonds. Therefore, availability of acrylamide for quenching to occur is little less in case of 12-4(OH)-12 than that in 12-4-12 gemini surfactant. Fluorescence maximum is 2 nm blue shifted in presence of 12-4(OH)-12 as compared to that in 12-4-12. Therefore, Trp

residues are present at more hydrophobic environment in 12-4(OH)-12 micelles as compared to the micelles of 12-4-12. Polar acrylamide molecules are less accessible to the micelles of the former surfactant.

9.4 Interaction of gemini surfactant with unfolded BSA

Interaction of gemini surfactant with unfolded BSA has been studied by steady-state and time resolved fluorescence methods. BSA has been denatured by guanidine hydrochloride (GdHCl). Fluorescence spectra of BSA have been recorded in presence of various concentration of GdHCl. Recorded fluorescence spectra of BSA in presence of GdHCl are similar to that reported in the literature.⁷ Intensity of fluorescence decreases and fluorescence maximum shifts towards longer wavelength with increasing the amount of GdHCl. At 4M GdHCl, the fluorescence peak maximum of BSA appears at 358 nm. Figure 9.10 shows the variation of average excited state lifetime of Trp with increasing concentration of GdHCl. Excited state lifetime initially increases and then decreases with increasing the concentration of GdHCl. These results clearly show the unfolding of BSA in presence of GdHCl.

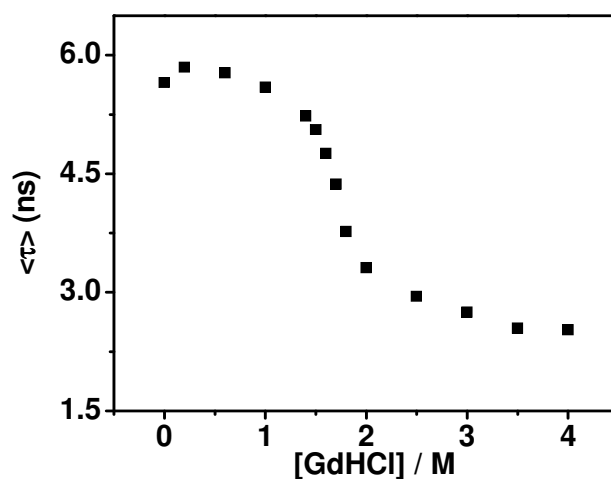


Figure 9.10: Variation of excited state lifetime of BSA in presence of GdHCl. [BSA] = 5 μ M, λ_{ex} = 300 nm

Mukherjee *et al.*⁵ have studied the interaction of BSA by β -cyclodextrin. They have reported that β -cyclodextrin remains inactive for refolding of BSA denatured by GdHCl. Present study have demonstrated the interaction of gemini surfactants, 12-4-12 and 12-4(OH)-12 with unfolded BSA. BSA is first denatured by using 4.0 M GdHCl and

then gemini surfactant of varying concentration are added. Circular dichromism (CD) spectra do not show any change in peak position with changing concentration of gemini surfactant. So, refolding does not take place in presence of gemini surfactants. Figure 9.11 shows the steady-state fluorescence spectra to demonstrate the interaction of BSA with various concentrations of 12-4-12 and 12-4(OH)-12. Fluorescence intensity of BSA progressively increases with increasing the concentration of gemini surfactants. Therefore, gemini surfactant molecule create hydrophobic environment around Trp and Try residues along the protein chain, may be by forming micelles-like structures. Enhancement in fluorescence intensity is more in case of 12-4-12 than that with 12-4(OH)-12. Fluorescence peak maximum is shifted from 358 nm to shorter wavelength with increasing the concentration of 12-4-12 and 12-4(OH)-12. In presence of 20 mM of 12-4-12, the fluorescence peak maximum appears 347nm. However in case of 10 mM of 12-4(OH)-12, fluorescence peak maximum appears at 353 nm.

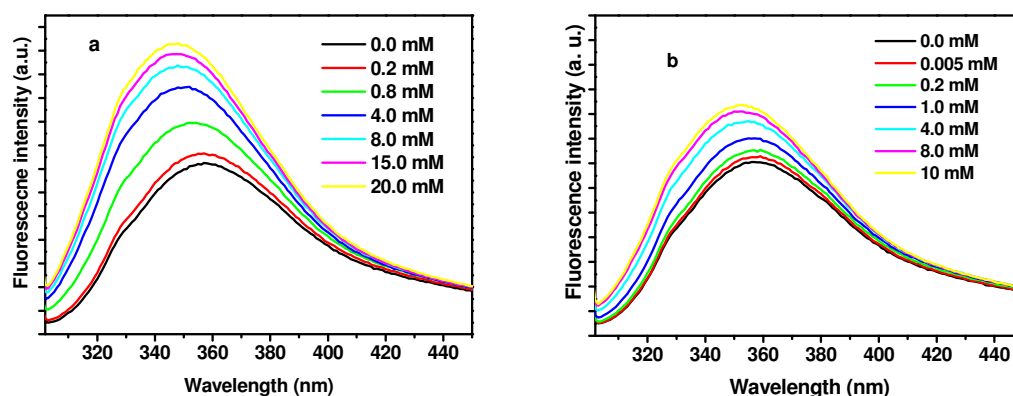


Figure 9.11: Fluorescence spectra of unfolded BSA to demonstrate interaction process in presence of (a) 12-4-12 and (b) 12-4(OH)-12. $\lambda_{exc} = 295$ nm

It was not possible to record the fluorescence spectra of BSA with 12-4(OH)-12 of concentration above 10 mM due to the precipitation. For 10 mM of 12-4-12 fluorescence peak maximum of BSA also appears at 347 nm. It is noteworthy that fluorescence peak maximum of pure BSA is also located at 347 nm. In presence of 20 mM and 10 mM concentration of 12-4-12 the intensity gains are 68% and 63%, respectively. For 12-4(OH)-12 at 10 mM concentration the gain in intensity is about 51%. These observations indicate that in presence of gemini surfactants, the denatured BSA regain substantial amount of hydrophobic environment and gain in that environment is more in presence of 12-4-12 than that of 12-4(OH)-12. Excited state

lifetimes also have been measured to support the above mentioned process. Figure 9.12 shows fluorescence decays for interaction process in presence of various concentrations of 12-4-12. Figure 9.13 shows the variation of excited state lifetime for interaction with various concentrations of gemini surfactants.

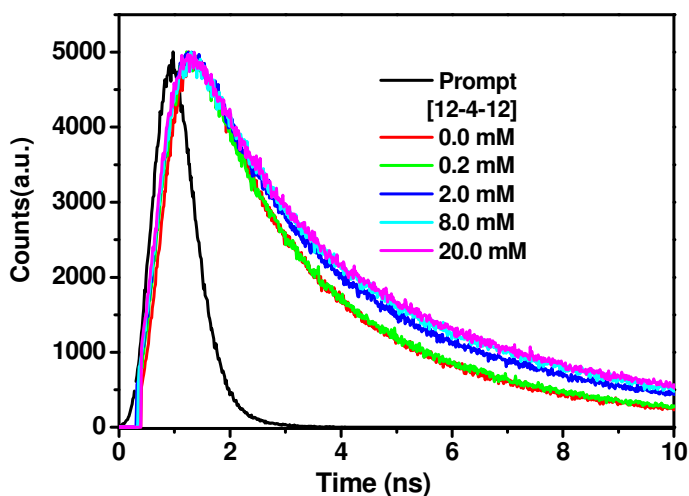


Figure 9.12: Time resolved fluorescence spectra of unfolded BSA in presence of different concentrations of 12-4-12 to show interaction process. $\lambda_{ex} = 300$ nm, λ_{em} is the fluorescence maxima in respective system, [BSA] = $5\mu\text{M}$

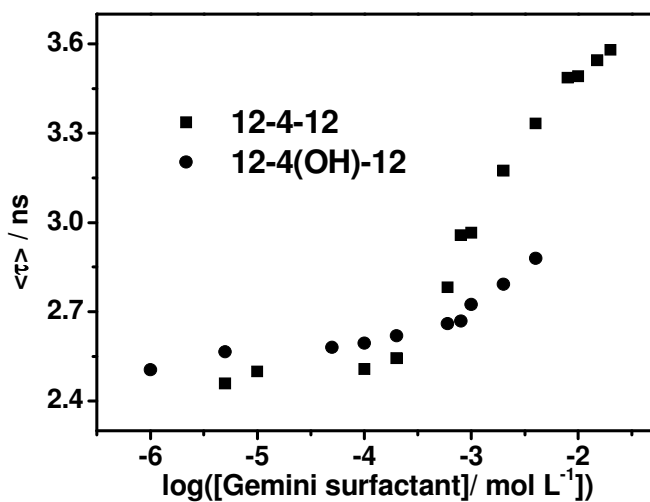


Figure 9.13: Average excited state lifetime of BSA for surfactant interaction process in presence of 12-4-12 and 12-4(OH)-12. $\lambda_{ex} = 300$ nm, λ_{em} is the fluorescence maxima in respective system, [BSA] = $5\mu\text{M}$

Like isotherm plot (Figure 9.7) the interaction of denatured BSA surfactant at higher concentration range also occurs in step wise manner. Upto 1mM concentration of both the gemini surfactants the increment in the lifetime is almost same. Above 1mM concentration the increment in the lifetime is more in presence of 12-4-12 than in presence of 12-4(OH)-12. Average excited state lifetime for pure BSA is 5.71 ns. In presence of 4M GdHCl the average excited state lifetime is 2.40 ns. During interaction process with 20 mM of 12-4-12 and 8 Mm 12-4(OH)-12 the average excited state lifetime are found to be 3.59 ns and 2.89 ns, respectively. It shows that the gain in excited state lifetime for 12-4-12 and 12-4(OH)-12 are 62.9 % and 50.6 %, respectively. These results depict that 12-4(OH)-12 is more effective for denaturation of native protein because of hydrogen bonding interaction with protein due to presence of -OH group in the spacer group. On the other hand 12-4-12 is more effective in creating hydrophobic environment around Trp and Tyr residues could be because of presence of more hydrophobic spacer group in this case as compared to that in 12-4(OH)-12.

9.5 Conclusions

This work has demonstrated interactions of gemini surfactants with bovine serum albumin. Effect of spacer group of gemini surfactants has been observed. Gemini surfactant with hydroxyl group in the spacer part (12-4(OH)-12) interact with native BSA more strongly than the gemini surfactant without hydroxyl group (12-4-12) in the spacer. Both the gemini surfactants interact with BSA in a sequential manner. Hydrophobic and electrostatic interactions of gemini surfactant show specific, noncooperative and cooperative bindings with BSA. Increasing the concentration of gemini surfactant, BSA unfolds and wraps around the micelles of gemini surfactant. Steady-state fluorescence data suggest that microenvironment around Trp residues altered during the interaction of gemini surfactant. Excited singlet state lifetime data also support the fact of sequential manner of interaction of gemini surfactants with BSA. Gemini surfactant with hydroxyl group in the spacer unfolds the native BSA more efficiently than the gemini surfactant without hydroxyl group in the spacer. Fluorescence of Trp is quenched by acrylamide to a greater extent in presence of 12-4-12. BSA unfolded by GdHCl shows interaction with gemini surfactants. Steady-state fluorescence and excited state fluorescence lifetime data of Trp residues of BSA show that 12-4-12 interact the unfolded BSA to a greater

extent than that by 12-4(OH)-12. 12-4-12 creates more hydrophobic environment around Trp and Try residues of BSA than that by 12-4(OH)-12 could be because of presence of more hydrophobic spacer group in the former. Interaction with unfolded BSA by gemini surfactants at high concentration also occurs in a sequential manner.

References:

- (1) X. Zhao, R. Liu, Z. Chi, Y. Teng, P. Qin. *J. Phys. Chem. B* **2010**, *114*, 5625.
- (2) D. Wu, G. Xu, Y. Sun, H. Zhang, H. Mao, Y. Feng. *Biomacromolecule* **2007**, *8*, 708.
- (3) Y. Pi, Y. Shang, C. Peng, H. Liu, Y. Hu, J. Jiang, *Biopolymers* **2006**, *83*, 243.
- (4) V. I. Martín, A. Rodríguez, A. Maestre, M. L. Moya, *Langmuir* **2013**, *29*, 7629.
- (5) U. Anand, S. Mukherjee, *Phys. Chem. Chem. Phys.* **2013**, *15*, 9375.
- (6) R. Das, D. Guha, S. Mitra, S. Kar, S. Lahiri, S. Mukherjee, *J. Phys. Chem. A* **1997**, *101*, 4042.
- (7) U. Anand, C. Jash, S. Mukherjee, *Phys. Chem. Chem. Phys.* **2011**, *13*, 20418.
- (8) Y. Shu, M. Liu, S. Chen, X. Chen, J. Wang, *J. Phys. Chem. B* **2011**, *115*, 12306.
- (9) S. De, A. Girigoswami, S. Das, *J. Colloid Interface Sci.* **2005**, *285*, 562.
- (10) T. Cserhádi. *Env. Health Perspect.* **1995**, *103*, 358.
- (11) B. K. Paul, N. Guchhait, *Photochem. Photobiol. Sci.*, **2011**, *10*, 980.
- (12) J. R. Lakowicz, *Principles of Fluorescence Spectroscopy*, 3rd ed.; Springer: New York, **2006**.
- (13) A. G. Szabo, D. M. Rayner, *J. Am. Chem. Soc.* **1980**, *102*, 554

Overall conclusions

To get a systematic overview of the research outcomes it is necessary to draw an overall conclusion for the whole thesis. In this thesis work, we have studied the physicochemical properties of some soft matter systems using fluorescence and conductometric methods. Photophysical properties of an ICT fluorescence probe molecule, 2-DMASP has been characterized experimentally as well as theoretically. 2-DMASP molecule exhibits solvent polarity dependent dual fluorescence. Theoretical studies based on TDDFT method shows that the donor twisting coordinate is a possible path for the creation of ICT excited state. Fluorescence properties of 2-DMASP have been explored to probe the microenvironment of micellar systems.

Mixed micellar properties of gemini and conventional surfactants have been studied in aqueous medium. This study shows that the surface active properties of a conventional surfactant can be improved by mixing it with a small amount of gemini surfactant. Microenvironment of mixed micellar systems have been characterized by the estimation of micropolarity and microviscosity values of the mixed micellar systems.

Solvation dynamics and rotational relaxation of C-153 molecule have been studied in presence of micelles of a series of cationic gemini surfactants, 12-s-12, 2Br- containing a hydrophobic polymethylene spacer with $s = 3, 4, 6, 8, 12$. Solvation dynamics depends upon the degree of counterion dissociation of gemini surfactant. Time-dependent fluorescence anisotropy decays were bi-exponential in nature due to various types of rotational motion of the probe molecule. Solvation dynamics and rotational relaxation of C-153 molecule have also been studied in presence of mixed micelles of non-ionic surfactant, Triton X-100 and a series of cationic gemini surfactants, 12-s-12, 2Br- with varying polymethylene spacer chain length ($s = 3, 6, 8, 12$), at different bulk mole fractions of a surfactant. Solvation process becomes faster with increasing the mole fraction of gemini surfactant in the mixed micelles with Triton X-100.

Urea molecule affects the solvation time of C-480 in presence of aqueous micelles of gemini surfactant. While at low concentration of urea the process of solvation dynamics is fast due to the disruption of tetrahedral structure of water, at high concentration of urea solvation dynamics becomes slower which is due to hydrogen bonding interaction between water and

urea. Rotational relaxation time of C-480 decreases with increasing the concentration of urea which is due to decrease in microviscosity of the micellar system in presence of urea. In presence of reverse micelles of gemini surfactant, the probe molecule, C-490 moves towards the pool of the reverse micelles with increasing amount of water into the pool and that is why solvation time of C-490 becomes faster. The faster solvation dynamics in gemini surfactant reverse micelles as compared to reported AOT reverse micelles is due to the absence of hydrogen bonding interaction between water molecules and quaternary ammonium headgroups of gemini surfactant. Rotational relaxation time of C-490 depends on water loading into the reverse micelles.

Study on interaction of gemini surfactants, 12-4-12 and 12-4(OH)-12 with BSA shows that the gemini surfactant with hydroxyl group in the spacer interacts more strongly with the native BSA as compared to the gemini surfactant without hydroxyl group in the spacer. Gemini surfactant without hydroxyl group in the spacer interacts more strongly with unfolded BSA as compared to the gemini surfactant with hydroxyl group in the spacer.

Future scope of the work

In the present study, the highly sensitive TICT fluorescence properties of 2-DMASP to the polarity and viscosity of micellar media are explored. The use of a single TICT molecule to characterize multiple properties such as micropolarity, microviscosity, location of probe, binding interactions, aggregation behaviour of various biomimicking and biological systems is very rare. This molecule can be explored to probe the aggregation properties of reverse micelles, mixed micelles and vesicles. In addition, the TICT fluorescence characteristics of 2-DMASP can be applied to probe various biological systems such as DNA, enzymes etc.

In this thesis work, several cationic gemini surfactants have been synthesized and their micellization behavior and mixed micellar properties with some conventional surfactants have been studied in aqueous medium. Gemini surfactants are having several attractive properties such as lower *cmc* value than their conventional counterparts, antimicrobial activities, foam formation, drug solubilizer, reverse micelles formation, lubricating agent etc. So the synthesized gemini surfactants can be used to carry out such kind of work. Mixed surfactants systems can be used for many industrial applications. In addition to cationic gemini surfactants, anionic and non-ionic gemini surfactants can also be synthesized and their various properties can be studied.

The solvation dynamics and rotational relaxation of some coumarin probe molecules have been studied in various micellar systems. The effect of spacer group of gemini surfactants on solvation dynamics and rotational relaxation of coumarin is an interesting finding. Further study can be carried out in terms of investigating the effect of nature of counterions and headgroups. Some systems such as protein-gemini surfactant, cyclodextrin-gemini surfactant, DNA-gemini surfactant etc. could be the choice for investigating the nature of solvation dynamics. Gemini surfactants with hydroxyl group substituted spacers can be used to study the effect of urea on solvation dynamics and rotational relaxation to focus more on the mechanism of action of urea. Interactions of gemini surfactants with the protein, BSA in its folded and unfolded forms have been studied. The work can be extended further to look for some gemini surfactant based additives to study the re-naturation of unfolded proteins.

Appendix A

$^1\text{H-NMR}$ spectra of synthesized gemini surfactants

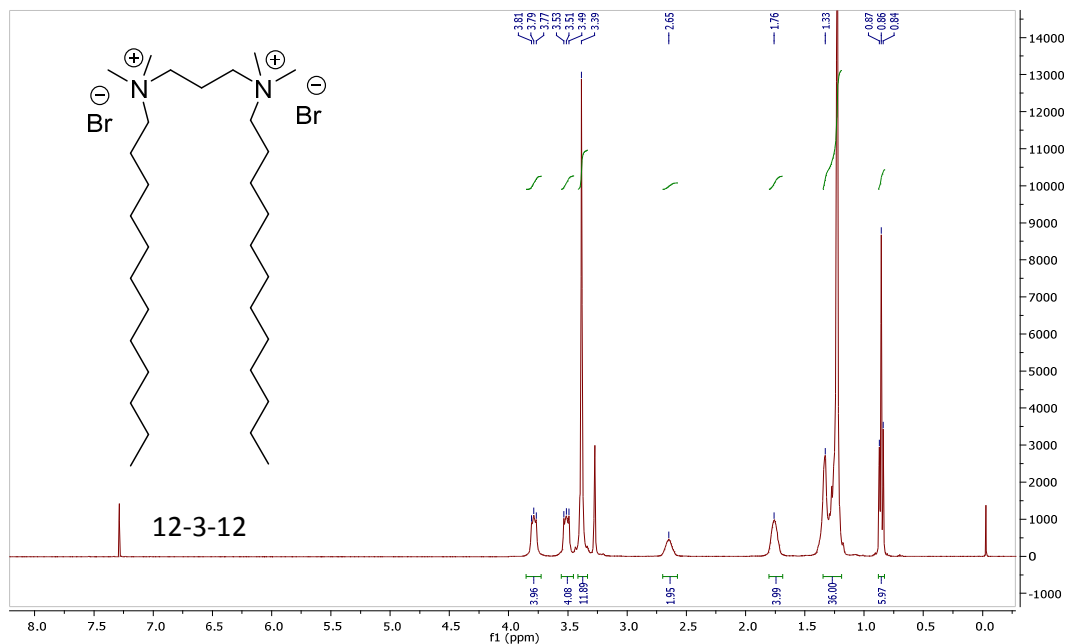


Figure A1: $^1\text{H-NMR}$ spectrum of 12-3-12

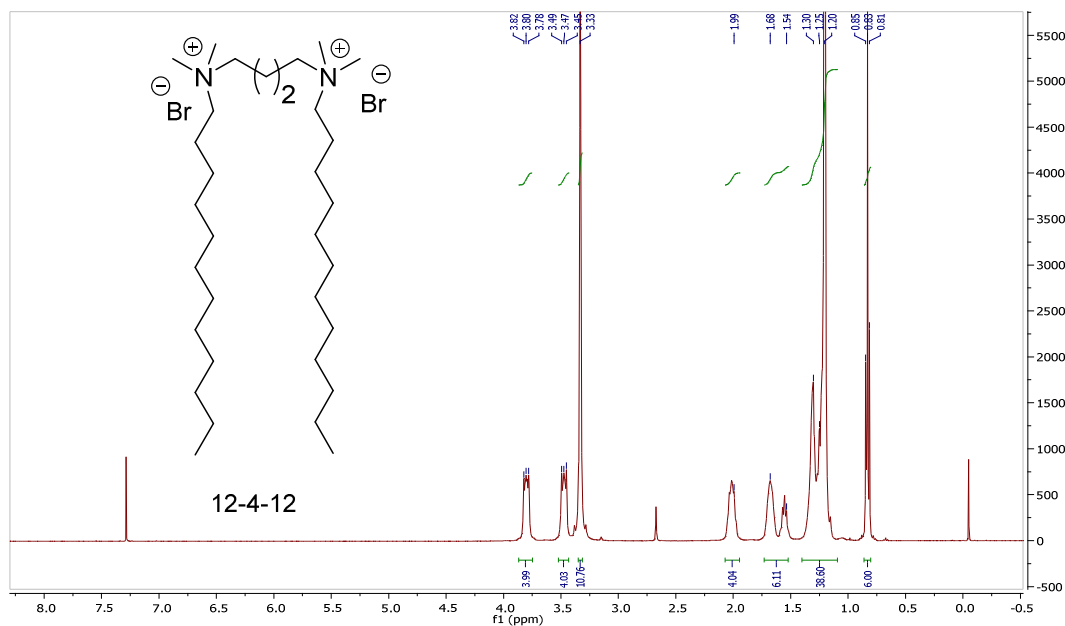


Figure A2: $^1\text{H-NMR}$ spectrum of 12-4-12

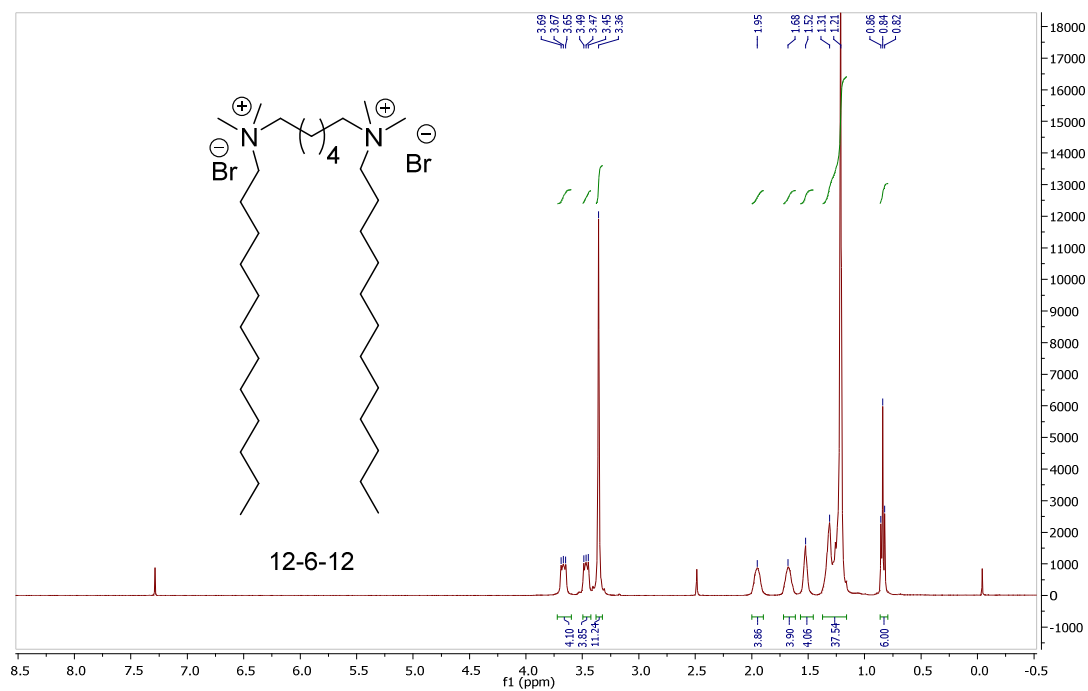


Figure A3: ¹H-NMR spectrum of 12-6-12

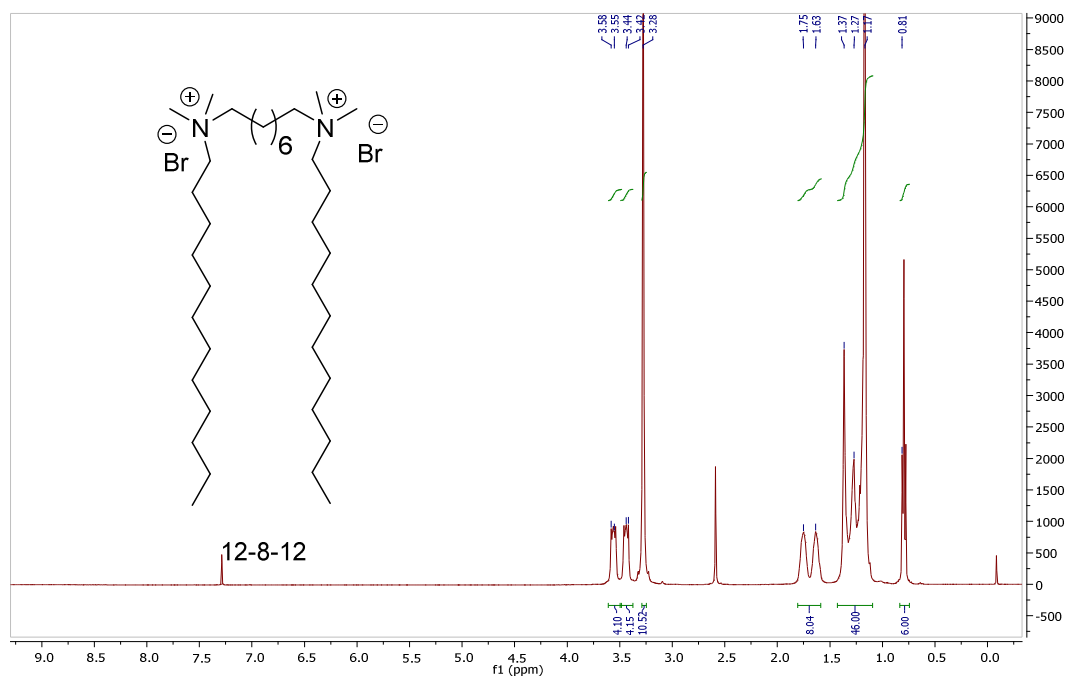


Figure A4: ¹H-NMR spectrum of 12-8-12

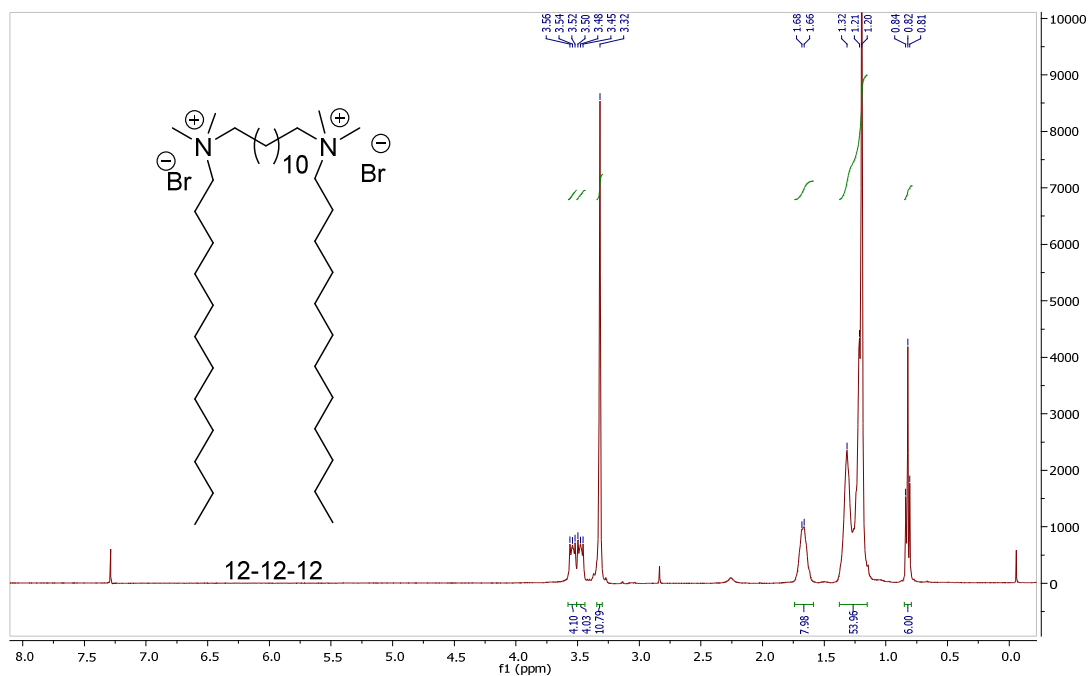


Figure A5: ¹H-NMR spectrum of 12-12-12

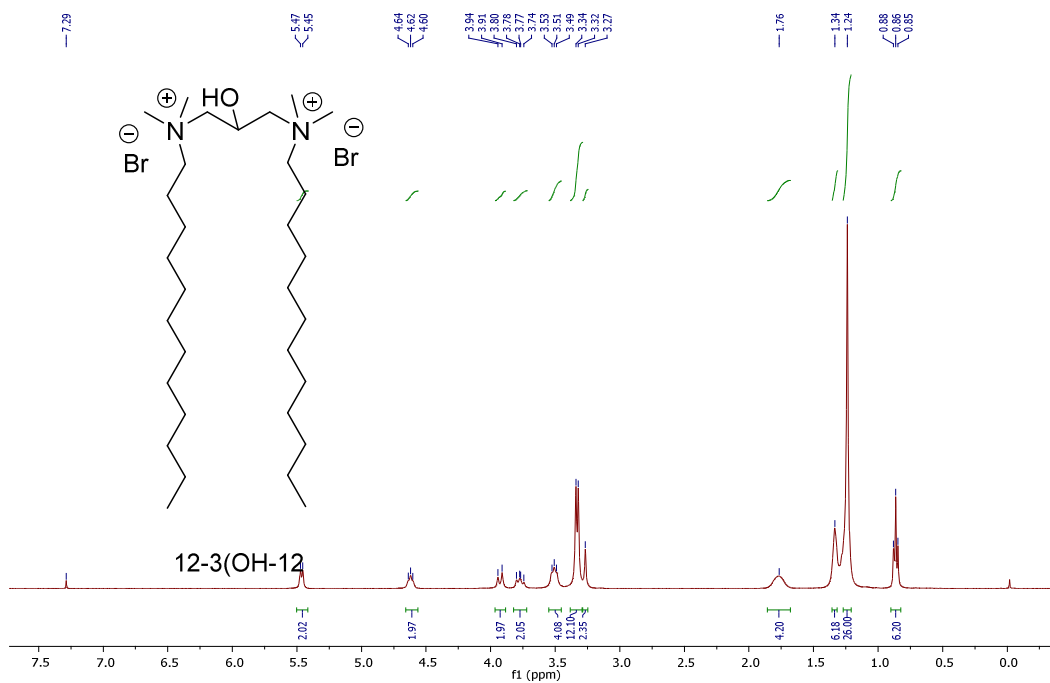


Figure A6: ¹H-NMR spectrum of 12-3(OH)-12

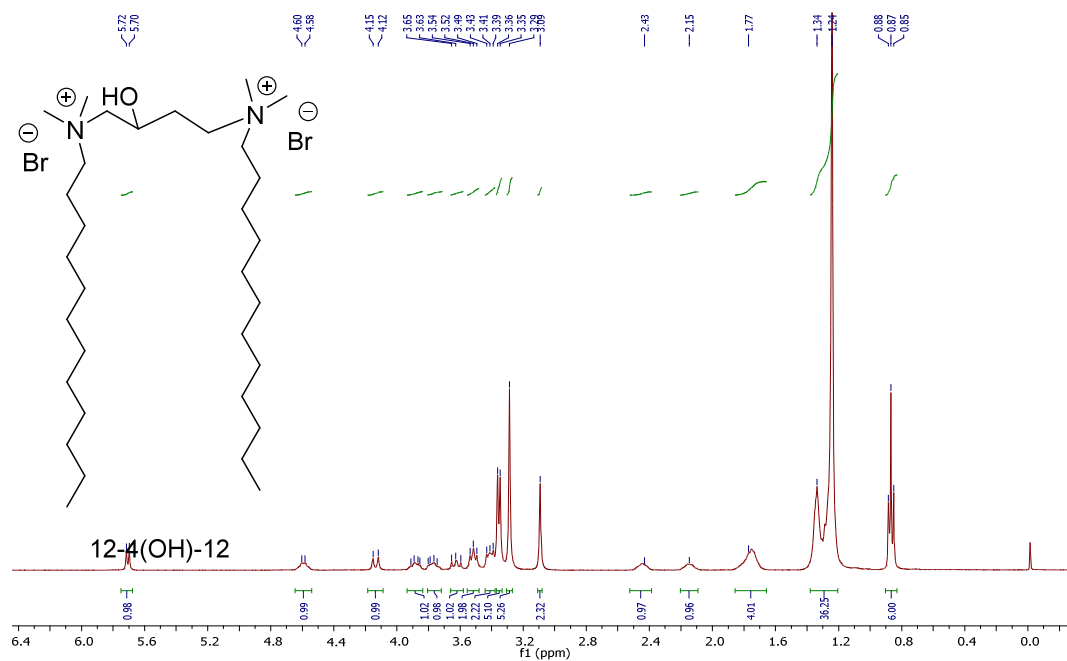


Figure A7: ¹H-NMR spectrum of 12-4(OH)-12

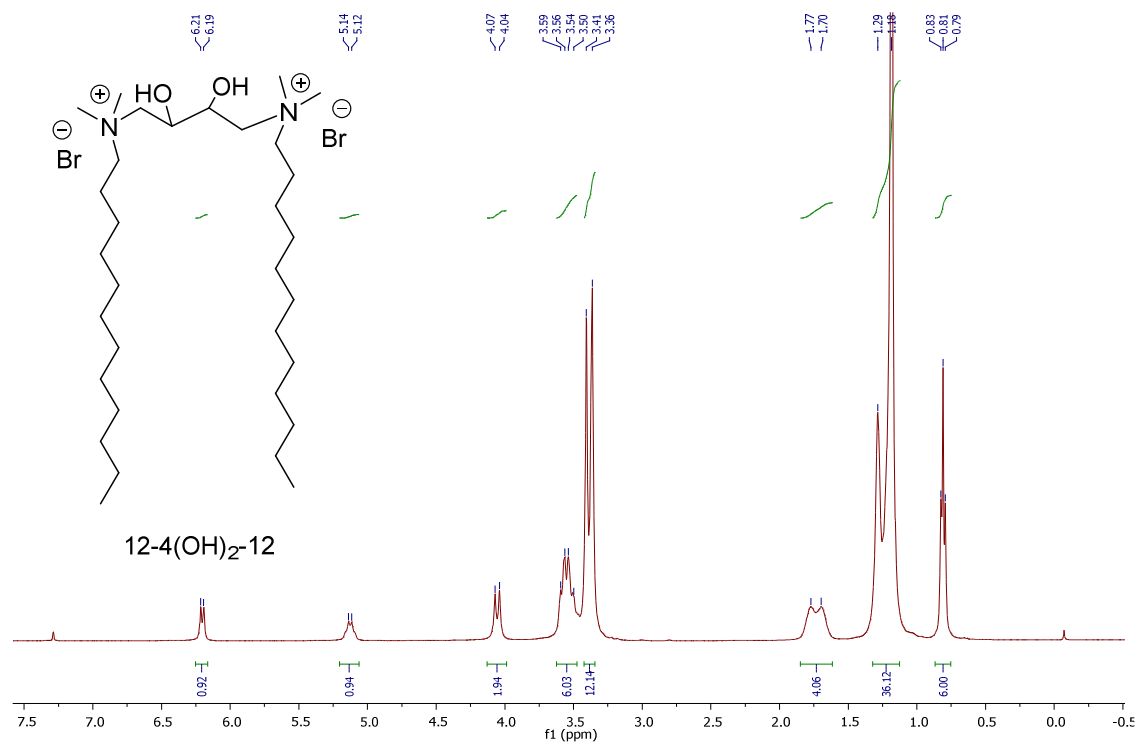


Figure A8: ¹H-NMR spectrum of 12-4(OH)₂-12

List of publications

From thesis work

Published

1. Sonu, Amit K. Tiwari, Subit K. Saha, Study on mixed micelles of cationic gemini surfactants having hydroxyl group in the spacers with conventional cationic surfactants: Effects of spacer group and hydrocarbon tail length, *Ind. Eng. Chem. Res.*, **2013**, *52*, 5895-5905.
2. Sonu, Amit K. Tiwari, Amrit Sarmah, Ram K. Roy, Subit K. Saha, Study on Photophysical Properties and Prototropic Equilibria of trans-2-[4'-(N,N'-dimethylaminostyryl)]pyridine, *Dyes and Pigments* **2014**, *102*, 114-125.
3. Sonu, Amit K. Tiwari, Sunita Kumari, Subit K. Saha Study on intramolecular charge transfer processes, solvation dynamics and rotational relaxation of coumarin 490 in reverse micelles of cationic gemini surfactant, *RSC Adv.*, **2014**, *4*, 25210-25219.
4. Sonu, Sunita Kumari, Subit K. Saha, Effect of polymethylene spacer of cationic gemini surfactants on solvation dynamics and rotational relaxation of coumarin 153 in aqueous micelles, *J. Phy. Chem. B* **2015**, *119*, 9751-9763.
5. Sonu, Sunita Kumari, Subit K. Saha, Solvation dynamics and rotational relaxation of coumarin 153 in mixed micelles of Triton X-100 and cationic gemini surfactants: effect of composition and spacer chain length of gemini surfactants, *Phys. Chem. Chem. Phys.*, **2016**, *18*, 1551-1563.

To be communicated

6. Sonu, Subit K. Saha, Effect of added urea on solvation dynamics and rotational relaxation of Coumarin 480 in aqueous micelles of cationic gemini surfactant (to be communicated).
7. Sonu, Subit K. Saha, Study on interaction of bovine serum albumin with cationic gemini surfactants: The spacer group effect (to be communicated).

Publications other than thesis work

1. Amit K. Tiwari, Sonu, M. Sowmiya, Subit K. Saha, Study on premicellar and micellar aggregates of gemini surfactants with hydroxyl substituted spacers in aqueous solution using a probe showing TICT fluorescence properties, *J. Photochem. Photobiol. A* **2011**, 223, 6-13.
2. M. Sowmiya, Amit K. Tiwari, Sonu, Subit K. Saha, Study on intramolecular charge transfer fluorescence properties of trans-4-[4'-(N,N'-dimethylamino)styryl]pyridine: Effect of solvent and pH, *J. Photochem. Photobiol. A: Chem.* **2011**, 218, 76-86.
3. Amit K. Tiwari, Sonu, M. Sowmiya, Subit K. Saha, Micellization behavior of gemini surfactants with hydroxyl substituted spacers in water and water-organic solvent mixed media: The spacer effect, *J. Mol. Liq.* **2012**, 167, 18-27.
4. S. Muthusubramanian, Amit K. Tiwari, Sonu, Subit K. Saha, A cationic surfactant-concentration dependent binding of a guest molecule with the nanotubes of β - cyclodextrin and its release from the nanotubular cavities, *Soft Matter*, **2012**, 8, 11072-11084
5. Amit K. Tiwari, Sonu, Subit K. Saha, Aggregation behaviour and thermodynamics of mixed micellization of gemini surfactants with a room temperature ionic liquid in water and water-organic solvent mixed media, *J. Chem. Thermo.* **2013**, 60, 29-40.
6. Amit K. Tiwari, Sonu, Subit K. Saha, Aggregation properties of gemini surfactants containing diethyl ether group in spacer group in water and water-organic solvent mixed media, *J. Chem. Thermo.* **2014**, 70, 24-32.
7. Amit K. Tiwari, Sonu, Subit K. Saha, Effect of hydroxyl group substituted spacer group of cationic gemini surfactants on solvation dynamics and rotational relaxation of Coumarin-480 in aqueous micelles, *J. Phy. Chem. B* **2014**, 118, 3582-3592.
8. M. Sowmiya, Amit K. Tiwari, Sonu, G. Eranna, Ashok K. Sharma, Subit K. Saha, Study on binding interactions of a hemicyanine dye with nanotubes of β -cyclodextrin and effect of a Hofmeister series of potassium salts on it, *J. Phy. Chem. C* **2014**, 118, 2735-2748.

Papers presented in National/International Conferences

1. Nano and Functional Materials (NFM-2014), Department of Chemistry, BITS Pilani, November 7, 2014 (Poster presentation).
2. 5th Asian Conference on Colloid and Interface Science, Department of Chemistry, University of North Bengal, Darjeeling, West Bengal, November 20-23, 2013 (Oral Presentation).
3. International Conference on Interdisciplinary Areas with Chemical Sciences-2013 (ICIACS-2013), Punjab University, Chandigarh in association with Institute of Nanoscience and Technology, Mohali, October 30-November 1, 2013 (Poster Presentation).
4. National Conference on Global Challenges New Frontiers In Chemical Sciences (GC: NFCS-2012), Kurukshetra University, Kureukshetra, September 22-23, 2013 (Poster Presentation).
5. Chemical Constellation Cheminar–2012 (CCC-2012) (An International Conference), Department of Chemistry, Dr. B. R. Ambedkar National Institute of Technology, Jalandhar, Punjab, September 10-12, 2012 (Poster Presentation).
6. Symposium on Recent Trends in Chemical Sciences, BITS Pilani, March 25, 2012 (Poster Presentation).
7. National Conference on Condensed Matter Physics (NCCMP-2012), BITS Pilani, February 24-25, 2012 (Poster Presentation).
8. National Fluorescence Workshop (FCS-2011), JNU New Delhi, November 14-18, 2011 (Poster Presentation).
9. National conference on Thermodynamics of Chemical and Biological Systems (NCTCBS-2011), M. D. University, Rohtak (Haryana), November 2-4, 2011 (Poster Presentation).
10. National Seminar on Membranes, Microemulsions, and Self-Assembled Systems (MMSAS) held at Department of Chemistry, Sikkim Manipal Institute of Technology, Majitar, Rangpo, Sikkim, September 28-30, 2010 (Oral Presentation).

Brief biography of the candidate

Mr. Sonu obtained his B.Sc. degree (B.Sc., Chemistry) in 2005 and M.Sc., degree (M.Sc., Physical Chemistry Specialization) in 2007 from Kurukshetra University, Kurukshetra, Haryana, India. He joined in Birla Institute of Technology & Science, Pilani in the year 2009, to pursue his Doctor of Philosophy (Ph.D) under the supervision of Prof. Subit Kumar Saha. Till date, he has published 13 papers in peer-reviewed international journals and has presented 10 papers in various international/national conferences. He qualified National Eligibility Test (NET/JRF) conducted by CSIR-UGC (HRDG, Govt. of India).

Brief biography of the supervisor

Dr. Subit Kumar Saha is Professor in the Department of Chemistry, Birla Institute of Technology & Science (BITS) Pilani, Pilani Campus, Rajasthan. He obtained his B.Sc. degree (B.Sc., Chemistry Honours) in 1988 and M.Sc. degree (M.Sc., Specialization in Physical Chemistry) in 1990 from University of Kalyani, Kalyani, West Bengal. He obtained his PhD in the year 1998 from IIT Kanpur. His title of thesis is “Spectroscopic study of new molecular probes for micelles using steady-state and nanosecond fluorescence spectroscopy”. Later, he worked as a CSIR Research Associate till November, 1999 in IIT Kanpur. He joined Department of Chemistry, BITS, Pilani in December, 1999 as Lecturer. He became Assistant Professor in December, 2003 and Associate Professor in August 2010. Currently, he is working as Professor in the same institute. His research interests are in the areas of characterization of ICT/TICT fluorescent probes and their application in the characterization of micelles, mixed micelles, reverse micelles, proteins, DNA, cyclodextrins and their supramolecular structures, synthesis and study of thermodynamics and aggregation behaviour of different Gemini surfactants etc. He successfully completed major research projects financially supported by CSIR, Aditya Birla Groups and UGC. A major research project supported by the UGC-DAE Consortium for Scientific Research, Mumbai Centre is going on in his laboratory. As a result of his research accomplishment, he has published number of research articles in the national and international journals. He acted as an Associate Editor of “Global Journal of Physical Chemistry”. He is also a co-author of a book ‘Thermodynamics – A Core Course’. He is a reviewer of a number of reputed national and international journals. Currently, Prof. Saha is guiding two Ph.D. students.